

2m14

SYNTHESIS OF OSCILLATING ADAPTIVE FEEDBACK SYSTEMS

(NASA-CR-136940) SYNTHESIS OF OSCILLATING
ADAPTIVE FEEDBACK SYSTEMS (Colorado Univ.)
239 p HC \$15.00 CSCL 09C

N74-16977

238

Unclas

G3/10 16034

by
John W. Smay

This research was supported by the National Aeronautics and
Space Administration under Research Grant NGR 06-003-083, and
by the National Science Foundation under NSF Grant GK-33485.

DEPARTMENT OF ELECTRICAL ENGINEERING
UNIVERSITY OF COLORADO
BOULDER, COLORADO
JUNE 1, 1973


SYNTHESIS OF OSCILLATING ADAPTIVE FEEDBACK SYSTEMS

by

John W. Smay

This research was supported by the National Aeronautics and Space Administration under Research Grant NGR06-003-083, and by the National Science Foundation under NSF Grant GK-33485.


John W. Smay


Isaac M. Horowitz
Research Supervisor

Department of Electrical Engineering
University of Colorado
Boulder, Colorado

June 1, 1973

SYNTHESIS OF OSCILLATING
ADAPTIVE FEEDBACK SYSTEMS

Abstract--It has been known for many years that insertion of certain types of nonlinear elements in the forward loop of a feedback system will produce a limit cycle and give the system the laudable property of zero sensitivity to plant gain changes. Some such systems have been built and tested, but no genuine synthesis theory has appeared. In this paper a synthesis theory is developed which allows system design to proceed from practical specifications on system command and/or disturbance response to a design which is very nearly optimal in terms of feedback sensor noise effects. The approach taken is to replace the nonlinear element by a mean square error minimizing approximation (dual-input describing function), and then use linear frequency domain synthesis techniques subject to additional constraints imposed by the limit cycle and the approximator. Synthesis techniques are also developed for a similar system using an externally excited oscillating signal with the above approach.

The results, to a large extent, remove the design of the systems considered from the realm of simulation and experimentation, permitting true synthesis and the optimization that accompanies it.

TABLE OF CONTENTS

CHAPTER		PAGE
I	PRELIMINARY BACKGROUND FOR OSCILLATING SYSTEM DESIGN	
1.1	Introduction	1
1.2	Description of the Nonlinear Element in an Oscillating System	3
1.3	Statement of the Design Problem	13
1.4	Optimization Criterion	22
II	SOAS SYNTHESIS FOR SIMULTANEOUSLY SATISFYING QUASI-LINEARITY AND OUTPUT LIMIT CYCLE CONSTRAINTS	
2.1	Synthesis of an Elementary SOAS	27
2.2	An Idealization for Lowering the SOAS Oscillating Frequency	40
2.3	Satisfying Quasi-Linearity and Output Limit Cycle Constraints with Minimum Oscillating Frequency and Practical Specifications	50
2.4	Design Example	61
III	SATISFYING SOAS SENSITIVITY SPECIFICATIONS WITH UNCERTAINTY IN PLANT DYNAMICS	
3.1	The Approach	71
3.2	The Equivalent Plant P_f for Forced Signals	73
3.3	Synthesis of SOAS Loop Transmission to Satisfy Sensitivity Specifications	77
3.4	Design Example	86
3.5	Additional Considerations in the P_h Parameter Sensitivity Design	98
IV	DESIGN CONSIDERATIONS FOR DISTURBANCE INPUTS TO THE SOAS	
4.1	Satisfying Quasi-Linearity and Output Limit Cycle Constraints	102
4.2	Design to Satisfy Disturbance Attenuation Specifications	109
V	EXAMPLE OF SOAS DESIGN AND SIMULATION	
5.1	Design Specifications	113
5.2	System Design	116
5.3	Digital Simulation of Command Response ...	131
5.4	Digital Simulation of Disturbance Response	142

CHAPTER		PAGE
VI	SYNTHESIS OF AN EXTERNALLY EXCITED OSCILLATING ADAPTIVE SYSTEM	
6.1	Introduction	152
6.2	EEAS Nonlinear Element	153
6.3	EEAS Sensitivity to Plant Gain Ignorance .	157
6.4	Synthesis of an Elementary EEAS	161
6.5	EEAS Design to Satisfy Quasi-Linearity and Output Oscillation Magnitude Constraints with Practical Specifications.	168
6.6	Satisfying Transfer Function Sensitivity Specifications	175
6.7	EEAS Design for Disturbance Inputs	180
VII	EEAS SIMULATION	183
VIII	SUMMARY AND CONCLUSIONS	192
	BIBLIOGRAPHY	195
APPENDIX A	Nonlinearity Forced Input Function	198
APPENDIX B	Determination of the Extreme Plant and Transfer Function	204
APPENDIX C	Derivation of Bounds for $L(j\omega)$ from Transfer Function Sensitivity or Disturbance Response Specifications	211

LIST OF TABLES

TABLE		PAGE
2.1	Data for $L_f/(1+L_f)$ for L_f of Eq. 2.4.....	38
2.2	Parameters of prefilter F	39
2.3	Parameters of $L_f/(1+L_f)$ using L_f from Eq. 2.42.....	46
2.4	Parameters of prefilter F	47
2.5	Parameters of rational H shown in Fig. 2.11.	67
3.1a	Parameters of G for L_f shown in Fig. 3.8..	90
3.1b	Parameters of $L_f = GP_f$ with G given in Table 3.1a.....	92
3.2a	Parameters of G for L_{f1} of Fig. 3.9.....	93
3.2b	Parameters of L_f using G from Table 3.2a..	95
3.3a	Parameters of G for L_{f1} of Fig. 3.10.....	95
3.3b	Parameters of L_f using G from Table 3.3a..	96
5.1	Parameters of G_2	118
5.2a	Parameters of G for L_{f1} shown in Fig. 5.4.	119
5.2b	Parameters of L_f using G from Table 5.2a..	120
5.3	Parameters of G_1	123
5.4	Parameters of H	124
5.5	Parameters of $L_{fe}/(1+L_{fe})$	124
5.6	Parameters of F	125
7.1	Parameters of EEAS L_f	188
7.2	Comparison of SOAS and EEAS step response characteristics	189
A.1	Tabulation of some trial functions $X_f(s)$	201

LIST OF ILLUSTRATIONS

FIGURE		PAGE
1.1	Representation of nonlinear element for derivation of multiple-input describing function	4
1.2	Oscillating system two degree-of-freedom feedback structure	14
1.3	Illustration of noise power reduction with loop transmission bandwidth reduction	25
2.1	SOAS structure	28
2.2	Constraint on ω_0 due to limitation on output limit cycle	33
2.3	Frequency response of functions applicable to design example	37
2.4	Frequency response of functions applicable to design example	45
2.5	SOAS feedback structure	51
2.6	Ideal limit cycle filter H and corresponding X_e	56
2.7	λ vs. ω_0' for fixed γ	57
2.8	Behavior of functions of interest as ω_0' is reduced	58
2.9	Frequency response of functions determining lower bound for ω_0'	65
2.10	Plot of λ vs. ω_0' calculated using ideal limit cycle filter with 500 db/dec slopes and $\gamma = 1.12$	67
2.11	Ideal and rational limit cycle filters	68
2.12	Time response $\alpha x_{e1}(t)/q_x$ and $\alpha x_e(t)/q_x$ using rational limit cycle filter from Table 2.5	69
3.1	SOAS structure	71
3.2	Illustration of gain factor variation with parameters of P_h	75
3.3	Permissible variation of $\ln T(j\omega) $ vs. variation of $\ln P_h(j\omega) $	77
3.4	Boundaries for optimal $L_f(j\omega)$	78

FIGURE	PAGE
3.5 Violation of boundary B_d which applies to all L_f	81
3.6 Hypothetical loop transmission satisfying all boundaries	83
3.7a Permissible variation of $ T(j\omega) $	88
3.7b Comparison of plant variation with permissible variation of transfer function	89
3.8 Bounds for $L_f(j\omega)$ and plots of rational L_f using G of Table 3.1a	91
3.9 Bounds for $L_{f1}(j\omega)$ after obtaining first G , and $L_{f1}(j\omega)$ using second G from Table 3.2a	94
3.10 Bounds for $L_{f1}(j\omega)$ after obtaining second G , and $L_{f1}(j\omega)$ using third G from Table 3.3a	97
3.11 Illustration of oscillation frequency variation proportional to phase slope	99
3.12 Shaping of L_f to reduce ω_o variation ..	100
4.1 SOAS structure with disturbance input D ..	102
4.2 Comparison of forced inputs to N for commands R and disturbances D	104
4.3 Composite boundary for $L_{f1}(j\omega_i)$ due to sensitivity and disturbance specifications.	111
5.1 SOAS structure	113
5.2 Saturation characteristic	114
5.3 Specification envelope for $ T(j\omega) $	116
5.4 Bounds for $L_{f1}(j\omega)$ and plot of $L_{f1}(j\omega)$ using G of Table 5.2	121
5.5 Frequency responses of L_f	122
5.6 Equivalent linear transfer functions for several plant values	126
5.7 $c(t)$ obtained with unit step input and transfer functions on Fig. 5.6	128
5.8 Design value of extreme $x_e(t)$	128
5.9 Digital simulation plot of prefilter F output	133
5.10 Digital simulation plot of nonlinearity input function	134
5.11 System response to unit step applied at $t = 1$. sec.	136

FIGURE	PAGE
5.12	System output for unit step disturbance .. 144
5.13	Comparison of nonlinearity forced signal input for step command and disturbance inputs 146
5.14	System output for step disturbance input . 147
5.15	System response to disturbance input 149
6.1	EEAS feedback structure 152
6.2	Character of $\max_B N_B(A,B) = \xi(A)$ 155
6.3	ϕ vs. $\sqrt{L_O(j\omega_o)}$ with A_O/M_O as a parameter 159
6.4	$ L_O(j\omega_o) $ vs. A_O/M_O with ϕ as a parameter 159
6.5	Variation of $L_O(j\omega_o)$ on Nichols chart coordinates 160
6.6	Boundaries for EEAS oscillating signal loop transmission 164
6.7	Location of oscillating frequency 166
6.8	EEAS structure with notch filter 168
6.9	Behavior of X_e and bounds for L_{Om} as oscillating frequency is decreased 172
6.10	Illustration of forced signal loop transmission shaping for EEAS 178
6.11	Location of ω_o 179
7.1	EEAS feedback structure 183
7.2	Phase characteristic of loop transmission. 184
7.3a	Input signal to nonlinear element in SOAS and EEAS 186
7.3b	System output in SOAS and EEAS modes 187
7.4	Bounds for $L_{fm}(j\omega)$ and $L_{fm}(j\omega)$ using G of Table 5.2b and $A_O = 1.2M_O = 3.05$.. 188
7.5	EEAS response to unit step command 190
A.1	Oscillating system structure 198
B.1	Illustration of extreme plant selection .. 207
B.2	Variation of $x_f(t)$ for several selections of P_{he} 209
C.1	A two degree-of-freedom feedback structure 211
C.2	Construction of the plant template 213

FIGURE		PAGE
C.3	Method for locating one point on the boundary of acceptable $L_1(j\omega_i)$	214
C.4	Location of boundary points for $L_1(j\omega_i)$ to satisfy disturbance transmission specification	216
C.5	Graphical representation of Eq. C.11	217

CHAPTER I
PRELIMINARY BACKGROUND FOR OSCILLATING
SYSTEM DESIGN

1.1 Introduction

The limit cycling or self-oscillating adaptive system (SOAS) has appeared in the literature several times over the preceding decade and before^[1-6]. Indeed one version of an oscillating system^[7] (externally excited and somewhat different from those in this paper, but with the same adaptive philosophy) was produced by Minneapolis-Honeywell and successfully flight tested in the F-94C aircraft in the role of pitch rate controller, and separately in the role of pitch attitude controller. An oscillating system was also used on the X-15 aircraft^[8]. The adaptive properties of oscillating systems have thus been proven to have useful practical application. In fact, out of many adaptive schemes that have been investigated, the oscillating system is one of few that have been shown to have practical application to systems where there is large plant parameter uncertainty or variation. The primary attractiveness of oscillating systems arises from their inherent zero sensitivity to plant gain factor changes. Even so, as pointed out in [6], a careful study must be made to determine whether,

in a given problem, a proposed oscillating system is indeed superior to a purely linear system.

Noticably absent from the literature, however, are specific synthesis techniques. Rather, the existing theory has been presented on a largely qualitative basis and actual hardware design entails much experimentation and simulation. Synthesis techniques are needed that permit the designer to proceed from a realistic set of specifications through a step by step design procedure which insures that these specifications are met, while optimizing in some sense over the free parameters. In addition, the designer should be able to see any trade-offs involved in the synthesis steps, and to succinctly determine what advantages his design has over other possible designs, e.g., a linear design.

In this paper a systematic synthesis procedure is presented. The criterion for optimization adopted is to minimize the effect of output sensor noise at the plant input (or the system output). Rather broad system performance specifications are assumed, and from these a design that is quite close to optimum is developed. The systematic procedure for approaching this nearly optimum design is given and at each step the designer has a good "feel" for what his chosen degree of optimization is costing in terms of system complexity.

In Chapter I we first consider the class of non-linear elements that are suitable for oscillating systems,

how these elements will be mathematically described in synthesis, and the constraints imposed by this description. Next, a detailed statement of the synthesis problem and the type of specifications to be satisfied is given. Finally, the criterion for optimizing the oscillating system design is discussed.

1.2 Description of the Nonlinear Element in an Oscillating System

In the following, some basic properties of a class of nonlinearities will be enumerated and the synthesis theory of this paper will then apply to the class of nonlinear elements possessing these properties. The multiple-input describing function is used for analysis. The multiple-input describing function has been treated rather thoroughly and elegantly by Gelb and Vander Velde^[9], and the abbreviated derivation below follows that work closely.

The nonlinearity in Fig. 1.1 has input $x(t)$ composed of three known signal types. We shall use in place of the nonlinear element N a quasi-linear approximator for each of the signal components and require that the approximators be such that the total mean squared error

$$E[e^2(t)] = E[(y(t) - \hat{y}(t))^2]$$

be minimized. By quasi-linear it is meant that for a

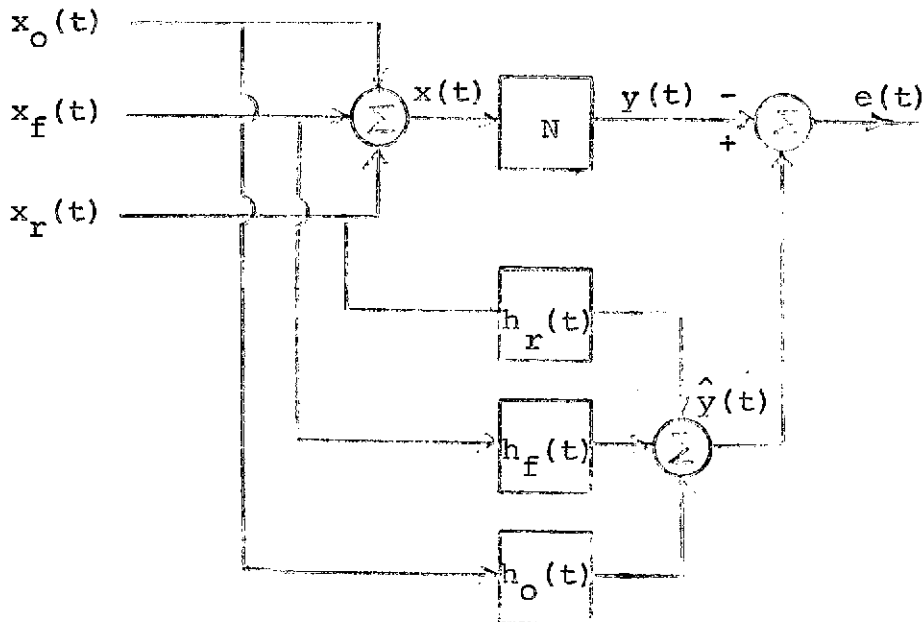


Figure 1.1 Representation of nonlinear element for derivation of multiple-input describing function.

fixed input signal each of the $h_i(t)$ in Fig. 1.1 perform as a linear system to the particular signal type for which it is derived, however, an h_i may depend on some parameters of its input signal type, e.g., magnitude, and therefore is not truly linear. We shall consider only time-invariant N and stationary inputs $x(t)$ so the resultant h_i are thus time-invariant. Forming the error, minimizing via the calculus of variations, and requiring that the input signals be statistically independent, the following decoupled set of equations in h_i

is obtained.

$$\int_0^{\infty} h_i(t) R_{x_i}(t-\tau) dt = R_{yx_i}(\tau) ; \quad \tau \geq 0. \quad (1.1)$$

In this equation $R_{x_i}(\tau)$ is the autocorrelation for input $x_i(t)$ and $R_{yx_i}(\tau)$ is the cross-correlation between nonlinearity output $y(t)$ and input component $x_i(t)$. Eq. 1.1 has identically the form of the Wiener-Hopf integral of linear mean square filtering theory.

Letting $x_o(t) = A \sin(\omega_o t + \theta)$ where θ is the random variable distributed uniformly over $[0, 2\pi]$ radians gives $R_{x_o}(\tau) = \frac{1}{2}A^2 \cos \omega_o \tau$. Then

$$\begin{aligned} \frac{A^2}{2} \int_0^{\infty} h_o(t) \cos[\omega_o(t-\tau)] dt = \\ \frac{A^2}{2} \left[\cos \omega_o \tau \int_0^{\infty} h_o(t) \cos \omega_o t dt + \sin \omega_o \tau \int_0^{\infty} h_o(t) \sin \omega_o t dt \right]. \quad (1.2) \end{aligned}$$

$R_{yx_o}(\tau) = E[y(t)A \sin[\omega_o(t-\tau) + \theta]] = AE[y(0) \sin[\theta - \omega_o \tau]] = A \cos \omega_o \tau E[y(0) \sin \theta] - A \sin \omega_o \tau E[y(0) \cos \theta]$. Equating the last expression to (1.2) for all $\tau \geq 0$ yields

$$\int_0^{\infty} h_o(t) \cos \omega_o t dt = \frac{2}{A} E[y(0) \sin \theta] \quad (1.3a)$$

$$\int_0^{\infty} h_o(t) \sin \omega_o t dt = -\frac{2}{A} E[y(0) \cos \theta]. \quad (1.3b)$$

These equations are satisfied by

$$h_o(t) = \frac{2}{A} \left[E[y(0) \sin\theta] \delta(t) + \frac{1}{\omega_o} E[y(0) \cos\theta] \dot{\delta}(t) \right], \quad (1.4a)$$

or upon taking the Fourier transform

$$N_o = H_o(j\omega_o) = \frac{2}{A} \left[E[y(0) \sin\theta] + jE[y(0) \cos\theta] \right]. \quad (1.4b)$$

N_o is the describing function for the sinusoidal component of input at frequency ω_o . If the total input $x(t)$ is taken to be a single sinusoid in computing N_o , (1.4b) yields the more conventional describing function obtained using harmonic analysis of $y(t)$. The expression here is valid for the sinusoidal component at ω_o of any stationary, but otherwise arbitrary, input provided the sinusoidal component and the remainder of the input are independent. If there are, for example, two sinusoidal components at different frequencies ω_o and ω_1 the describing function for each may be obtained from (1.4b) by two separate calculations. The two gains thus obtained are known as the two sinusoid input describing function (TSIDF). N_o has quite simple form, being a complex gain, but calculation of the expectations in (1.4b) is not in general simple. It is shown in [9] that N_o is real for static and single-valued nonlinearities.

Taking $x_f(t) = b$, a constant, gives $R_{x_f}(\tau) = b^2$ and $R_{yx_f}(\tau) = bE[y(t)] = bE[y(0)]$. Thus using (1.1) again

$$\int_0^{\infty} h_f(t) dt = \frac{E[y(0)]}{b}, \quad (1.5)$$

which is satisfied by

$$h_f(t) = \frac{E[y(0)]}{b} \delta(t) \quad (1.6a)$$

and this represents a pure gain in the frequency domain, viz.,

$$N_f = \frac{E[y(0)]}{b}. \quad (1.6b)$$

The nonlinearity must have no constant output component when there is no constant input (static nonlinearities must be odd) in order that N_f be finite as $b \rightarrow 0$. This condition is always assumed in subsequent discussion.

If the input to N is restricted to be the sum of a sinusoid plus a constant signal, the two gains N_o , N_f are known as the dual-input describing function (DIDF). For use in an oscillating system we shall require that

$$N_o \approx M_o/A \quad (1.7a)$$

$$N_f \approx M_f/A \quad (1.7b)$$

for $A/|b| > 1$ by a sufficient margin, where M_o , M_f do not depend on $x(t)$. Actually, we require even more. Instead of just a constant we shall allow $x_f(t)$ to be some transient function of time, therefore not stationary, and require it to be slow and small with respect to the

sinusoidal input in the following sense.

$$\max_t |x_f(t)| \leq A_1/\alpha \quad (1.8a)$$

$$\omega_b \leq \omega_o/\beta, \quad (1.8b)$$

where ω_b is the bandwidth of $X_f(j\omega)$ and A_1 is the minimum value that A can assume in the given application. If for a given nonlinearity there exists α, β such that when (1.8) holds, then (1.7) gives a sufficiently good approximation to the DIDF with α, β, M_o , and M_f dependent only on the physical parameters of the nonlinearity, i.e., independent of input provided the input has the assumed form, then such a nonlinearity is a candidate for use in an oscillating system. It will be seen that (1.7) is necessary to obtain the zero gain sensitivity property in oscillating systems. It is stated in [10] that $\alpha > 3$ and $\beta > 3$ give less than 5% error in the approximations of (1.7) for an ideal relay when $x_f(t)$ is a sinusoid and this reference indicates these values hold closely for a wide range of common nonlinearities. The error for any given nonlinearity can be obtained by expanding the TSIDF, obtained from (1.4b), and DIDF in Taylor series in b/A with b as the bias magnitude or the magnitude of the lower frequency sinusoid.

It may appear that by now we have restricted ourselves to a nearly empty class of nonlinearities, but

this is not the case. In order that (1.7a) hold it is seen that N must have a saturating property, or for large A the output sinusoidal component must approach $|M_0|$ in magnitude, independent of A . In [11] it is shown that for all odd, static, and single-valued nonlinearities, if the input is the sum of two sinusoids $x(t) = x_f(t) + x_o(t) = b\cos\omega_b t + A\cos\omega_o t$ with ω_o/ω_b irrational then

$$\lim_{b \rightarrow 0} N_f(A, b) = N_o(A, 0) + \frac{A}{2} \frac{dN_o(A, 0)}{dA} . \quad (1.9)$$

The limit holds also for $\omega_b = 0$, i.e., when $x_f(t) = b$. Of course dN_o/dA must exist. The above limit has been called the incremental input describing function (IIDF). Applying this limit to the right side of (1.7a) we get that $N_f \approx N_o/2 \approx M_o/2A$ when x_f is a sufficiently small constant. Thus we can conclude that every odd, saturating, static, and single-valued nonlinearity is in the class of candidates for oscillating systems. In a practical design situation one must of course determine that (1.7) is a satisfactory approximation with acceptable values of α and β . We remark also that there may be some lower bound set by the nonlinearity on A_1 in (1.8a), e.g., for a saturation nonlinearity A_1 must be large enough to cause saturation. The above in no way limits the possible nonlinearities that may prove satisfactory for an oscillating system. Smisek^[16] has

studied a dynamic nonlinearity for which M_0 is complex with phase lead, and used this element in an SOAS simulation. The above conditions, viz., nonlinearities that are odd, saturating, static, single-valued, and such that dn_0/dA is finite are theoretically sufficient for (1.7) to hold for some α and β , but they are not necessary.

The IIDF has another useful application. Since it holds for any ω_b not rationally related to ω_0 it can be used to predict stability of the forced signal loop transmission for small perturbations. For large signal stability the TSIDF can be used.

Next a random process input $x_r(t)$ to the nonlinear element is considered. For this input $R_{yx_r}(\tau) = E[y(t)x_r(t-\tau)]$ and Eq. 1.1 becomes

$$\int_0^{\infty} h_r(t) R_{x_r}(t-\tau) dt = R_{yx_r}(\tau); \quad \tau \geq 0. \quad (1.10)$$

For the general nonlinearity $R_{yx_r}(\tau)$ is quite difficult to obtain, and even if it were known the solution of (1.10) is not apparent except in special cases, e.g., if the Fourier transform of $R_{yx_r}(\tau)$ is known and rational, the Wiener-Hopf type integral can be solved by spectral factorization. However, as shown in [9], for the special case of gaussian zero mean $x_r(t)$ (if it is not zero mean the constant component may be included in x_f), and

for static single-valued nonlinearities only, $R_{yx_r}(\tau) = R_{x_r}(\tau)E[y(0)x_r(0)]/\sigma^2$. σ is the standard deviation of the process amplitude distribution. In this case (1.10) is seen to be satisfied by

$$h_r(t) = E[y(0)x_r(0)]\delta(t)/\sigma^2 \quad (1.11a)$$

and

$$N_r = E[y(0)x_r(0)]/\sigma^2 . \quad (1.11b)$$

Thus the random input describing function (RIDF) component is a pure gain under the stated conditions.

Finally it is shown in [9] that with input $x(t) = b\cos\omega_b t + A\cos\omega_o t + x_r(t)$, an odd single-valued nonlinearity, and x_r gaussian, that

$$\lim_{b \rightarrow 0} N_f(A, b, \sigma) = N_r(A, 0, \sigma) . \quad (1.12)$$

Eq. 1.12 holds when $\omega_b = 0$ as well. This suggests that for small inputs $x_f(t)$ the mean square error minimizing quasi-linear approximator is a gain independent of the waveshape of $x_f(t)$. It is found also that if in addition to (1.8)

$$\sigma \leq A_1/\alpha_r \quad (1.13)$$

then

$$N_r \approx M_f/A . \quad (1.14)$$

More importantly, we want (1.7) to hold for forced and oscillating signals when there is also a noise input to N , i.e., the forced and oscillating signal components of the three input describing function, $N_f(A,b,\sigma)$ and $N_o(A,b,\sigma)$ must approach the asymptotic values of (1.7). This, of course, occurs when σ is vanishingly small. A check for two common nonlinearities, ideal relay and saturation, indicates that (1.7) holds for $\alpha_r \approx \alpha > 3$.

The nonlinearity N will be used in a feedback system (see Fig. 1.2). The output of N will always be non-gaussian (since only saturating nonlinearities are used) and in this structure the output is fed back so that the input to N is not in general gaussian. A linear system with gaussian input produces a gaussian output.^[17] Also, it has been empirically observed^[12,17] that when a non-gaussian signal is passed through a linear bandpass filter the output tends to a gaussian distribution (this can be proved for non-gaussian white noise or for vanishing bandwidth). Further, the RIDF has exhibited good agreement with experimental measurements^[13] obtained from a feedback structure using two nonlinearities of the type considered here, viz., an ideal relay and a relay with dead zone. Therefore we shall assume that the noise input to N is reasonably well approximated by a gaussian distribution.

In the development of subsequent synthesis theory the nonlinear element will be represented by the quasi-linear

approximations on the right of Eq. 1.7 and (1.8) will be taken as a specification to insure the validity of this approximation. Eq. 1.13 will not be taken as a specification because it is not possible to simultaneously achieve this and the feedback specifications that are assumed in the following section. Rather, for any completed design the maximum tolerable noise input to the nonlinearity can be calculated and the describing function holds as long as this limit is respected.

1.3 Statement of the Design Problem

The system structure of Fig. 1.2 will be assumed throughout. P is the plant transfer function which may contain varying or uncertain parameters. The designer has access to its input and output only. The remaining transfer functions are compensations to be synthesized, with the exception of N , which is a nonlinear element of the type discussed in the preceding section. A sensor with unity transfer function which introduces noise with power spectrum η is assumed. $D(s)$ is a disturbance input and A_0 is the applied excitation, present only in the case of an externally excited oscillating system (EEAS).

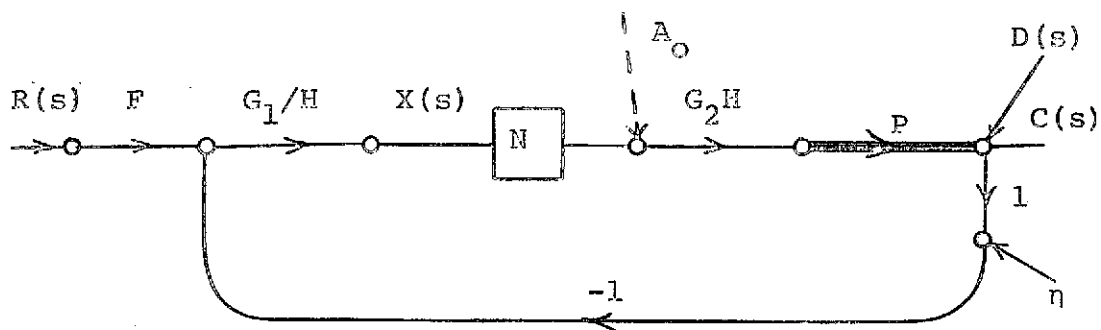


Figure 1.2 Oscillating system two degree-of-freedom feedback structure.

The feedback system in Fig. 1.2 is a two degree-of-freedom structure, so called because there are two signals that can be independently processed and used to control the plant output, viz., the command input $R(s)$ and the system output $C(s)$. For linear systems, all two degree-of-freedom structures are equivalent with respect to the attainable benefits of feedback (sensitivity to plant parameters and disturbance attenuation), and with respect to the effect of sensor noise η on the plant. [18] Since we replace N by a quasi-linear approximator, all other two degree-of-freedom structures are equivalent to Fig. 1.2 in the above respect provided two constraints imposed by the nonlinear element are observed. First, the nonlinear element must be in the forward path in series with the plant to provide the zero gain sensitivity property. Second, the nonlinear element must be embedded between two compensations to allow for simultaneously satisfying the quasi-linearity constraints

and a limit on output oscillation magnitude.

The oscillating signal component at the input of N in Fig. 1.2 will be taken as sinusoidal so the usual filter hypothesis of describing function theory must be invoked. In particular the output from N will be a periodic signal with fundamental frequency ω_o and G_1G_2P must filter out higher harmonics well enough that they may be neglected at the input to N .

The synthesis problem is to design the compensation functions in Fig. 1.2 so that the system output always satisfies given specifications in spite of bounded ignorance or variation of plant parameters and disturbance inputs. Some a priori knowledge of command and disturbance inputs must of course be assumed.

Below we give a statement of the specifications, in their most general form, that the subsequent synthesis theory is capable of dealing with. In any particular design example one or more of these may be absent.

Specifications

Nonlinear Element

The nonlinear element N is taken to be adequately characterized by the DDF

$$N_o = M_o/A \quad (1.15a)$$

$$N_f = M_f/A \quad (1.15b)$$

when quasi-linearity constraints

$$\max_t |x_f(t)| \leq A/\alpha \quad (1.16a)$$

$$\omega_b \leq \omega_o/\beta \quad (1.16b)$$

are satisfied. Some specific nonlinear element must of course be selected before a numerical design can be executed, so that $M_o, M_f, \alpha,$ and β are known or can be determined by the designer. $x_f(t)$ is the forced signal component of input to N arising from command or disturbance inputs. ω_b is the bandwidth of $X_f(j\omega)$. A is the magnitude of the oscillating signal input to N . Eq. 1.16 must hold for all possible x_f and A as the plant and input vary, so extremes will be treated in synthesis. As noted previously there may be a lower bound on A , e.g., a saturation nonlinearity must be driven well into saturation before (1.15) can hold. Also, it was noted in Sect. 1.2 from [10] that $\alpha > 3, \beta > 3$ gives 5% accuracy for the approximation to obtain (1.15) for some nonlinearities when x_f is a sinusoid with frequency in the closed interval $[0, \omega_b]$. Since x_f considered here will be a transient signal, β may depend to some extent upon its waveshape. Ultimately the choice of α and β is left to the designer, who must consider a particular nonlinearity and the nature of the forced signals in his system. It will be seen in design examples presented later that in practical systems where the SOAS or EEAS is most appropriate, that ω_o/ω_b is forced by

other design constraints to be rather large.

Plant

In the subsequent synthesis theory the plant is assumed to be a rational transform with known structure, written as

$$P(s,w) = K(w)P_h(s,w); \quad \begin{cases} w \in W \\ K(w) \in [K_1, K_2] \end{cases} \quad (1.17)$$

w is a vector of all plant parameters bounded by the set W and $K(w)$ is the high frequency gain factor, i.e., $P(s,w) \rightarrow K(w)/s^e$ as $|s| \rightarrow \infty$. $K_1 = \min_{w \in W} K(w)$ and $K_2 = \max_{w \in W} K(w)$. The plant parameters may have any value within the bounding set, or may vary slowly within this set. By "slowly" it is meant that the change in any parameter over the time period required to process an input command or disturbance is negligible. The feedback may be quite effective for fast parameter variations also, [19] but since time-invariant synthesis theory is used herein the results are valid for slow variations, and fast variations are not considered.

Extreme Input

The extreme command or disturbance input that the system is required to accept must be specified. By extreme, we mean the forcing signal input that most nearly causes the system to violate the quasi-linearity

constraints. This input denoted by $R_e(s)$ or $D_e(s)$ will be the largest magnitude and/or the fastest input to be applied to the system. For example, if the command inputs are steps, then $R_e(s) = q_r/s$ where q_r represents the largest step.

Transfer Function and Parameter Sensitivity

The transfer function for commands in Fig. 1.2 is denoted by $T(s) = C_f(s)/R(s)$ where $C_f(s)$ is the forced signal component of output. We assume that a nominal transfer function T_n is specified along with bounds on permissible magnitude variation $\Delta \ln|T(j\omega)|$ as a function of ω . The nominal response and sensitivity may initially be given in the time domain as $c_n(t)$ and an envelope of permissible responses, e.g., $g_1(t) \leq c_f(t) \leq g_2(t)$, where $c_f(t)$ is the response due to a specific command input, say a step. Such specifications may be translated approximately to the frequency domain as discussed in [22].

Although the oscillating systems treated herein may be used for nonminimum phase^[20] designs, there is not available at present a complete synthesis theory to satisfy sensitivity specifications of the above nature, i.e., regarding time response. For this reason we assume T is minimum phase and since $T(j\omega)$ in this case is completely determined by $|T(j\omega)|$ ^[21] we treat only the magnitude in the design procedure for satisfying

sensitivity specifications. However, if one is presented with specifications on both magnitude and angle variation for $T(j\omega)$, these may be handled with the synthesis method presented.

Disturbance Response

In this paper the disturbance $D(s)$ of Fig. 1.2 is treated as a deterministic input (a random input with sufficient restrictions could be treated using the RIDF). Specifications are assumed given as an upper bound on the disturbance transmission magnitude $|T_D(j\omega)| = |C_D(j\omega)/D(j\omega)|$. For minimum phase systems such a bound can be obtained approximately from a time domain specification of the form $|c_d(t)| \leq g_3(t)$ provided the form of the disturbance inputs is known. [22]

When command transmission sensitivity dominates in a design, but nevertheless disturbance inputs exist, it is usually desirable to place a damping constraint on the disturbance response. Even though T_D may not be specified over an entire frequency band, we require that it have no significantly underdamped poles. Since $T_D = 1/(1+L_f)$ where $L_f = N_f G_1 G_2 P$ is the forced signal loop transmission in Fig. 1.2, we require

$$\left| \frac{L_f(j\omega)}{1+L_f(j\omega)} \right| \leq \ell ; \forall \omega. \quad (1.18)$$

This places an approximate constraint on the complex pole pair nearest to the $j\omega$ axis in $1/(1+L_f)$, and thus

loosely limits settling time and overshoot of $c_d(t)$. Also, one may verify on the Nichols chart that (1.18) establishes minimum gain and phase margins.

Output Oscillation Constraint

For a useful oscillating control system there must be some constraint on the magnitude of the oscillating signal component of signal at some point in the system. In Fig. 1.2 we have a sinusoid of magnitude A at the input to N . For this sinusoid N is represented by gain M_o/A (Eq. 1.15a), so the output from N has magnitude $|M_o|$. Thus specifying that the system output have magnitude less than m , the constraint is written

$$|M_o G_2(j\omega_o) H(j\omega_o) K_{mP_{hm}}(j\omega_o)| \leq m, \quad (1.19)$$

where $|K_{mP_{hm}}(j\omega_o)| = \max_{\omega \in W} |P(j\omega_o)|$.

Oscillation Frequency Variation

In the SOAS the frequency of oscillation ω_o occurs at the frequency of 180° phase lag in the loop transmission. This will vary some due to inevitable inaccuracies in the loop compensation elements. In the EEAS we must have a generator that cannot be perfect. Thus, let ω'_o be the center or average value of ω_o . The variation due to the above sources is parameterized by γ_c where

$$\omega_o \in [\omega'_o/\gamma_c, \omega'_o \gamma_c] = \Omega_c. \quad (1.20)$$

γ_C is assumed known as a specification in the synthesis procedure. Note that ω_0 may vary even more due to plant parameter variations, but this component is dealt with separately in the design.

Limit Cycle Quenching Gain Margin

Let $L_O = N_O G_1 G_2 P$ from Fig. 1.2 be the open-loop transmission for the oscillating signal component. In the EEAS it will be necessary to quench the natural limit cycle of the system. As will be shown later, this introduces a gain margin requirement on L_O , written

$$|L_O(j\omega_\pi)| \leq \rho, \quad (1.21)$$

where ω_π satisfies $\angle L_O(j\omega_\pi) = -180^\circ$. ρ will depend on the nonlinear element that is used. This specification does not apply to the SOAS.

Aside from the optimizing criterion, which is treated in the next section, the above completes a statement of design specifications and constraints. Admittedly some of the above are rather broad in nature and some approximations are required. However, they represent a reasonable compromise between the desire to be as analytical as possible on the one hand, and on the other, to get results that have practical application.

1.4 Optimization Criterion

The specifications of the preceding section will be taken as inviolate, but upon quasi-linearization of the system in Fig. 1.2 these can be satisfied by an unlimited number of designs provided the plant is minimum phase. Therefore it is desirable to use this reservoir of design freedom to optimize in some fashion. In particular, the rms noise power at the plant input (or output) due to sensor noise input η will be minimized, as shown below.

As explained in Sect. 1.2 the RIDF, $N_r = M_r/A$, for odd, static, and single-valued nonlinearities with gaussian inputs is a pure gain. Assuming N in this class, the sensor noise η in Fig. 1.2 sees an equivalent linear loop transmission $L_r = N_r G_1 G_2 P$. This is related to $L_o = N_o G_1 G_2 P$, the oscillating signal loop transmission, by the gain factor N_o/N_r (from Sect. 1.2 $N_o/N_r \approx N_o/N_f \approx 2$ for some common nonlinearities) so we can equivalently discuss optimization of L_o which is more closely related to the specifications. Letting e denote the excess of poles over zeros in L_o , a number which of course remains fixed while comparing the quality of any two designs, then at high frequencies

$$|L_o(j\omega)| \rightarrow \frac{K_\infty}{\omega^e} \text{ as } \omega \rightarrow \infty. \quad (1.22)$$

The optimum L_o will be taken as the one with minimum K_∞ . This criterion has been used previously for linear systems. [22,23]

In Fig. 1.2 the noise transmission to the plant input is

$$T_{\eta} = \frac{-L_r}{P(1+L_r)} . \quad (1.23)$$

Using $L_r = QP$ we see that

$$|T_{\eta}(j\omega)| \approx \begin{cases} \left| \frac{1}{P(j\omega)} \right| ; & |L_r(j\omega)| > 1 \\ |Q(j\omega)| ; & |L_r(j\omega)| < 1 . \end{cases} \quad (1.24)$$

η is the power density spectrum of the sensor noise input, so writing $\eta(\omega) = \eta^+(j\omega)\eta^-(-j\omega)$ and $\bar{T}_{\eta} = T_{\eta}(-j\omega)$, the mean square noise at the plant input is

$$\sigma_i^2 = \frac{1}{2\pi} \int_{-\infty}^{\infty} \eta^+ \eta^- T_{\eta} \bar{T}_{\eta} d\omega . \quad (1.25)$$

With the aid of Parseval's formula [24], this may also be written

$$\sigma_i^2 = \int_0^{\infty} \mathcal{L}^{-1} [\eta^+ T_{\eta}]^2 dt . \quad (1.26)$$

Let us temporarily take η as white gaussian noise.

In a nontrivial oscillating system design problem it will be seen subsequently that the oscillating frequency ω_0 is constrained to fall above some lower limit. For the SOAS the magnitude of L_0 is constrained by $(L_0(j\omega_0) = -1)$ the choice of ω_0 . A similar constraint is later shown for the EEAS arising from $|L_0(j\omega_{\pi})| \leq \rho$.

Approximately over the frequency range $(0, \omega_0)$ the designer has little control over noise transmission T_η in (1.24). First, because at low frequencies the sensitivity and disturbance attenuation specifications generally dictate some loop transmission magnitude $|L_r(j\omega)| > 1$ and the designer of course has no control over P . Above this frequency range but still below ω_0 , L_o or L_r cannot be reduced significantly because of the magnitude constraint at ω_0 . It is only beyond ω_0 that L_o can be reduced with a steep slope and the accompanying large phase lag. In Fig. 1.3a we show a hypothetical frequency response for P . With the oscillating frequency at ω_0 as shown, the resultant oscillating loop transmission L_a is shown along with $N_o Q_a / N_r$. These are in decibels vs. $\log \omega$. The noise power integral (1.25) is on an arithmetic scale so the mean square noise power at the plant input is proportional to the area under the $|Q_a|$ curve on the arithmetic scale of Fig. 1.3b. Choosing a smaller oscillating frequency, say $\omega_0/2$, the new Q_b and L_b are shown and noise power is now proportional to the area under the dashed $|Q_b|$ curve of Fig. 1.3b. In the frequency region where $|L_r(j\omega)| < 1$, but $|L_r(j\omega)| > |P(j\omega)|$, the noise is amplified by the loop compensation Q (Eq. 1.24), and from Fig. 1.3a $|Q(j\omega)|$ becomes larger over a larger frequency span as ω_0 is increased. Clearly, we should design for the smallest ω_0 possible, and because noise

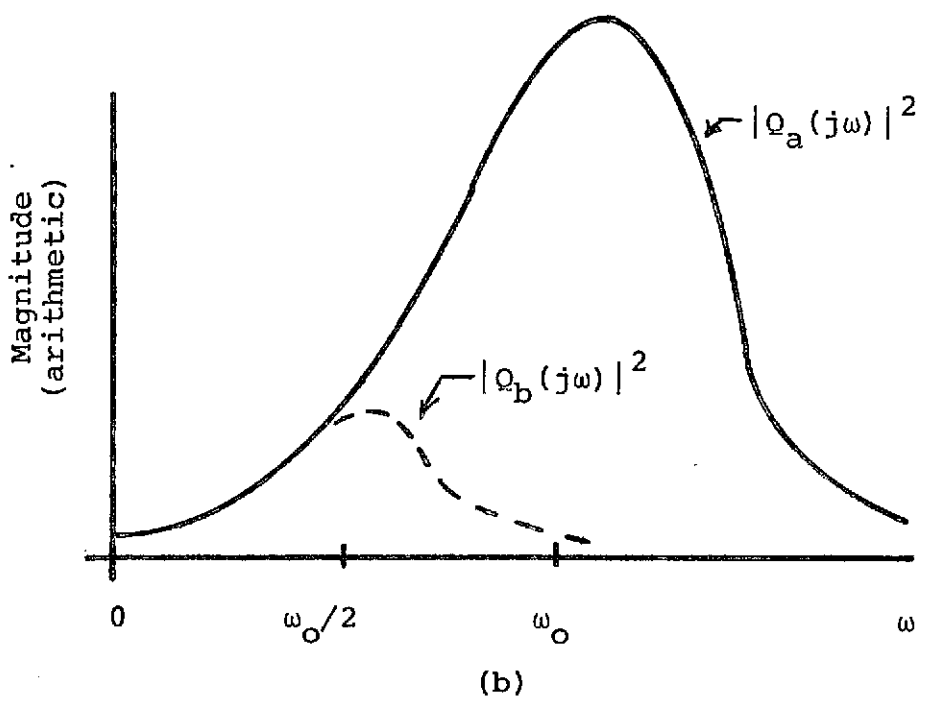
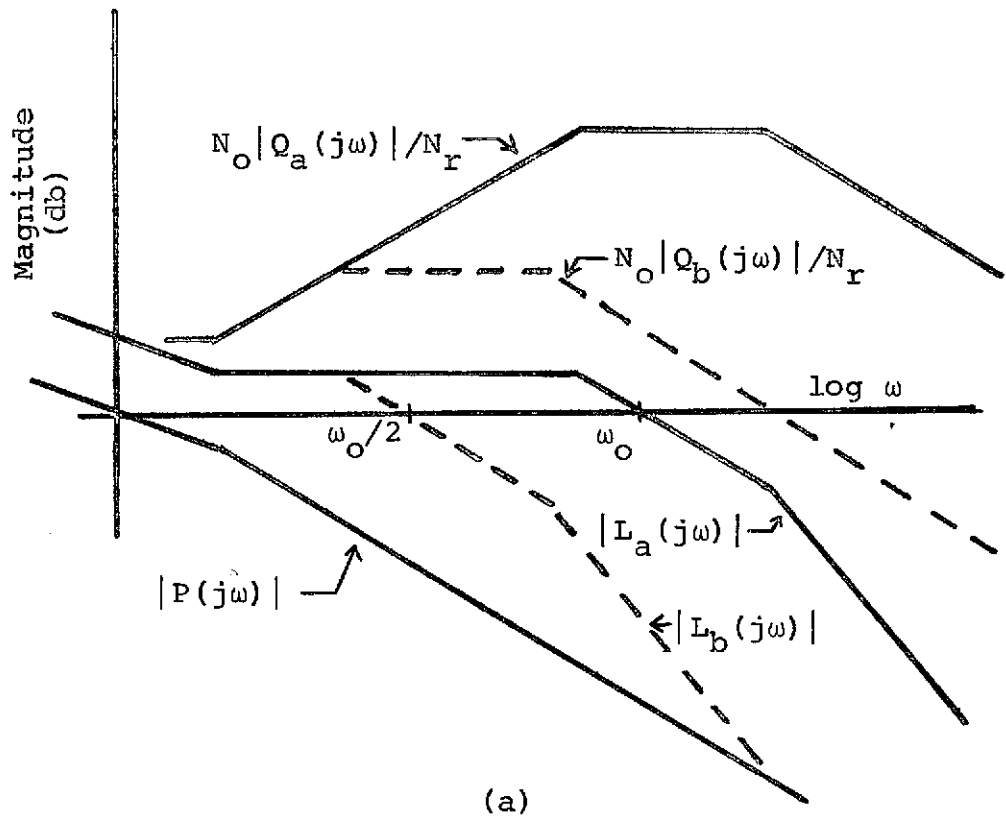


Figure 1.3 Illustration of noise power reduction with loop transmission bandwidth reduction.

power is computed on an arithmetic scale, even a fraction of an octave improvement in ω_0 may give a significant improvement.

Now suppose the noise is not white, but has finite bandwidth. If the noise power is concentrated in the frequency range above ω_0 then the design is still optimized by obtaining minimum ω_0 , and hence K_∞ in Eq. 1.22. This is often the case in control systems since they generally have small bandwidths and it is relatively easy to obtain sensors that are free of very low frequency noise. It will be seen in Chapter III that ω_0 is minimized by making $|L_0(j\omega)|$ as small as specifications permit over the low frequency range ($\omega < \omega_0$). Thus, even if the input noise spectrum is concentrated in a neighborhood of ω_0 there is probably little improvement possible over the above optimization scheme.

The above optimization criterion was based on the nonlinearity having a pure gain RIDF, however, it is reasonable to expect that it may also produce an optimum design, at least for the case of white noise, for a broader class of nonlinearities.

In summary, as each design specification is considered the synthesis theory will be developed with the goal of minimizing oscillating frequency ω_0 (ω_π for the EEAS) which in turn yields minimum K_∞ and rms noise power at the plant input.

CHAPTER II

SOAS SYNTHESIS FOR SIMULTANEOUSLY SATISFYING
QUASI-LINEARITY AND OUTPUT LIMIT CYCLE CONSTRAINTS2.1 Synthesis of an Elementary SOAS.

In this section the synthesis of a simple SOAS is described. The SOAS adaptive property of zero sensitivity to plant gain changes is shown as well as the basic cost in terms of loop transmission bandwidth required to obtain this property. It is found that three basic factors are the determinants of the loop transmission bandwidth, and that they all influence the bandwidth with equal weight. These three factors are the spread of plant gain variation, the maximum input that the system is required to process, and the maximum limit cycle magnitude permitted at the system output.

The structure shown in Fig. 2.1 is used with N a nonlinear element characterized by the DIDF components

$$N_o = M_o/A \quad (2.1a)$$

$$N_f = M_f/A \quad (2.1b)$$

when quasi-linearity constraints

$$\max_t |x_f(t)| \leq A_1/\alpha \quad (2.2a)$$

$$\omega_b \leq \omega_o/\beta \quad (2.2b)$$

are satisfied. M_o , M_f , α , and β are parameters of N , A_1 is the minimum limit cycle magnitude input to N , and $x_f(t)$ is the forced signal input at N having bandwidth ω_b .

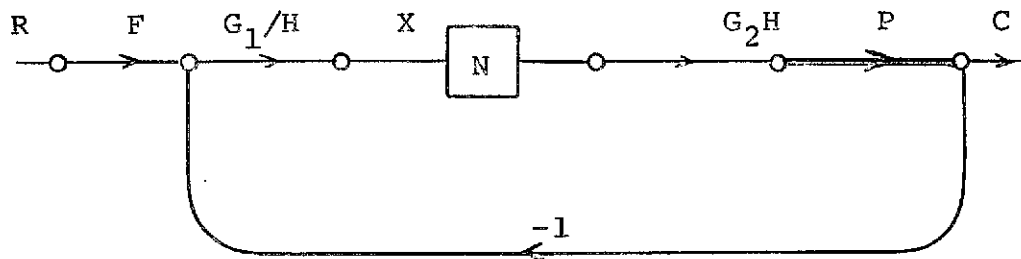


Figure 2.1 SOAS structure.

In Fig. 2.1 P is the given plant which the designer cannot alter, and containing uncertainty in its gain factor only, say $P = KP_h = K/[s(s+a)]$ with the gain factor uncertainty bounded by $K \in [K_1, K_2]$ and a known. The remaining elements in the structure are compensations to be obtained in the synthesis procedure. It is assumed that no disturbances are acting on the system.

The transfer function is specified, and for illustration suppose it is $T(s) = \omega_a^2 / (s + \omega_a)^2$. The limit cycle component appearing in C , the system output, is to have magnitude less than m , and let the extreme input be a step $R_e(s) = q_r/s$.

It is necessary that the describing function N_f be valid for the significant frequency components that must appear in the system output, hence the oscillating frequency is constrained to be above the transfer function bandwidth by the ratio β of Eq. 2.2b. $|T(j\omega_m)| = 1/\sqrt{2}$ gives $\omega_m = \omega_a(\sqrt{2}-1)$, so

$$\omega_o \geq \beta\omega_m = \beta\omega_a(\sqrt{2}-1). \quad (2.3)$$

The loop transmissions for oscillating and forced signal components are respectively

$$L_o = N_o G_1 G_2 P = \frac{M_o}{A} G_1 G_2 K P_h \quad (2.4a)$$

and

$$L_f = N_f G_1 G_2 P = \frac{M_f}{A} G_1 G_2 K P_h. \quad (2.4b)$$

L_o has a valid linear transmission interpretation at the oscillating frequency only and L_f is interpreted as a linear transmission over $(0, \omega_o/\beta)$. To sustain a limit cycle in the system we must have $L_o(j\omega_o) = -1$, which yields from (2.4a)

$$\frac{A}{K} = |M_o G_1(j\omega_o) G_2(j\omega_o) P_h(j\omega_o)|. \quad (2.5)$$

The right side of (2.5) contains no uncertainty or variation so A/K must be constant and therefore can be written $A/K = A_1/K_1$. Putting this in (2.4b),

$$L_f = \frac{M_f K_1}{A_1} G_1 G_2 P_h, \quad (2.6)$$

which shows that the forced signal loop transmission does not change with plant gain, i.e., for any change in plant gain K an exactly compensating change occurs in $1/A$ of N_f . Since $T = FL_f/(1+L_f)$ there is no uncertainty related to the transfer function in this design with only plant gain variation.

Similarly, the only uncertainty in the forcing input to N , X_f , arises from changes in the command input R . Using the extreme input and the specified transfer function, we write with the aid of Fig. 2.1,

$$X_e = \frac{R_e T}{N_f G_2 P} = \frac{A R_e T}{M_f K G_2 P_h} = \frac{A_1 R_e T}{M_f K_1 G_2 P_h} \quad (2.7)$$

We are assuming $H = 1$ throughout this section. The design is carried out to insure that X_e satisfies quasi-linearity constraints (2.2) using R_e , then for all other R , X_f also satisfies these constraints. Introducing the maximum magnitude limitation m on output limit cycle gives, from Fig. 2.1,

$$|M_o G_2(j\omega_o) K_2 P_h(j\omega_o)| \leq m. \quad (2.8)$$

Solving (2.7) for G_2 and substituting in (2.8),

$$\left| \frac{X_e(j\omega_o)}{A_1} \right| \geq \frac{M_o K_2}{M_f K_1 m} |R_e(j\omega_o) T(j\omega_o)|. \quad (2.9)$$

The last inequality is entirely equivalent to (2.8), but written in this form it provides some helpful insight for choosing X_e . The right side of (2.9) is completely given by specifications. The left side is determined entirely by the choice of X_e , but this constraint on X_e is partly in the time domain and partly in the frequency domain. This is seen by using equality in (2.2a) to write $|X_e(j\omega_o)|/A_1 = |X_e(j\omega_o)|/[\alpha_t^{\max}|x_e(t)|]$. ω_o is constrained by $\omega_o > \beta\omega_m$ to be above the transfer function bandwidth so $|R_e(j\omega)T(j\omega)|$ will be a decreasing function of ω in the range of permissible ω_o . Since the objective is to minimize ω_o , we want to maximize $|X_e(j\omega_o)|/A_1$ at fixed ω_o , subject to the quasi-linearity constraints (2.2) on X_e . Observe that using $R_e = q_r/s$, the right side of (2.9) contains the factor $q_r K_2/K_1 m$, thus for any fixed choice of X_e the oscillating frequency ω_o increases or decreases with this factor. These three specifications all influence the required loop transmission bandwidth in the same fashion. This will continue to be the case even in the most complex SOAS designs.

The selection of X_e is discussed in some detail in Appendix A, and it is seen there that if $|X_e(j\omega)|$ is required to be a relatively smooth function of ω , then

$$X_e = \frac{q_x \omega_b}{s + \omega_b} \quad (2.10)$$

is a good choice that also has the advantage of simplicity. Of course X_e will have some constraints imposed by the particular plant structure and input form.

Eq. 2.10 is for Type 1 plants (one pole at the origin) and step inputs. Adopting (2.10) for X_e gives

$\max_t |x_e(t)| = q_x \omega_b$ and hence $A_1 = \alpha q_x \omega_b$. The determination of q_x and ω_b will be discussed presently.

Using X_e from (2.10) and A_1 as above in Eq. 2.7, the compensation G_2 is now

$$G_2 = \frac{A_1 R_e T}{M_f K_1 X_e P_h} = \frac{\alpha (s + \omega_b) R_e T}{M_f K_1 P_h} \quad (2.11)$$

To obtain the constraint on ω_o due to (2.8), G_2 from (2.11) is substituted giving

$$\begin{aligned} & |M_o G_2(j\omega_o) P_h(j\omega_o)| \\ &= \frac{\alpha}{M_f K_1} |M_o (j\omega_o + \omega_b) R_e(j\omega_o) T(j\omega_o)| \leq \frac{m}{K_2} \quad (2.12) \end{aligned}$$

Since we must have $\omega_b \leq \omega_o/\beta$, the center quantity in (2.12) is approximately independent of ω_b , therefore any $\omega_b < \omega_o/\beta$ will not influence the ω_o satisfying (2.12). It is reasonable to give $x_e(t)$ a response time comparable to that of the system output. Thus take ω_b near ω_a or ω_m . If we take it at $\omega_b = \omega_a$ the pole

of X_e cancels one pole of T in G_2 (Eq. 2.11) and thus simplifies G_2 .

Using the given specific form for $R_e T$ in (2.12),

$$|M_o G_2(j\omega_o) P_h(j\omega_o)| = \frac{\alpha q_r \omega_a^2}{M_f K_1} \left| \frac{M_o}{j\omega_o (j\omega_o + \omega_a)} \right| \leq \frac{m}{K_2} \quad (2.13)$$

The quantities of (2.13) are sketched in Fig. 2.2 and the minimum ω_o due to this constraint is labeled. The larger

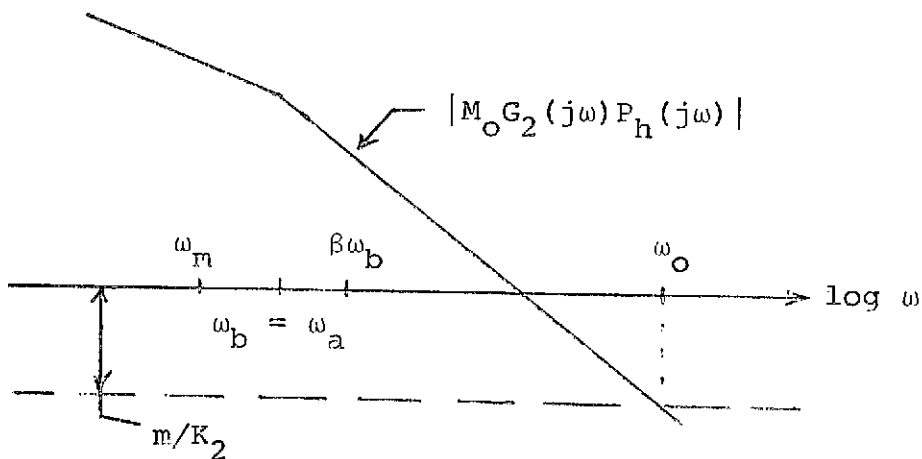


Figure 2.2 Constraint on ω_o due to limitation on output limit cycle.

of $\beta\omega_b$, or the minimum ω_o that satisfies (2.13) must be taken as the design value of ω_o . We can further approximate in (2.13) using $\omega_a < \omega_o$ to get

$$\omega_o > \omega_a \left[\frac{|M_o| K_2 \alpha q_r}{M_f K_1 m} \right]^{1/2}, \quad (2.14)$$

which again shows the basic importance of the quantity $q_r K_2 / K_1 m$. An approximation equivalent to (2.14) is given in [6]. One may observe in Fig. 2.2 that addition of more poles to T , which then appear as poles of G_2 (see Eq. 2.11), have a very beneficial effect on reducing ω_o .

Since no disturbances have been assumed for the present design and there is no uncertainty in P_h , there is no gain-bandwidth requirement for loop transmission L_f . Thus the only requirement for G_1 is to shape L_o to establish the limit cycle at the proper frequency. Finally, after G_1 is selected, the pre-filter F may be obtained directly from the relation $F = T(1+L_f)/L_f$. The design procedure is next demonstrated by a numerical example.

Example

Specifications

Nonlinearity:

$$\left. \begin{array}{l} \text{Ideal Relay} \\ \text{with output} \\ \text{level } M. \end{array} \right\} \begin{array}{l} N_o = M_o/A = 4M/\pi A \\ N_f = M_f/A = 2M/\pi A \end{array} \quad \begin{array}{l} (2.15a) \\ (2.15b) \end{array}$$

$$\left. \begin{array}{l} \text{Quasi-linearity} \\ \text{Constraints} \end{array} \right\} \begin{array}{l} \max_t |x_e(t)| \leq A_1/\alpha; \alpha \geq 3 \\ \omega_b \leq \omega_o/\beta; \beta \geq 3 \end{array} \quad \begin{array}{l} (2.16a) \\ (2.16b) \end{array}$$

Transfer function:

$$T(s) = \frac{(6)^2 (15)^2}{(s+1)^2 (s+6)^2 (s+15)^2} \quad (2.17)$$

Plant:

$$P(s) = KP_h(s) = \frac{K}{s(s+1)}; \quad K \in [K_1, K_2] = [1, 100] \quad (2.18)$$

Maximum input:

$$R_e(s) = q_r/s = 10/s \quad (2.19)$$

Maximum limit cycle output:

$$m = 0.1 \quad (2.20)$$

Design

The constraint on ω_o due to the required bandwidth of T is $\omega_o \geq \beta\omega_m = 3(\sqrt{2}-1)$. Taking $\omega_b = 1$, at one of the poles of T, and using X_e in the form of Eq. 2.10 yields

$$X_e = \frac{q_x b}{s+\omega_b} = \frac{q_x}{s+1} \quad (2.21)$$

Then $A_1 = \alpha q_x \omega_b = 3q_x$ giving from (2.7)

$$\begin{aligned} M_f G_2 &= \frac{A_1 R_e^T}{K_1 X_e P_h} \\ &= \frac{30(6)^2(15)^2}{(s+6)^2(s+15)^2} = M_o G_2/2 \quad (2.22) \end{aligned}$$

Applying the output limit cycle constraint,

$$M_o |G_2(j\omega_o)P_h(j\omega_o)|$$

$$= \left| \frac{60(6)^2(15)^2}{s(s+1)(s+6)^2(s+15)^2} \right|_{j\omega_o} \leq .001 = \frac{m}{K_2} \quad (2.23)$$

The quantities in (2.23) are plotted in Fig. 2.3 and the minimum oscillating frequency is found to be $\omega_o \geq 26.5$ rps. To see the beneficial effect of extra poles in T , note that if the two poles at -15 were deleted the minimum oscillating frequency would be 37 rps as shown by the dashed segment on Fig. 2.3.

In the absence of disturbance inputs and parameter uncertainty in P_h there is no gain-bandwidth requirement for L_f . The only specific requirement is that $L_f(j\omega_o) = -\frac{1}{2} = L_o(j\omega_o)/2$. We choose the minimum $\omega_o = 26.5$ rps and design L_f accordingly, making $|L_f(j\omega)|$ quite small for $\omega < \omega_o$ as shown in Fig. 2.3. The resultant rational loop transmission is

$$L_f = L_o/2$$

$$= \frac{7.585 \times 10^{12} (s+1)}{s[(s^2 + 2(.6)35s + 35^2)(s^2 + 2(.4)60s + 60^2)]^2} \quad (2.24)$$

Thus

$$G_1 = \frac{L_f}{N_f G_2 P} = \frac{A_1 L_f}{K_1 M_f G_2 P_h}$$

$$= \frac{A_1 3.12 \times 10^7 [(s+1)(s+6)(s+15)]^2}{[(s^2 + 2(.6)35s + 35^2)(s^2 + 2(.4)60s + 60^2)]^2} \quad (2.25)$$

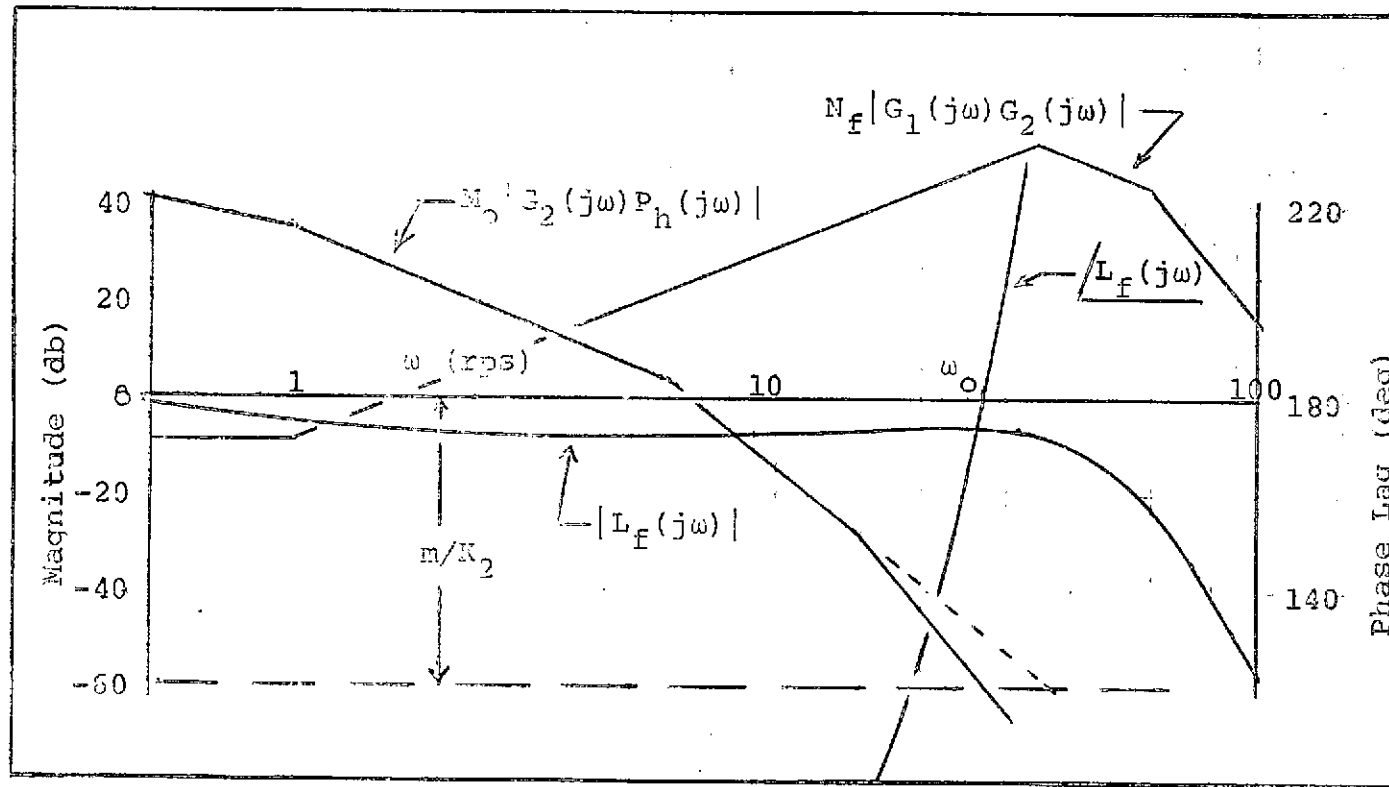


Figure 2.3 Frequency response of functions applicable to design example.

Only the prefilter remains to complete the design.

Factoring the numerator of $1 + L_f$ the data in Table 2.1 is obtained. The prefilter is then obtained

Poles			Zeros		
p	ζ	ω	z	ζ	ω
	.164	26.8	1		
	.813	48.			
	.255	60			
	.468	67			
$K_0 = 1$			$K_\infty = 7.585 \times 10^{12}$		

Table 2.1*

Data for $L_f/(1+L_f)$ for L_f of Eq. 2.24

from

$$F = T(1+L_f)/L_f \quad (2.26)$$

Inspection of the data in Table 2.1 for $L_f/(1+L_f)$ and in Eq. 2.17 for T shows that F has 8 zeros and 7 poles which is not realizable. Additional far poles must be added to T and therefore to X_e in Eq. 2.7.

* For any rational function $F(s)$, K_0 and K_∞ are defined by $F(s) \rightarrow K_0/s^n$ as $|s| \rightarrow 0$ and $F(s) \rightarrow K_\infty/s^m$ as $|s| \rightarrow \infty$.

From Fig. 2.1 we can write $(H = 1) X_e = R_e F G_1 / (1 + L_f)$ so X_e must always have the same excess of poles as $R_e F G_1$ (≥ 3 for step R). If such poles are added to X_e at frequencies well above ω_o they will have negligible effect on $\max_t |x_e(t)|$ and they will not alter the calculation for minimum oscillating frequency in Eq. 2.23. Thus we add complex pole pairs to T and X_e at 60 and 67 rps respectively which cancel the zeros of $1 + L_f$ at those locations. The resultant prefilter has parameters as given in Table 2.2. Since H is

Poles			Zeros		
p	ζ	ω	z	ζ	ω
1				.164	26.8
1				.813	48.
1					
6					
6					
15					
15					
$K_o = 1$			$K_\infty = 4.9 \times 10^{-3}$		

Table 2.2. Parameters of prefilter F.

being taken as unity this completes the design of all the compensation blocks in Fig. 2.1 except for choosing the two constants A_1 , and the relay output level M . With an ideal relay the design theory leaves these constants completely arbitrary. For some other nonlinearities, e.g., saturation, there will be a lower bound for A_1

given in terms of the parameters of M_f . These constants will in practice be chosen from consideration of signal levels within a given system. q_x was not given a value either, however, we have used $A_1/q_x \omega_b = \alpha = 3$ and taken $\omega_b = 1$, so q_x is determined by the selection of A_1 .

2.2 An Idealization for Lowering the SOAS Oscillation Frequency.

In the previous section the smallest possible oscillation frequency was obtained under the assumption that X_e was to be in some sense a smooth function of ω . It was found that the most significant factor requiring ω_o to be large was the combination of input magnitude q_r , range of plant gain variation K_2/K_1 , and the demand for a small output limit cycle component m , so that the basic determinant of ω_o was the magnitude of the quantity $q_r K_2/K_1 m$. Recall the following equations (Eqs. 2.7-9).

$$X_e = \frac{A_1 R_e T}{K_1 M_f G_2 P_h} \quad (2.27)$$

$$|M_o G_2(j\omega_o) P_h(j\omega_o)| \leq m/K_2 \quad (2.28)$$

$$\frac{|X_e(j\omega_o)|}{A_1} \geq \frac{M_o K_2}{M_f K_1 m} |R_e(j\omega_o) T(j\omega_o)| \quad (2.29)$$

Eqs. 2.27 and 28 are obtained from Fig. 2.1 with $H = 1$,

and (2.29) is obtained from substitution of G_2 from (2.27) into (2.28). Eq. 2.29 shows that if one could place large magnitude peaking in $X_e(j\omega)$ at ω_0 , and still maintain control of the time domain quasi-linearity constraints, a significantly smaller ω_0 may satisfy this inequality. Recall the quasi-linearity constraints are

$$\max_t |x_e(t)| \leq A_1/\alpha \quad (2.30a)$$

$$\omega_b \leq \omega_0/\beta \quad (2.30b)$$

To provide for peaking in $|X_e(j\omega)|$ a pair of underdamped poles are introduced at ω_0 in such a way that $\max_t |x_e(t)|$ can be simultaneously controlled^[25]. $x_e(t)$ is written

$$\begin{aligned} x_e(t) &= x_{e1}(t) + x_{e2}(t) \\ &= q_{x\omega_b} e^{-\omega_b t} + q_{x\omega_b} (\lambda-1) e^{-\zeta\omega_0 t} \cos[\omega_0 t \sqrt{1-\zeta^2}]. \end{aligned} \quad (2.31)$$

In the frequency domain

$$\begin{aligned} X_e(s) &= X_{e1}(s) + X_{e2}(s) \\ &= \frac{q_{x\omega_b}}{s+\omega_b} + \frac{q_{x\omega_b} (\lambda-1) (s+\zeta\omega_0)}{s^2 + 2\zeta\omega_0 s + \omega_0^2} \\ &\equiv X_{e1}(s)/H(s) \quad (2.32) \end{aligned}$$

Solving for H gives

$$H = \frac{1}{\lambda} \left[\frac{s^2 + 2\zeta\omega_0 s + \omega_0^2}{s^2 + \frac{[(\lambda+1)\zeta\omega_0 + (\lambda-1)\omega_b]s}{\lambda} + \frac{\omega_0[\omega_0 + (\lambda-1)\zeta\omega_b]}{\lambda}} \right] \quad (2.33)$$

With the above choice of x_e , $\max_t |x_e(t)| = \lambda q_x \omega_b$ can be taken as close as desired to $q_x \omega_b$ by taking λ sufficiently close to unity, while ζ is independently adjusted to make $|1/H(j\omega_0)|$, and thus $|x_e(j\omega_0)|$, as large as desired. This means that with the ideal x_e in (2.32), (2.29) can be satisfied for any ω_0 . Therefore, the bound on output limit cycle component (2.28) does not constrain ω_0 .

We prefer to treat the peaking compensation function H as a separate function so in Eq. 2.27 G_2 is replaced by $G_2 H$ giving

$$x_e = \frac{x_{e1}}{H} = \frac{A_1 R_e T}{K_1 M_f G_2 H P_h} \quad (2.34)$$

and

$$x_{e1} = \frac{A_1 R_e T}{K_1 M_f G_2 P_h} \quad (2.35)$$

The function in (2.33) is the compensation H shown at the output of N in Fig. 2.1 so the constraint on output limit cycle from (2.27) is now replaced by

$$|M_0 G_2(j\omega_0) H(j\omega_0) P_h(j\omega_0)| \leq m/K_2 \quad (2.36)$$

It is undesirable to have the highly underdamped zeros of H appearing in the loop transmissions L_o and L_f so $1/H$ is inserted at the nonlinearity input as shown by Fig. 2.1. The following example demonstrates a design using the ideal limit cycle filter H .

Example

Specifications

The specifications are the same as those in the example of Sect. 2.1, Eqs. 2.15 through 20.

Design

The constraint on oscillating frequency due to required transfer function bandwidth is, as in the example of Sect. 2.1, $\omega_o \geq \beta\omega_m = 3(\sqrt{2}-1)$.

X_{e1} , the low frequency dominant part of X_e is taken as

$$X_{e1} = \frac{q_x \omega_b}{s + \omega_b} = \frac{q_x}{s+1}, \quad (2.37)$$

with $\omega_b = 1$. This constrains $\omega_o \geq \beta\omega_b = 3$ due to quasi-linearity constraint (2.30b). With the narrow limit cycle filter H it is possible to design for any $\omega_o \geq 3$. Let us use $\omega_o = 10$, ($\omega_o = 3$ could be used, but it is seen later that even 10 is not practical) and choose $\lambda = 3/2$. Then from (2.30a and 31) $A_1 = \lambda \alpha q_x \omega_b = 4.5 q_x$, since $\alpha = 3$ from the specifications. Using X_{e1} from (2.37) in (2.35) gives

$$M_f G_2 = \frac{A_1 R_e T}{K_1 X_{el} P_h} = \frac{45(6)^2(15)^2}{(s+6)^2(s+15)^2}$$

$$= M_o G_2 / 2 . \quad (2.38)$$

The output limit cycle magnitude constraint is

$$M_o |G_2(j\omega_o)H(j\omega_o)P_h(j\omega_o)|$$

$$= |H(j\omega_o)| \left| \frac{90(6)^2(15)^2}{s(s+1)(s+6)^2(s+15)^2} \right|_{j\omega_o} \leq .001 = m/K_2 . \quad (2.39)$$

We find at $\omega_o = 10$, $M_o |G_2(j10)P_h(j10)| = -15.7\text{db}$, so that $|H(j10)| = -60 + 15.7 = -44.3\text{db}$. H , given by Eq. 2.33 is completely determined except for ζ . Solving for ζ that provides the required $|H(j10)|$ gives $\zeta = 0.0015$ and

$$H(s) = \frac{2}{3} \left[\frac{s^2 + 2(.0015)10s + 10^2}{s^2 + 2(.0219)8.17s + 8.17^2} \right] . \quad (2.40)$$

The quantities on both sides of Eq. 2.39 are plotted on Fig. 2.4.

Shaping G_1 to establish the oscillating frequency at 10 rps, a satisfactory compensation is

$$G_1 = \frac{A_1 1.26 \times 10^4 [(s+1)(s+6)(s+15)]^2}{[(s^2 + 2(.6)13s + 13^2)(s^2 + 2(.4)25s + 25^2)]} , \quad (2.41)$$

and the corresponding loop transmission is

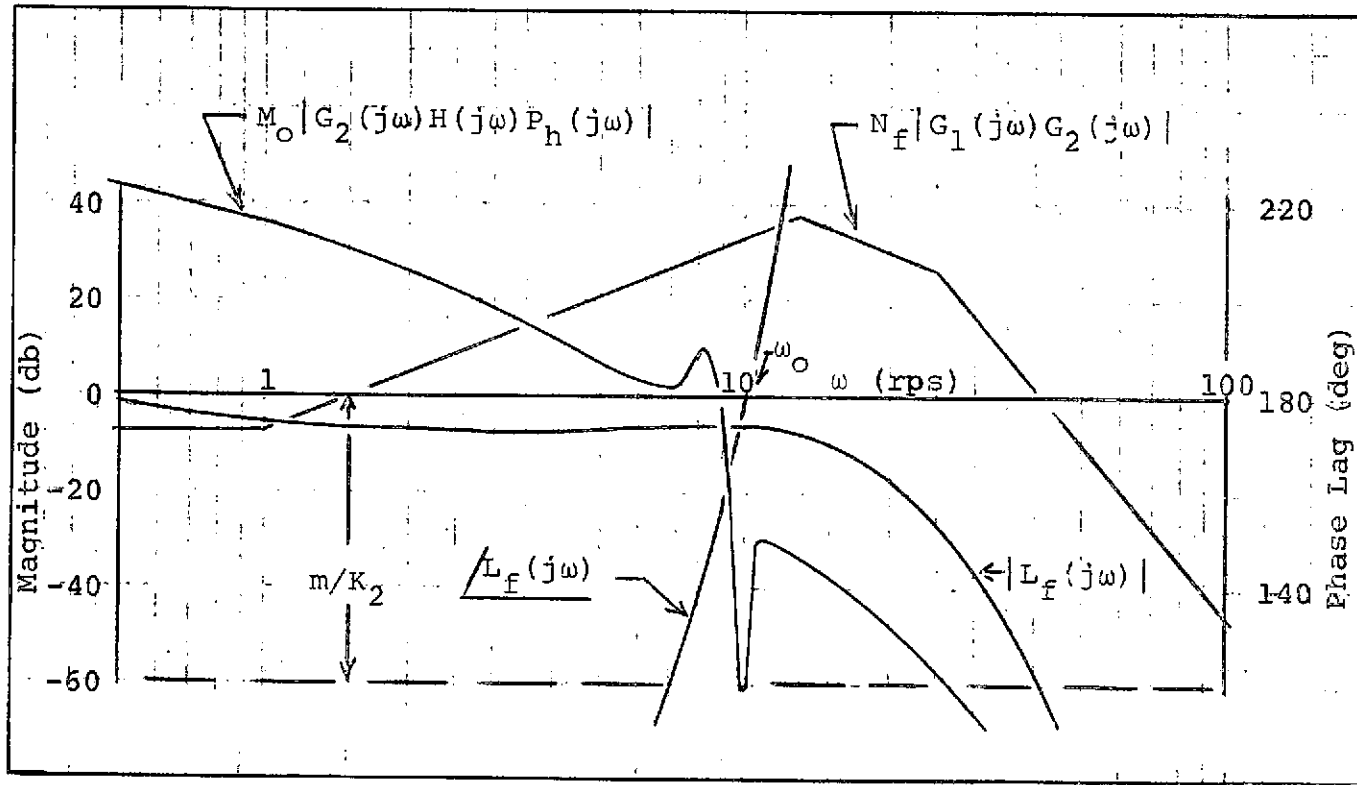


Fig. 2.4 Frequency response of functions applicable to design example.

$$L_f = L_o/2$$

$$= \frac{4.58 \times 10^9 (s+1)}{s[(s^2 + 2(.6)13s + 13^2)(s^2 + 2(.4)25s + 25^2)]^2} \quad (2.42)$$

There is no magnitude or bandwidth requirement on L_f other than that $L_f(j\omega_o) = L_f(j10) = -1/2$, so $|L_f(j\omega)|$ has been chosen rather small. A plot of L_f is shown on Fig. 2.4. Factoring $1 + L_f$ gives the data on Table 2.3.

Poles			Zeros		
p	ζ	ω	z	ζ	ω
	.172	10.1	1		
	.797	18.2			
	.278	24.4			
	.455	27.3			
$K_o = 1$			$K_\infty = 4.58 \times 10^9$		

Table 2.3. Parameters of $L_f/(1+L_f)$ using L_f from Eq. 2.42.

The prefilter is found from

$$F = T(1+L_f)/L_f, \quad (2.43)$$

and comparing data for T (Eq. 2.17) and $(1+L_f)/L_f$ from Table 2.3, it is found as in the previous example that F has an excess of zeros over poles, and is therefore not realizable. With the justification given in the design example of Sect. 2.1, we add additional far pole pairs to T and X_e at 24.4 and 27.3 rps with

proper damping to cancel the zeros of $1 + L_F$ at these locations. These are well above ω_0 and so have

Poles			Zeros		
p	ζ	ω	z	ζ	ω
1				.172	10.1
1				.497	18.2
1					
6					
6					
15					
15					
$K_0 = 1$			$K_\infty = 0.24$		

Table 2.4 Parameters of prefilter F.

negligible effect on the design. The design is now complete, except for a choice of q_x and the relay output level M , neither of which are important to what is demonstrated in this example. Note that H in Eq. 2.40 is unrealizable because it has an equal number of poles and zeros. In the structure of Fig. 2.1, G_1/H and G_2H may be realized as single compensation functions so it is not necessary to make H realizable by itself.

Consider again the idealized

$$\begin{aligned}
 x_e(t) &= x_{e1}(t) + x_{e2}(t) \\
 &= q_x \omega_b e^{-\omega_b t} + q_x \omega_b (\lambda - 1) e^{-\zeta \omega_0 t} \cos[\omega_0 t \sqrt{1 - \zeta^2}]. \quad (2.44)
 \end{aligned}$$

The quasi-linearity constraint $\omega_o \geq \beta\omega_b$ implies that $x_e(t)$ should have no significant frequency components above ω_b , but $x_{e2}(t)$ is at frequency $\omega_o\sqrt{1-\zeta^2} \approx \omega_o$. In fact $x_{e2}(t)$ will be a very lightly damped sinusoid at this frequency. In Sect. 1.2 it was observed that for odd, static, and single-valued nonlinearities the incremental input describing function (IIDF), Eq. 1.9, holds for small sinusoidal components of any frequency not rationally related to ω_o . Also it was noted that the IIDF was N_f , the describing function being used for the total signal $x_e(t)$. Hence, if λ in (2.44) is taken near unity, one should expect N_f to satisfactorily describe the nonlinearity transmission for both $x_{e1}(t)$ and $x_{e2}(t)$. In the following section we will not be able to make $x_{e2}(t)$ arbitrarily small, so a simulation will be necessary to verify the validity of N_f for the total $x_e(t)$.

We have shown in the above example that the SOAS oscillating frequency can be reduced to the limit required by quasi-linearity, i.e., $\omega_o = \max[\beta\omega_b, \beta\omega_m]$, by using narrow and high peaking in $X_e = X_{e1}/H$. Reducing ω_o will in general reduce the sensor noise power that is transmitted to the plant input. As discussed in Sect. 1.4 this noise power is approximately proportional to the area under the $|L_f(j\omega)/P(j\omega)|^2 = N_f|G_1(j\omega)G_2(j\omega)|^2$ curve on an arithmetic scale. The quantity $N_f|G_1(j\omega)G_2(j\omega)|$ in db has been plotted

in Fig. 2.3 and 2.4 to illustrate its significant reduction as a result of the decreased oscillating frequency ω_o . However, the ideal design scheme in this section is not practical. Consider, in Fig. 2.4, the effect of a small variation of ω_o , say from 10 to 9 rps. The system output limit cycle magnitude is given by $K_2 M_o |G_2(j\omega_o)H(j\omega_o)P_h(j\omega_o)|$, and at 9 rps this quantity has increased by 60 db or a factor of 10^3 . Thus, even small variations in ω_o , which will always be present due to imperfections of the compensating elements, can cause the limit cycle component of system output to far exceed its specified bound.

In Sect. 2.1 a rather simple synthesis scheme gave a large value of ω_o , basically determined by the ratio $q_r K_2 / K_1 m$. In the present section an idealization in the design of X_e has essentially eliminated this constraint and allows ω_o to be determined by other, and frequently less severe, constraints. The idealization has very limited, if any, practical use, but it indicates that one can possibly do considerably better than in Sect. 2.1. In the following section we shall explore the middle ground between these two extremes, and in the process develop a synthesis scheme that can be applied to real systems.

2.3 Satisfying Quasi-Linearity and Output Limit Cycle Constraints with Minimum Oscillating Frequency and Practical Specifications.

In Sect. 2.1 it was shown that the combination of SOAS output limit cycle magnitude limit, range of plant gain variation, and command input magnitude places a severe limitation on the minimum achievable loop transmission bandwidth (or oscillation frequency). This phenomenon is accentuated when the plant gain variation is large, which is just the situation where the SOAS is most useful. In Sect. 2.2, by using a very special kind of limit cycle filter the above constraint on bandwidth of loop transmission was removed completely, however, it was pointed out that this limit cycle filter was too much idealized to work in practice. Nevertheless, this ideal filter has provided the insight and motivation for the design procedure to be developed in this section. In the following development the anticipated range of oscillation frequency variation is taken as a specification and a notch limit cycle filter is used to reduce the oscillation frequency as much as is practical in a given design situation. It is found that the cost of reducing the oscillation frequency is the necessity to realize an increasingly complex filter and its inverse in the system.

The same feedback structure is used, and it is shown again in Fig. 2.5 for easy reference. The constrained

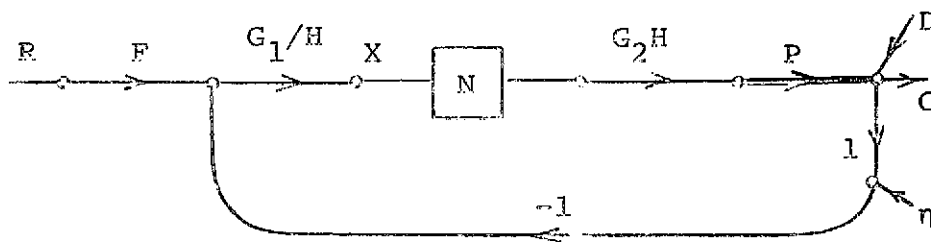


Fig. 2.5 SOAS feedback structure.

part of the system, the plant P , is now assumed to have uncertainty associated with its dynamics as well as the gain factor, written

$$P(s, w) = K(w)P_h(s, w); \begin{cases} w \in W \\ K(w) \in [K_1, K_2] \end{cases} \quad (2.45)$$

w is the vector of all plant parameters and $K(w)$ is the high frequency gain factor ($P(s, w) \rightarrow K(w)/s^e$ as $|s| \rightarrow \infty$). $K_1(w) = \min_{w \in W} K(w)$ and $K_2 = \max_{w \in W} K(w)$. In subsequent notation the functional dependence on w will be omitted unless specifically needed for clarity. The oscillating frequency ω_o is assumed to vary about a center value ω_o' with the variation quantified by the given parameter γ , i.e.,

$$\omega_o \in [\omega_o'/\gamma, \omega_o'\gamma] = \Omega \quad (2.46)$$

ω_o' is not known at this point, rather it emerges from the synthesis. $\gamma = \gamma_c \gamma_h$ is made up of a component of

specification γ_c due to compensation uncertainty from Eq. 1.20, and a component from plant parameter uncertainty γ_h treated in Chapter III.

In Fig. 2.5 let z_f be the forced component of plant output signal due to either a command or disturbance input and x_f is the corresponding input to N . Then $x_f = z_f/[N_f G_2 H K P_h] = A z_f/[M_f G_2 H K P_h]$. There is some more restrictive set of plant parameters $W_e \subset W$ and input that produce the extreme nonlinearity input x_e , i.e., the fastest and/or largest x_f which comes closest to violating quasi-linearity constraints

$$\max_t |x_e(t)| \leq A_e/\alpha \quad (2.46a)$$

$$\omega_b \leq \omega_o/\beta \quad (2.46b)$$

All the extreme parameters and functions are so denoted with a sub-e and we have

$$x_e = \frac{A_e z_e}{M_f G_2 H K_e P_{he}} \quad (2.47)$$

For the remainder of this section the discussion is restricted to command inputs so z_e is made up of the extreme input R_e and an extreme transfer function T_e which is the transfer function only when P_h is at the value P_{he} . Thus,

$$x_e = \frac{A_e R_e T_e}{M_f G_2 H K_e P_{he}} \quad (2.48)$$

There is a distinct pairing of T_e with P_{he} and Appendix B discusses how P_{he} is obtained and paired with T_e . Here we assume the pairing has been made and both functions are known. In general P_h may be independent of some elements of the parameter vector w so that when it is fixed at P_{he} , K_e can still have uncertainty $K_e \in [K_{e1}, K_{e2}] \subset [K_1, K_2]$. However, A_e/K_e in (2.48) is constant by the same arguments used earlier when P_h had no uncertainty at all. Thus any value in the set $[K_{e1}, K_{e2}]$ may be used in the following synthesis calculations. We shall simply denote this choice by K_e and when A_e is obtained it is the A that exists when $P = K_e P_{he}$. To clarify the above consider the following plant. $P(s) = K_\ell a / [s(s+a)]$ where $w = [K_\ell, a]$ with K_ℓ and a varying independently in $[K_{\ell 1}, K_{\ell 2}]$ and $[a_1, a_2]$, giving $K \in [K_1, K_2] = [K_{\ell 1} a_1, K_{\ell 2} a_2]$. Then $P_{he} = 1 / [s(s+a_e)]$ while $K_e \in [K_{e1}, K_{e2}] = [K_{\ell 1} a_e, K_{\ell 2} a_e]$, and one might choose $K_e = K_{\ell 1} a_e$ to use in the synthesis calculations.

It is again convenient to separate X_e into the "smooth" part and the part due to the complex limit cycle filter H as

$$X_e = \frac{X_{e1}}{H} = \frac{q_x \omega_b}{s + \omega_b} \frac{\phi_x}{H} \quad (2.49)$$

with

$$X_{e1} = \frac{q_x \omega_b}{s + \omega_b} \phi_x \quad (2.50)$$

The $q_x \omega_b / (s + \omega_b)$ part of X_{e1} is chosen in accord with Appendix A and assumes step inputs and one pole at the origin in the plant. In Sects. 2.1 and 2.2 it was found that X_e cannot be realized with a single pole, so Φ_x allows for the addition of far poles. To emphasize that the absolute value of A_e or q_x are not determined by the design procedure, the notation

$$A_e \equiv \lambda \alpha q_x \omega_b \quad (2.51)$$

is introduced.

Summarizing the above we have

$$X_e = \frac{X_{e1}}{H} = \frac{\lambda \alpha q_x \omega_b R_e^T e}{M_f K_e G_2^{HP} P_{he}} \quad (2.52)$$

where

$$X_{e1} = \frac{\lambda \alpha q_x \omega_b R_e^T e}{M_f K_e G_2^{HP} P_{he}} = \frac{q_x \omega_b}{s + \omega_b} \Phi_x, \quad (2.53)$$

and X_e must satisfy quasi-linearity constraints

$$\max_t |x_e(t)| \leq A_e / \alpha = \lambda q_x \omega_b \quad (2.54a)$$

$$\omega_b \leq \omega_0 / \beta.$$

Simultaneously the output limit cycle constraint,

$$|M_0 G_2(j\omega_0) H(j\omega_0) P_{hm}(j\omega_0)| \leq m / K_m, \quad (2.55)$$

must be satisfied, where $|K_m P_{hm}(j\omega_o)| = \max_{\omega \in \Omega} |P(j\omega_o)|$.

Solving (2.53) for G_2 and substituting in (2.55) gives, after some rearrangement,

$$\left| \frac{X_{e1}(j\omega_o)}{A_e H(j\omega_o)} \right| = \left| \frac{X_e(j\omega_o)}{A_e} \right| \geq \frac{K_m}{K_{em}} \left| \frac{M_o}{M_f} \right| |R_e(j\omega_o) T_e(j\omega_o)| \left| \frac{P_{hm}(j\omega_o)}{P_{he}(j\omega_o)} \right|. \quad (2.56)$$

The task now is to find a suitable combination of center oscillating frequency ω_o' , the filter H , and $A_e = \lambda \alpha q_x \omega_b$ to satisfy (2.56). Observe that λ depends on H because each H will produce a different $\max_t |x_e(t)|$ for Eq. 2.54a, and therefore demand a different λ . Given values for ω_o' and λ , the corresponding $|H(j\omega)|$ required is obtained from (2.55) as

$$|H(j\omega)| = \begin{cases} \frac{K_{em}}{\lambda \alpha q_x \omega_b K_m} \left| \frac{M_f}{M_o} \right| \left| \frac{X_{e1}(j\omega)}{R_e(j\omega) T_e(j\omega)} \right| \left| \frac{P_{he}(j\omega)}{P_{hm}(j\omega)} \right|; & \omega \in \Omega \\ 1 & ; \omega \notin \Omega. \end{cases} \quad (2.57)$$

The ideal limit cycle filter of (2.57) is shown in Fig. 2.6a using a straight line approximation over Ω . An obvious modification of (2.57) will give H with finite slopes shown dashed in Fig. 2.6a. Substituting (2.57) into the first relation of (2.52)

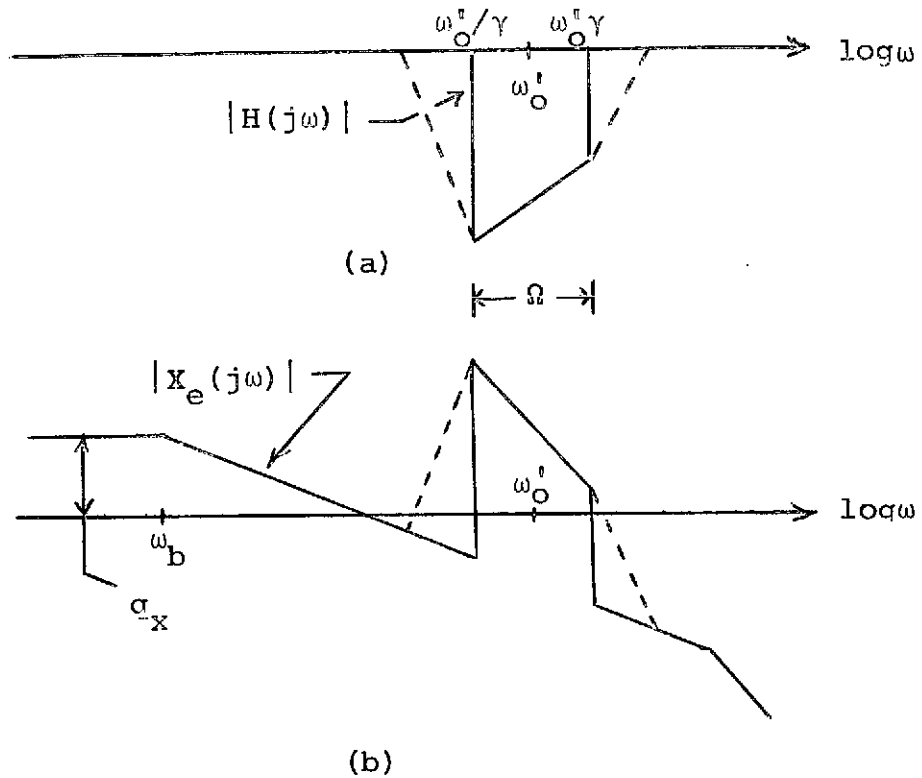


Fig. 2.6 Ideal limit cycle filter H and corresponding X_e .

yields

$$|X_e(j\omega)| = \begin{cases} \frac{\lambda \alpha q_x \omega_b K_m}{K_e m} \left| \frac{M_o}{M_f} \right| |R_e(j\omega) T_e(j\omega)| \left| \frac{P_{hm}(j\omega)}{P_{he}(j\omega)} \right|; & \omega \in \Omega \\ |X_{e1}(j\omega)| & ; \omega \notin \Omega. \end{cases} \quad (2.58)$$

Using X_{e1} from Eq. 2.53 combined with $|H(j\omega)|$ shown in Fig. 2.6a, the plot of Fig. 2.6b for $|X_e(j\omega)|$ results.

Observe that (2.57) is independent of q_x , while

q_x is just a scale factor in (2.58). Similarly, since $|H(j\omega)|$ is evaluated at $\omega_0 \geq \beta\omega_b$ in (2.57) where $|X_{e1}(j\omega)| \approx q_x \omega_b / \omega$, the value is closely independent of ω_b , i.e., the choice of ω_b has an insignificant influence on the determination of minimum ω_0 . Therefore it is reasonable to take ω_b near the maximum transfer function bandwidth, $\omega_b \approx \omega_m$.

$X_e(j\omega)$ is minimum phase, so using the Hilbert transform^[26] as applied to this problem by Bode^[27] the phase can be obtained from the magnitude characteristic. With both phase and magnitude the time response may then be calculated as $x_e(t) = \mathcal{L}^{-1}[X_e(s)]$. The following scheme is used to obtain satisfactory combinations of ω_0' , λ , and $H(j\omega)$. First choose a value for ω_0' . Then iterate on λ to find a solution of

$$\max_t |x_e(t)| = \max_t |\mathcal{L}^{-1}[X_e(s, \lambda)]| = \lambda q_x \omega_b \quad (2.59)$$

For each ω_0' , λ pair $H(j\omega)$ is given by (2.57). In this manner one can obtain a plot of λ vs. ω_0' as shown in Fig. 2.7. A good estimate for a starting value of ω_0' is

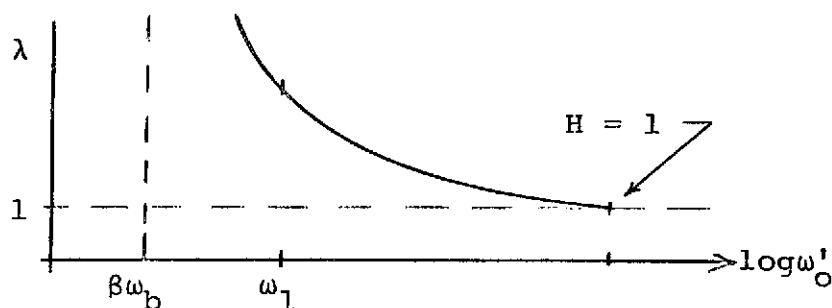


Fig. 2.7 λ vs. ω_0' for fixed γ .

obtained by letting $H = 1$. Then from Eq. 2.53 (assuming negligible contribution to the time response $x_e(t)$ from the far poles in Φ_x) $\lambda = 1$, and

$$\left| \frac{M_o G_2(j\omega) P_{hm}(j\omega)}{M_f X_{el}(j\omega) P_{he}(j\omega)} \right| = \left| \frac{M_o \alpha \omega_b q_x R_e(j\omega) T_e(j\omega) P_{hm}(j\omega)}{M_f X_{el}(j\omega) P_{he}(j\omega)} \right|$$

as shown in Fig. 2.8a. Where this quantity equals m/K_m (Eq. 2.55) gives a suitable value for ω'_o/γ . This is the solution found in Section 2.1

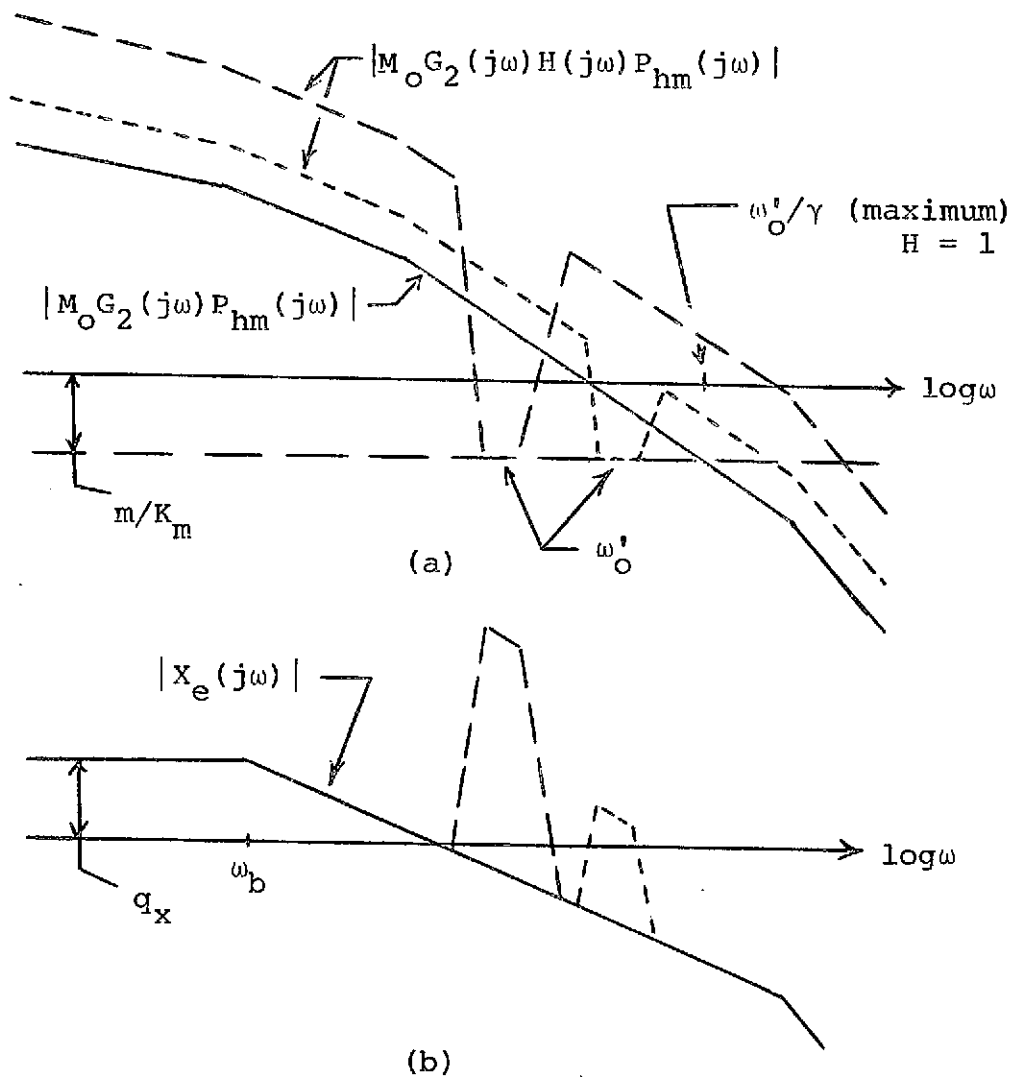


Fig. 2.8 Behavior of functions of interest as ω'_o is reduced.

generalized to permit variation in ω_0 . From here we work to lower frequencies with ω_0' . Each reduction of ω_0' causes H to become a deeper and more complex filter and it causes $\max_t |x_e(t)|$ to increase, thereby increasing the gain of $G_2 = \lambda \alpha \omega_b R_e T_e / [M_f K X_{e1} G_2 P_{he}]$ at all frequencies. The behavior of H , G_2 and X_e with decreasing ω_0' is illustrated in Fig. 2.8.

Assume now that Fig. 2.7 has been constructed in the manner explained above. How does the designer use this curve? First there is some lower bound dictated for the oscillating frequency by the bandwidth of the transfer function, $\omega_0 \geq \beta \omega_m$. Also, a minimum oscillating frequency is dictated by disturbance response and/or P_h parameter sensitivity considerations which are treated in the next chapter. Let the largest of these lower bounds be ω_1 shown in Fig. 2.7, such that some freedom remains to reduce ω_0' by taking $H \neq 1$. Any $\omega_0' \geq \omega_1/\gamma$ can then be chosen as the center value of oscillation frequency. The designer must choose a value by making an acceptable tradeoff between loop transmission bandwidth and the complexity of the limit cycle filter H , which must be realized twice in the loop of Fig. 2.5. Having made such a tradeoff, ω_0' and λ are available from Fig. 2.7. The magnitude characteristic for $H(j\omega)$ is given by (2.57), or its finite slope replacement, from which a rational approximation is obtained. The compensation function G_2 is obtained from (2.52) as

$$G_2 = \frac{\lambda \sigma \Gamma_x \omega_b R_e T_e}{M_f K_e X_{e1} P_{he}} \quad (2.60)$$

The compensation G_1 is then shaped to provide the level of loop transmission required for disturbance attenuation and/or P_h parameter sensitivity over the low and intermediate frequency ranges, and to provide

$L_{oe} = \frac{M_o}{A_e} K_e G_1 G_2 P_{he}$ with 180° of phase lag at the chosen oscillating frequency ω'_o . Finally,

$L_{fe} = \frac{M_f K_e}{A_e} G_1 G_2 P_{he}$, and the prefilter of Fig. 2.5 can be designed from

$$F = T_e (1 + L_{fe}) / L_{fe} \quad (2.61)$$

We mention that for a significant class of design problems some simplifications are appropriate. Recall that P_h was defined (Eq. 2.45) so that it has vanishing uncertainty at high frequencies, i.e., $P_h(s) \rightarrow 1/s^e$ for large $|s|$. It follows that when the specifications are such that a high oscillating frequency is required, $K_m |P_{hm}(j\omega_o)| / |P_{he}(j\omega_o)| \rightarrow K_m \rightarrow K_2$, and this result can be used to simplify Eqs. 2.56, 57 and 58. Also, some far poles above ω_o may be assigned coincident in T_e and X_{e1} giving a reduction of order of G_2 seen in Eq. 2.60. Further, if these poles are a reasonable distance above ω_o , neglecting them will have no significant effect on the calculation of $|H(j\omega)|$ or $|X_e(j\omega)|$ from Eqs. 2.57 and 58 respectively, nor will they effect

$x_e(t)$ significantly. This means their location need not be known during the preparation of the curve of Fig. 2.7; all we must know is that they lie well above the oscillating frequency, say above the ω'_0 resulting when $H = 1$ in Fig. 2.7 and 2.8a. Therefore they need not be assigned at any specific frequency until ω'_0 is determined and L_{fe} designed. Since $L_{fe}(j\omega'_0) = 180^\circ$, there are inevitable poles of L_{fe} above ω'_0 which result in far off zeros of $1 + L_{fe}$. Once L_{fe} is known these zeros of $1 + L_{fe}$ can be assigned as far poles in T_e and X_e which by (2.60) reduces the order of G_2 , and by (2.61) reduces the order of F . This is precisely the technique used in the examples of Sects. 2.1 and 2.2.

The synthesis technique of this section is next demonstrated with a numerical example.

2.4 Design Example

In this section a design example with significant plant ignorance is worked out. The objective here is to assume that the minimum oscillating frequency is determined by the combined constraints of output limit cycle magnitude and quasi-linearity, and then select the oscillating frequency and design X_e and H using the methods of Sect. 2.3. This portion of the design is later incorporated into a complete SOAS design and simulation in Chapter V.

Specifications

Nonlinearity:

$$\left. \begin{array}{l} \text{Ideal relay} \\ \text{with output} \\ \text{level } M \end{array} \right\} \begin{array}{l} N_o = M_o/A = 4M/\pi A \\ N_f = M_f/A = 2M/\pi A \end{array} \quad \begin{array}{l} (2.62a) \\ (2.62b) \end{array}$$

$$\left. \begin{array}{l} \text{Quasi-linearity} \\ \text{constraints} \end{array} \right\} \begin{array}{l} \max_t |x_e(t)| A_e/\alpha = \lambda q_x \omega_b; \alpha \geq 3 \\ \omega_b \leq \omega_o/\beta; \beta \geq 3 \end{array} \quad \begin{array}{l} (2.63a) \\ (2.63b) \end{array}$$

Transfer function:

$$T_e(s) = \frac{(6)^2 (25)^2 (50)^2}{(s+6)^2 (s+25)^2 (s+50)^2} \quad (2.64)$$

Plant:

$$P(s) = KP_h(s) = \frac{K}{s(s+a)}; \quad \begin{cases} a \in [a_1, a_2] = [1, 10] \\ K \in [K_1, K_2] = [1, 10] \end{cases} \quad (2.65)$$

The plant parameters a and K are independent.

Extreme command input:

$$R_e(s) = q_r/s = 1/s \quad (2.66)$$

Maximum limit cycle output:

$$m = 0.1 \quad (2.67)$$

Limit cycle frequency variation:

The limit cycle may vary $\pm 12\%$ about the nominal ω_o' , i.e.,

$$\omega_o \in [\omega_o'/\gamma, \omega_o'/\gamma] = \Omega; \quad \gamma = 1.12. \quad (2.68)$$

Design

The first step is to determine what plant parameter set constitutes the extreme plant P_{he} . This is considered in Appendix B and in accord with the conclusions there we select

$$P_{he} = \frac{1}{s(s+a_2)} = \frac{1}{s(s+10)}. \quad (2.69)$$

We also note that for the plant given in Eq. 2.65,

$|K_m P_{hm}(j\omega_o)| = \max_{a,K} |P(j\omega_o)|$ is obtained from

$$K_m P_{hm}(s) = \frac{K_2}{s(s+a_1)} = \frac{10}{s(s+1)}, \quad (2.70)$$

without regard to the particular ω_o that emerges from the design.

The low frequency dominant part of X_e is chosen as

$$X_{e1} = \frac{q_x \omega_b}{s + \omega_b} = \frac{6q_x}{s+6}, \quad (2.71)$$

and the far poles that will eventually appear in X_{e1} are neglected for the present. If no limit cycle filter is used, i.e., $H = 1$, then $x_e(t) = x_{e1}(t)$ and Eqs. 2.63a and 71 give $\max_t |x_e(t)| = 6q_x = A_e/\alpha$, while $K_e = K_1 = 1$ is satisfactory. Therefore

$$\begin{aligned} M_f G_2 &= \frac{\alpha q_x \omega_b R_e^T}{K_e X_{e1} P_{he}} \\ &= \frac{3(6)^2 (25)^2 (50)^2 (s+10)}{(s+6)(s+25)^2 (s+50)^2} \\ &= M_o G_2 / 2. \end{aligned} \quad (2.72)$$

This is the design value for G_2 only if $H = 1$, which permits $\lambda = 1$ in Eq. 2.63a. Otherwise G_2 in (2.72) will be multiplied by $\lambda > 1$. Using G_2 from above and P_{hm} from (2.70),

$$\begin{aligned} M_o |G_2(j\omega_o)P_{hm}(j\omega_o)| &= \left| \frac{6(6)^2(25)^2(50)^2(s+10)}{s(s+1)(s+6)(s+25)^2(s+50)^2} \right|_{j\omega_o} \\ &\leq .01 = m/K_m. \end{aligned} \quad (2.73)$$

The functions on each side of inequality (2.73) are plotted on Fig. 2.9, from which the minimum ω_o' is read as $\omega_o' = 48.6\gamma = 54.5$ rps. A smaller oscillating frequency is desired if possible so the limit cycle filter design steps are carried out. From Eq. 2.57

$$\begin{aligned} H(j\omega) &= \begin{cases} \frac{K_e m}{K_m \lambda \alpha q_x \omega_b} \left| \frac{M_f}{M_o} \right| \left| \frac{X_{e1}(j\omega)}{R_e(j\omega)T_e(j\omega)} \right| \left| \frac{P_{he}(j\omega)}{P_{hm}(j\omega)} \right|; & \omega \in \Omega \\ 1 & ; \omega \notin \Omega \end{cases} \\ &= \begin{cases} \frac{2.77 \times 10^{-5}}{\lambda} \left| \frac{10s(s+1)(s+6)(s+25)^2(s+50)^2}{6(25)^2(50)^2(s+10)} \right|_{j\omega} & ; \omega \in \Omega \\ 1 & ; \omega \notin \Omega. \end{cases} \end{aligned} \quad (2.74)$$

Then

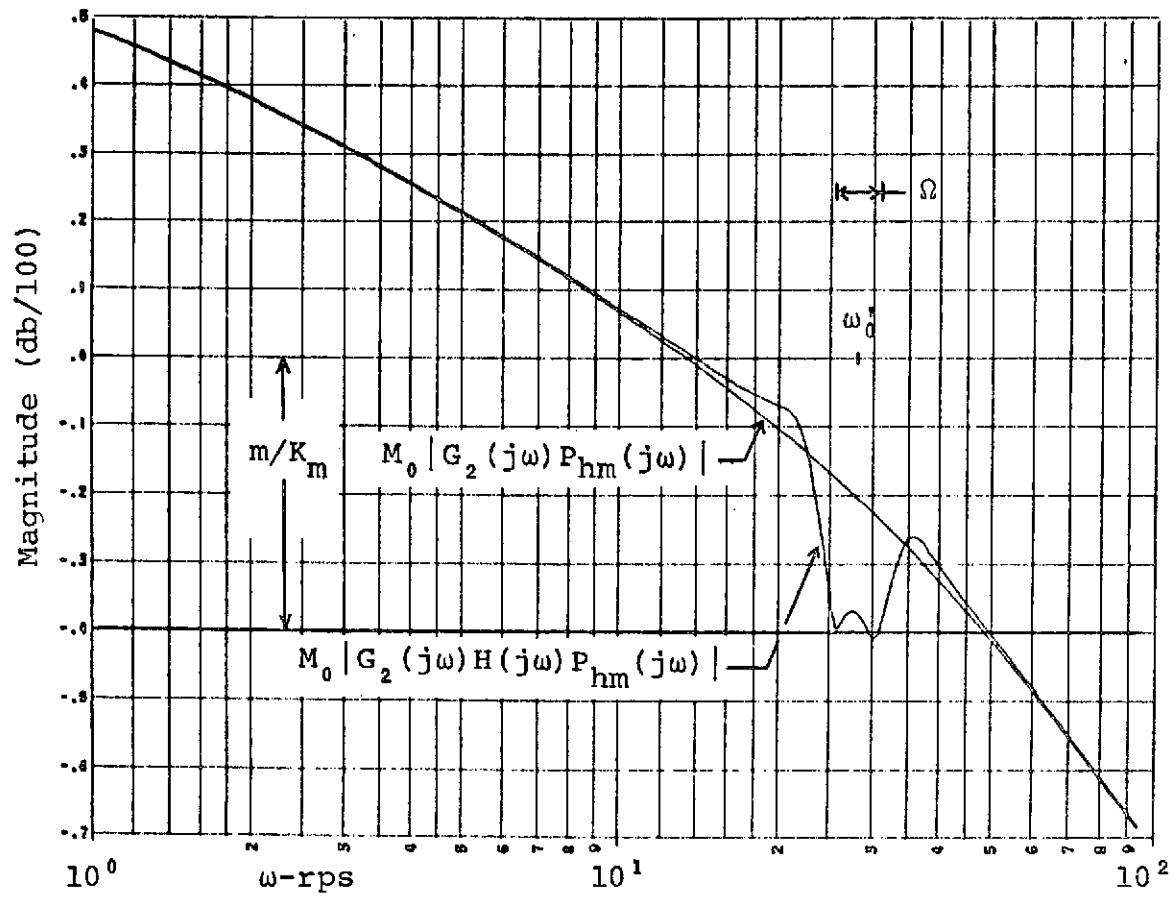


Fig. 2.9 Frequency responses for functions determining lower bound for ω_0' .

$$\begin{aligned}
 \left| \frac{X_e(j\omega)}{q_x} \right| &= \begin{cases} \frac{K_m \lambda \alpha \omega_b}{K_{em}} \left| \frac{M_o}{M_f} \right| |R_e(j\omega) T_e(j\omega)| \left| \frac{P_{hm}(j\omega)}{P_{he}(j\omega)} \right|; & \omega \in \Omega \\ |X_{e1}(j\omega)|/q_x & ; \omega \notin \Omega \end{cases} \\
 &= \begin{cases} 3.6\lambda \times 10^4 \left| \frac{(6)^2 (25)^2 (50)^2 (s+10)}{10s(s+1)(s+6)^2 (s+25)^2 (s+50)^2} \right|_{j\omega} & ; \omega \in \Omega \\ \left| \frac{6}{s+6} \right|_{j\omega} & ; \omega \notin \Omega. \end{cases}
 \end{aligned}
 \tag{2.75}$$

The next task is to use Eq. 2.75 to calculate ω'_o , λ pairs to produce the λ vs. ω'_o plot. This is implemented by getting the phase of X_e using the Bode method^[27], followed by inversion to time response using the Discrete Fast Fourier Transform (DFFT)^[28,29]. Several points are plotted on Fig. 2.10 and connected by a continuous curve.

From consideration of the rapid rise in λ below 30 rps in Fig. 2.10 and the complexity of the required filter H , $\omega'_o = 28.2$ rps is chosen as a center value of oscillating frequency that appears achievable. The ideal filter with 500 db/dec slopes centered at $\omega'_o = 28.2$ rps is shown in Fig. 2.11. A rational approximation to the ideal filter is also shown in Fig. 2.11 and has the parameters tabulated on Table 2.5. Also the plot of $M_o |G_2(j\omega)H(j\omega)P_{hm}(j\omega)|$ has been added to Fig. 2.9.

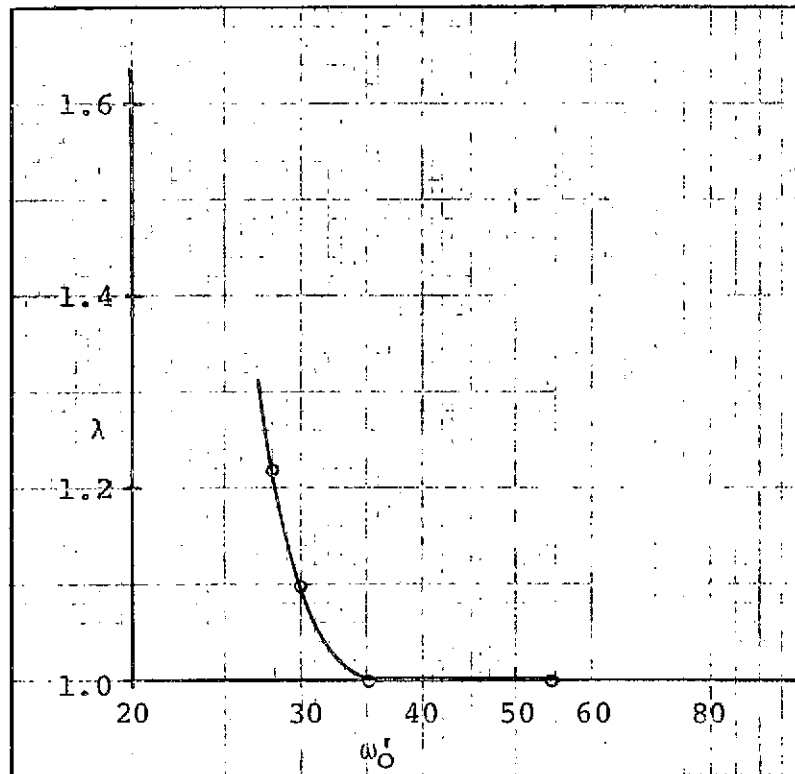


Fig. 2.10 Plot of λ vs. ω' calculated using ideal limit cycle filter with 500 db/dec slopes and $\gamma = 1.12$.

Poles			Zeros		
p	ζ	ω	z	ζ	ω
	.08	22		.025	25.6
	.08	35		.04	30.5
$K_0 = .838$			$K_\infty = .82$		

Table 2.5 Parameters of rational H shown in Fig. 2.11.

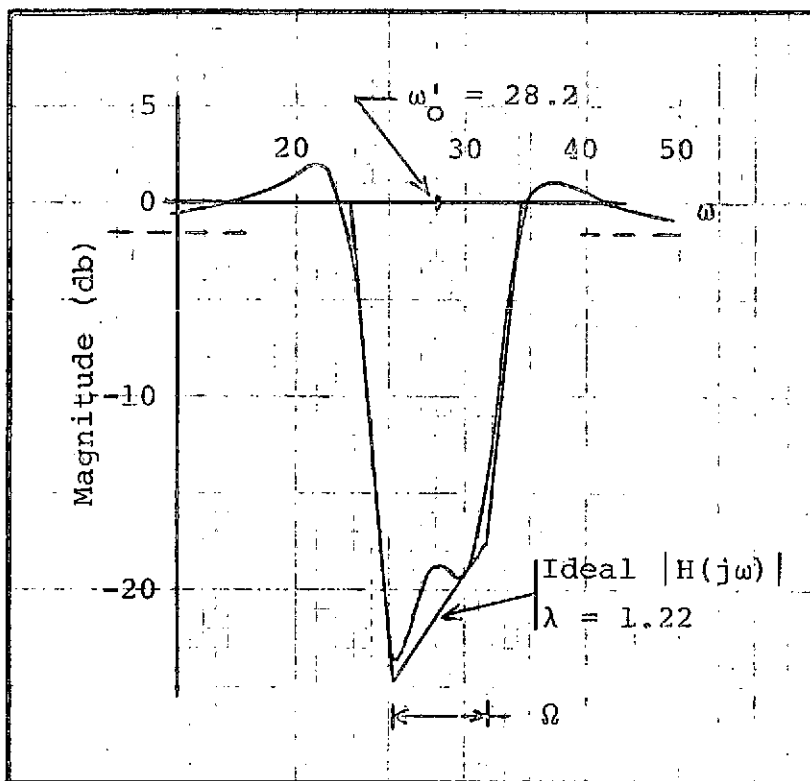


Fig. 2.11 Ideal and rational limit cycle filters.

Shown in Fig. 2.12 are time responses of the original $x_{e1}(t)$ from Eq. 2.71 and the resultant $x_e(t)$ after modification by H . Of course some far poles must eventually be added to $X_e(s)$ when designing the final loop transmission and these will set $x_e(0) = 0$. With $\lambda = 1.22$ we get $A_e/q_x = \lambda\alpha\omega_b = 22$ which is very close to the peak value of $x_e(t)$ shown in the figure.

The design value of $M_f G_2$ is now obtained by multiplying the quantity on the right of (2.72) by $\lambda = 1.22$, completing the portion of the design to be demonstrated in this section. Use of the limit cycle

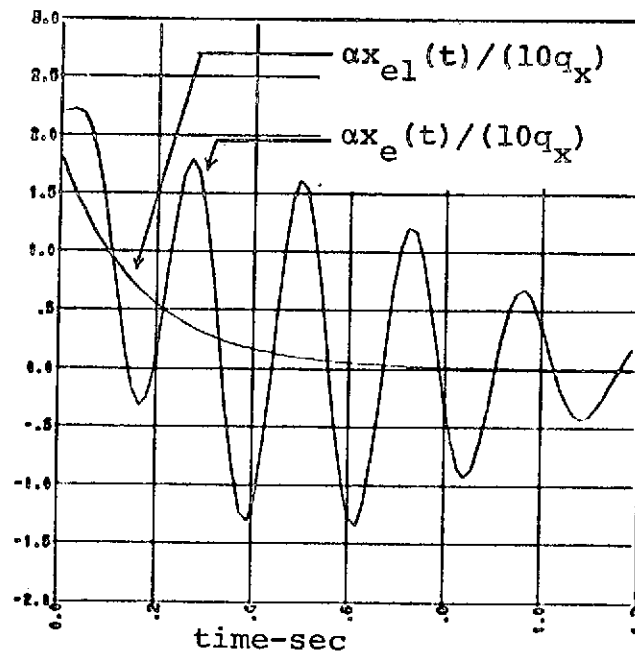


Fig. 2.12. Time response $\alpha x_{el}(t)/q_x$ and $\alpha x_e(t)/q_x$ using rational limit cycle filter from Table 2.5.

filter has reduced the oscillating frequency by the factor $54.5/28.2 = 1.93$, or nearly an octave.

The filter in Fig. 2.11 is not quite as deep as it should be at some frequencies. The maximum error in the interval Ω is about 2.5 db, which will manifest itself in the completed system design by producing an output limit cycle in excess of the specification by the factor 1.34. Of course this is only a violation when the plant has maximum gain $K_2 = 10$. Note the clear visibility of the tradeoffs among various specifications. The compromises available to avoid redesigning H are a) allow the larger limit cycle, i.e., set $m = .134$, b) demand smaller K_2/K_1 and reduce $|G_2(j\omega)|$ (Eq. 2.73)

to bring the limit cycle in tolerance, c) reduce $|G_2(j\omega)|$ and require smaller inputs, $q_r \leq 1/1.3 = .75$, d) reduce $|G_2(j\omega)|$ and attempt to get by with a small violation of quasi-linearity constraint (2.63b) when the maximum step input is present. We shall consider the remainder of the system design for this example in Chapter V.

CHAPTER III

SATISFYING SOAS SENSITIVITY SPECIFICATIONS
WITH UNCERTAINTY IN PLANT DYNAMICS

3.1 The Approach

The constrained part of the system, the plant, in Fig. 3.1 is described by transfer function

$$P(s,w) = K(w)P_h(s,w); \begin{cases} w \in W \\ K(w) \in [K_1, K_2], \end{cases} \quad (3.1)$$

($P(s,w) \rightarrow K(w)/s^e$ as $|s| \rightarrow \infty$) with the parameter bounding sets $W, [K_1, K_2]$, and the plant structure known. The SOAS property gives zero sensitivity to variations in

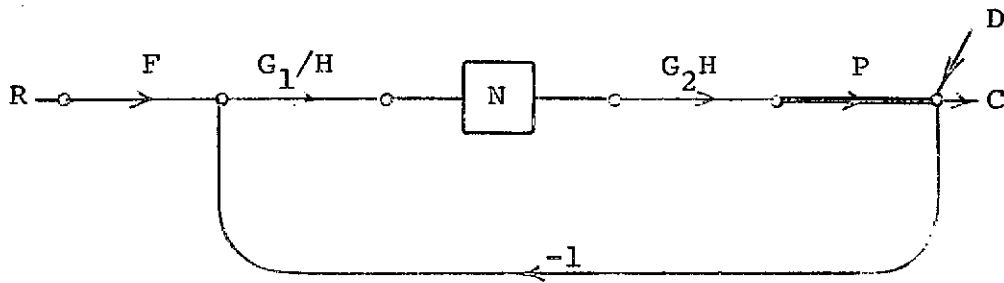


Fig. 3.1 SOAS structure.

the high frequency gain factor $K(w)$. In this chapter a synthesis method is given for satisfying fixed specifications on sensitivity to plant dynamics with a minimum

bandwidth loop transmission, i.e., a loop transmission that is optimal in the sense of Sect. 1.4.

The forced signal loop transmission is

$$L_f = N_f G_1 G_2 P = \frac{M_f K}{A} G_1 G_2 P_h, \quad (3.2)$$

and the transmission for command inputs is

$$T = FL_f / (1 + L_f). \quad (3.3)$$

It is assumed that specifications are given as bounds of acceptable variation $\Delta \ln[T(j\omega)]$ as a function of ω . A method for satisfying such specifications in linear systems has been given by Horowitz and Sidi^[22], and this method will be adapted to the present problem. The prefilter F is a fixed transmission so $\Delta \ln[T(j\omega)] = \Delta \ln[F(j\omega)L_f(j\omega)/(1+L_f(j\omega))] = \Delta \ln|L_f(j\omega)/(1+L_f(j\omega))| + j\Delta \angle L_f(j\omega)/(1+L_f(j\omega))$. Similarly, if we assume A/K does not change with P_h , then $\Delta \ln[L_f(j\omega)] = \Delta \ln[P_h(j\omega)]$ since the remaining fixed parts of L_f cancel in the difference. Thus the specifications and plant uncertainty are both in terms of $L_f(j\omega)$, viz, $\Delta \ln[L_f(j\omega)/(1+L_f(j\omega))]$ and $\Delta \ln[L_f(j\omega)]$ respectively. The two quantities are conveniently related on the Nichols chart which has coordinates of $\ln|L_f(j\omega)|$ vs. $\angle L_f(j\omega)$. For a given range of plant uncertainty $\Delta \ln[P_h(j\omega)] = \Delta \ln[L_f(j\omega)]$, the specifications $\Delta \ln[T(j\omega)] = \Delta \ln[L_f(j\omega)/(1+L_f(j\omega))]$ may be translated into bounds on acceptable $L_f(j\omega)$. The

details of this translation are given in Appendix C. A loop transmission L_f is then synthesized which has minimum gain-bandwidth while satisfying the sensitivity bounds.

3.2 The Equivalent Plant P_f for Forced Signals

To apply the method of [22] to the SOAS it is necessary to write the loop transmission as $L_f = GP_f$, where P_f contains all the parameter ignorance of the loop. P_f is the equivalent linear plant seen by forced signals in the SOAS. From the nonlinearity describing functions

$$N_o = M_o/A \quad (3.4a)$$

$$N_f = M_f/A, \quad (3.4b)$$

the forced and oscillating loop transmission are

$$L_o = N_o G_1 G_2 K P_h, \quad (3.5)$$

and

$$\begin{aligned} L_f &= N_f G_1 G_2 K P_h = \frac{M_f}{A} G_1 G_2 K P_h \\ &= \frac{N_f}{N_o} L_o = \frac{M_f}{M_o} L_o. \end{aligned} \quad (3.6)$$

To sustain the limit cycle $L_o(j\omega_o) = -1$, and using this in (3.6) gives

$$\frac{A}{K} = |M_o G_1(j\omega_o) G_2(j\omega_o) P_h(j\omega_o)|. \quad (3.7)$$

If only the plant gain factor changes, A/K in (3.7) remains constant. However, when the parameters of P_h change then $|P_h(j\omega)|$ will be changed as well as $\angle P_h(j\omega)$. The phase change in P_h in turn causes the oscillating frequency ω_o to shift and the net result is that the right side of (3.7) changes in a rather complicated way with the varying parameters of P_h . To obtain an expression for the equivalent plant, A/K from (3.7) is substituted back in L_f of (3.6) yielding

$$\begin{aligned} L_f &= \frac{M_f G_1 G_2 P_h}{|M_o G_1(j\omega_o) G_2(j\omega_o) P_h(j\omega_o)|} \\ &= G \left[\frac{M_f P_h}{|M_o G_1(j\omega_o) G_2(j\omega_o) P_h(j\omega_o)|} \right] \\ &= G P_f, \end{aligned} \quad (3.8)$$

where we have defined

$$G = G_1 G_2 \quad (3.9a)$$

and

$$P_f = K_f P_h = \frac{M_f P_h}{|M_o G(j\omega_o) P_h(j\omega_o)|}. \quad (3.9b)$$

The quantity $K_f = M_f / |M_o G(j\omega_o) P_h(j\omega_o)|$ is a varying gain factor that is part of the equivalent plant P_f . For example, suppose $M_f/M_o = 1/2$, $G = 1/(s+10)$, and $P_h = 1/[s(s+a)]$ with $a \in [1,4]$. Then $L_f = M_f/A[s(s+a)(s+10)]$. For $a = 1$, the oscillating

frequency is determined by $\angle L_f(j\omega_1) = -180^\circ$ which gives $\omega_1 = 3.16$. Solving for $|L_f(j3.16)| = 1/2$ gives $M_f/A_1 = 55$. Thus $L_{f1} = 55/[s(s+1)(s+10)]$ and this function is plotted in Fig. 3.2. Now letting $a = 4$,

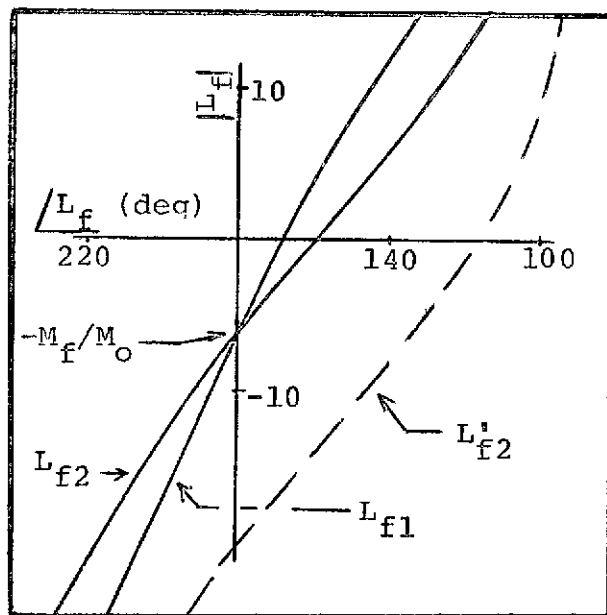


Fig. 3.2 Illustration of gain factor variation with parameters of P_h .

we get $L'_{f2} = L_{f1}(s+1)/(s+4)$ which is shown dashed in Fig. 3.2. $\angle L'_{f2}(j\omega_2) = -180$ gives the new oscillating frequency at $\omega_2 = 6.32$, but at this frequency $|L'_{f2}(j\omega_2)|$ is -20 db so A must change value so that $L_{f2}(j\omega_2) = -1/2$. Solving, $M_f/A_2 = 280$, and $L_{f2} = 280/[s(s+4)(s+10)]$. As a varies from 1 to 4, A varies by the ratio $A_1/A_2 = 280/55 = 5.1$. This gain variation must be expressed as part of the uncertainty of the loop

transmission and accounted for in the design to satisfy transfer function sensitivity specifications. The magnitude of the gain uncertainty depends on the compensation G , as well as the parameter uncertainty of P_h . In the above example $L_{f1}(j\omega_1) = L_{f2}(j\omega_2) = -1/2$ and the ratio of these two loop transmissions gives $A_1/A_2 = |G(j\omega_1)P_{h1}(j\omega_1)/G(j\omega_2)P_{h2}(j\omega_2)|$. Thus we write the equivalent plant P_f as a function of G as given by Eq. 3.9b. In summary, we have the loop transmission

$$L_f = GP_f, \quad (3.10a)$$

where

$$P_f = K_f P_h = M_f P_h / |M_o G(j\omega_o) P_h(j\omega_o)|, \quad (3.10b)$$

which is to be synthesized to satisfy given transfer function sensitivity specifications with minimum bandwidth. Due to the constraint $L_f(j\omega_o) = -M_f/M_o$, minimizing loop transmission bandwidth is equivalent to obtaining the smallest possible ω_o subject to the sensitivity specifications. Neither ω_o nor G are known at the outset, while the equivalent plant P_f depends on both of these quantities. Thus an iteration scheme will be implemented whereby we converge to the minimum oscillating frequency and the required compensation G simultaneously.

3.3 Synthesis of SOAS Loop Transmission to Satisfy Sensitivity Specifications

In this section a method for determining the minimum bandwidth (minimum ω_o) $L_f(j\omega)$ to satisfy given sensitivity specifications is developed. Assume that bounds on the acceptable magnitude variation, $\ln|T(j\omega)|$, are given as shown in Fig. 3.3a and b. Also shown in

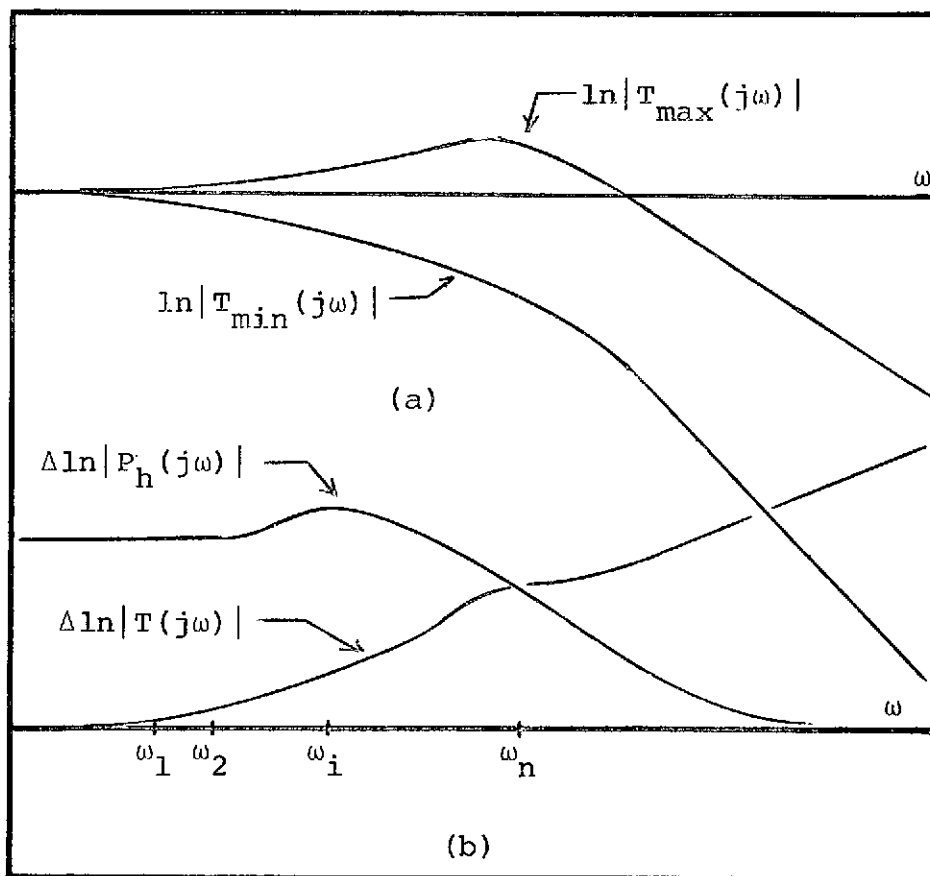


Fig. 3.3 Permissible variation of $\ln|T(j\omega)|$
vs. variation of $\ln|P_h(j\omega)|$.

Fig. 3.3b is a hypothetical set of bounds for plant uncertainty $\Delta\ln|P_h(j\omega)|$. In general the loop transmission is $L_f = GP_f = GK_fP_h$ with P_f dependent on G and

ω_0 in the manner given by Eq. 3.10b. However, since neither of these are known at this point, we first neglect the gain factor K_f of P_f , and use $P_h(j\omega)$ to obtain a set of bounds for $L_f(j\omega)$ using the specifications on $\Delta \ln|T(j\omega)|$ and the method detailed in Appendix C. Since L_f varies with P_h , the bounds apply to some reference value of plant parameters denoted by $L_{f1} = GP_{h1}$. The bounds are conveniently displayed on Nichols

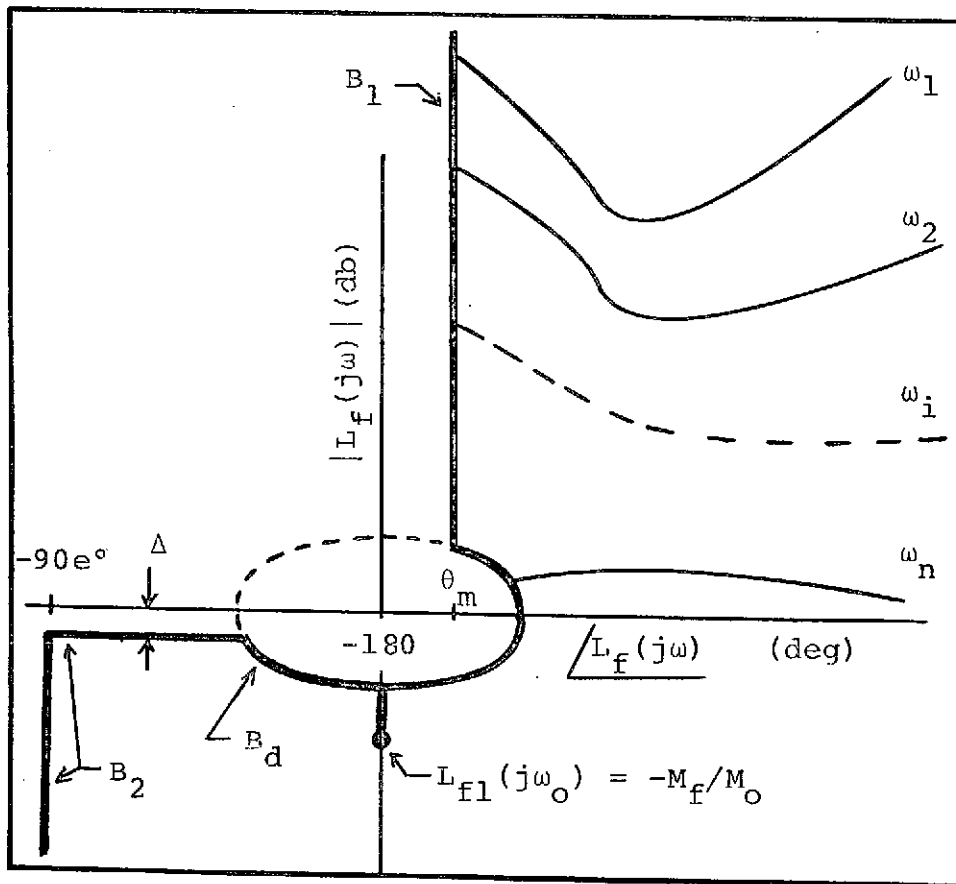


Fig. 3.4 Boundaries for optimal $L_f(j\omega)$.

chart coordinates ($\ln|L_f(j\omega)|$ vs. $\angle L_f(j\omega)$) as shown in Fig. 3.4 labeled $\omega_1, \omega_2, \dots, \omega_n$. $L_{f1}(j\omega_i)$ must lie on or above the bound at ω_i in order to satisfy the

sensitivity specification $\Delta \ln|T(j\omega_i)|$. It is noted in Appendix C that these bounds can also include specifications on $\Delta/T(j\omega_i)$ if desired, however, for minimum phase design the magnitude specification is sufficient. There are in theory an infinite number of bounds, but in practice the designer chooses enough frequencies to provide high confidence that $L_f(j\omega)$ will satisfy the intermediate bounds that have not been computed. At some frequency near, or possibly as much as an octave above, the $\Delta \ln|T(j\omega)|$, $\Delta \ln|P_h(j\omega)|$ crossing in Fig. 3.3b the bounds will cease to exist or become insignificant because the permitted variation in $\ln|T(j\omega)|$ is larger than that exhibited by the plant, i.e., no feedback is required in this frequency range. Several other bounds are shown in Fig. 3.4 whose construction is investigated next.

In the SOAS we permit only one frequency to satisfy $\angle L_f(j\omega) = -180^\circ$, which is the oscillating frequency ω_o . Therefore, there is some maximum phase lag boundary, B_1 in Fig. 3.4, given by $\angle L_f(j\omega) \geq \theta_m > -180^\circ$ which applies over the intermediate frequency range. In the next frequency range the bound B_d comes into effect. This bound is derived from the disturbance response damping constraint

$$\left| \frac{L_f(j\omega)}{1+L_f(j\omega)} \right| \leq \ell ; \forall \omega . \quad (3.11)$$

The significance of (3.11) has been discussed in Sect. 1.3. At the oscillating frequency L_f is constrained to pass through the point $L_f(j\omega_0) = -M_f/M_0$. Of course ℓ in (3.11) must be large enough so that B_d excludes this point. Above ω_0 , where the final poles of L_f are introduced, some limit on maximum peaking is imposed, $|L_f(j\omega)| \leq -\Delta$ (db) for $\omega > \omega_0$. This gives the horizontal segment of B_2 of Fig. 3.4. Finally, L_f must have some specified excess of poles over zeros e , so that eventually $\angle L_f(j\omega) \rightarrow -90e^\circ$, giving the vertical segment of B_2 .

The boundaries at $\omega_1, \omega_2, \dots, \omega_n$ are applicable to L_{f1} only, but they are constructed to guarantee satisfaction of the transfer function sensitivity specifications over all possible plant parameters provided the specific value L_{f1} satisfies its bounds (and assuming for the present the gain factor variation in P_f is negligible). This allows the designer to work only with L_{f1} in full confidence that all other L_f will be satisfactory.

The above is not true for the heavy boundaries B_1 , B_d , and B_2 of Fig. 3.4 which apply to all L_f . It is possible to design L_{f1} to satisfy these bounds as indicated by Fig. 3.5, and then find for another plant, say P_{h2} , that L_{f2} violates the bounds as shown. It can be seen from Fig. 3.5 that the situation would not be

improved by using P_{h2} as the reference plant to design with. A reasonable approach to this problem is to choose P_{h1} as the parameter set that gives maximum phase lag

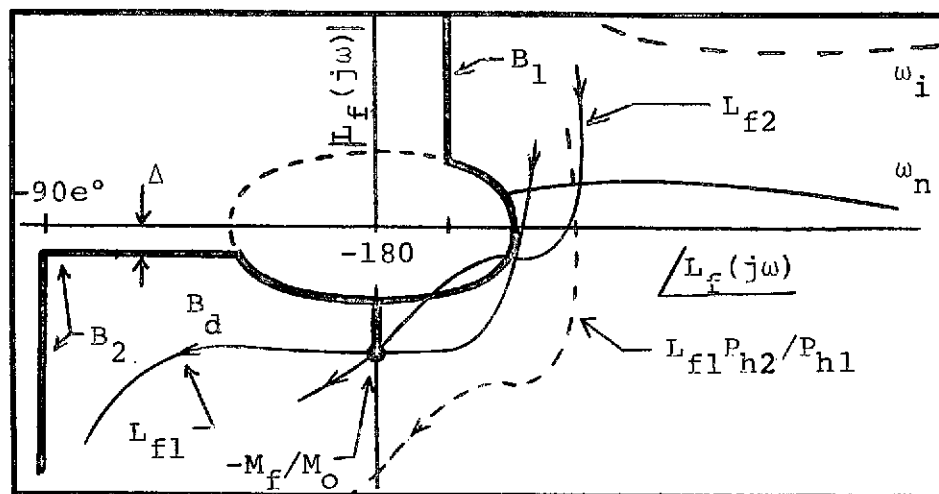


Fig. 3.5 Violation of boundary B_d which applies to all L_f .

over the low frequency band. Then L_{f1} must be designed to avoid the higher frequency portions of B_d , B_2 by some margin. The margin can only be found by checking the remaining $L_f(j\omega)$.

Finally, one additional constraint is placed on the oscillating frequency ω_o . Recall that the describing function N_f has a valid frequency interpretation over $(0, \omega_o/\beta)$, where β is the quasi-linearity parameter from Eq. 1.16b. Therefore, to insure the validity of L_f over the frequency range where sensitivity reduction is required we require that

$$\omega_o \geq \beta \omega_n \quad (3.12)$$

for all P_h .

A summary of properties of $L_f(j\omega)$ which will be quite close to optimal in the gain-bandwidth sense of Sect. 1.4 is given below.

- Property 1. $L_f(j\omega_0) = -M_f/M_0$ for all P_h .
2. $\omega_0 \geq \beta\omega_n$ for all P_h .
 3. $L_f(j\omega)$ does not cross the bounds B_1 , B_d , and B_2 for any P_h .
 4. $L_{f1}(j\omega_i)$, $i = 1, 2, \dots, n$, is on or above the respective bound at ω_i . If $L_{f1}(\omega_i)$ is above the bound at ω_i , then it has the maximum phase lag permitted by Property 3. (For example, if $L_{f1}(j\omega_2)$ has maximum phase lag of all possible $L_f(j\omega_2)$, then if $L_{f1}(j\omega_2)$ is above the ω_2 bound of Fig. 3.4, it is on B_1 .)
 5. For $\omega > \omega_n$, $L_{f1}(j\omega)$ is as close to bounds B_d and B_2 as permitted by Properties 1. and 3.

These properties follow closely those given in [22,23] for linear design, but are modified to allow for the special constraints of the SOAS loop transmission. They are intended to serve as a guide to the designer for shaping a real rational loop transmission. A practical $L_{f1}(j\omega)$ might appear as shown by Fig. 3.6.

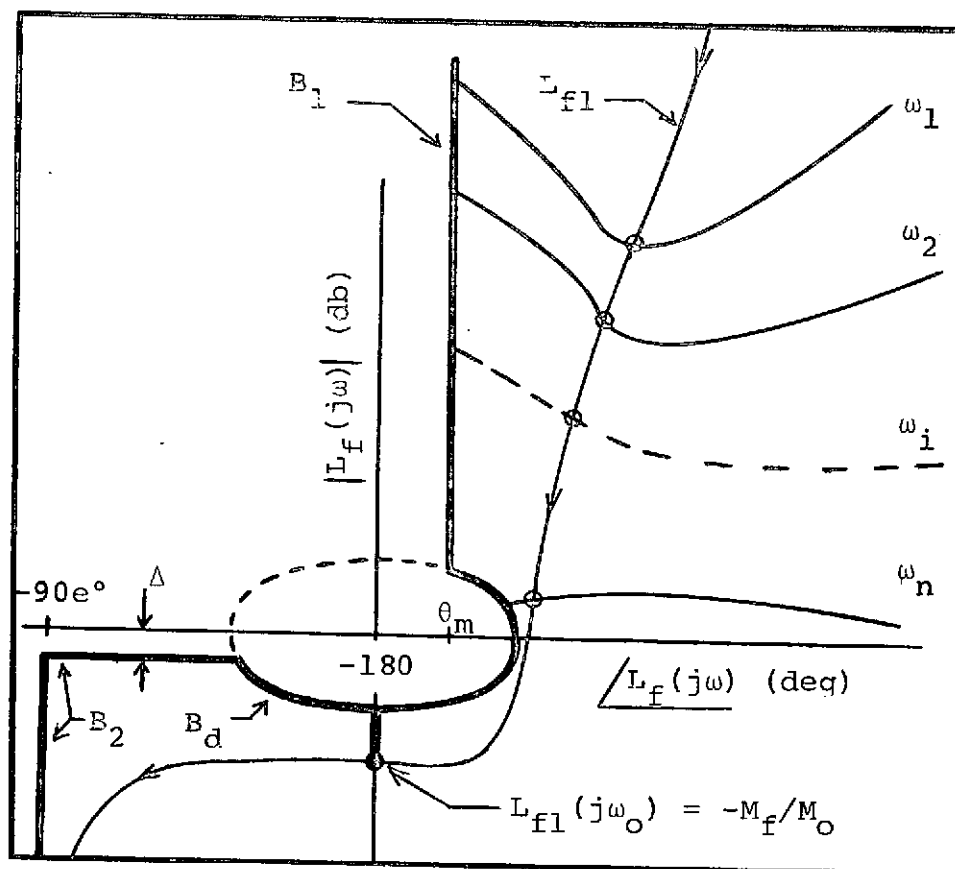


Fig. 3.6 Hypothetical loop transmission satisfying all boundaries.

Next we consider the gain factor of P_f that has been thus far neglected. We have

$$L_f = GP_f \quad (3.13)$$

with

$$P_f = K_f P_h = M_f P_h / |M_0 G(j\omega_0) P_h(j\omega_0)|. \quad (3.14)$$

The sensitivity bounds at $\omega_1, \omega_2, \dots, \omega_n$ are first obtained by neglecting the gain factor uncertainty in P_f and using P_h in the manner of Appendix C. Then $L_{f1}(j\omega) = GP_{h1}(j\omega)$ is designed such that L_{f1} satisfies

the sensitivity bounds and all L_f satisfy the bounds B_1 , B_d , and B_2 . From the design for L_{f1} the value of ω_0 for plant P_{h1} may be obtained, and the compensation is $G = L_{f1}/P_{h1}$. With any other plant value the loop transmission is $L_f = GK_f P_h$ where $K_f = M_f / |M_0 G(j\omega_0) P_h(j\omega_0)|$ is the gain factor required to satisfy $L_f(j\omega_0) = -M_f/M_0$. For a significant class of design problems this gain factor will exhibit very small variation, and can therefore be neglected completely. The reason that this is true is that ω_0 tends to be well above the varying plant dynamics and P_h is defined with vanishing uncertainty at high frequencies (see Fig. 3.3b). If it is ascertained that the gain uncertainty is negligible, then the design of L_f for sensitivity is complete.

In any particular design problem the gain factor variation may not be insignificant, in which case we must insure that the sensitivity specifications are met with the smallest possible bandwidth loop transmission, taking the K_f uncertainty into account. From the design of L_{f1} above, a function G is obtained. This G can now be used to calculate P_f for any plant parameter set, and with P_f we can obtain a new set of Nichols chart bounds for sensitivity at $\omega_1, \omega_2, \dots, \omega_n$. Then we reshape L_{f1} as required to satisfy the new bounds, obtaining a new G and repeating. The above procedure is summarized in the following design algorithm.

Algorithm:

- Step 1. Choose a reference plant parameter set denoted by P_{hl} . Take $P_{f1} = P_{hl}$ and approximate $P_f \approx P_h$ for remaining plant parameter values. Use P_h as the plant for obtaining bounds on $L_{f1}(j\omega_i)$, $i = 1, 2, \dots, n$ in accord with Appendix C.
2. Synthesize $L_{f1} = GP_{hl}$ approximating the optimality properties given earlier in this section.
3. Use $G = L_{f1}/P_{hl}$ to calculate P_f in Eq. 3.14, and use P_f to obtain new bounds for $L_f(j\omega_i)$, $i = 1, 2, \dots, n$. Repeat Steps 2 and 3 until the realized L_{f1} and the bounds computed using G from this L_{f1} are arbitrarily close.

If the gain factor $M_f/|M_o G(j\omega_o)P_h(j\omega_o)|$ of P_f has negligible uncertainty this will be evident the first time Step 3 of the algorithm is executed and this portion of the design is complete at that point.

Each time an L_{f1} is formed it is constrained by Property 1 to pass through the value $-M_f/M_o$ and the frequency at this point is the oscillating frequency ω_o . It will be minimized in accord with how well the remaining properties are satisfied.

When a satisfactory design has been completed by the

methods of this section one may check the extremes of oscillating frequency variation and obtain

$$\omega'_0 = \sqrt{\omega_{0\max} \omega_{0\min}} \quad (3.15)$$

and

$$\gamma_h = \sqrt{\omega_{0\max} / \omega_{0\min}} \quad (3.16)$$

γ_h parameterizes the maximum variation in oscillating frequency due to parameter uncertainty in P_h . This number is used in the design procedure of Sect. 2.3 to determine the required width of the notch limit cycle filter. ω'_0 is the minimum center value for oscillating frequency permitted by the present design consideration, i.e., transfer function sensitivity to parameter uncertainty of P_h . However, other design considerations, e.g., those of Chapter II, may dictate a higher oscillating frequency.

3.4 Design Example

A numerical design example is carried out below to demonstrate the design techniques of the preceding section.

Specifications

Nonlinearity:

$$\left. \begin{array}{l} \text{Ideal relay} \\ \text{with output} \\ \text{level } M \end{array} \right\} \begin{array}{l} N_o = M_o/A = 4M/\pi A \\ N_f = M_f/A = 2M/\pi A \end{array} \quad \begin{array}{l} (3.17a) \\ (3.17b) \end{array}$$

$$\left. \begin{array}{l} \text{Quasi-linearity} \\ \text{Constraint} \end{array} \right\} \omega_o \geq \beta \omega_n ; \quad \beta = 3 \quad (3.18)$$

In Eq. 3.18 ω_n is the highest frequency at which there is a nontrivial sensitivity specification.

Plant:

$$P_h(s) = \frac{1}{s(s+a)} ; \quad a \in [a_1, a_2] = [1, 10] \quad (3.19)$$

This plant has been deliberately chosen with the pole variation not confined to the low frequency range so that it is likely to produce some variation in oscillating frequency.

Disturbance Response Damping:

$$\left| \frac{L_f(j\omega)}{1+L_f(j\omega)} \right| \leq \ell = 2; \quad \forall \omega \quad (3.20)$$

Transfer Function Sensitivity:

The upper and lower bounds for acceptable transfer functions are shown in Fig. 3.7a below. The lower bound is $T_{\min} = [(6)(25)(50)/[(s+6)(s+25)(s+50)]]^2$. In Fig. 3.7b the permissible variation in the transfer function is compared with the existing plant variation or uncertainty.

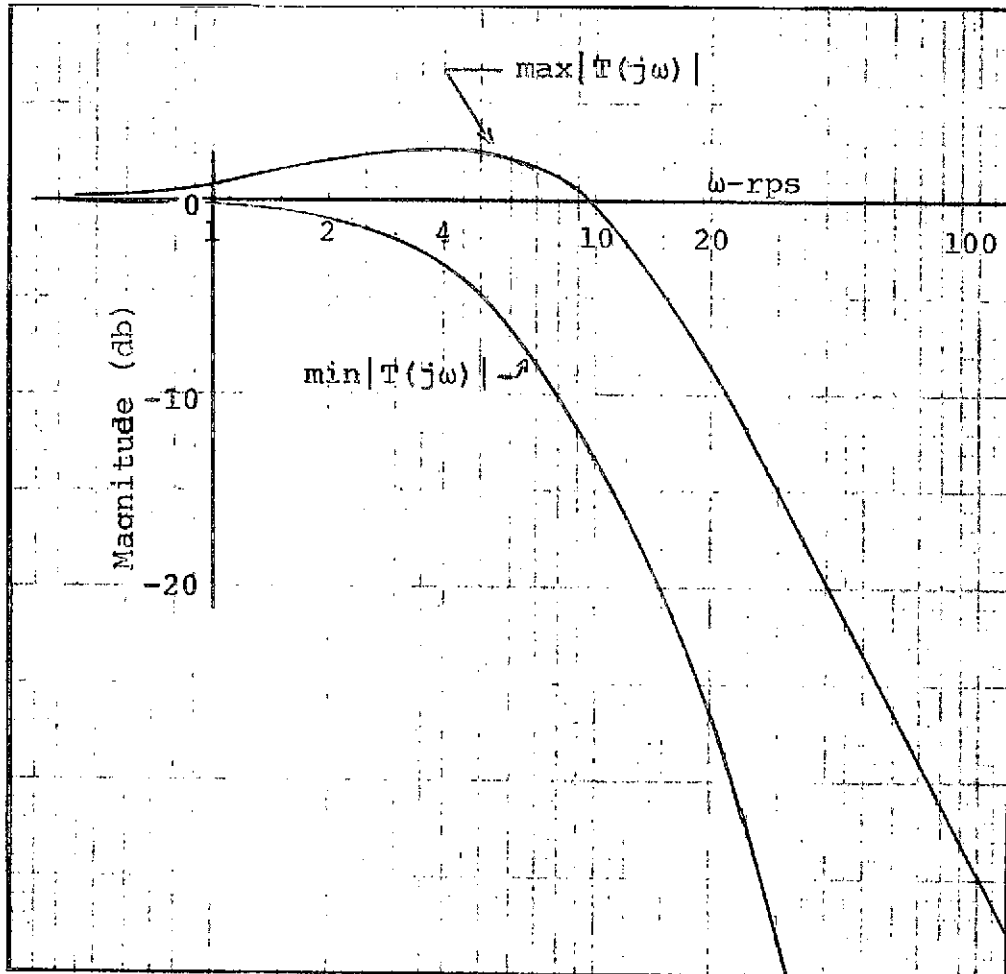


Fig. 3.7a Permissible variation of $|T(j\omega)|$.

C-2

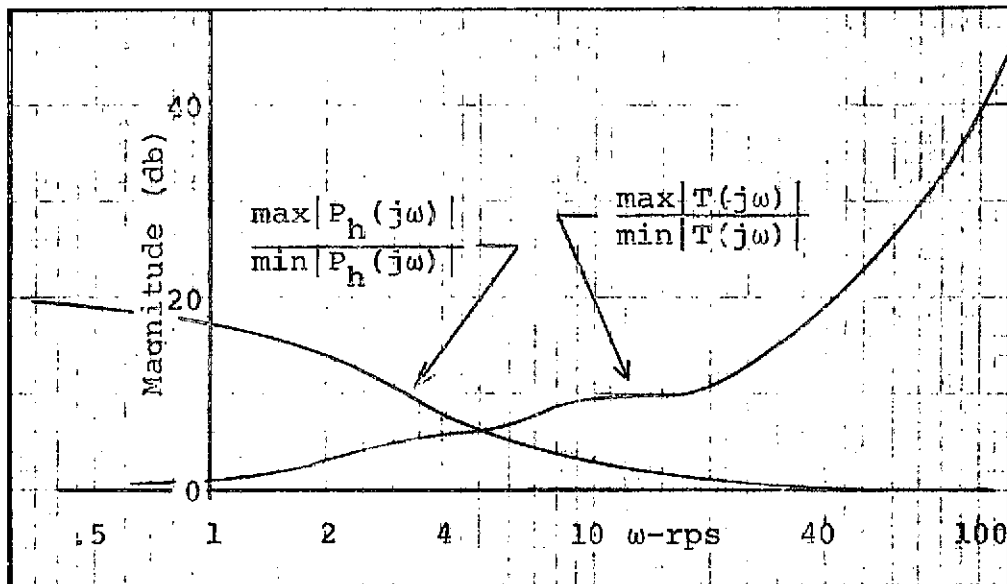


Fig. 3.7b Comparison of plant variation with permissible variation of transfer function.

Design

The first step in the design algorithm in Sect. 3.3 is to obtain bounds for $L_{f1}(j\omega)$ using the method of Appendix C. The forced signal loop transmission is

$$L_f = GP_f, \quad (3.21)$$

with

$$P_f = K_f P_h = \frac{M_f P_h}{|M_o G(j\omega_o) P_h(j\omega_o)|}. \quad (3.22)$$

To obtain the initial bounds, the uncertainty of $K_f = M_f / |M_o G(j\omega_o) P_h(j\omega_o)|$ is neglected, and we use $P_f \approx P_h$.

As a reference plant

$$P_{hl} = \frac{1}{s(s+a_1)} = \frac{1}{s(s+1)} \quad (3.23)$$

is chosen and the resultant bounds for $L_{f1} = GP_{hl}$ are shown as the solid bounds at $\omega = .4, .8, \dots, 4.8$ in Fig. 3.8. Also shown is the boundary B_d due to Eq. 3.20.

A rational function L_{f1} is found as plotted in Fig. 3.8. The plotted points correspond to the boundary frequencies in sequence, a convention that we shall follow throughout. The parameters of the compensation G are listed in Table 3.1a and further data on L_f is

Poles			Zeros		
p	ζ	ω	z	ζ	ω
	.6	15	3		
	.4	60	18		
	.4	100			
	.5	120			
$K_o = 21.23$			$K_\infty = 4.59 \times 10^{13}$		

Table 3.1a Parameters of G for L_f shown in Fig. 3.8.

given in Table 3.1b. L_f has been shown dashed on Fig. 3.8 when $P_h = 1/[s(s+10)]$. Of course each L_f must pass through the point $-M_f/M_o = -1/2$ (-6 db, -180°).

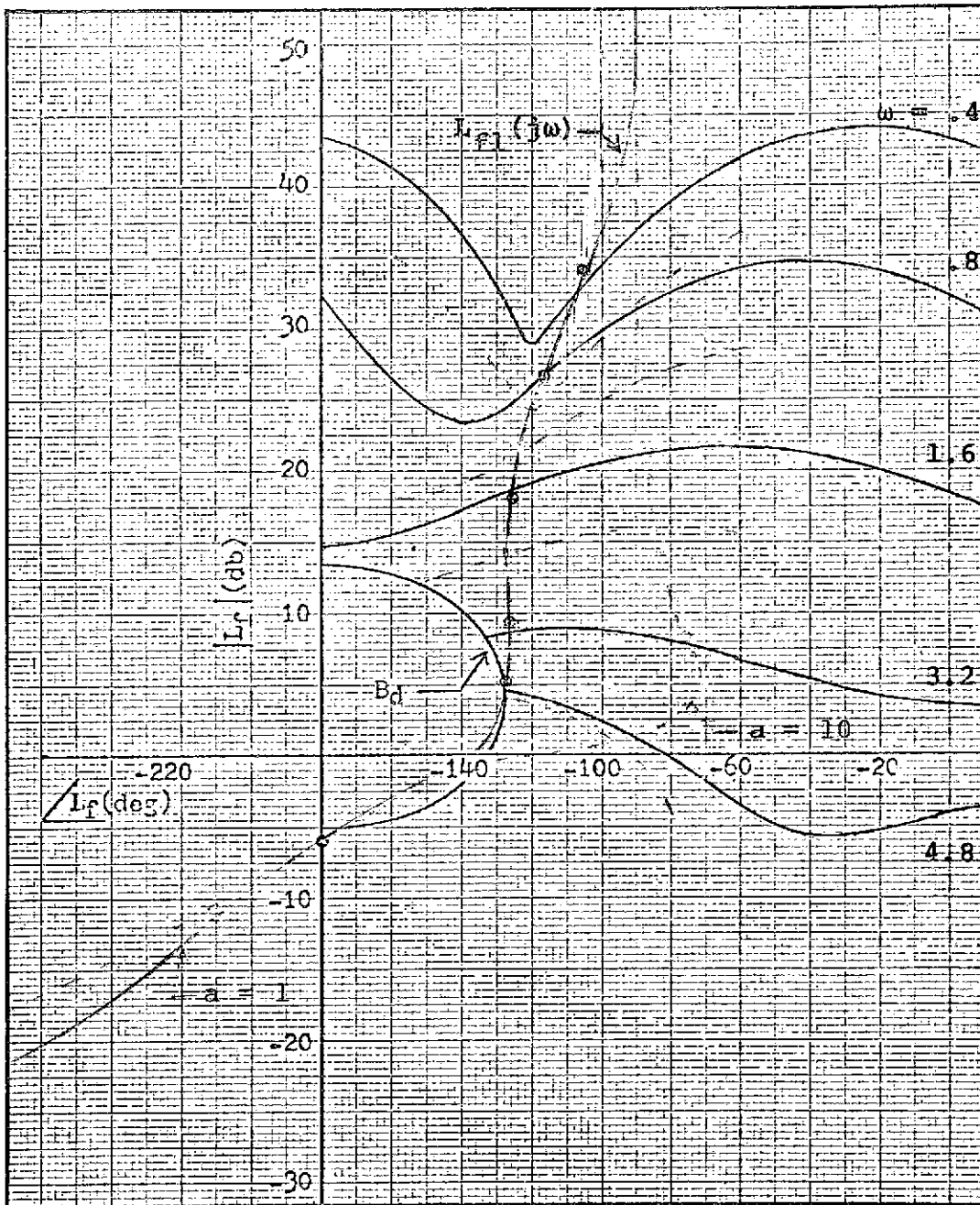


Fig. 3.8 Bounds for $L_{f1}(j\omega)$ and plots of rational L_f using G of Table 3.1a.

ω_o	K_f	K_o	K_∞	a
16.1	1.0	21.23	4.59×10^{13}	1
17.3	1.15	8.11	5.26	3
18.4	1.31	5.56	6.01	5
19.4	1.49	4.51	6.82	7
20.8	1.78	3.77	8.14	10
$\omega_o' = 18.4$			$\gamma_h = 1.14$	

Table 3.1b Parameters of $L_f = GP_f$
with G given in Table 3.1a.

Obtaining a rational function for L_{f1} to give a reasonable fit of the boundaries is a difficult task, which is largely accomplished by a process of cut and try. Some help may be obtained by using the average relationships between magnitude slope and phase for minimum phase functions as explained in [22]. The problem here is considerably more difficult than in linear system design. For example, in Fig. 3.8 the last sensitivity boundary is at 4.8 rps while $L_{f1}(j16.1) = -1/2$. If this were a linear system loop transmission one could add a complex pole pair, at say 30 rps, having virtually no effect at 4.8 rps and below where the sensitivity bounds are located. However, for the SOAS loop transmission the same pair of poles at 30 rps will have a significant phase effect at 16.1 rps, hence shifting the oscillating frequency. The gain factor is then adjusted so that at the new oscillating frequency, say ω_1 , $L_{f1}(j\omega_1) = -1/2$.

The resultant effect is that L_{f1} is shifted away from all the sensitivity bounds.

Next we use the gain factor K_f obtained from the first compensation G to calculate bounds for the plant $P_f = K_f P_h$. K_f is listed in Table 3.1b where a spread of 1.78 (5 db) is noted. The new bounds are shown dashed on Fig. 3.8 for comparison with those obtained previously. Note they are considerably lower allowing a smaller bandwidth L_{f1} than the first bounds yielded. The new bounds are shown solid on Fig. 3.9 along with the second iteration for L_{f1} . Data for this L_{f1} is listed on Tables 3.2a and 3.2b. Comparing the data of Tables 3.1b with 3.2b, the oscillating frequency

Poles			Zeros		
p	ζ	ω	z	ζ	ω
1.5	.6	12	1		
	.4	60	3		
	.4	100	18		
	.4	120			
$K_o = 12.7$			$K_\infty = 2.63 \times 10^{13}$		

Table 3.2a Parameters of G used for L_{f1} of Fig. 3.9.

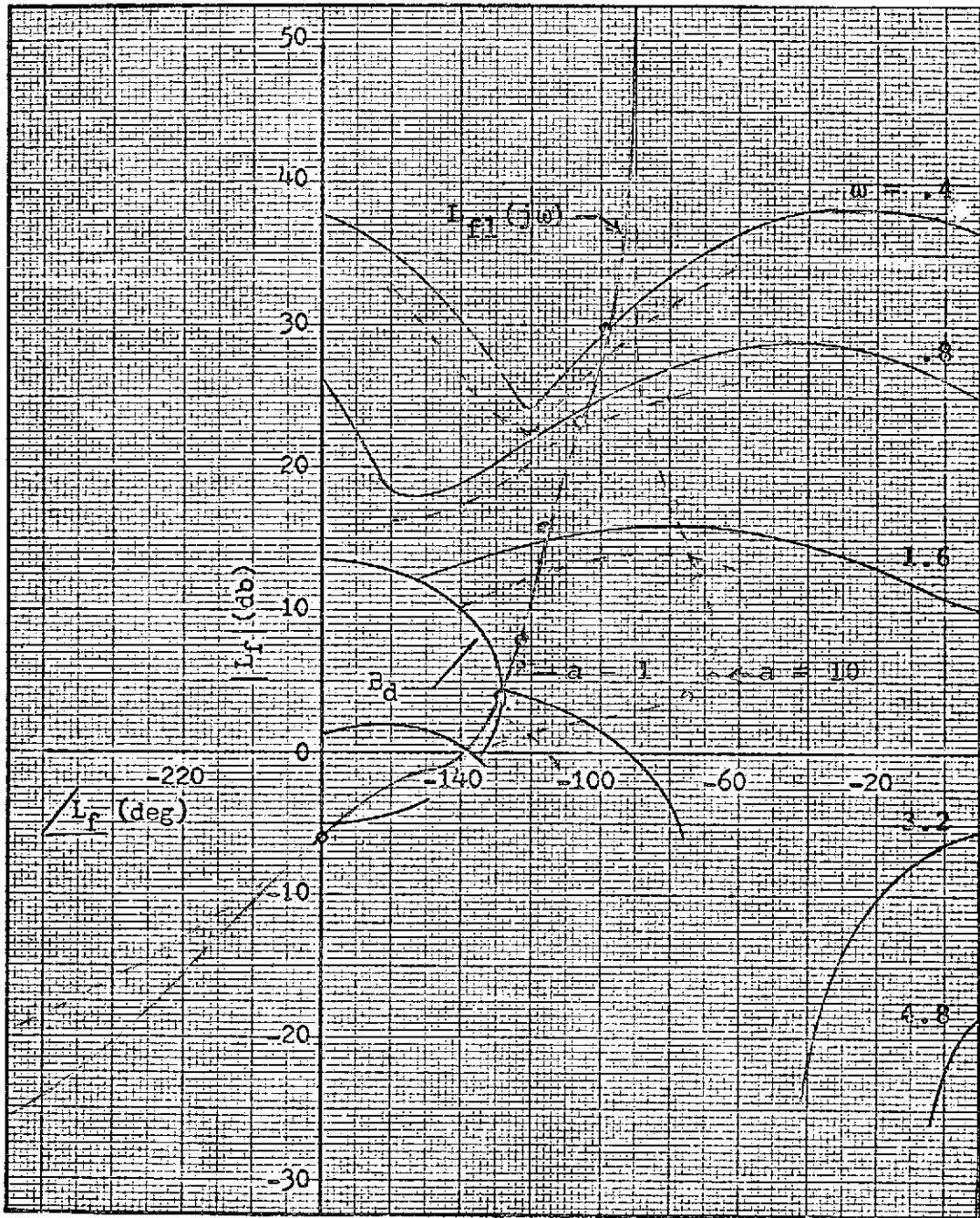


Fig. 3.9 Bounds for $L_{f1}(j\omega)$ after obtaining first G , and $L_{f1}(j\omega)$ using second G from Table 3.2a.

ω_o	K_f	K_o	K_∞	a
12.9	1.00	12.69	2.63×10^{13}	1
14.2	1.22	5.16	3.21	3
15.3	1.47	3.74	3.88	5
16.4	1.76	3.19	4.63	7
17.2	2.24	2.84	5.88	10
$\omega_o' = 16.2$		$\gamma_h = 1.16$		

Table 3.2b Parameters of L_f using
G from Table 3.2a.

has been reduced by $18.4/16.2 = 1.17$ and the high frequency gain by $4.59/2.63 = 1.74$ (4.8 db).

The next set of bounds are obtained using $P_f = K_f P_h$ with K_f from Table 3.2b. These bounds are again displayed with dashed lines on Fig. 3.9 for comparison with

Poles			Zeros		
p	ζ	ω	z	ζ	ω
1.8	.7	3.2	1	.45	3.2
	.6	11	3.3		
	.8	50	18		
	.4	100			
	.5	120			
$K_o = 10.8$		$K_\infty = 1.43 \times 10^{13}$			

Table 3.3a Parameters of G for
 L_{f1} of Fig. 3.10.

ω_o	K_f	K_o	K_∞	a
11.1	1.00	10.8	$1.43 \cdot 10^{13}$	1
12.2	1.21	4.36	1.73	3
13.1	1.46	3.15	2.08	5
13.9	1.74	2.68	2.48	7
15.0	2.21	2.39	3.16	10
$\omega_o^* = 13.4$		$\gamma_h = 1.17$		

Table 3.3b Parameters of L_f using
G from Table 3.3a

with the previous set, and are shown solid on Fig. 3.10. Data for the next L_f is given in Tables 3.3a and 3.3b while L_{f1} is sketched on Fig. 3.10.

The next set of bounds are calculated using K_f from Table 3.3b. These are shown dashed on Fig. 3.10, where it is observed that they are quite close to the previous set, i.e., the algorithm has converged to an acceptable G.

Comparing data from Tables 3.1b and 3.3b, the iteration has reduced oscillating frequency by the ratio $18.4/13.4 = 1.37$ while lowering the high frequency asymptote of L_{f1} by $20\log[4.59/1.43] = 10.1$ db. This is a significant improvement that should not be ignored.

It is notable that if the entire plant were $P = P_h$ from Eq. 3.19, i.e., no high frequency gain variation, then the loop transmission required in a linear design is specified by the bounds in Fig. 3.8. For the SOAS the

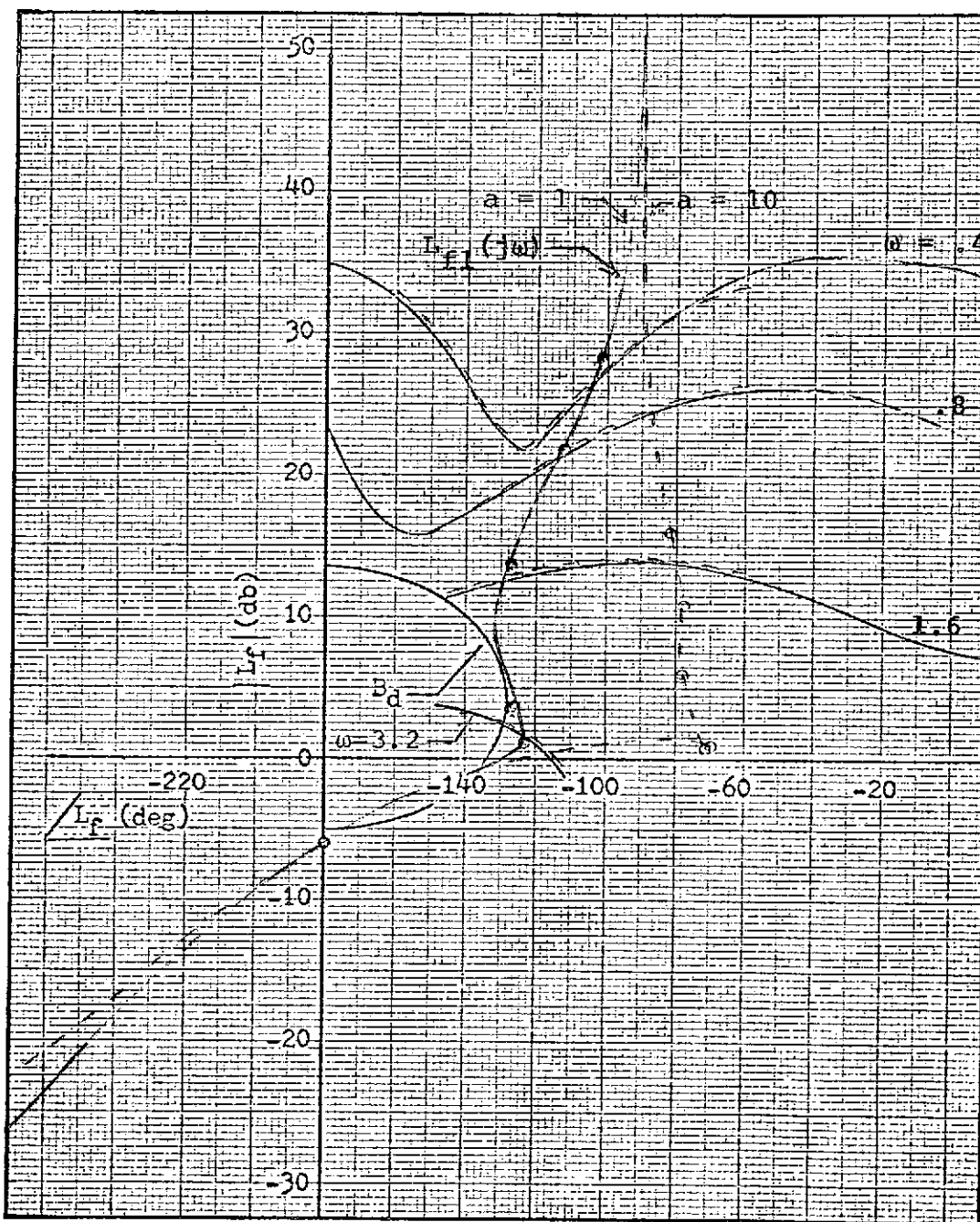


Fig. 3.10 Bounds for $L_{f1}(j\omega)$ after obtaining second G, and $L_{f1}(j\omega)$ using third G from Table 3.3a.

lower bounds of Fig. 3.10 are sufficient. Hence, provided the remaining SOAS design considerations allow the loop transmission to be obtained, the SOAS is superior to a linear design in this example even without any plant gain factor uncertainty.

3.5 Additional Considerations in the P_h Parameter Sensitivity Design

The method of synthesis in Sect. 3.3 which has been demonstrated in Sect. 3.4 provides the designer with the means for finding the minimum mean oscillating frequency ω'_0 permitted by P_h parameter uncertainty, as well as the uncertainty which is written

$$\omega_0 \in [\omega'_0/\gamma_h, \omega'_0\gamma_h] = \Omega_h . \quad (3.24)$$

γ_h may then be used in determining the width required for the limit cycle filter in Sect. 2.3. There are other lower bounds for ω'_0 , e.g., the bound established by the spread of gain uncertainty in Chapter II. Thus it may not be possible to achieve the ω'_0 dictated by Sect. 3.3. When this is the case some freedom is permitted to reduce the uncertainty parameter γ_h . The variation of ω_0 is caused by the phase variation of P_h in the interval Ω_h . Recalling that P_h has vanishing uncertainty at high frequencies (see Eq. 3.1 and Fig. 3.3), any increase in ω'_0 can be expected to decrease the ω_0 variation. On Tables 3.1b and 3.3b in the numerical example of the preceding section it is seen that a change of ω'_0 from 13.4

to 18.4 reduces γ_h from 1.17 to 1.14. In addition, for a change in plant phase $\Delta\theta$ in the neighborhood of ω'_0 , the corresponding change in ω_0 is proportional to the slope of the loop transmission phase characteristic.

This phenomenon is illustrated in Fig. 3.11, where we see that it is desirable to make the $\angle L_f(j\omega)$ characteristic as steep as possible in this neighborhood. When ω'_0 must

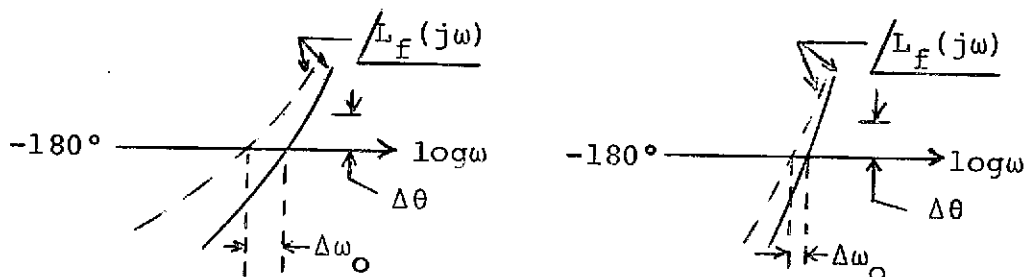


Fig. 3.11 Illustration of oscillation frequency variation proportional to phase slope.

be significantly above the value found from Sect. 3.3, the frequency range between ω_n and the required ω'_0 can be used to shape $\angle L_f(j\omega)$ for $\omega \in \Omega_n$ with a very steep slope. This is done by removing some phase lag above ω_n and then introducing underdamped poles near ω'_0 . Fig. 3.12 qualitatively illustrates the appearance of L_f on Nichols chart coordinates when the above is implemented.

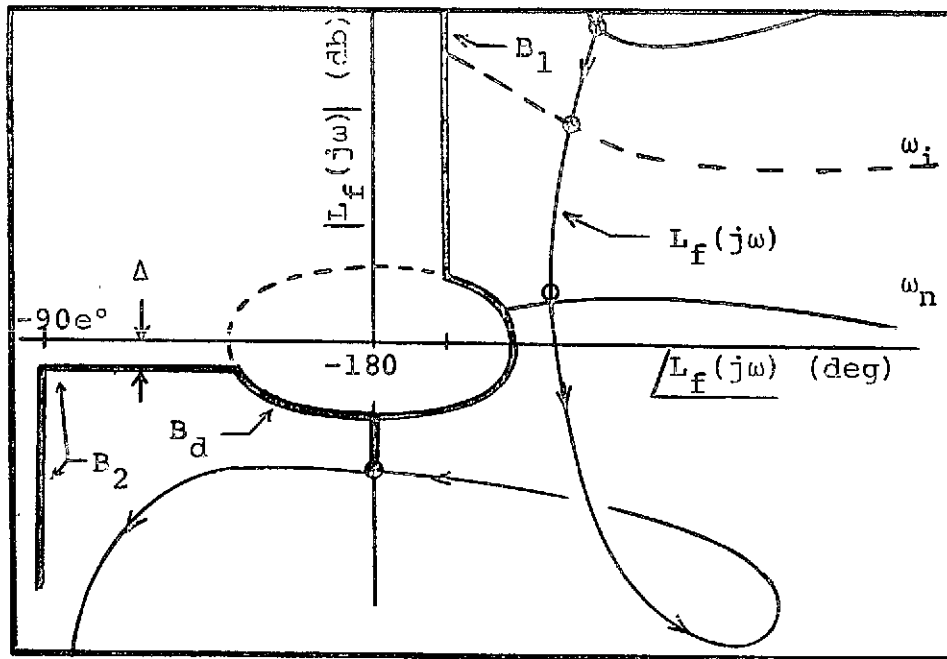


Fig. 3.12 Shaping of L_f to reduce ω_o variation.

The validity of the disturbance damping boundary B_d , and boundary B_2 , is open to question at frequencies above ω_o/β (β is the quasi-linearity parameter of Eq. 1.16b) where the forced signal describing function N_f becomes ambiguous. The conservative approach is to avoid these boundaries, although it might be shown experimentally that this is not entirely necessary.

Clearly the synthesis procedure of Sect. 3.3 entails a considerable amount of design effort, while we have noted that other design considerations such as adapting to large gain uncertainty with small limit cycle in Chapter II may preclude the use of the minimum ω_o' found in Sect. 3.3. Therefore, the designer should ascertain

approximately the achievable ω'_0 to handle gain variation and output limit cycle requirements before carrying out the synthesis of Sect. 3.3 in detail. In many situations the tedious design of that section may be avoided completely, because the gain uncertainty and output limit cycle magnitude considerations obviously demand a larger loop transmission.

CHAPTER IV
DESIGN CONSIDERATIONS FOR
DISTURBANCE INPUTS TO THE SOAS

4.1 Satisfying Quasi-Linearity and Output Limit
Cycle Constraints for Disturbance Inputs.

Disturbance inputs are taken as deterministic signals D applied to the plant output as depicted by Fig. 4.1. Disturbance signals that act internally, or at the plant input, can be translated to equivalent signals at the output. The nonlinear element N is characterized by DIDF

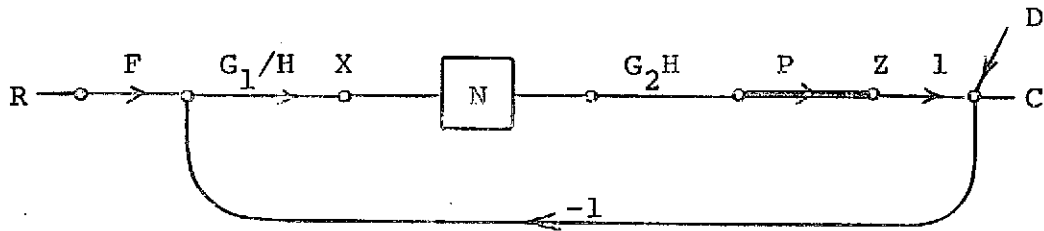


Fig. 4.1 SOAS structure with disturbance input D .

$$N_o = M_o/A \quad (4.1a)$$

$$N_f = M_f/A, \quad (4.1b)$$

when quasi-linearity constraints

$$\max_t |x_e(t)| \leq A_e/\alpha \quad (4.2a)$$

$$\omega_b \leq \omega_o/\beta \quad (4.2b)$$

are satisfied. Simultaneously, the limit on maximum magnitude of output limit cycle component,

$$|M_o G_2(j\omega_o)H(j\omega_o)P_{hm}(j\omega_o)| \leq m/K_m, \quad (4.3)$$

must be satisfied. In this equation $|K_m P_{hm}(j\omega_o)| = \max_{\omega \in W} |P(j\omega_o)|$, where the plant ignorance is characterized as in Sect. 1.3, Eq. 1.17. Chapter II presented a design technique to satisfy (4.2) and (4.3) when $x_e(t)$, the extreme forced signal input to N , is due to a command input R in Fig. 4.1. Here some modifications of that procedure are considered when $x_e(t)$ is the forced input to N due to disturbance D .

The plant output signal due to a disturbance in Fig. 4.1 is

$$Z_f = -DL_f/(1+L_f), \quad (4.4)$$

where L_f is the forced signal loop transmission

$$L_f = N_f G_1 G_2 K P_h. \quad (4.5)$$

Let us take an analysis viewpoint temporarily. Suppose X_R is the forced input at N due to commands and X_D is that resulting from disturbances. From Fig. 4.1,

$$\begin{aligned} X_R &= \frac{TR}{N_f G_2 H K P_h} = \frac{A_1 TR}{K_1 M_f G_2 H P_h} \\ &= \frac{A_1 R}{K_1 M_f G_2 H P_h} \left[\frac{L_f}{1 + L_f} \right] F, \end{aligned} \quad (4.6)$$

where we have used $A/K = A_1/K_1$, and $T = FL_f/(1+L_f)$.

For a disturbance input $-D$, we get similarly,

$$\begin{aligned} X_D &= \frac{A_1 D}{K_1 M_f G_2 H P_h} \left[\frac{L_f}{1 + L_f} \right] \\ &= X_R \left[\frac{D}{RF} \right]. \end{aligned} \quad (4.7)$$

Suppose X_R has been designed as in Chapter II (for step commands and a Type 1 plant), so that the dominant part of X_R is

$$X_R = \frac{q_x \omega_b}{s + \omega_b} \quad (4.8)$$

The frequency response, $|X_R(j\omega)|$, is sketched in Fig. 4.2 showing $\omega_b < \omega_o/\beta$, as is often the case because the limit cycle constraint, Eq. 4.3, forces ω_o to be high. If the disturbance inputs $\mathcal{L}^{-1}[D(s)]$ have approximately the

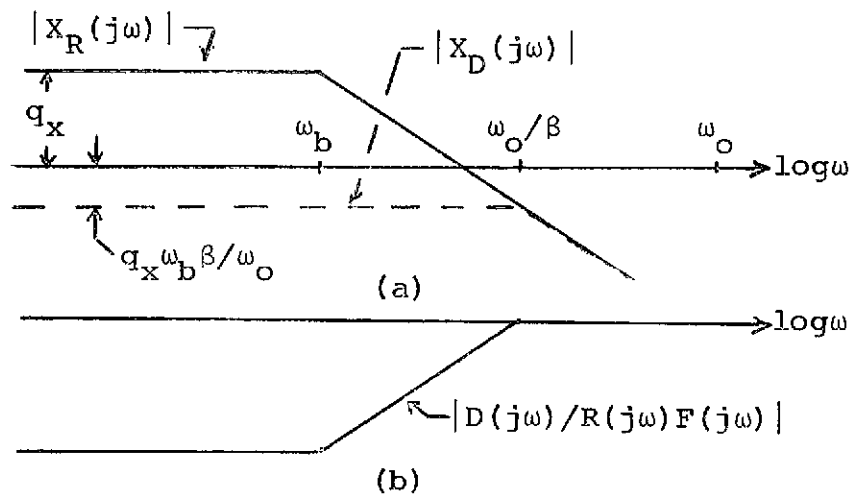


Fig. 4.2 Comparison of forced inputs to N for commands R and disturbances D.

same speed and magnitude as the prefilter output signal in Fig. 4.1, $\mathcal{L}^{-1}[R(s)F(s)]$, due to command inputs, then by (4.7) the two forced signals at N will be the same, and will both satisfy the quasi-linearity constraints. Since $x_R(t)$ is slower than required to satisfy (4.2b) ($\omega_b < \omega_o/\beta$), we could speed up $x_D(t)$ to $x_D(t) = x_R(\omega_o t/\beta\omega_b)$ without violating (4.2b). This gives

$$X_D(s) = \frac{a_x^{(n)} b}{s + \omega_0 / \beta}, \quad (4.9)$$

which is also sketched in Fig. 4.2a.

For the system structure being considered here (step R and Type 1 plant) F tends to be a low-pass filter. Thus, if D(s) and R(s)F(s) are to be comparable signals with respect to their propensity to violate the quasi-linearity constraints on N, then D(s) must have smaller bandwidth than R(s). In particular, a step D(s) will probably be an unacceptable input to an SOAS that has been designed on the basis of step R(s). We now return to the synthesis problem.

The nonlinearity forced input is obtained in terms of the plant output signal Z_f as

$$X_f = \frac{Z_f}{N_f G_2^{HKP_h}}, \quad (4.10)$$

with

$$Z_f = RT = RFL_f / (1 + L_f) \quad (\text{command input}), \quad (4.11)$$

and

$$Z_f = -DL_f / (1 + L_f) \quad (\text{disturbance input}). \quad (4.12)$$

When there is plant uncertainty there is some extreme set of plant parameters P_{he} which produce the extreme X_e due to disturbance input $-D_e$, so that

$$Z_e = D_e L_{fe} / (1 + L_{fe}). \quad (4.13)$$

In view of Eqs. 4.10 thru 4.12, the synthesis procedure when Z_e and X_e are due to a disturbance input is exactly the same as explained in Sect. 2.3 when X_e is

due to a command input, except that in all the equations of that section $Z_e = R_e T_e$ is replaced by $Z_e = D_e L_{fe} / (1 + L_{fe})$. Thus we can parallel many of the equations from Sect. 2.3 in the following. Beginning with

$$A_e = \lambda \alpha q_x \omega_b, \quad (4.14)$$

we get

$$\begin{aligned} X_e &= \frac{X_{e1}}{H} = \frac{A_e Z_e}{M_f G_2 H K_e P_{he}} \\ &= \frac{\lambda \alpha q_x \omega_b D_e L_{fe}}{M_f K_e G_2 H P_{he} (1 + L_{fe})}, \end{aligned} \quad (4.15)$$

and

$$X_{e1} = \frac{\lambda \alpha q_x \omega_b D_e L_{fe}}{M_f K_e G_2 P_{he} (1 + L_{fe})} = \frac{q_x \omega_b}{s + \omega_b} \phi_x. \quad (4.16)$$

q_x and ω_b are parameters of X_e due to a disturbance, and the chosen form for X_{e1} on the right of (4.16) is appropriate only if D_e has one pole at the origin. Recall that $L_{fe}(j\omega_0) = -M_f/M_0$. Using this, solving for G_2 from (4.16), and substituting in (4.3) yields

$$\begin{aligned} \left| \frac{X_e(j\omega_0)}{A_e} \right| &= \left| \frac{X_{e1}(j\omega_0)}{A_e H(j\omega_0)} \right| \\ &\geq \frac{K_m |M_0|}{K_e m |M_f - M_0|} |D_e(j\omega_0)| \left| \frac{P_{hm}(j\omega_0)}{P_{he}(j\omega_0)} \right|. \end{aligned} \quad (4.17)$$

This is the equation corresponding to (2.56), but now applying to X_e generated by a disturbance input.

Suppose $D_e = q_d/s$, and no limit cycle filter is used so $H = 1$, and $\max_t |x_e(t)| \approx q_x \omega_b$, giving $A_e = \alpha q_x \omega_b$.

Then (4.17) reduces approximately to

$$\left| \frac{1}{s+\omega_b} \right|_{j\omega_0} \geq \frac{\alpha K_m q_d |M_0|}{K_e m |M_f - M_0| \omega_0} \quad (4.18)$$

or approximating $|j\omega_0 + \omega_b| \approx \omega_0$ we get

$$q_d \leq \frac{K_e m |M_f - M_0|}{\alpha K_m |M_0|} \quad (4.19)$$

For step D_e and $H = 1$, there will be a value of ω_0 satisfying (4.17) only if the step magnitude satisfies (4.19). In other words, without a limit cycle filter the system will only tolerate very small step disturbances and continue to operate in a quasi-linear fashion. For example, using numbers from the design of Sect. 2.4, i.e., $K_e/K_m = m = .1$, $\alpha = 3$, and $|(M_f - M_0)/M_0| = 1$, yields $q_d \leq .0033$. This is smaller than the smallest value of limit cycle magnitude, which has peak value $m/K_m = .01$.

Continuing with the design equations (which are not just valid for step D_e , but for any D_e with one pole at the origin), we assume that ω_0 can vary in

$$\omega \in [\omega_0'/\gamma, \omega_0'\gamma] = \Omega. \quad (4.20)$$

Solving for $|H(j\omega)|$ from (4.17),

$$|H(j\omega)| = \begin{cases} \frac{K_e m |M_f - M_0| |X_{e1}(j\omega)| \left| \frac{P_{he}(j\omega)}{P_{hm}(j\omega)} \right|}{K_m \lambda \alpha q_d \omega_b |M_0| |D_e(j\omega)|} & ; \omega \in \Omega \\ 1 & ; \omega \notin \Omega. \end{cases} \quad (4.21)$$

Again taking $D_e = q_d/s$, we get $|H(j\omega)| \approx K_e m |M_f - M_0| / [K_m \lambda \alpha q_d |M_0|]$ for $\omega \in \Omega$, which is entirely given by specifications and is independent of the choice of ω_0 .

If D_e has at least one additional finite pole, then the

right side of (4.21) will increase with ω and the higher the choice of ω_0 , the less depth required in $H(j\omega)$. In any event, the design problem is to find a suitable combination of ω_0' , λ , and $H(j\omega)$, and this is accomplished by iteration on ω_0' and λ in precisely the manner explained in Sect. 2.3 when the extreme X_e is due to a command. The only difference is that a new defining function for $H(j\omega)$, (4.21), is used. If no narrow limit cycle filter is used, then the minimum permissible oscillating ω_0'/γ is the smallest frequency satisfying (4.17) with $H = 1$.

Suppose now that ω_0' , λ , and H have been found. How is the design completed? Solving Eq. 4.15 for G_2 gives

$$G_2 = \frac{\lambda \alpha q_x \omega_b^D L_{fe}}{M_f K_e X_{el} P_{he} (1 + L_{fe})} \cdot \quad (4.22)$$

We cannot determine G_2 uniquely until L_{fe} has been designed. L_{fe} can be designed in the manner detailed in Sects. 3.3 and 4.2 to satisfy both parameter sensitivity and/or disturbance attenuation specifications over the low and intermediate frequency bands, while constraining it to satisfy $L_{fe}(j\omega_0) = -M_f/M_0$ at the ω_0 selected above. When L_{fe} is thus obtained, G_2 is completely determined and G_1 is solved from

$$G_1/q_x = \frac{\lambda \alpha \omega_b L_{fe}}{M_f K_e G_2 P_{he}} \cdot \quad (4.23)$$

Lastly, the prefilter F is obtained in the same manner as in Sect. 2.3 as

$$F = T_e (1 + L_{fe}) / L_{fe} . \quad (4.24)$$

This completes the synthesis steps for the case when minimum ω'_0 is determined by the need to satisfy quasi-linearity constraints (4.2) and output limit cycle constraint (4.3) with a disturbance input.

We have seen that the constraints of this section are difficult to satisfy (if they can be satisfied at all) when the disturbance inputs are steps. However, this will not always preclude the use of an SOAS when step disturbance inputs are present. Usually one is more interested in simply attenuating the effect of the disturbance at the system output, rather than shaping the disturbance response function in any particular manner. Therefore, it may, in some cases, be acceptable to design the system so that it remains quasi-linear for all commands, but operates nonlinearly for some disturbance inputs.

4.2 Design to Satisfy Disturbance

Attenuation Specifications

As suggested in Sect. 1.4, specifications on the maximum disturbance transmission magnitude as a function of frequency may be given. The synthesis scheme for satisfying such specifications is considered below, and shown to be a simple extension of the technique used in Chapter III for sensitivity specifications.

We assume the bounded plant ignorance

$$P(s,w) = K(w)P_h(s,w); \begin{cases} w \in W \\ K(w) \in [K_1, K_2], \end{cases} \quad (4.25)$$

with $P(s,w) \rightarrow K(w)/s^e$ as $|s| \rightarrow \infty$, and the bounding sets $W, [K_1, K_2]$, and the plant structure known. As derived in Sect. 3.2, the equivalent plant for forced signals (command or disturbance) is

$$P_f = K_f P_h, \quad (4.26)$$

where

$$K_f = M_f / |M_o G(j\omega_o) P_h(j\omega_o)|, \quad (4.27)$$

when the forced signal loop transmission is written

$$L_f = N_f G_1 G_2 K P_h = G P_f. \quad (4.28)$$

From the system structure of Fig. 4.1 the disturbance transmission to the system output is

$$T_D = \frac{1}{1+L_f}. \quad (4.29)$$

Specifications are taken as an upper bound on $\ln|T_D(j\omega)|$ vs. ω , which is to be satisfied over the range of parameter ignorance for the equivalent plant P_f . The specifications on $\ln|T_D(j\omega)| = \ln|1/(1+L_f(j\omega))|$ is easily translated to a set of boundaries on $L_{f1}(j\omega) = G(j\omega)P_{f1}(j\omega)$ when bounds on the ignorance of P_f are known. The method for doing so is explained in Appendix C. As in the sensitivity design, the ignorance in K_f is

not known at the outset so it is neglected in finding the first set of bounds for which $P_f \approx P_h$ is used. The net result is a set of Nichols chart bounds for L_{f1} . Once such bounds are obtained the design procedure for finding an optimal L_{f1} satisfying them is exactly the same as given in Chapter III to satisfy sensitivity bounds. In fact, if both sensitivity and disturbance attenuation specifications are given, the design should be carried out to satisfy both simultaneously. At any frequency, say ω_i , a boundary, B_s in Fig. 4.3, for $L_{f1}(j\omega_i)$ is obtained by the technique of Appendix C to satisfy the sensitivity specification. Similarly the boundary B_d of

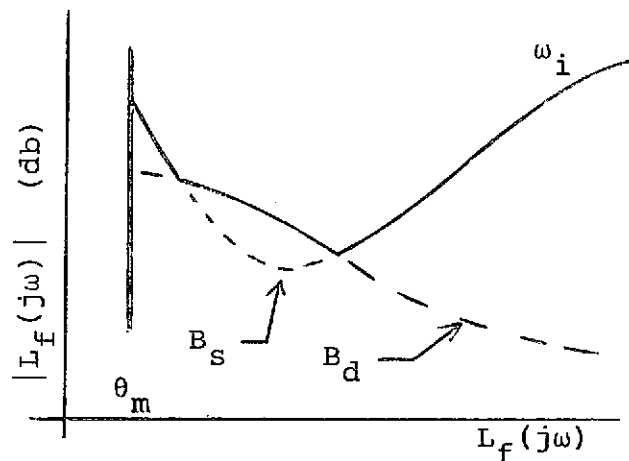


Fig. 4.3 Composite boundary for $L_{f1}(j\omega_i)$ due to sensitivity and disturbance specifications.

Fig. 4.3 is obtained from the disturbance response specification for the same $L_{f1}(j\omega_i)$. Then the boundary with greater $|L_{f1}(j\omega_i)|$ must be respected to satisfy both

sensitivity and disturbance response specifications.

Hence, the only alteration of the design technique in

Chapter III is in the calculation of the bounds for

$L_{f1}(j\omega_i)$.

CHAPTER V

EXAMPLE OF SOAS DESIGN AND SIMULATION

5.1 Design Specifications

Listed below are the necessary specifications for a complete SOAS design in the context of this paper. It will be evident that the specifications are selected to take maximum advantage of the design efforts previously invested in Sects. 2.4 and 3.4.

Structure

The design will be implemented with the same feedback structure of previous sections, shown again in Fig. 5.1.

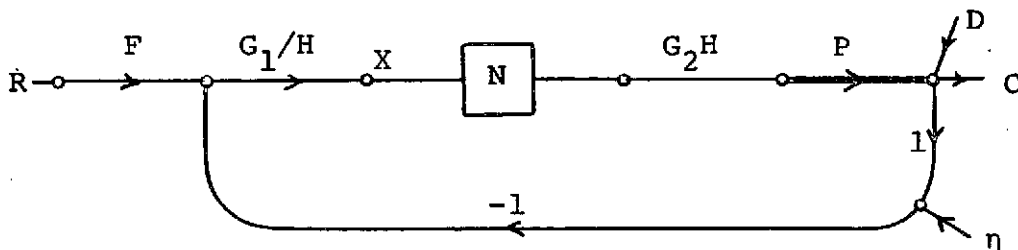


Fig. 5.1 SOAS structure.

Nonlinear element (saturation)

The nonlinear element is taken as a saturation with parameters of the characteristic defined by Fig. 5.2.

The DIDF is

$$N_o = M_o/A = 4M/\pi A \quad (5.1a)$$

$$N_f = M_f/A = 2M/\pi A, \quad (5.1b)$$

with quasi-linearity constraints

$$\max_t |x_f(t)| \leq A/\alpha; \quad \alpha \geq 3 \quad (5.2a)$$

$$\omega_b \leq \omega_o/\beta; \quad \beta \geq 3. \quad (5.2b)$$

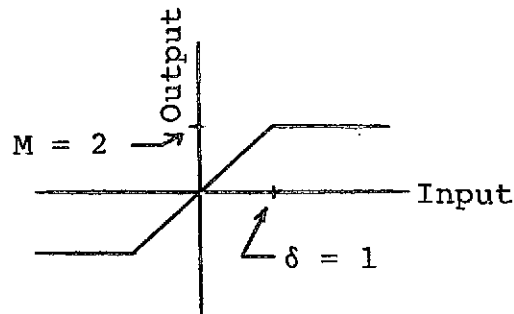


Fig. 5.2 Saturation characteristic.

Plant

The plant is specified by

$$P(s) = KP_h(s) = \frac{K}{s(s+a)}; \quad \begin{cases} a \in [a_1, a_2] = [1, 10] \\ K \in [K_1, K_2] = [1, 10] \end{cases} \quad (5.3)$$

where a and K are uncorrelated.

Disturbance response damping

To avoid excessive overshoot and ringing due to disturbance inputs the specification

$$\left| \frac{L_f(j\omega)}{1+L_f(j\omega)} \right| \leq \ell = 2; \quad \forall \omega \quad (5.4)$$

is imposed. This specification was discussed in Sect.1.3, Eq. 1.18. The disturbance inputs are assumed sufficiently small that no specific transmission requirements are imposed, and also that such inputs will not intolerably violate the quasi-linearity specifications.

Transfer function and sensitivity

The transfer function magnitude must lie between the bounds given in Sect. 3.4, Fig. 3.7a, repeated here as Fig. 5.3 for convenient reference. These bounds establish both sensitivity and the absolute level for $|T(j\omega)|$.

Extreme command input

The extreme (largest and fastest) command input anticipated is

$$R_e(s) = q_r/s; \quad |q_r| = 1. \quad (5.5)$$

Output limit cycle magnitude

The maximum output limit cycle magnitude over all plant conditions is

$$m = 0.1. \quad (5.6)$$

Note that this is a 'peak' value.

Oscillation frequency uncertainty

We assume in the absence of plant uncertainty the oscillation frequency may vary by $\pm 6\%$ due to parameter

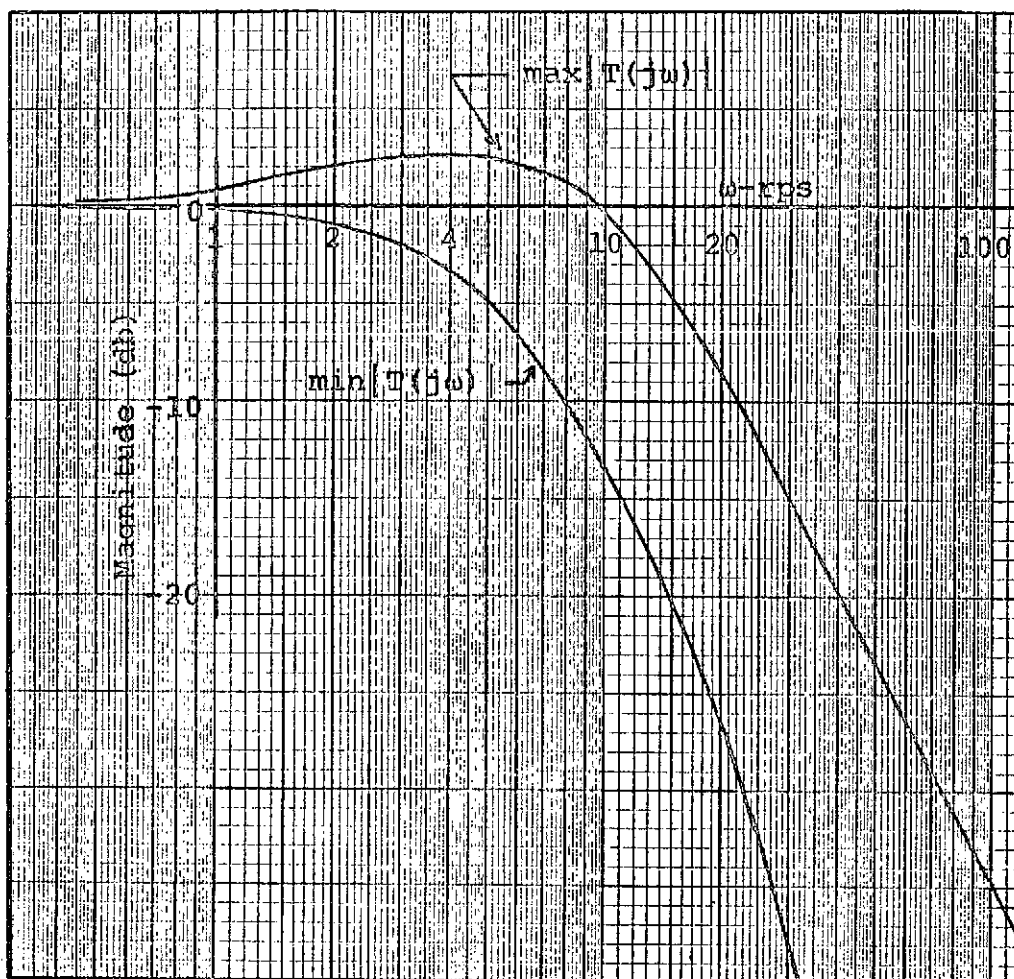


Fig. 5.3 Specification envelope for $|T(j\omega)|$.

variation in the compensating elements. Thus

$$\omega_0 \in [\omega_0'/\gamma_c, \gamma_c \omega_0'] = \Omega_c; \quad \gamma_c = 1.06, \quad (5.7)$$

when the plant parameters are fixed.

5.2 System Design

The first step is to determine the minimum oscillating frequency allowed by the transfer function sensitivity specification. This has been done in Sect.3.4,

and the minimum frequency found to be $\omega_0 = 13.4$ rps with variation parameter due to plant uncertainty of $\gamma_h = 1.17$. The data for this minimum bandwidth sensitivity design is given on Tables 3.3a & b.

Next the combined constraints of quasi-linearity (5.2) and output limit cycle limit (5.6) are considered. This part of the problem with the present specifications was treated in Sect. 2.4. There it was found that $\omega_0' = 28.2$ rps is an achievable oscillating frequency with a moderately complex limit cycle filter H , which is significantly better than is possible without the filter. This value of course takes precedence over the smaller value demanded by sensitivity.

Before proceeding with the design we need to consider two additional requirements on the oscillating frequency. First, recall that ω_0 must be high enough so that the assumed N_f is appropriate over the transfer function bandwidth. Fig. 5.3 shows that this bandwidth is permitted to range over approximately [4,13] rps. However, the actual variation will be considerably less because of the inherent SOAS property of removing nearly all high frequency gain variation (of course at high frequency N_f is ambiguous anyway, but the effect extends to the intermediate frequency range also). The crucial question is does the transfer function vary from 4 rps upward, or from 13 rps downward. The former is

true in the present problem because in Sect. 2.4 the extremes of plant and transfer function, T_e and P_{he} , used for the extreme X_e were the small gain-bandwidth cases. Thus $\omega'_0 = 28$ rps is judged to be sufficiently high for transfer function bandwidth requirements.

Lastly, ω'_0 must be large enough to render the sensitivity design meaningful. There is little question that 28 is sufficient, since the last sensitivity specification was at about 3 to 5 rps (Fig. 3.10). Thus we proceed to design for $\omega'_0 = 28$ rps.

The design value of $M_f G_2$ was determined in Sect. 2.4, and is obtained by multiplying Eq. 2.72 by the appropriate $\lambda = 1.22$ found in that section. The parameters are listed on Table 5.1.

Poles			Zeros		
p	ζ	ω	z	ζ	ω
6			10		
25					
25					
50					
50					
$K_0 = 220/M_f$			$K_\infty = 2.06 \times 10^8 / M_f$		

Table 5.1 Parameters of G_2 .

Now G_1 must be obtained such that the Nichols chart sensitivity boundaries are satisfied over the low and

intermediate frequency ranges, and so that the limit cycle is established about the chosen nominal $\omega_0 = 28$ rps. For this purpose it is easier to work with the entire loop compensation G , defined in Sect. 3.2 as $G_1 G_2$, and the forced signal equivalent plant P_f , i.e.,

$$L_f = G P_f, \quad (5.8)$$

$$P_f = \frac{M_f P_h}{|M_0 G(j\omega_0) P_h(j\omega_0)|} = K_f P_h. \quad (5.9)$$

A function for G which satisfies the sensitivity bounds, but sets ω_0 too small, is available from Table 3.3a. This function is modified, primarily by moving the complex pole pair near ω_0 up in frequency, enough to establish the new center oscillating frequency near 28 rps. This is again a cut and try process and the result is tabulated on Table 5.2. By increasing ω_0' significantly the spread of ω_0 variation is

Poles			Zeros		
p	ζ	ω	z	ζ	ω
	.5	27	4		
	.4	60	18		
	.4	100			
	.5	120			
$K_0 = 24$			$K_\infty = 1.26 \times 10^{14}$		

Table 5.2a Parameters of G for L_{f1} shown in Fig. 5.4.

ω_o	K_f	K_o	K_∞	a
26.9	1	24.0	1.26×10^{14}	1
27.6	1.03	8.26	1.30	3
28.4	1.07	5.14	1.35	5
29.1	1.11	3.82	1.40	7
30.0	1.19	2.85	1.49	10
$\omega_o^i = 28.4$		$\gamma_h = 1.057$		

Table 5.2b Parameters of L_f using G from Table 5.2a.

considerably reduced, as is the spread of K_f variation; both may be checked by comparing data from Table 3.3b and 5.2b. Recalling the iterative procedure for satisfying the sensitivity bounds, from Sect. 3.3, the new G has to be checked and possibly adjusted somewhat to insure that the final L_{f1} satisfies the bounds corresponding to the final G . Here only the completed design is given with the data of Table 5.2 and the plots on Fig. 5.4. In this figure $L_{f1} = GP_{h1}$ with $P_{h1} = 1/[s(s+1)]$. Frequency responses of L_f for several values of P_h are given in Fig. 5.5.

To extract G_1 , $L_{fe} = GP_{fe} = GK_{fe}P_{he} = \frac{M_f}{A_e} K_e G_1 G_2 P_{he}$.

Thus

$$G_1 = \frac{A_e K_{fe} G}{K_e M_f G_2} = \frac{q_x \alpha \lambda \omega_b K_{fe} G}{K_e M_f G_2} \quad (5.10)$$

Recall that $A_e = \alpha \lambda q_x \omega_b$ is the value of A when the plant is $P = K_e P_{he}$, where $K_e = 1$ was used for this

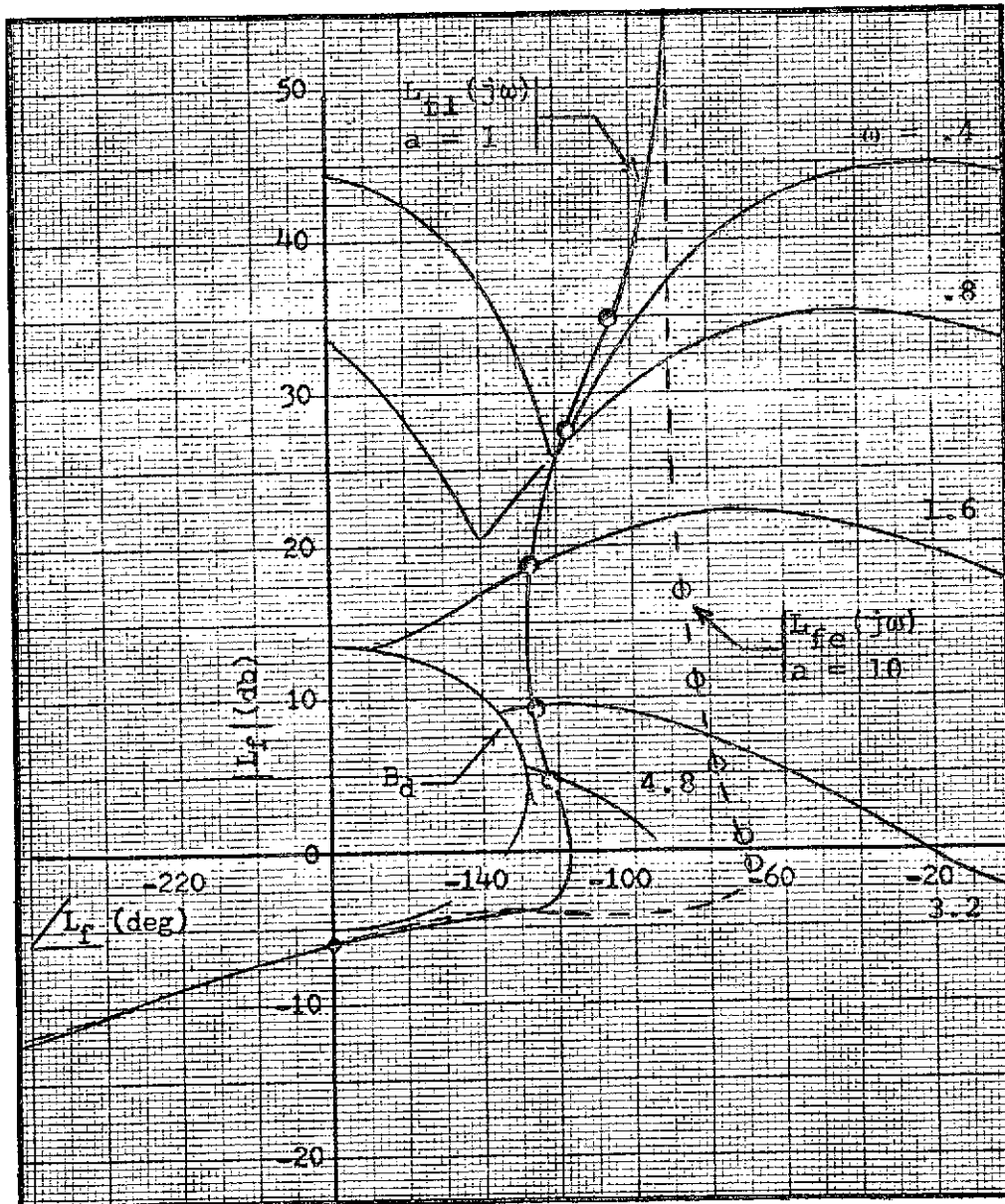


Fig. 5.4 Bounds for $L_{fl}(j\omega)$ and plot of $L_{fl}(j\omega)$ using G of Table 5.2.

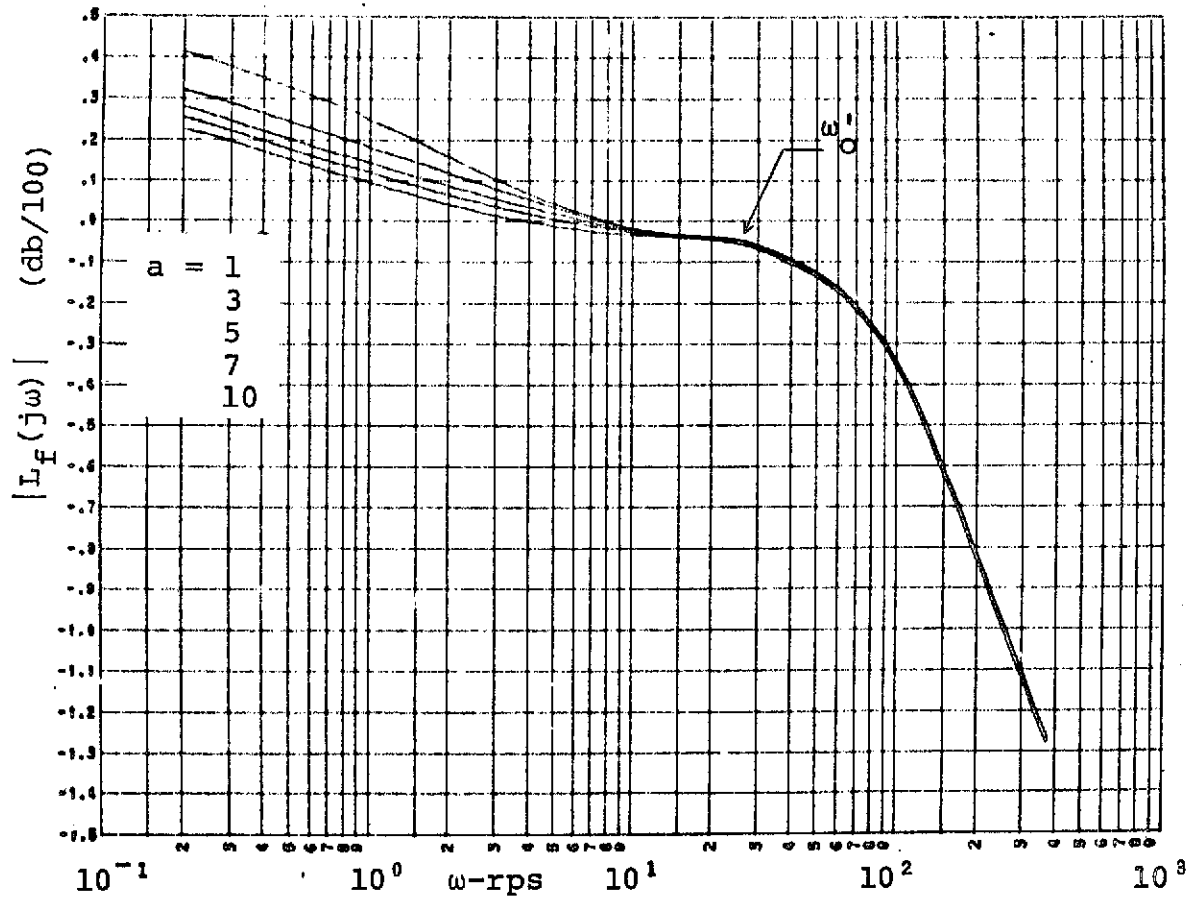


Fig. 5.5 Frequency responses of L_f .

design in Sect. 2.4. K_{fe} is the K_f from Table 5.2b that pairs with $P_{he} = 1/[s(s+10)]$ used in Sect. 2.4, i.e., $K_{fe} = 1.19$. Also from Sect. 2.4, $\lambda = 1.22$ and $\omega_b = 6$. $M_f G_2$ and G are given by Tables 5.1 and 5.2a respectively. Collecting the data, G_1 has the parameters tabulated on Table 5.3. For completeness

Poles			Zeros		
p	ζ	ω	z	ζ	ω
10	.5	27	4		
	.4	60	6		
	.4	100	18		
	.4	120	25		
			25		
			50		
		50			
$K_O = .95q_x$			$K_\infty = 5.32q_x \times 10^6$		
$= .13A_e$			$= 7.27A_e \times 10^5$		

Table 5.3 Parameters of G_1 .

the parameters of H are given in Table 5.4.

The system prefilter F is obtained from

$$F = T_e (1 + L_{fe}) / L_{fe}, \quad (5.11)$$

where

$$T_e = \frac{(6)^2 (25)^2 (50)^2}{(s+6)^2 (s+25)^2 (s+50)^2}. \quad (5.12)$$

Poles			Zeros		
p	ζ	ω	z	ζ	ω
	.08	22		.025	25.6
	.08	35		.04	30.5
$K_0 = .838$			$K_\infty = .82$		

Table 5.4 Parameters of H.

This T_e is the lower bound in Fig. 5.3 and the extreme transfer function used in Sect. 2.4. The parameters of $L_{fe}/(1+L_{fe})$ are listed in Table 5.5. One

Poles			Zeros		
p	ζ	ω	z	ζ	ω
1.88	.194	28.3	4		
12.7	.511	64	18		
	.379	98			
	.499	121			
$K_0 = 1$			$K_\infty = 1.49 \times 10^{14}$		

Table 5.5 Parameters of $L_{fe}/(1+L_{fe})$.

finds F in (5.11) with 10 zeros and 8 poles, hence unrealizable. We assign additional pole pairs to X_e and T_e at 98 and 121 rps with damping factors to cancel these zeros of $1 + L_{fe}$. These poles are sufficiently far off that they should have no appreciable effect on the time responses $x_f(t)$ or $c(t)$.

Poles			Zeros		
p	ζ	ω	z	ζ	ω
4			1.88	.194	28.3
6			12.7	.511	64
6					
18					
25					
25					
50					
50					
$K_o = 1$			$K_\infty = 51.7$		

Table 5.6 Parameters of F.

The resultant prefilter is given by Table 5.6. The design is now finished, with all functions in Fig. 5.1 completely identified except for the selection of q_x or A_e .

Before proceeding to simulation of the completed design we can do some verification by using the quasi-linear model, i.e., we calculate the linear response functions for Fig. 5.1 when N is replaced by the gain factor M_f/A . The particular A that goes with a given plant is accounted for by using the appropriate gain factors from Table 5.2b. First the transfer functions $T(j\omega)$ are calculated and the magnitudes are shown by Fig. 5.6. In this figure the lower response ($a = 10$) is identically T_e which is also the lower

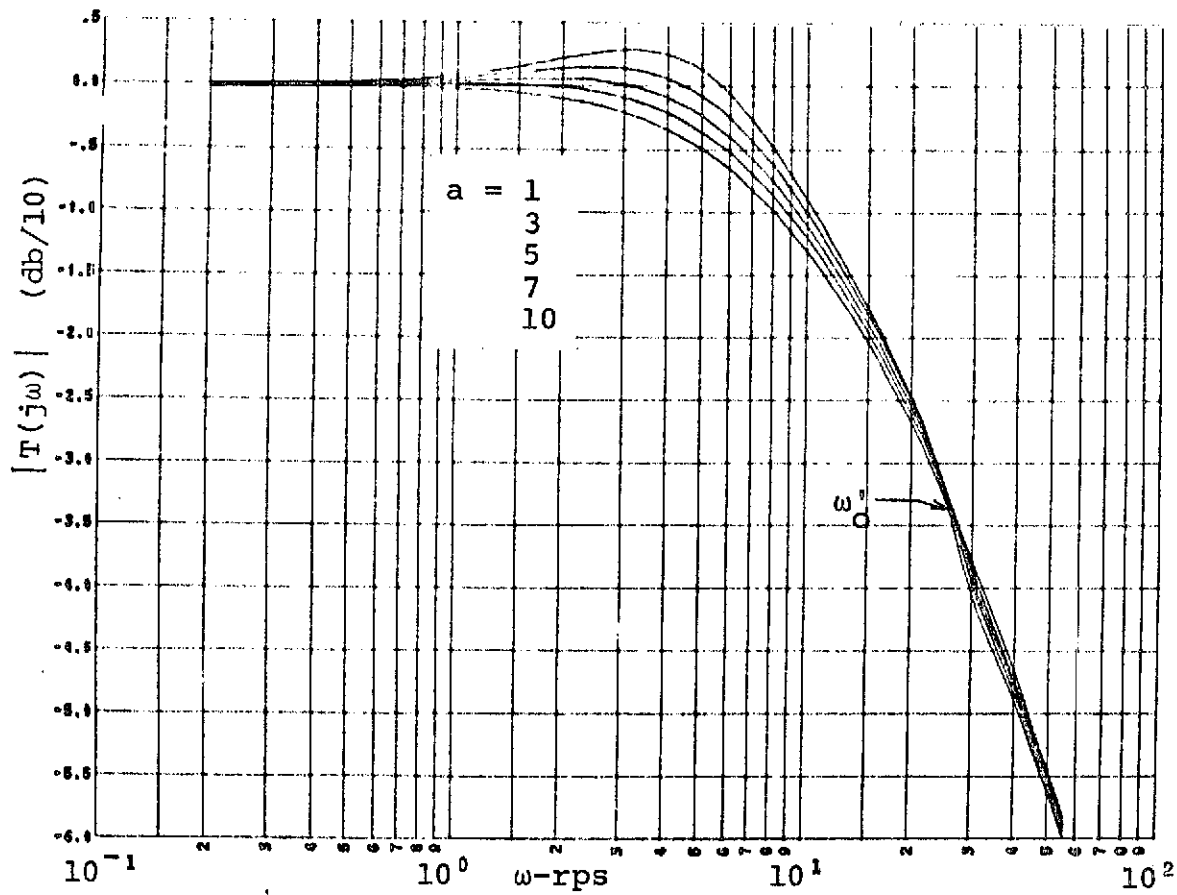


Fig. 5.6 Equivalent linear transfer functions for several plant values.

bound in Fig. 5.3. The upper bound ($a = 1$) is very close to the upper bound of Fig. 5.3 up to about 5 rps and then falls below the specification bound. Thus our goal of barely achieving the sensitivity specifications is met and not exceeded except at higher frequencies where it is unavoidable (and where $T(j\omega)$ is ambiguous). Finally we verify that the bandwidth, -3db point, lies within [3.5,7.5] rps which seems compatible with $\omega'_0 = 28$ rps.

Shown in Fig. 5.7 are the system outputs $c(t)$, which will be useful in evaluating simulation results later. For $a = 1$ the overshoot is rather large ($\approx 35\%$), but this is permitted by the transfer function specifications.

Next, shown in Fig. 5.8 are several $x_f(t)$. From these we can check the validity of the selections made for P_{he} and T_e when designing the limit cycle filter in Sect. 2.4, i.e., does the a priori selection made truly yield the largest and/or fastest $x_f(t)$. Figure 5.8d permits easy comparison. At small t they are identical since for large ω in the frequency domain the $X_f(j\omega)$ are identical. For larger t the designed $x_e(t)$ ($a = 10$) consistently has larger magnitude peaks than the remaining two signals. It does not seem possible to detect any meaningful difference in speed of the $x_f(t)$ by simple inspection of Fig. 5.8.

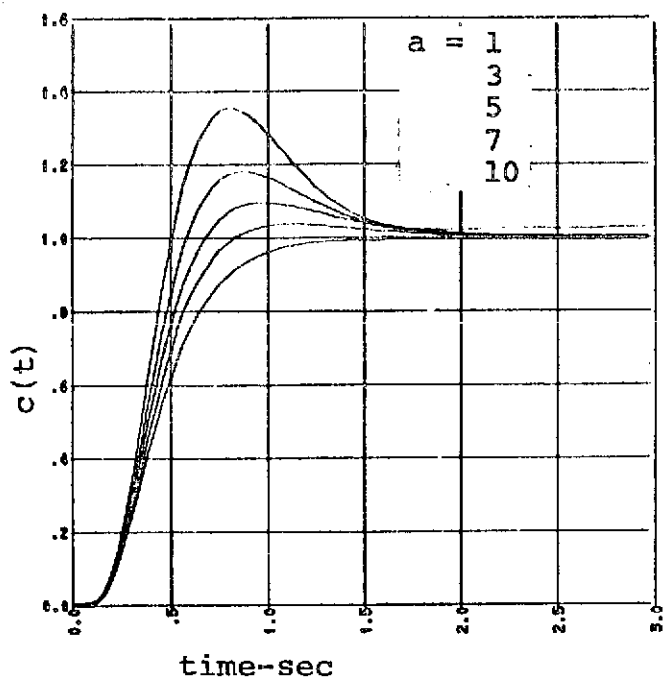


Fig. 5.7 $c(t)$ obtained with unit step input and transfer functions in Fig. 5.6.

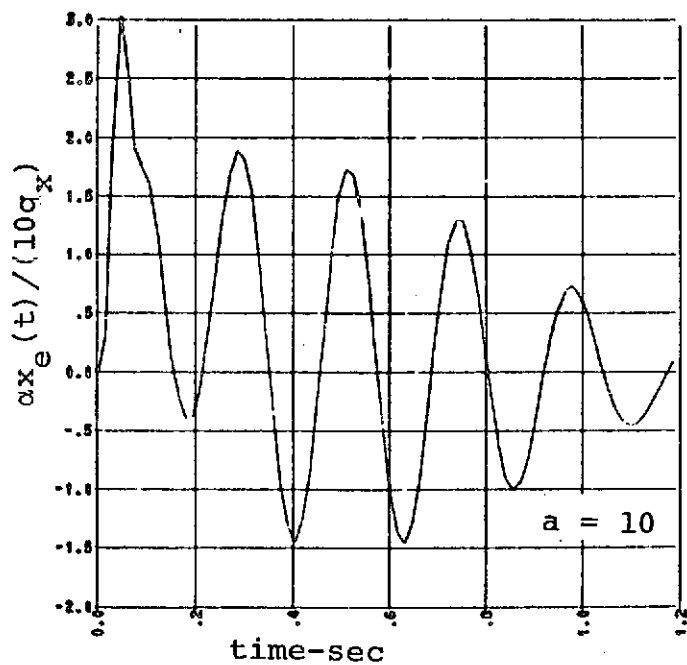
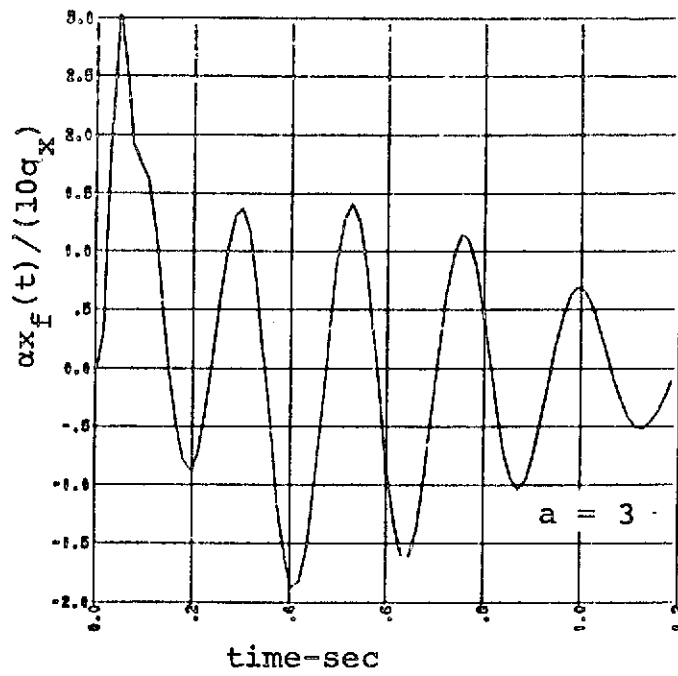
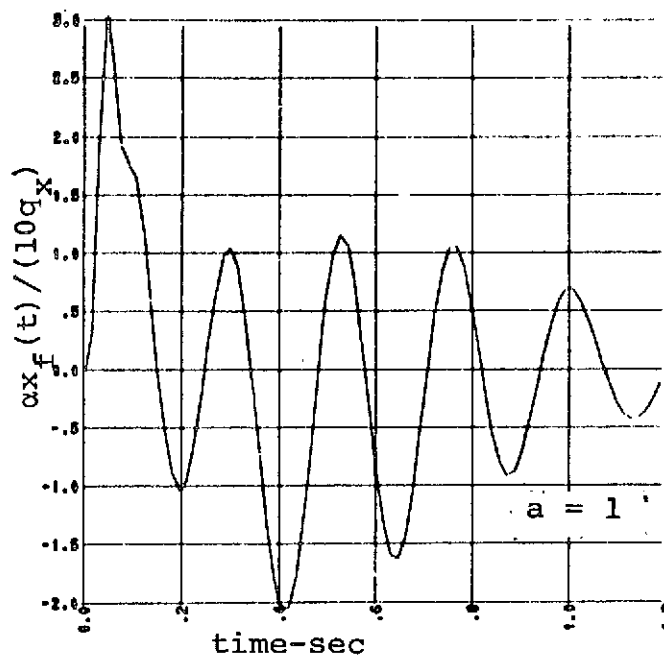


Fig. 5.8a Design value of extreme $x_e(t)$.



(b)



(c)

Fig. 5.8 (cont) Additional values of $x_f(t)$.

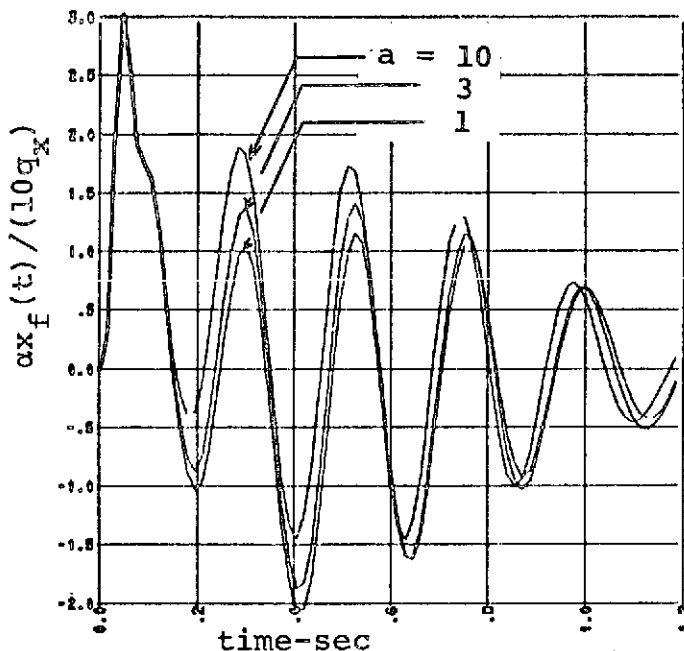


Fig. 5.8d Simultaneous plots of $x_f(t)$.

The conclusion drawn is that the selections of P_{he} , T_e are quite satisfactory. However, the change in $x_f(t)$ with P_h in the present example is rather small so the selection of P_{he} is probably not a critical factor in this design. Note that the proper pairing of T_e with P_{he} is verified by Fig. 5.6. That is, we designed the transfer function T_e on the lower specification bound so that for values of P_h other than P_{he} , $|T(j\omega)|$ should increase, as it does in Fig. 5.6. Finally let us compare the resultant $x_e(t)$ in Fig. 5.8a with the design value in Sect. 2.4, Fig. 2.12. The two signals are identical after an initial transient in

Fig. 5.8a which is the effect of the added far poles. This transient does exceed the Sect. 2.4 design value of $\alpha \max_t |x_e(t)| = 22$. by about 35%. This narrow pulse should not cause any appreciable effect on the output $c(t)$, because even if the nonlinear element does transmit it, the smoothing effect of the plant integrator will essentially remove it from the system output.

5.3 Digital Simulation of Command Response

The system design of the previous section was simulated using the MIMIC digital simulation language as adapted for the CDC 6400 computer.

It is noteworthy that the simulation was first attempted with an ideal relay nonlinearity. In propagating the limit cycle through the ideal relay the zero-crossing times must be detected with rather high accuracy, and errors in the detection produce low frequency transients, or ideally subharmonics, in the nonlinearity output signal. The difficulty is highly accentuated in the oscillating system because of the extremely high low frequency gain compared to the gain at the limit cycle frequency ω_0 (see Fig. 2.9) between the nonlinearity output and the system output. This causes the low frequency error terms to be greatly amplified at the system output, and these components swamp out the limit cycle signal. The net result was that an

extremely small digital simulation integration step size was required, making the simulation very expensive in terms of computer running time. This difficulty was removed by changing the nonlinear element to a saturation. For an ideal relay with output level M the output error is $2M$ when the simulation fails to detect a zero crossing. For saturation, the output error will be proportional to the time increment by which the zero-crossing is missed, and therefore reduces rapidly with integration step size, making it possible to execute the simulation at reasonable cost. The lesson of this experience is that, although the synthesis is independent of the particular nonlinearity used, there will indeed be practical considerations that give some nonlinearities advantages over others in a given application.

Shown below are simulation results using a saturation nonlinearity with the parameters listed on Fig.5.2, and using $q_x = 1$, $A_e = \lambda \alpha q_x \omega_b = 22$. The system input is a unit step $R_e(s) = q_r/s = 1/s$ in all cases. Fig. 5.9 shows the output from prefilter F of Fig.5.1. This signal is of course the same for all plant parameter cases. Figure 5.10 shows the nonlinearity input signal for two parameter cases. The forced signal component $x_f(t)$ is essentially indistinguishable in these plots. The system output $c(t)$ is shown for several plant parameter cases in Fig. 5.11. Comparison of these step

responses with those of Fig. 5.7 shows that the non-linear system response closely approximates the response of the quasi-linear approximation used in synthesis. The specified limit cycle magnitude has been scaled on several plots of Fig. 5.11 and shows satisfactory agreement with the observed limit cycle.

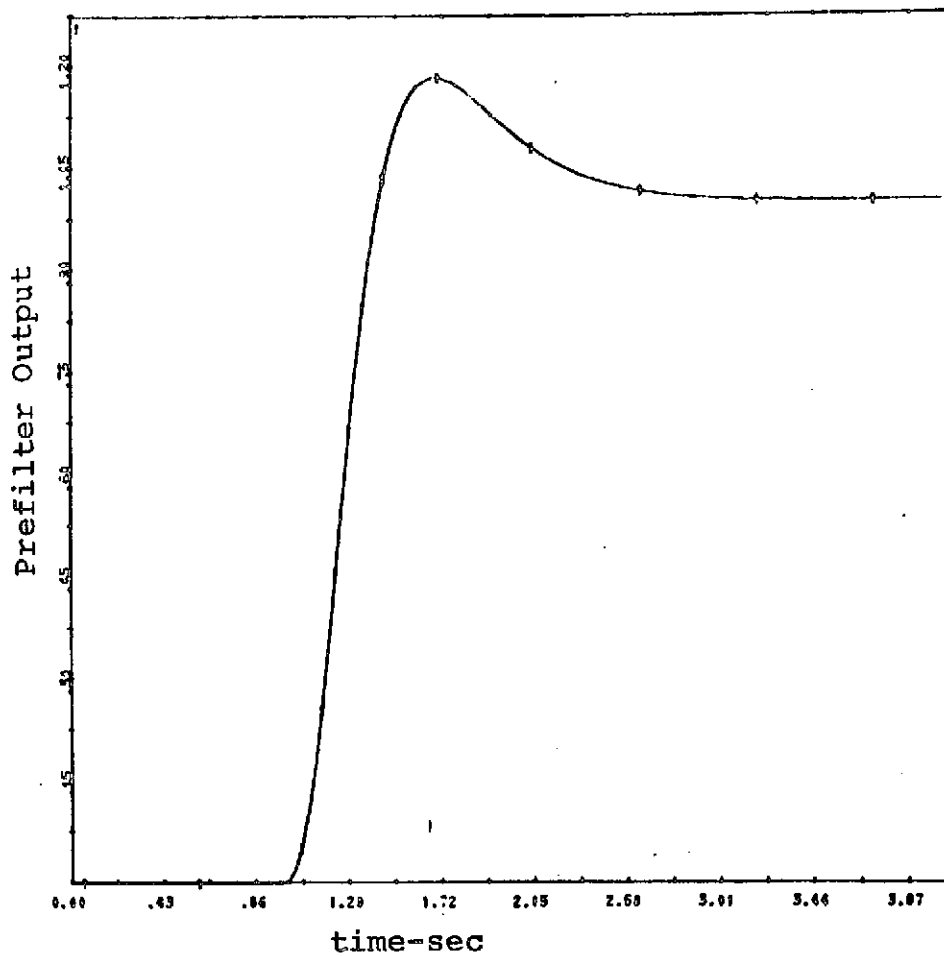


Fig. 5.9 Digital simulation plot of prefilter F output.

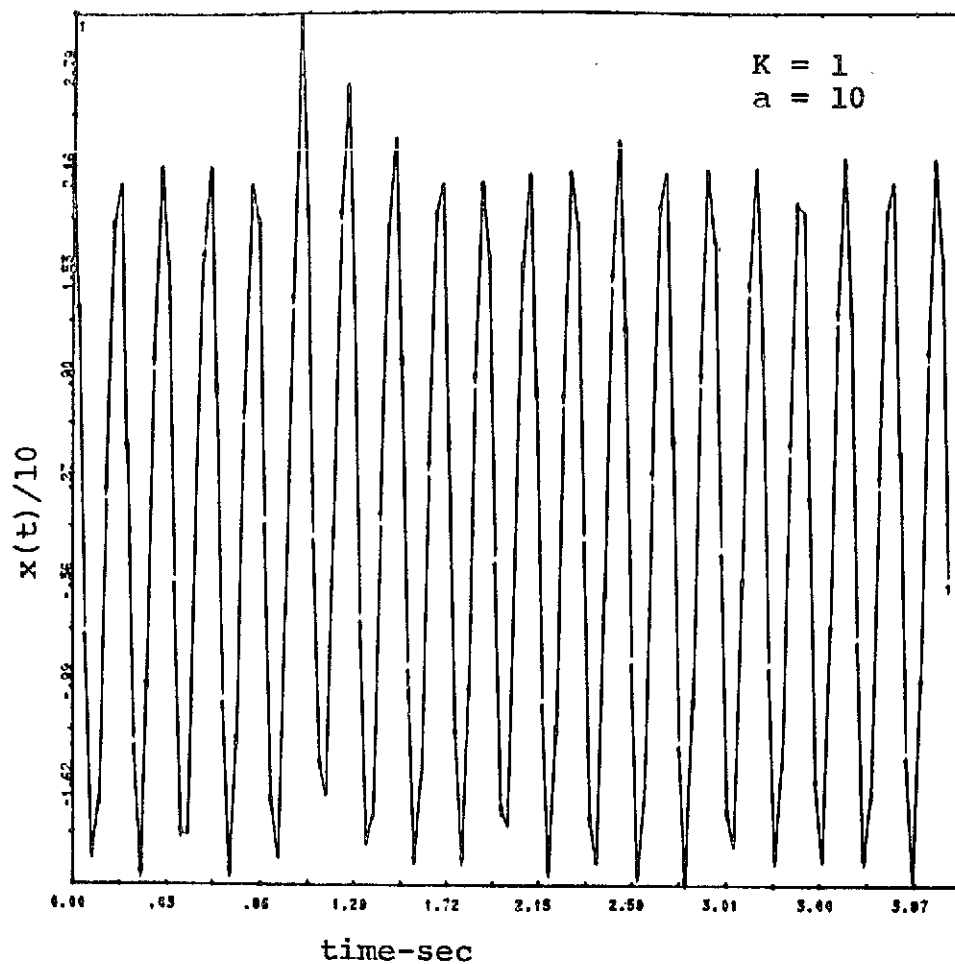


Fig. 5.10a Digital simulation plot of nonlinearity input function.

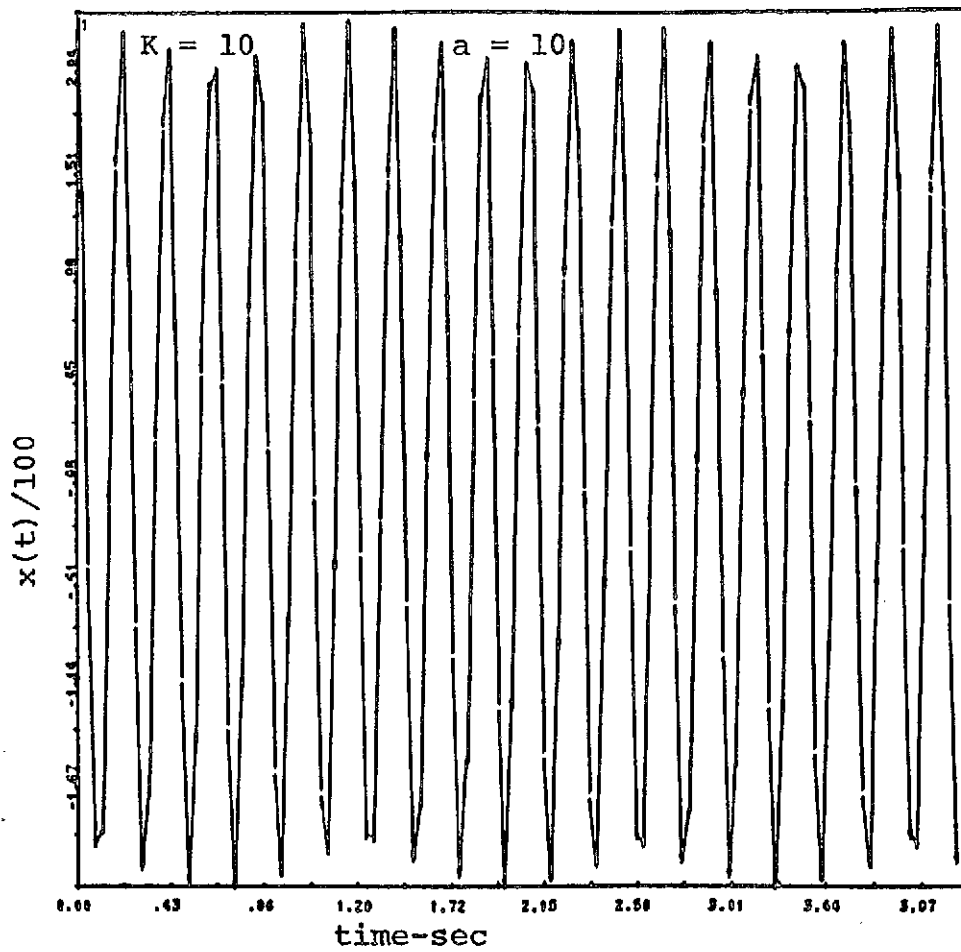


Fig. 5.10b Digital simulation plot of nonlinearity input function.

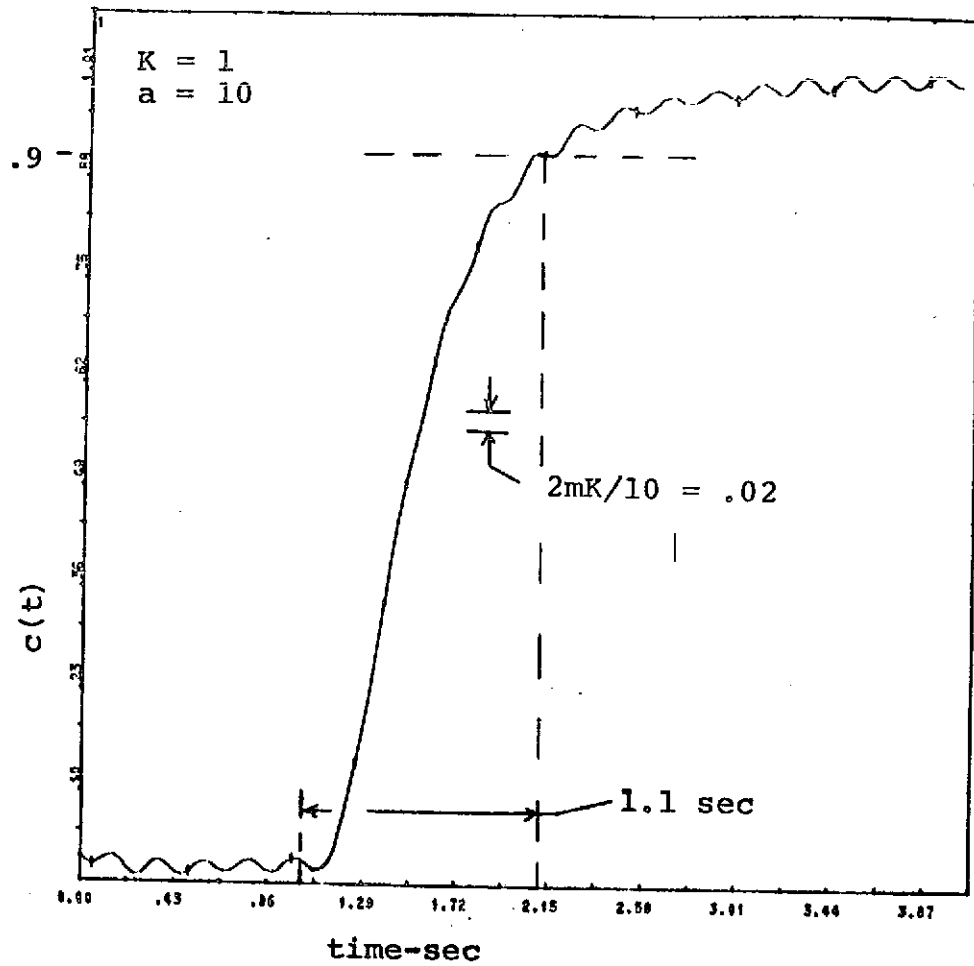


Fig. 5.11a System response to unit step applied at $t = 1.0$ sec.

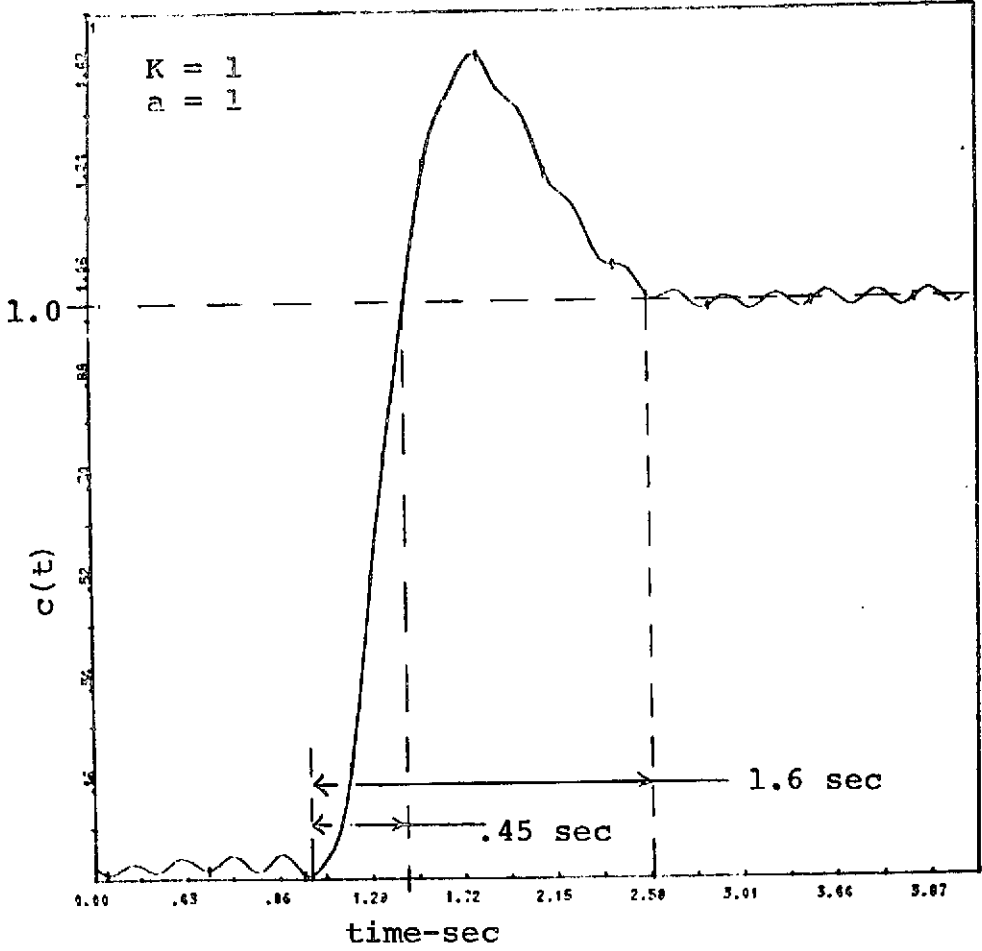


Fig. 5.11b System response to unit step applied at $t = 1$. sec.

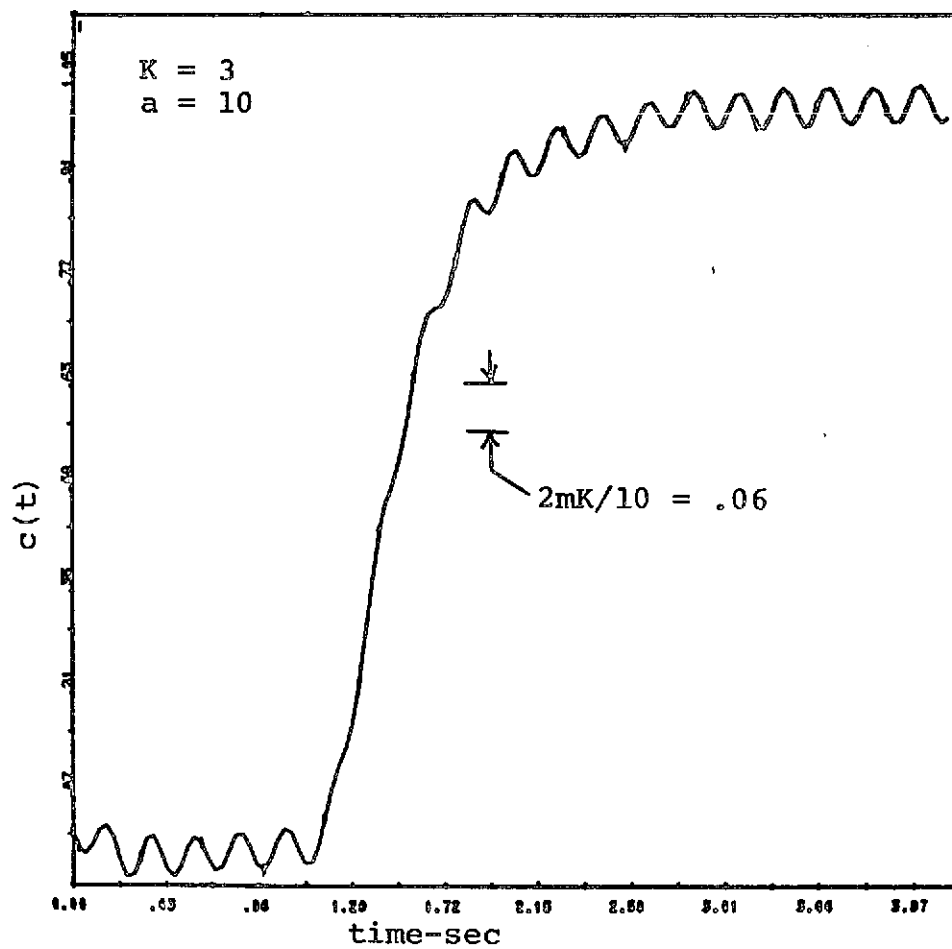


Figure 5.11c System response to unit step applied at $t = 1.0$ sec.

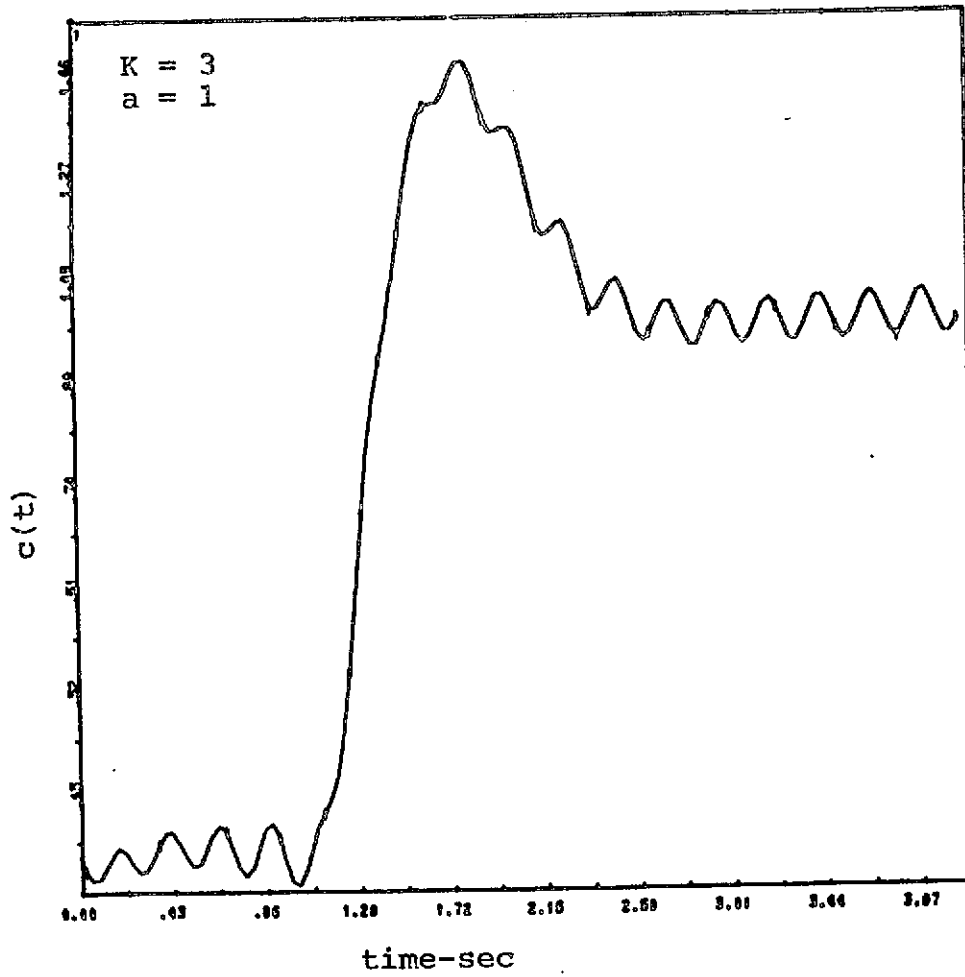


Fig. 5.11d System response to unit step applied at $t = 1.0$ sec.

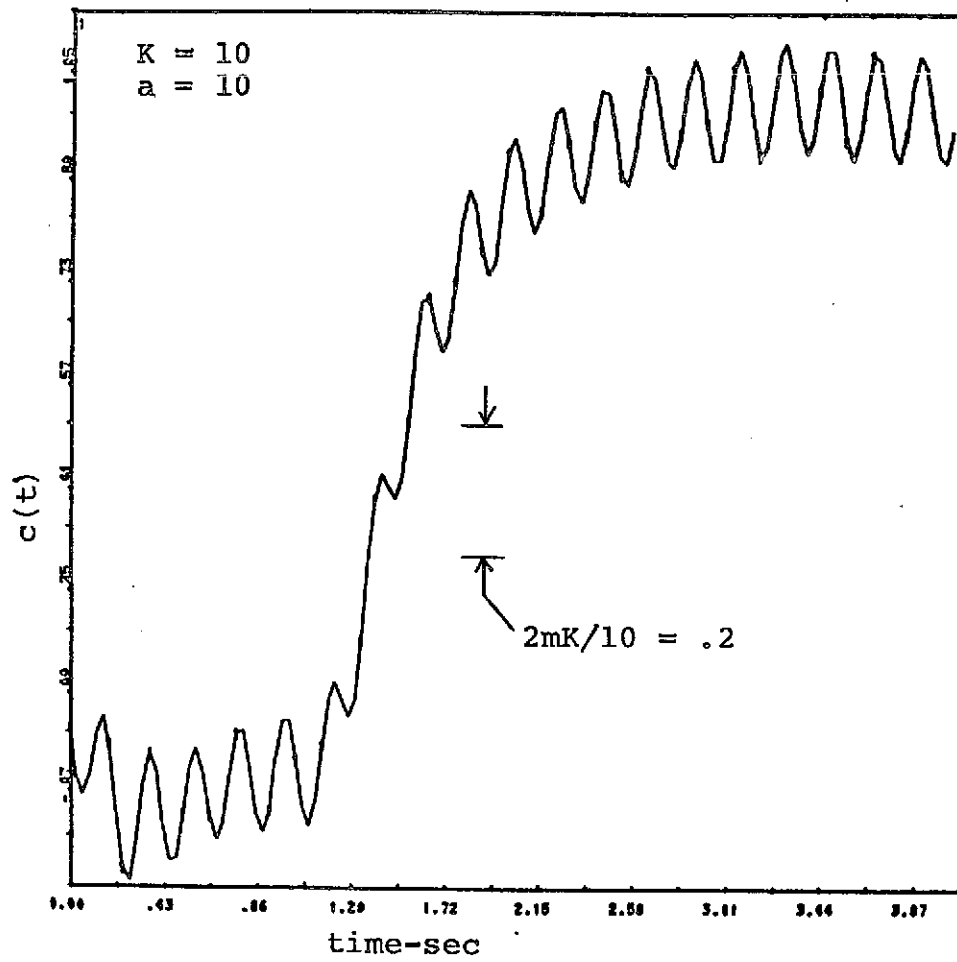


Fig. 5.11e System response to unit step applied at $t = 1.0$ sec.

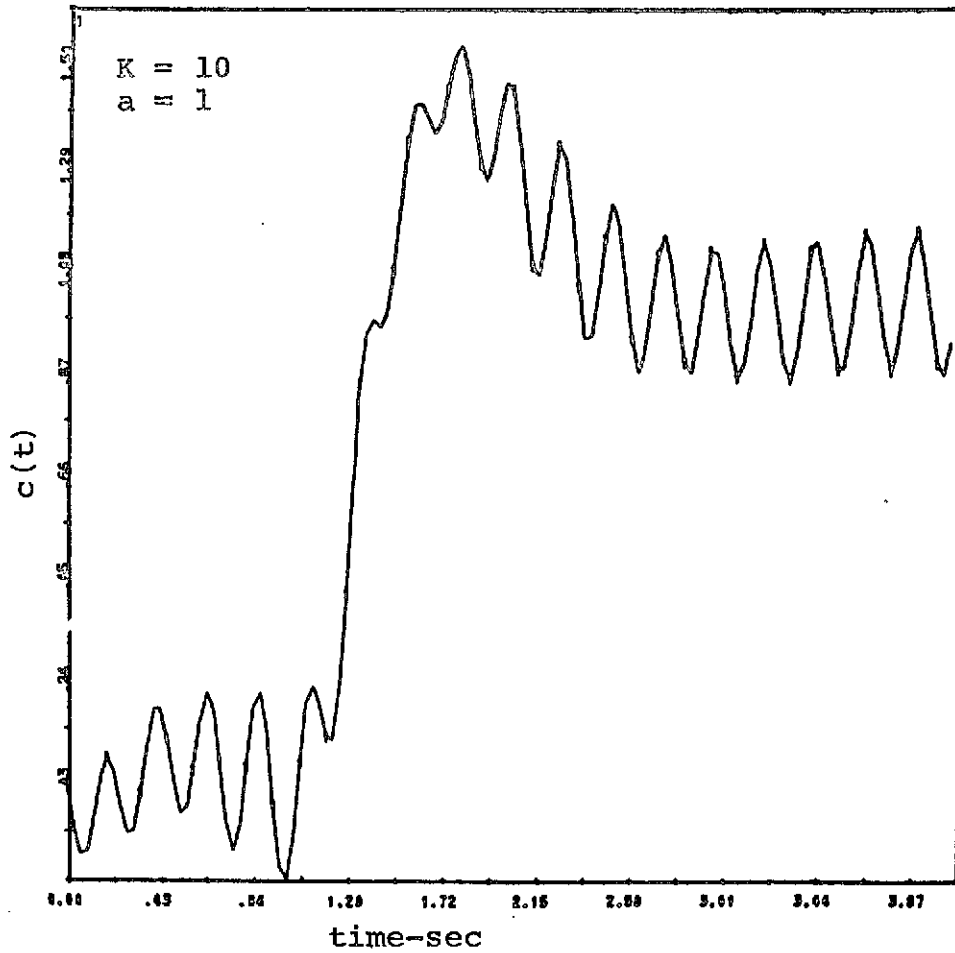


Fig. 5.11f System response to unit step applied at $t = 1$. sec.

5.4 Digital Simulation of Disturbance Response

This section presents some disturbance response simulation results obtained from the system design of Sect. 5.2. Any evaluation of these results must be rather qualitative, since the design does not conform to any specifications on the disturbance response. Nevertheless, they do provide useful information about system performance for disturbance inputs. All simulations were performed with $P(s) = K_1 P_{he}(s) = 1/[s(s+10)]$, because this parameter set is the worst case in terms of magnitude quasi-linearity constraint (5.2a).

It is obvious from the treatment in Chapter IV that the system will not be quasi-linear in the presence of a unit step disturbance. Regardless, a unit step input, $D = q_d/s = -1/s$ in Fig. 5.1, was simulated and the resultant system output is shown in Fig. 5.12. In Fig. 5.12b the disturbance input is applied at one half the limit cycle period (π/ω_0) later than in Fig. 5.12a. The radical difference in the two responses demonstrates the well known phenomenon that the oscillating system response is time dependent when the quasi-linearity constraints are violated. Both responses exhibit a predominant time constant τ which is believed to be the time required to return to quasi-linear operation. Later plots show this time constant to be dependent on the magnitude of step input. Both responses of Fig. 5.12 appear quite undesirable for most applications.

Next, a smaller step, $q_d = -.025$, was simulated. The magnitude of this input was obtained by using the design values of X_{el} , P_{he} , P_{hm} , H , and other required parameters from this chapter in Eq. 4.21. Evaluating this equation at $\omega_o = 30$ rps (corresponding to P_{he} from Table 5.2b), the given q_d is obtained. This does not guarantee quasi-linear performance however, because the present design values of G_1 , G_2 , and H have not been selected to produce quasi-linear operation for any step disturbance input. In Fig. 5.13 the frequency responses of the forced input to N are compared for $R_e = 1/s$ and $D_e = -.025/s$. It is observed that the signal due to D_e is rich in frequency components above ω_o . This will be the case irrespective of the step magnitude, i.e., a step disturbance input can be made small enough to satisfy the magnitude quasi-linearity constraint, but the frequency constraint cannot be satisfied. Fig. 5.14 shows simulated outputs for the input $D_e = -.025/s$. These exhibit time dependence and overshoots an order of magnitude greater than the input, hence they are quite undesirable responses.

We know that if the signal $f(t) \equiv \mathcal{L}^{-1}[R_e(s)F(s)]$ is applied as a disturbance input, then $x_e(t)$ will be the same as for command inputs. The signal $f(t)$ is shown in Fig. 5.9. This signal was time scaled to increase its speed by factors of $\sqrt{2}$ and 2, and applied as

a disturbance input in the digital simulation. The system outputs obtained are shown in Fig. 5.15, and appear quite reasonable.

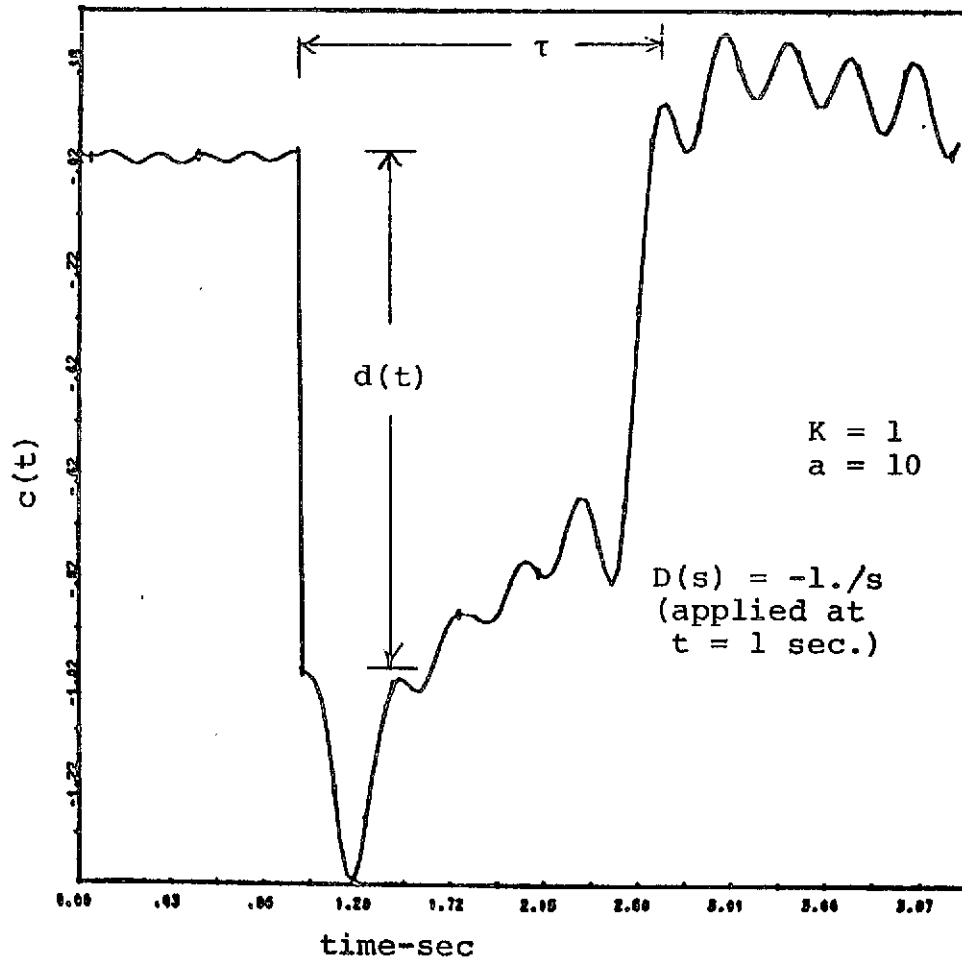


Fig. 5.12a System output for unit step disturbance.

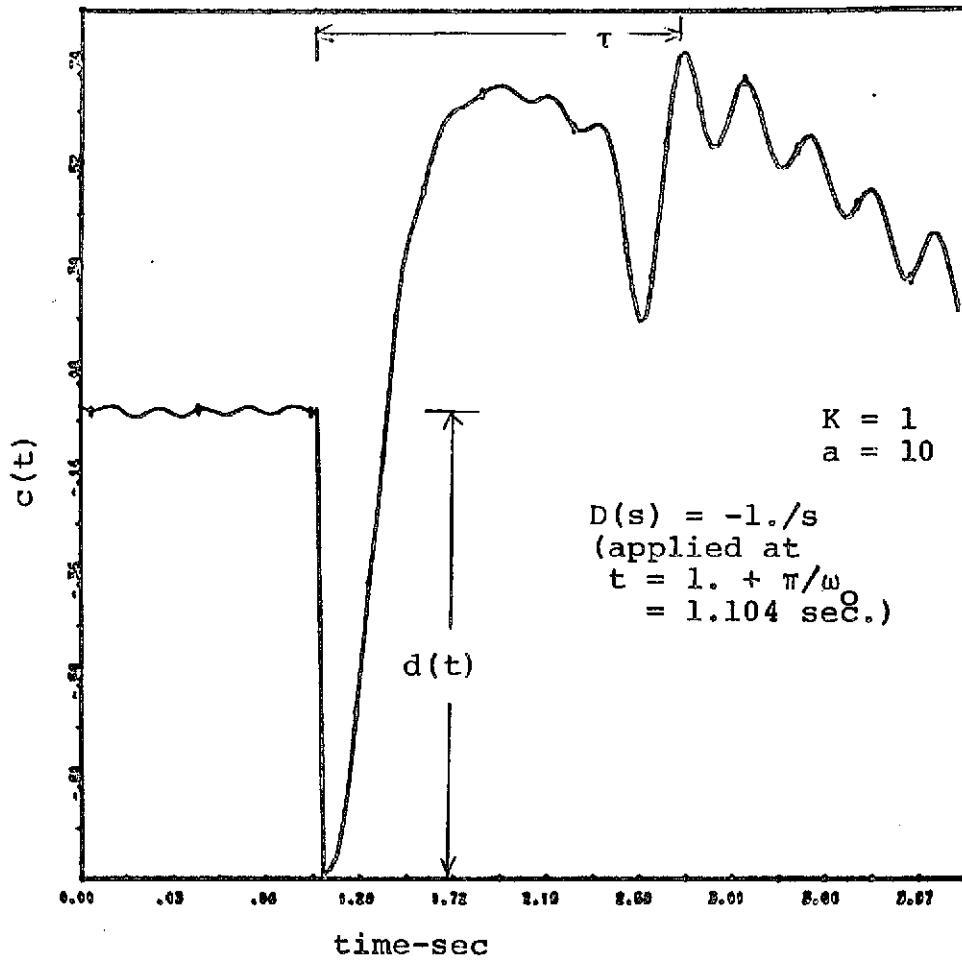


Fig. 5.12b System output for unit step disturbance.

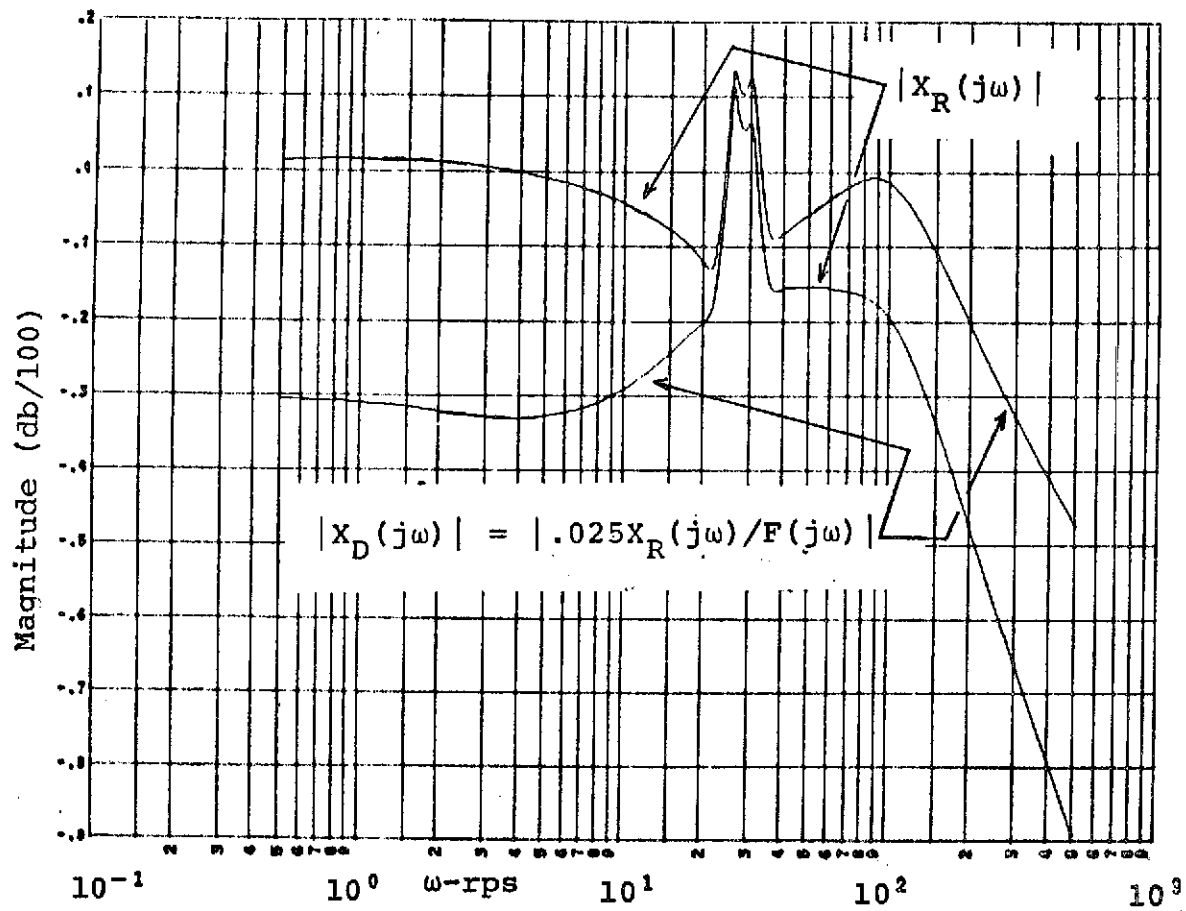


Fig. 5.13 Comparison of nonlinearity forced signal input for step command and disturbance system inputs.

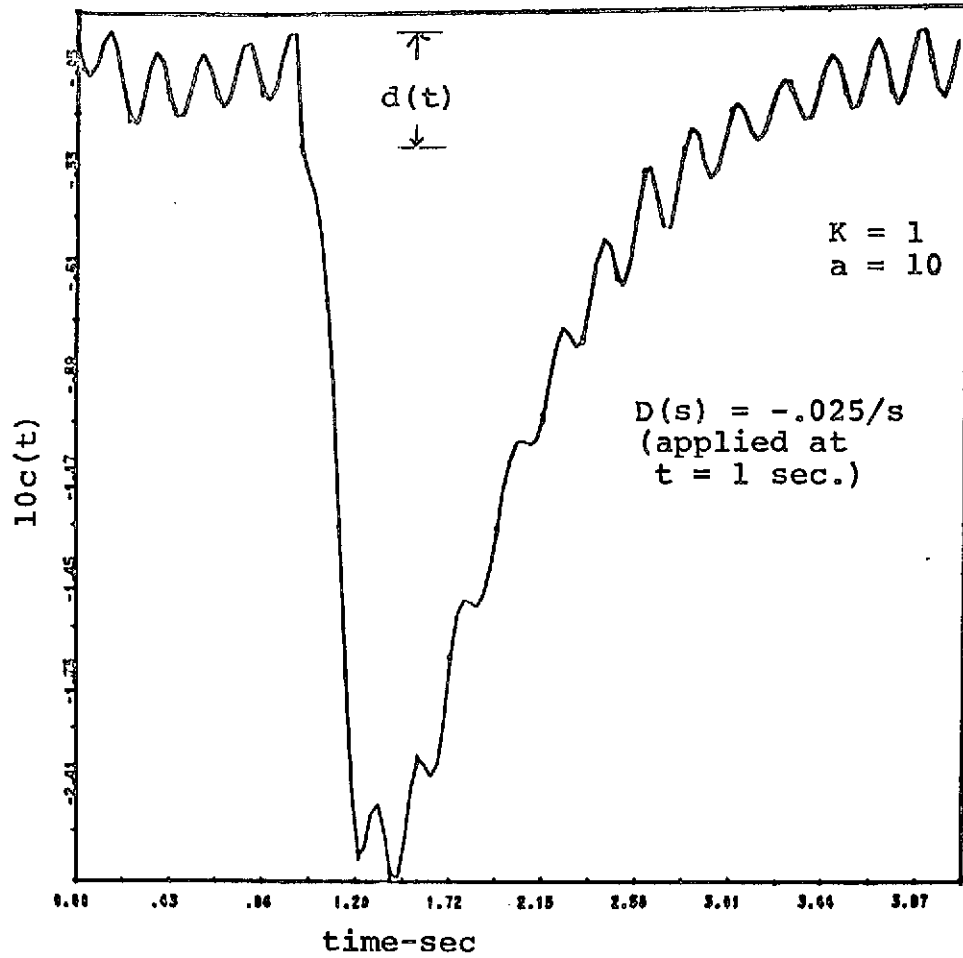


Fig. 5.14a System output for step disturbance input.

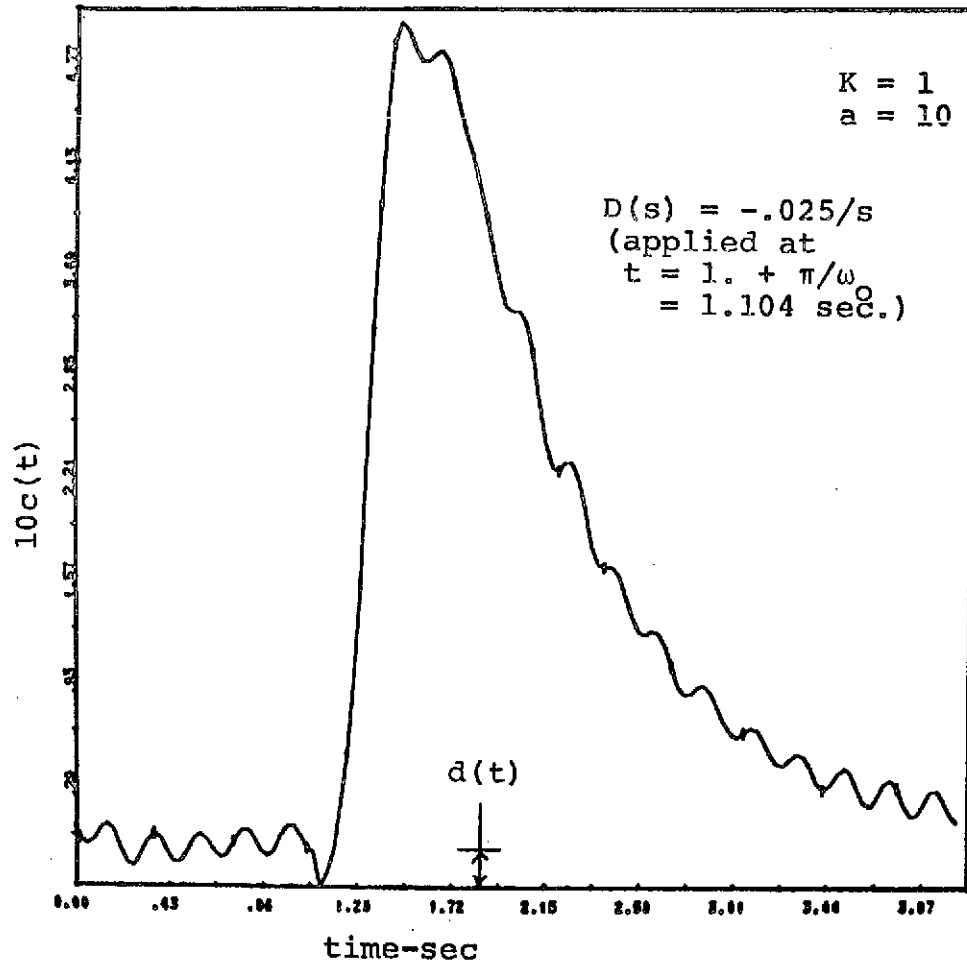


Fig. 5.14b System output for step disturbance input.

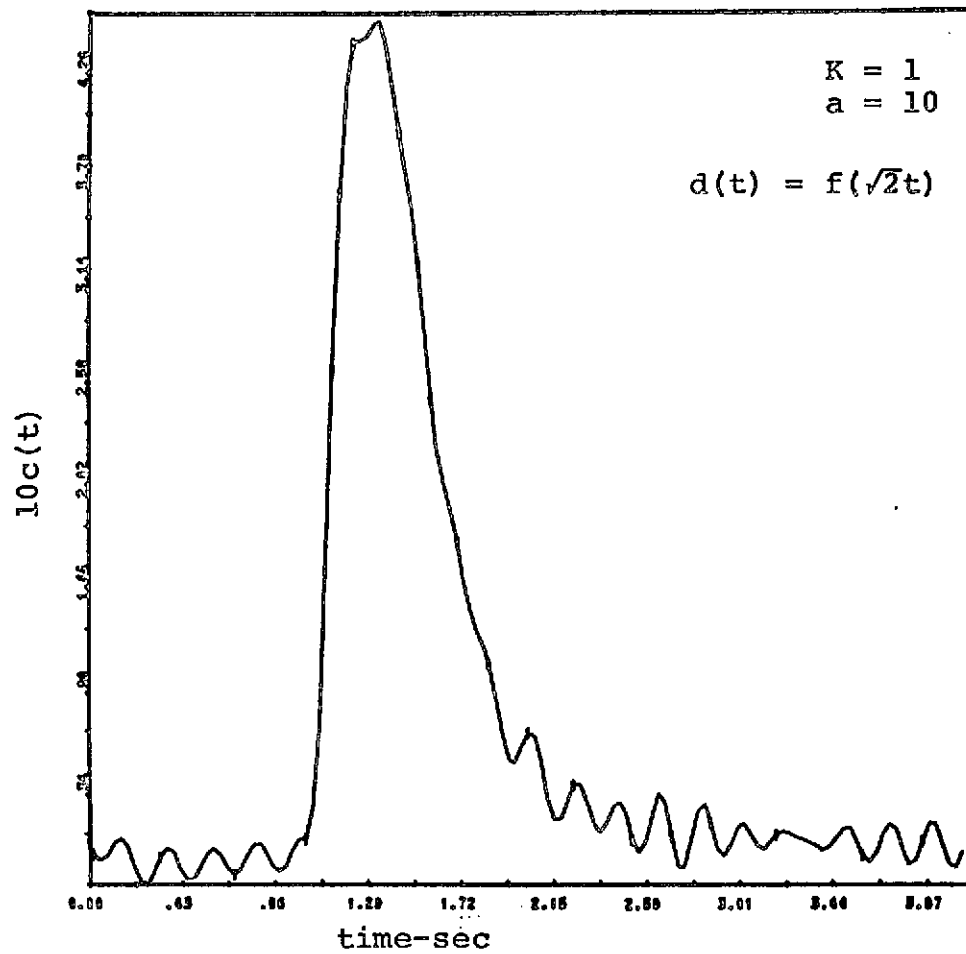


Fig. 5.15a System response to disturbance $f(\sqrt{2}t)$.

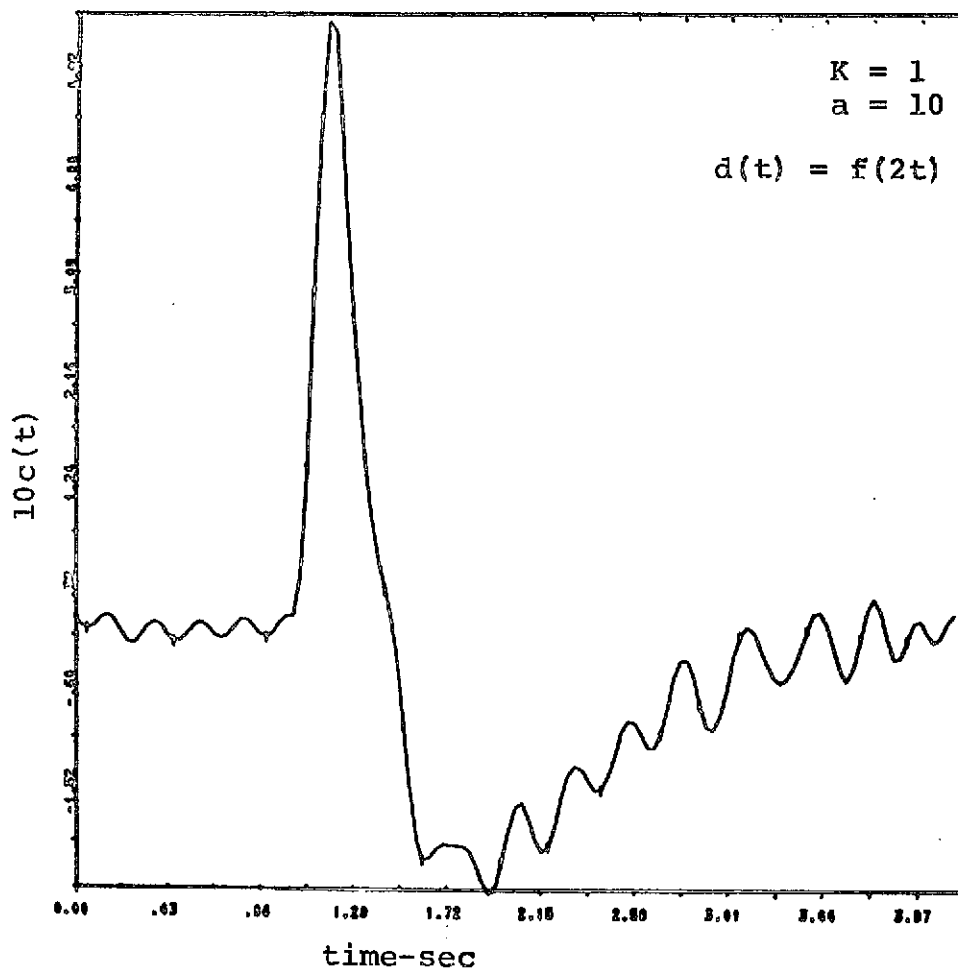


Fig. 5.15b System response to disturbance $f(2t)$.

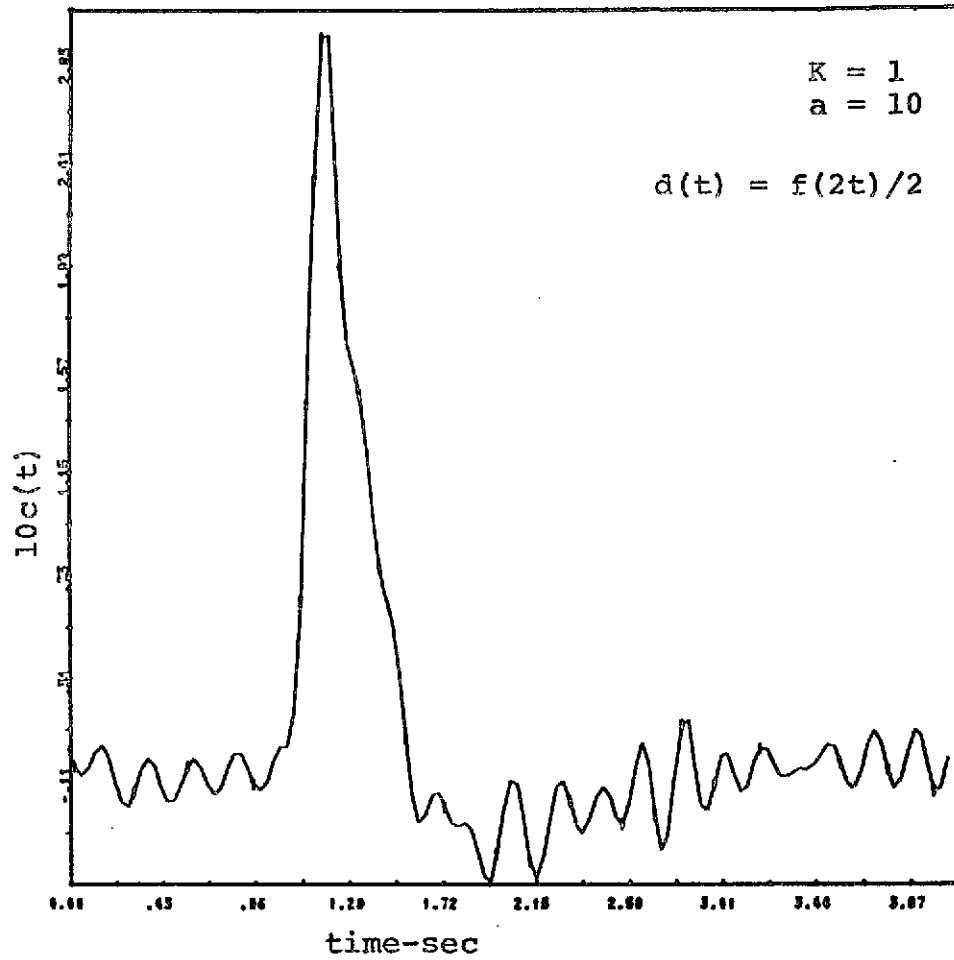


Fig. 5.15c System response to disturbance $f(2t)/2$.

CHAPTER VI
 SYNTHESIS OF AN EXTERNALLY
 EXCITED OSCILLATING ADAPTIVE SYSTEM

6.1 Introduction

It is possible, with the proper type of nonlinear element, to externally excite the oscillating signal which circulates in an oscillating feedback system rather than using the limit cycle which occurs naturally in the SOAS. Such a system, discussed below, will be termed an externally excited oscillating adaptive system (EEAS). The two degree-of-freedom feedback structure to be used is depicted in Fig. 6.1. A_0 is a zero mean periodic excitation signal of frequency ω_0 which we take to be sinusoidal. This input need not be sinusoidal provided $G_1 G_2 P$ is of sufficient low pass character to maintain the validity of the describing function used for N . F , G_1 , and G_2 are linear time-invariant compensations to be synthesized, and P is the plant or constrained

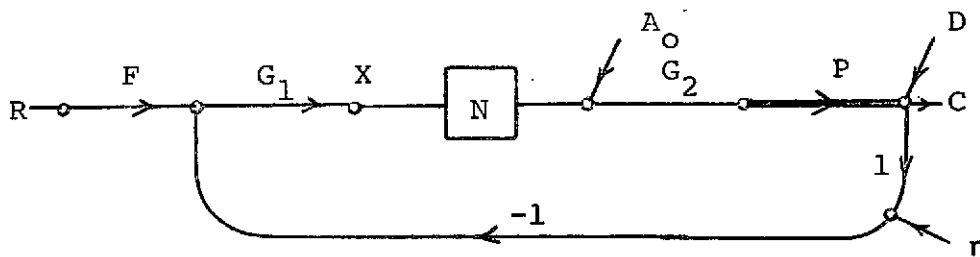


Fig. 6.1 EEAS feedback structure

part of the system for which parameter ignorance as detailed in Sect. 1.3, Eq. 1.17, is assumed. The generality and limitations of this structure have been pointed out in Sect. 1.3.

System performance specifications and optimization criterion for the EEAS are identical to those taken for the SOAS and stated in Sects. 1.3 and 1.4 respectively.

With the exception of one new constraint, to be developed in the following section, it will be observed that the EEAS synthesis methods developed below in large measure parallel those for the SOAS.

6.2 EEAS Nonlinear Element

At the outset it is required that the nonlinear element N in the EEAS possess all the properties required for the SOAS. These properties were treated in Sect. 1.2. In particular it is necessary that the DIDF components

$$N_o \approx M_o/A \quad (6.1a)$$

$$N_f \approx M_f/A \quad (6.1b)$$

represent a satisfactory quasi-linear approximator when

$$\max_t |x_f(t)| \leq A/\alpha, \quad (6.2a)$$

and

$$\omega_b \leq \omega_o/\beta. \quad (6.2b)$$

All quantities in the preceding two equations are as previously defined, e.g., in Sect. 1.2, Eq. 1.7 and 1.8.

If A_0 is zero or sufficiently small in Fig. 6.1, and the loop transmission has in excess of 180° phase lag, then the system will self-oscillate. Indeed, with $A_0 = 0$, we have the SOAS treated in the preceding chapters. Thus if the DIDF in (6.1) is to be used, the system must be synthesized under conditions that prevent the occurrence of the natural limit cycle, i.e., there must be only one sinusoidal input at N . We shall give sufficient conditions for limit cycle quenching below.

Assume there are two sinusoidal inputs to N giving $x(t) = A \sin \omega_0 t + B \sin \omega_\pi t$, where ω_π is the limit cycle frequency and ω_0 is the frequency of the excitation A_0 . Using the techniques of Sect. 1.2, the two sinusoid input describing function (TSIDF) may be calculated by repeated application of Eq. 1.4b, and the components labeled $N_A(A,B)$ and $N_B(A,B)$. Letting L_B denote the loop transmission seen by the $B \sin \omega_\pi t$ component, the limit cycle will be quenched provided

$$|L_B(j\omega_\pi)| < 1. \quad (6.3)$$

Suppose that $\max_B |N_B(A,B)| \equiv \xi(A)$ exists and is finite. Then the limit cycle quenching condition may be written

$$\xi(A) |G_1(j\omega_\pi)G_2(j\omega_\pi)P(j\omega_\pi)| < 1; \forall P. \quad (6.4)$$

In general this condition may be quite complicated to

satisfy. A survey of a few odd, static, single-valued nonlinearities seems to indicate the following. For nonsaturating nonlinearities $\xi(A)$ does not exist. However, these are of no interest because their DIDF's are not of the form required in (6.1). For three saturating nonlinearities (ideal relay, relay with dead zone, and saturation) whose TSIDF's are plotted in [14], $\xi(A)$ has the characteristic shown in Fig. 6.2, and asymptotic value $\xi(A) \rightarrow \psi/A$ where ψ is a constant. The departure from the

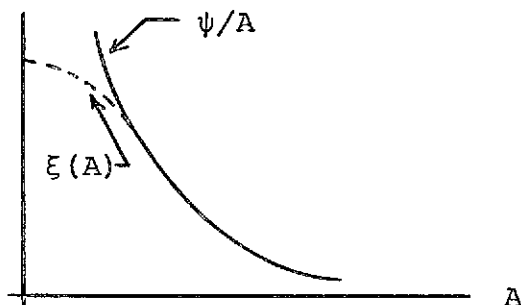


Fig. 6.2 Character of $\max_B |N_B(A,B)| = \xi(A)$.

asymptote occurs when A is so small that the nonlinearity is rapidly changing character, e.g., saturation when A is so small that the element is linear. For the ideal relay with output M , $\xi(A) = \psi/A = .855M/A$ for all $A > 0$ [15]. We restrict the EEAS synthesis theory to nonlinear elements such that ψ exists and $\xi(A) \leq \psi/A$ for all $A > 0$. Using this restriction

$$\frac{\psi}{A} |G_1(j\omega_\pi)G_2(j\omega_\pi)P(j\omega_\pi)| < 1 \quad (6.5)$$

is sufficient to quench the limit cycle and DIDF theory may be applied. Defining $M_o/\psi \equiv \rho$ and recalling the oscillating signal loop transmission is $L_o = N_o G_1 G_2 P =$

$\frac{M_o}{A} G_1 G_2 P$ we get

$$|L_o(j\omega_\pi)| < \rho, \quad (6.6a)$$

or

$$|L_f(j\omega_\pi)| < \rho |M_f/M_o|. \quad (6.6b)$$

Eq. 6.6 gives the limit cycle quenching constraint clearly in terms of the loop transmission to be synthesized, i.e., it is merely a minimum gain margin. This is the gain margin mentioned briefly under specifications in Sect. 1.3, Eq. 1.21, and it is taken as a specification for the EEAS design. It is not surprising that a gain margin emerges as the condition for limit cycle quenching, however, it may be somewhat surprising that $\rho > 1$ is satisfactory for some nonlinearities. For the ideal relay $\rho = M_o/\psi = 4/(\cdot 855\pi) = 1.49$. We have verified satisfactory limit cycle quenching by analog simulation with $|L_o(j\omega_\pi)| = 1.26(+2\text{db})$.

In all subsequent discussion of the EEAS, Eq. 6.6 is taken as a specification and it is therefore assumed that the nonlinearity input signal is composed of a forced signal component $x_f(t)$ and a single oscillating component due to the excitation input A_o .

6.3 EEAS Sensitivity to Plant Gain Changes and Behavior of $L_o(j\omega_o)$ with Changing Plant Dynamics

The most attractive property of the SOAS is its inherent zero sensitivity to plant gain changes. In this section it is shown that the EEAS retains this property.

If the oscillating component of X at the input to N in Fig. 6.1 is denoted by X_o , then

$$X_o = -A_o G_1 G_2 P - X_o L_o. \quad (6.7)$$

$L_o = N_o G_1 G_2 P = \frac{M_o}{A} G_1 G_2 K P_h$, and at $j\omega_o$, $X_o(j\omega_o) = Ae^{j\phi}$, thus (6.7) becomes

$$Ae^{j\phi} = -KG_1(j\omega_o)G_2(j\omega_o)P_h(j\omega_o)[A_o + M_o e^{j\phi}], \quad (6.8)$$

or

$$A/K = |G_1(j\omega_o)G_2(j\omega_o)P_h(j\omega_o)| |A_o + M_o e^{j\phi}|. \quad (6.9)$$

To obtain an expression for ϕ , observe that (6.8) is

$$Ae^{j\phi} = \frac{-L_o(j\omega_o)}{N_o} [A_o + M_o e^{j\phi}], \quad (6.10)$$

from which we write

$$\phi - \tan^{-1} \left[\frac{\sin\phi}{A_o/M_o + \cos\phi} \right] = \angle L_o(j\omega_o) + \pi \quad (6.11)$$

provided M_o is real. If M_o is complex, ϕ is replaced by $\phi + \angle M_o$ and M_o by $|M_o|$ in the \tan^{-1} term of (6.11). In either case ϕ is independent of K , and it follows that $A/K = A_1/K_1$ in (6.9) is also independent of K . Substituting this in $L_f = N_f G_1 G_2 P = \frac{M_f K_1}{A_1} G_1 G_2 P_h$

shows the desired zero sensitivity to pure gain changes.

Similar analysis will show that the zero gain sensitivity property is retained with the excitation A_0 in Fig. 6.1 applied to any point between the nonlinearity output and the varying gain factor. The input point shown has been chosen because it yields system equations in convenient form. If, for example, A_0 is applied at the input to N , the equation corresponding to (6.9) is $A/K = |A_0/K - e^{j\phi} M_0 G_1(j\omega_0) G_2(j\omega_0) P_h(j\omega_0)|$, and A/K is not constant due to the A_0/K term on the right.

Now consider the behavior of $L_0(j\omega_0)$ as plant dynamics change. From Eq. 6.11 the plot of ϕ vs. $\underline{L_0(j\omega_0)}$ of Fig. 6.3 is constructed. Taking the excitation frequency ω_0 constant, $\underline{L_0(j\omega_0)}$ will vary with plant parameters and cause ϕ to change along its respective A_0/M_0 contour. However, if $A_0/M_0 < 1$ there are either two solutions, or no solutions for ϕ . Fig. 6.3 shows that a unique ϕ is obtained for every $\underline{L_0(j\omega_0)}$ if $A_0/M_0 > 1$. For this reason $A_0/M_0 > 1$ is assumed for the remainder of the EEAS synthesis.

Rearranging (6.10) slightly,

$$L_0(j\omega_0) = \frac{-N_0 A e^{j\phi}}{[A_0 + M_0 e^{j\phi}]} = \frac{-e^{j\phi}}{[A_0/M_0 + e^{j\phi}]} \quad (6.12)$$

This is the relation that fixes the $|L_0(j\omega_0)|$ characteristic at a particular level. The magnitude of (6.12) is shown on Fig. 6.4, and it is easy to show that if

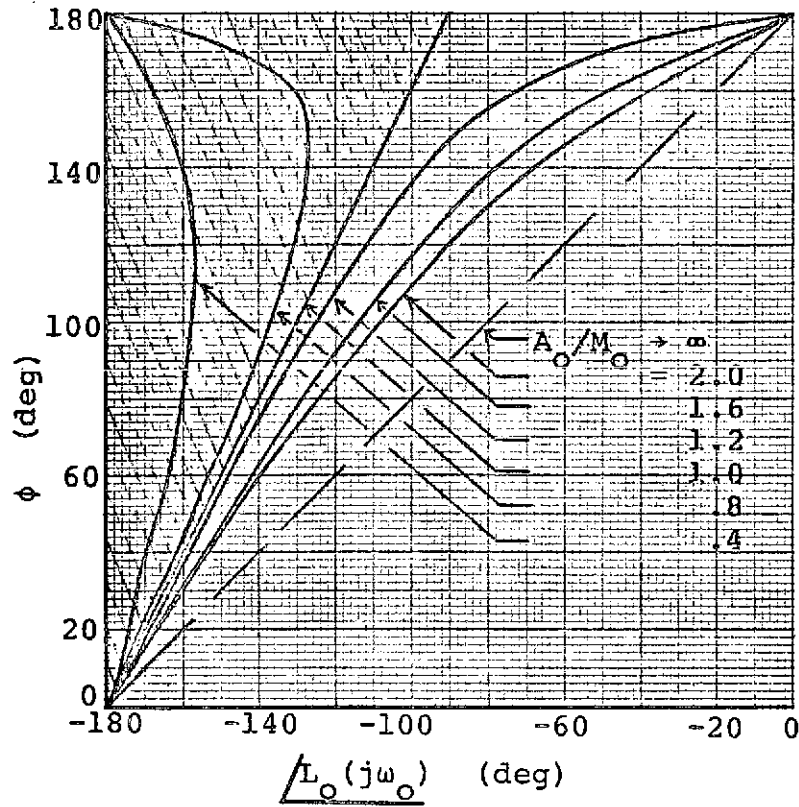


Fig. 6.3 ϕ vs. $\angle L_o(j\omega_o)$ with A_o/M_o as a parameter (ϕ is an odd function of $\angle L_o(j\omega_o) + \pi$).

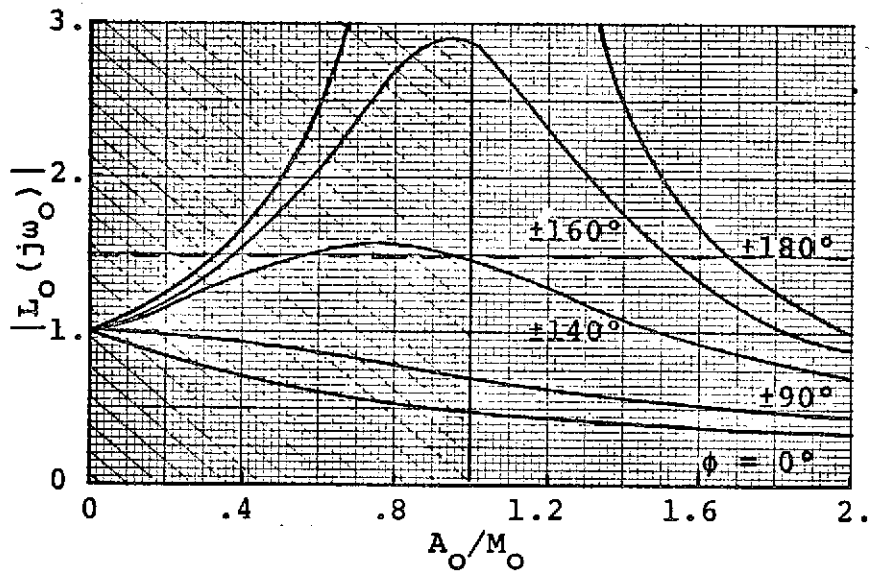


Fig. 6.4 $|L_o(j\omega_o)|$ vs. A_o/M_o with ϕ as a parameter.

$A_o/M_o > 1$, $|L_o(j\omega_o)| < 1$ for all $\phi \in [-120^\circ, +120^\circ]$.

From Fig. 6.3 this translates to the same result for

$\angle L_o(j\omega_o) + 180^\circ \in [-60^\circ, +60^\circ]$, or in an even larger range for larger A_o/M_o . This means that if ω_o is taken close to ω_π the loop transmission will be less than unity even though the limit cycle quenching gain margin ρ might permit a larger value.

From (6.12) we also get $|L_o(j\omega_o)/(1+L_o(j\omega_o))| = |-e^{j\phi} M_o/A_o| = M_o/A_o$, which is constant. Thus, as plant parameters vary $L_o(j\omega_o)$ varies along a contour of fixed $|L_o(j\omega)/(1+L_o(j\omega))|$ on the Nichols chart as shown by Fig. 6.5.

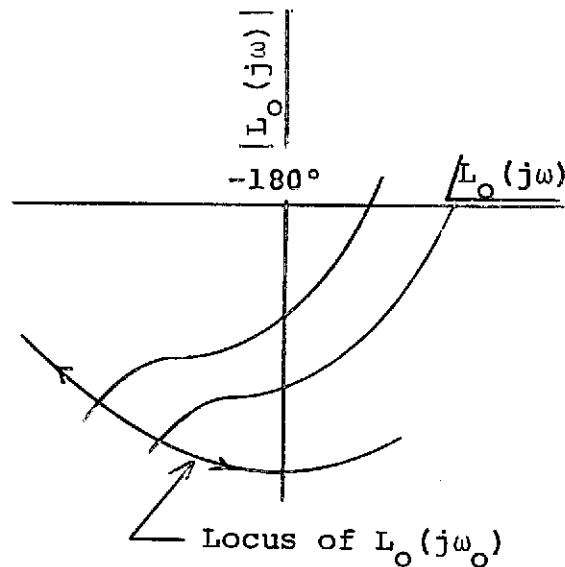


Fig. 6.5 Variation of $L_o(j\omega_o)$ on Nichols chart coordinates.

The above description applies to M_o real, as it is for all odd, static, and single-valued nonlinearities. M_o will be assumed real for the remainder of this chapter. Although somewhat more tedious, the extension to complex

M_o is straightforward.

6.4 Synthesis of an Elementary EEAS

In this section we shall develop the necessary equations and synthesis steps for a simple EEAS where the plant is assumed to have only gain uncertainty. The approach of Sect. 2.1 is followed with the intent of stripping away the complexity of the most general design and exposing the basic design conflicts.

The structure in Fig. 6.1 is taken with N having the usual DIDF,

$$N_o = M_o/A \quad (6.13a)$$

$$N_f = M_f/A, \quad (6.13b)$$

under quasi-linearity constraints

$$\max_t |x_f(t)| \leq A_1/\alpha \quad (6.14a)$$

$$\omega_b \leq \omega_o/\beta. \quad (6.14b)$$

In addition, we now have the limit cycle quenching gain margin

$$|L_o(j\omega_\pi)| \leq \rho, \quad (6.15)$$

where ω_π satisfies $L_o(j\omega_\pi) = -180^\circ$.

Let the plant be $P = KP_h = K/[s(s+a)]$ with the gain factor ignorance given by $K \in [K_1, K_2]$, and K_1, K_2 and a are known. To complete a set of specifications take $T = \omega_a^2/(s+\omega_a)^2$, $R_e = q_r/s$, and assume the maximum magnitude of oscillating signal at the system output is

bounded above by m .

The output oscillation magnitude $|C_o(j\omega_o)|$ is written from Fig. 6.1 as

$$|C_o(j\omega_o)| = \frac{A_o |G_2(j\omega_o)P(j\omega_o)|}{|1 + L_o(j\omega_o)|} \quad (6.16)$$

Taking maximum plant gain K_2 , and imposing the magnitude constraint gives

$$\frac{A_o K_2 |G_2(j\omega_o)P_h(j\omega_o)|}{|1 + L_o(j\omega_o)|} \leq m \quad (6.17)$$

From (6.12) $A_o/|1+L_o(j\omega_o)| = M_o/|L_o(j\omega_o)|$ giving in (6.17)

$$K_2 M_o |G_2(j\omega_o)P_h(j\omega_o)| \leq m |L_o(j\omega_o)| \quad (6.18)$$

The extreme forced input signal to N is

$$X_e = \frac{R_e T}{N_f G_2 P} = \frac{A_1 R_e T}{M_f K_1 G_2 P_h} \quad (6.19)$$

and solving for G_2 ,

$$G_2 = \frac{A_1 R_e T}{M_f K_1 X_e P_h} \quad (6.20)$$

Evaluating G_2 at ω_o and substituting in (6.18) yields

$$\left| \frac{X_e(j\omega_o)}{A_1} \right| \geq \frac{K_2 M_o}{K_1 m M_f} \left| \frac{R_e(j\omega_o) T(j\omega_o)}{L_o(j\omega_o)} \right| \quad (6.21)$$

This inequality is the counterpart to Eq. 2.9 for the SOAS, and indeed reduces to (2.9) if we recall that in the SOAS $|L_o(j\omega_o)| = 1$. Thus, the same arguments used in

choosing X_e to minimize ω_o would seem to apply to the EEAS. What we have not seen yet for the EEAS is that minimizing ω_o will optimize the design in the sense of noise transmission discussed in Sect. 1.4.

The constraints on $L_o(j\omega)$ are summarized as follows. For limit cycle quenching

$$|L_o(j\omega_\pi)| \leq \rho, \quad (6.22)$$

where ρ is now the design value of quenching gain margin, presumably smaller than the theoretical quenching limit.

Due to the limit on output oscillation magnitude

$$|L_o(j\omega_o)| \geq \frac{K_2 A_1 M_o}{K_1 m M_f} \left| \frac{R_e(j\omega_o) T(j\omega_o)}{X_e(j\omega_o)} \right|, \quad (6.23)$$

with A_1 satisfying quasi-linearity constraint (6.14a).

The loop transmission magnitude is fixed by

$$|L_o(j\omega_o)| = \left| \frac{-e^{j\phi}}{A_o/M_o + e^{j\phi}} \right|. \quad (6.24)$$

In contrast to the SOAS, the designer must fix $|L_o(j\omega_o)|$ in the EEAS by selecting a suitable combination of ϕ and A_o . This will make the loop transmission shaping task more difficult and some cut and try may be necessary.

Temporarily choose X_e in the form previously used for the Type 1 plant and step inputs, i.e.,

$$X_e = \frac{q_x \omega_b}{s + \omega_b}. \quad (6.25)$$

Then $A_1 = \alpha q_x \omega_b$, and inserting all the given quantities in the right side of (6.23) results in

$$|L_o(j\omega_o)| \geq \frac{\alpha q_x K_2 M_o}{m K_1 M_f} \left| \frac{\omega_a^2 (s + \omega_b)}{s (s + \omega_a)^2} \right|_{j\omega_o} \quad (6.26)$$

The bounds for $|L_o(j\omega)|$ are sketched on Fig. 6.6.

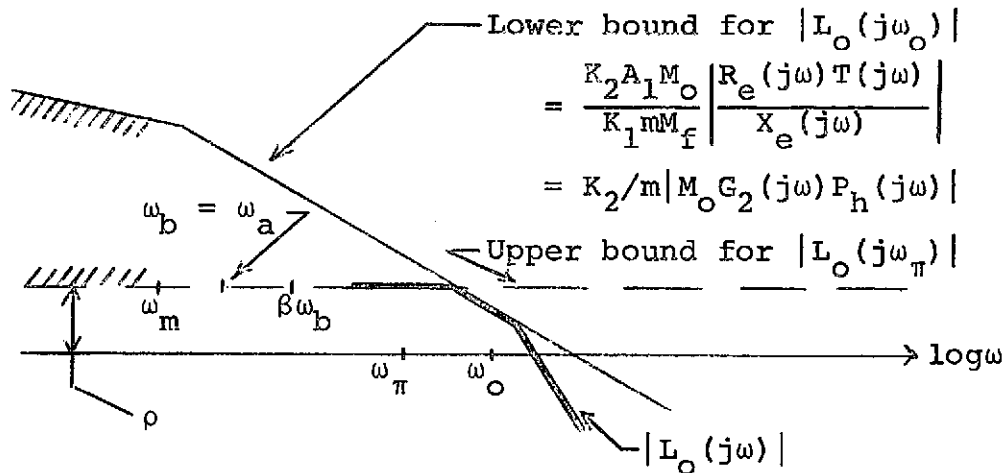


Fig. 6.6 Boundaries for EEAS oscillating signal loop transmission.

The foremost goal in shaping $L_o(j\omega)$ within the constraints of Fig. 6.6 is to optimize in terms of noise transmission as discussed in Sect. 1.4, i.e., to minimize the high frequency asymptote of the loop transmission. We assume that any sensitivity requirements due to parameter uncertainty other than plant gain will permit L_o to be below the lower bound in Fig. 6.6. Otherwise, the lower bound is not a constraint (in the present problem there are no such sensitivity requirements, but they will exist in the general design problem). $|L_o(j\omega)|$ cannot

assume its final asymptote until it has encountered the lower bound and ω_0 has been established along this bound. This reasoning indicates that ω_0 should be minimized, i.e., the final asymptote should be assumed at the lowest possible frequency. One may postulate ω_0 lower than ω_π , say at $\beta\omega_b$, in Fig. 6.6, in which case $|L_0(j\omega_0)| > \rho$. It is difficult if not impossible to satisfy (6.24) at this frequency with any reasonable L_0 when $\rho > 1/2$. However, ignoring this, note that the lower bound has an excess of two poles (more in practical designs), so if $|L_0(j\omega_0)| > \rho$, $|L_0(j\omega)|$ must then decrease slower than the lower bound to avoid having 180° of phase lag before reaching the upper bound at ρ .

The conclusion is that the optimum $L_0(j\omega)$ has closely the characteristic shown on Fig. 6.6. The shaping is now explained in detail. As ω approaches the boundary intersection of Fig. 6.6, $|L_0(j\omega)|$ lies between the bounds, joining the lower bound at the intersection, and following it until the far poles may be inserted. The poles must be inserted far enough out so $|L_0(j\omega_\pi)| \leq \rho$ and to permit $|L_0(j\omega_0)|$ to be established on the boundary. For example, suppose $\rho > 1$ and ω_π is at the boundary intersection. Further suppose that we attempt to choose $\omega_0 = \omega_\pi$. From Fig. 6.3 $\phi = 0^\circ$, and on Fig. 6.4 $|L_0(j\omega_0)| < 1/2$. Hence the necessary $|L_0(j\omega_0)|$ cannot be achieved; instead ω_0 must be positioned far enough above ω_π such that ϕ differs from zero by the

amount required to obtain some $|L_O(j\omega_o)| > 1/2$. Let L_O shown be a trial value and assume that it establishes ω_π at the point labeled. How do we find ω_o ? First, recalling from Sect. 6.3 that $\Lambda_o/M_o > 1$, choose $A_o = 1.2M_o$ for example. Using this Λ_o and $|L_O(j\omega)|$ in Eq. 6.11 to get $\phi(\omega)$ for Eq. 6.24, $|L_O^*(j\omega)|$ is plotted as on Fig. 6.7 over the frequency range where the trial $|L_O(j\omega)|$ is coincident with the lower bound in Fig. 6.6. $|L_O^*(j\omega)|$ represents the achievable $|L_O(j\omega_o)|$ with this specific trial. The oscillating frequency is

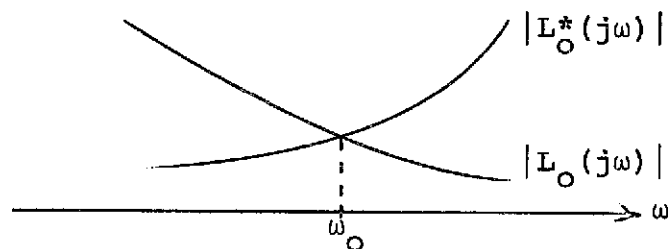


Fig. 6.7 Location of oscillation frequency.

then chosen at the intersection. If the two curves do not intersect A_o may be adjusted, or the far poles of the trial loop transmission adjusted. If $\rho < 1/2$ (see fig. 6.4) it will be beneficial to take $\omega_o \approx \omega_\pi$ because a smaller A_o results. In this case the design is considerably simplified in an obvious way, but for $\rho > 1/2$ this is not possible unless the optimality of the design is compromised by allowing $|L_O(j\omega_\pi)|$ to be smaller than required.

It is now clear that X_e should be chosen to minimize the lower bound given by (6.23), and this is accomplished by maximizing $|X_e(j\omega)|/A_1$ at ω_o . This is the same criterion obtained for X_e in the SOAS design, and it is treated in some detail in Appendix A.

The remainder of the design for plant gain uncertainty and no disturbances proceeds in essentially the same fashion as the SOAS design in Sect. 2.1. The selection of X_e determines G_2 completely from Eq. 6.20, then G_1 is shaped to obtain the desired L_o . Lastly, the prefilter is obtained using the specified transfer function from $F = T(1+L_f)/L_f$.

To compare the EEAS design of this section with the SOAS design in Sect. 2.1, note that the preceding arguments have shown that $|L_o(j\omega_o)| \leq |L_o(j\omega_\pi)| \leq \rho$. Using this in (6.26), and approximating $\omega_a \approx \omega_b \ll \omega_o$, gives

$$\omega_o \geq \omega_a \left[\frac{M_o K_2 \alpha q_r}{M_f K_1 m \rho} \right]^{\frac{1}{2}}. \quad (6.27)$$

Here it is seen $K_2 q_r / K_1 m \rho$ assumes the role in the EEAS which $K_2 q_r / K_1 m$ has for the SOAS in Eq. 2.14. If $\rho < 1$ the EEAS loop transmission must have larger bandwidth. For $\rho > 1$ it is conceivable that an EEAS design could have smaller bandwidth, however, ρ must be considerably greater than unity to realize any significant advantage from the EEAS design. The ideal relay and saturation nonlinearities have $\rho \leq 1.49$, which is not large enough to

give more than trivial advantage to the EEAS for the design problem considered in this section.

6.5 EEAS Design to Satisfy Quasi-Linearity and Output Oscillation Magnitude Constraints with Practical Specifications

Having looked at a rather idealized EEAS example in the preceding section, a more general design scheme is now developed. The plant will be characterized by

$$P(s,w) = K(w)P_h(s,w); \quad \begin{cases} w \in W \\ K(w) \in [K_1, K_2], \end{cases} \quad (6.28)$$

where w is the plant parameter vector and only the bounding sets W and $[K_1, K_2]$ are known. The oscillating signal at frequency ω_0 is supplied by an external generator which has frequency tolerance parameterized by γ , with

$$\omega_0 \in [\omega_0'/\gamma, \omega_0'\gamma] = \Omega. \quad (6.29)$$

A notch filter H is inserted at oscillating frequency ω_0 , as in the SOAS, giving the structure shown by Fig. 6.8. This filter has width Ω and it is presumed that

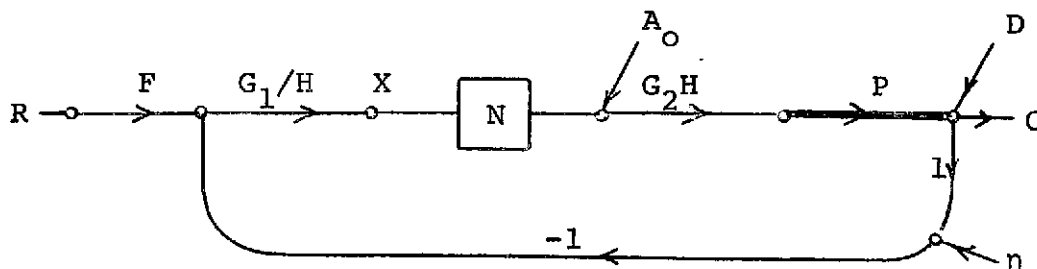


Fig. 6.8 EEAS structure with notch filter added.

γ in (6.29) is adjusted to account for inaccuracies and small parameter variations in H . The nonlinear element N is characterized by DIDF (6.13) under quasi-linearity constraints

$$\max_t |x_e(t)| \leq A_e/\alpha = \lambda q_x \omega_b \quad (6.30a)$$

$$\omega_b \leq \omega_o/\beta. \quad (6.30b)$$

The sub- e again denotes the extreme nonlinearity input signal (fastest and/or largest) and the function and parameter values that exist in the system simultaneously with $x_e(t)$.

With uncertainty in plant parameters of P_h the limit cycle quenching constraint is

$$\max_{w \in W} |L_o(j\omega_\pi)| \equiv |L_{om}(j\omega_\pi)| \leq \rho. \quad (6.31)$$

In the previous section we saw that ω_π tends to be less than ω_o , and Fig. 6.5 shows that when this is true the left side of (6.31) contains the plant parameter set producing maximum phase lag in the neighborhood of ω_o .

This parameter set will be used to define L_{om} .

Constraining the output oscillation to have magnitude bounded above by m ,

$$\begin{aligned} \max_{w \in W} \left[A_o K \frac{|G_2(j\omega_o)H(j\omega_o)P_h(j\omega_o)|}{|1 + L_o(j\omega_o)|} \right] = \\ \max_{w \in W} \left[M_o K \frac{|G_2(j\omega_o)H(j\omega_o)P_h(j\omega_o)|}{|L_o(j\omega_o)|} \right] \leq m. \end{aligned} \quad (6.32)$$

Variation in the factor $|P_h(j\omega_o)/L_o(j\omega_o)|$ with plant parameters is dependent upon the shaping of $\underline{L_o(j\omega)}$ near ω_o . For this reason the maximizing parameter set for (6.32) cannot be determined until the design is complete. Further, we want to use (6.31) and (6.32) as bounds for $|L_o(j\omega)|$, requiring that both inequalities refer to the same L_o , i.e., both be determined by the same plant parameter set. Let L_{om} contain the plant $K_m P_{hm}$ defined as follows. $\underline{P_{hm}(j\omega_o)} = \min_{w \in W} \underline{P_h(j\omega_o)}$, and $P_h = P_{hm}$ if and only if $w \in W_m \subset W$. Let $K_m = \max_{w \in W_m} K$. Then take

$$m^* = m \frac{K_m P_{hm}(j\omega_o)}{L_{om}(j\omega_o)} \left[\max_{w \in W} \left| \frac{L_o(j\omega_o)}{K P_h(j\omega_o)} \right| \right] \leq m. \quad (6.33)$$

Then

$$M_o K_m \left| \frac{G_2(j\omega_o) H(j\omega_o) P_{hm}(j\omega_o)}{L_{om}(j\omega_o)} \right| \leq m^* \quad (6.34)$$

defines the lower bound for $L_{om}(j\omega_o)$, while (6.31) defines the upper bound for $L_{om}(j\omega_o)$. The ignorance in (6.32) has been lumped in the factor m^* . The designer must estimate this from study of his particular plant, and then verify the estimate or make adjustments when the first design is complete.

Continuing the synthesis steps, there is a pairing P_{he} and T_e as discussed in Appendix B that gives the extreme forced input to N ,

$$\begin{aligned}
 X_e &= \frac{X_{el}}{H} = \frac{A_e R_e T_e}{M_f K_e G_2 H P_{he}} \\
 &= \frac{\lambda \alpha_x \omega_b R_e T_e}{M_f K_e G_2 H P_{he}} . \quad (6.35)
 \end{aligned}$$

In the preceding section it was shown that the optimal functional form for X_e is the same as for the SOAS. thus, in accord with Appendix A, assuming step commands and a Type 1 plant, the form

$$X_{el} = \frac{\alpha_x \omega_b}{s + \omega_b} \phi_x \quad (6.36)$$

is chosen. ϕ_x will be used to include the necessary far poles in X_e .

Solving (6.35) for G_2 and substituting in (6.34) yields, after some rearrangement,

$$\begin{aligned}
 \left| \frac{X_{el}(j\omega_o)}{A_e H(j\omega_o)} \right| &= \left| \frac{X_e(j\omega_o)}{A_e} \right| \\
 &> \frac{K_m M_o}{K_e m^* M_f} \left| \frac{R_e(j\omega_o) T_e(j\omega_o)}{L_{om}(j\omega_o)} \right| \left| \frac{P_{hm}(j\omega_o)}{P_{he}(j\omega_o)} \right| . \quad (6.37)
 \end{aligned}$$

This is the generalization of Eq. 6.21, and the EEAS counterpart to SOAS Eq. 2.56.

Eqs. 6.31 and 6.37 respectively provide the upper bound for $L_{om}(j\omega_\pi)$ and the lower bound for $L_{om}(j\omega_o)$. If no notch filter is used ($H = 1$) the resultant ω_π is shown on Fig. 6.9a. $L_{om}(j\omega_o)$ must be situated on the lowest (solid) boundary of Fig. 6.9a above ω_π and this

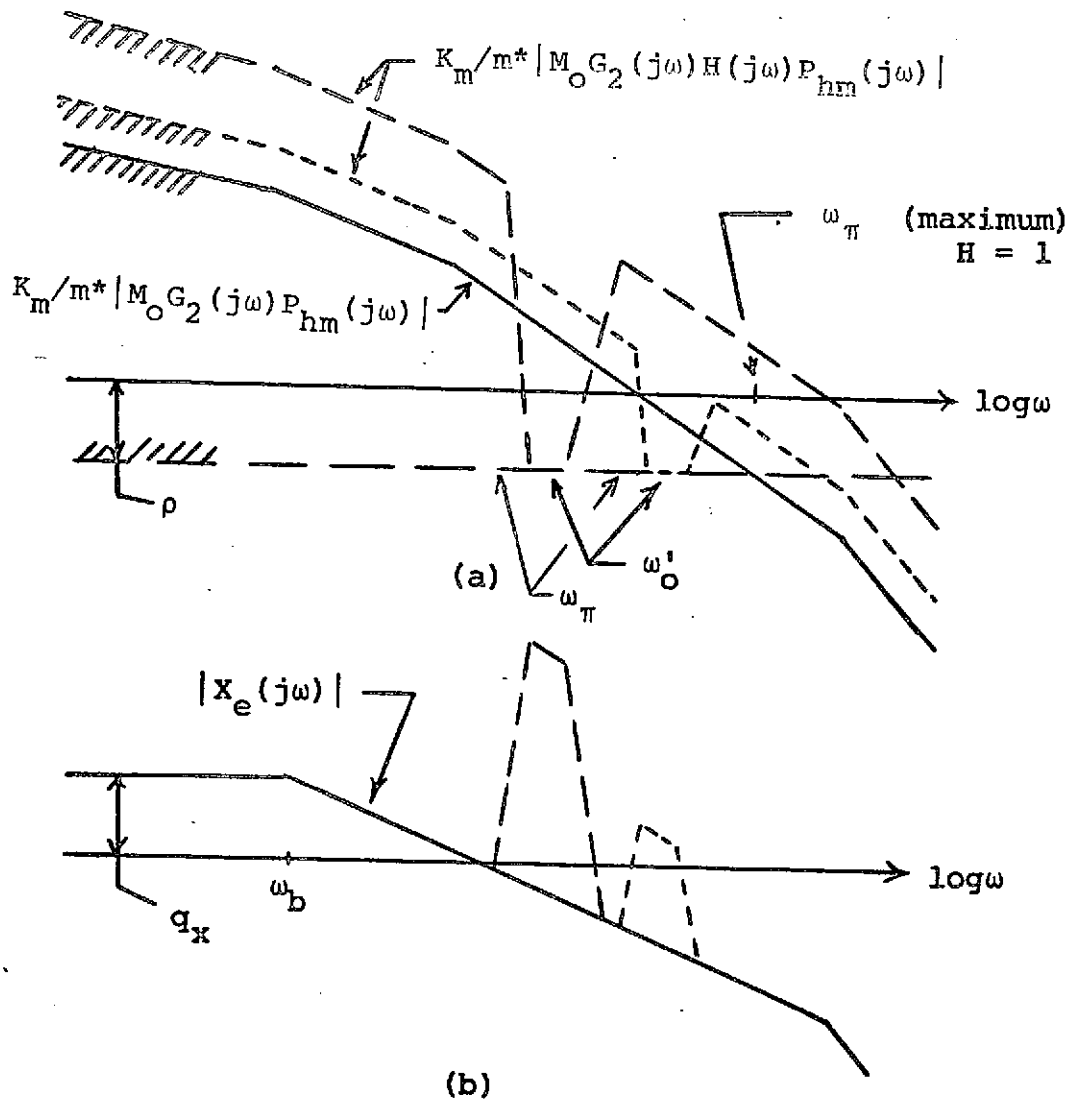


Fig. 6.9 Behavior of X_e and bounds for L_{om} as oscillating frequency ω_0 is decreased.

is accomplished by shaping $\underline{L_{om}(j\omega)}$ and selection of A_0 as detailed in Sect. 6.4. L_{om} must be above the bound for all $\omega_0 \in \Omega$. Study of Fig. 6.3 and 6.4 shows that as ω_0 moves away from ω_π , $|L_{om}(j\omega_0)|$ increases, thus one need only work with the worst case value of ω_0

which is ω_0^i/γ .

If the notch filter is employed we require its magnitude characteristic. The basic equation for obtaining $|H(j\omega)|$ is (6.37), however, the value of $|L_{om}(j\omega_0)|$ is unknown. We can assume that $|L_{om}(j\omega)|$ is flat over $[\omega_\pi, \gamma\omega_0^i]$ and take $|L_{om}(j\omega_0)| = \rho$, yielding from (6.37)

$$|H(j\omega)| = \begin{cases} \frac{m^* \rho K_e M_f}{\lambda \alpha q_x \omega_b K_m M_o} \left| \frac{X_{el}(j\omega)}{R_e(j\omega) T_e(j\omega)} \right| \left| \frac{P_{he}(j\omega)}{P_{hm}(j\omega)} \right|; & \omega \in \Omega \\ 1 & ; \omega \notin \Omega, \end{cases} \quad (6.38)$$

where $A_e = \lambda \alpha q_x \omega_b$. This should produce reasonable results when $\rho < 1/2$ and ω_0 and ω_π can be taken quite close together, i.e., $\phi \approx 0$ on Fig. 6.4. If $\rho > 1/2$ so that ϕ must differ significantly from zero, requiring that $\angle L_{om}(j\omega_0)$ differ significantly from -180° , the approximation $|L_{om}(j\omega_0)| \approx \rho$ will deteriorate. The alternative is to use smaller ρ or m^* in (6.38), but how much smaller must be determined by cut and try. Given a satisfactory ρ for (6.38), the problem of determining λ , ω_0^i , and H is identical to that in the SOAS detailed in Sect. 2.3, and therefore is not repeated here.

Once ω_0^i has been selected by the method of Sect. 2.3 and all remaining constraints, sensitivity to P_h , disturbances, etc. permit the use of this value, the design proceeds by the same steps detailed for the SOAS in

Sect. 2.3, except for the requirement to shape $\sqrt{L_{om}(j\omega)}$ and select A_o . λ is known from a λ vs. ω' plot as shown by Fig. 2.7, $|H(j\omega)|$ is given by (6.38) from which a rational function is synthesized, and G_2 is obtained from Eq. 6.33. Then G_1 is used to shape $L_{om}(j\omega)$ in accord with sensitivity and disturbance attenuation requirements (treated in the following sections), and to shape $\sqrt{L_{om}(j\omega)}$ at ω_o as explained in Sect. 6.4. Lastly, the prefilter is obtained from $F = T_e(1+L_{fe})/L_{fe}'$ where $L_{fe} = \frac{M_f}{A_e} K_e G_1 G_2 P_h e$.

The discussion in Sect. 2.3 regarding efficient assignment of far poles to the ϕ_x part of X_e and to T_e also applies to the present design.

To make a brief comparison of SOAS and EEAS, first note the position of ρ in H of Eq. 6.38. Comparing this H with that given in Eq. 2.57, the EEAS requires a deeper notch when $\rho < 1$. When $\rho > 1$ there is a possibility of obtaining a smaller bandwidth loop transmission with the EEAS. The aspect of the EEAS most likely to make it superior to the SOAS in some applications is that ω_o does not change with plant parameters. In the SOAS a significant portion of the oscillating frequency interval Ω is contributed by the variation of plant dynamics in P_h , and this effect is accentuated as the design is optimized by reduction of ω_o . In the EEAS ω_π will experience this variation, but ω_o will not, because this frequency is presumably fixed to much smaller tolerance

by the excitation source. Only ω_o must remain in the notch filter in the EEAS, hence the notch can be narrower, having less effect on $x_e(t)$, and ultimately can be moved to a lower frequency than the SOAS permits. There is no difficulty if ω_π is not within the notch filter as long as $|L_o(j\omega_\pi)| \leq \rho$, and this has been insured by using the worst case in (6.31). Of course, the requirement of an excitation source is a disadvantage in the EEAS.

6.6 Synthesis of EEAS Loop Transmission to Satisfy Transfer Function Sensitivity Specifications

The transfer function sensitivity specifications for the EEAS are assumed in the form detailed at the beginning of Sect. 3.3, i.e., we are given bounds on the maximum transfer function variation $\Delta \ln|T(j\omega)|$ (and possibly $\Delta/T(j\omega)$) as a function of frequency. The system structure remains as in Fig. 6.1, and the plant ignorance is as described in Sect. 1.3, Eq. 1.17. The approach for synthesizing the forced signal loop transmission $L_f(j\omega)$ will be basically the same as developed earlier for the SOAS.

First, it is necessary to write the forced signal loop transmission as the product of a compensation transmission G , and the equivalent plant P_f which contains all the loop transmission ignorance, i.e., $L_f = GP_f$. We have previously shown in Sect. 6.3, Eq. 6.12, that

$$\begin{aligned}
 L_o(j\omega_o) &= \frac{M_o}{A} K G_1(j\omega_o) G_2(j\omega_o) P_h(j\omega_o) \\
 &= \frac{-e^{j\phi}}{[A_o/M_o + e^{j\phi}]} \quad (6.39)
 \end{aligned}$$

where the oscillating input to N is $Ae^{j\phi}$. Thus

$$K/A = \frac{1}{|G_1(j\omega_o)G_2(j\omega_o)P_h(j\omega_o)| |A_o + M_o e^{j\phi}|} \quad (6.40)$$

and substituting this in the forced signal loop transmission,

$$\begin{aligned}
 L_f &= N_f G_1 G_2 P = \frac{M_f}{A} K G_1 G_2 P_h \\
 &= \frac{M_f G_1 G_2 P_h}{|G_1(j\omega_o)G_2(j\omega_o)P_h(j\omega_o)| |A_o + M_o e^{j\phi}|} \\
 &= G \left[\frac{1}{|G(j\omega_o)| |P_h(j\omega_o)| |A_o + M_o e^{j\phi}|} \right] \\
 &= G K_f P_h = G P_f \quad (6.41)
 \end{aligned}$$

In the last equation the definitions

$$G \equiv G_1 G_2 \quad (6.42a)$$

$$P_f \equiv K_f P_h \quad (6.42b)$$

$$K_f \equiv \frac{M_f}{|G(j\omega_o)| |P(j\omega_o)| |A_o + M_o e^{j\phi}|} \quad (6.42c)$$

have been applied. Recall from Sect. 6.3, Eq. 6.11, that

$$\phi - \tan^{-1} \left[\frac{\sin\phi}{A_o/M_o + \cos\phi} \right] = \angle L_o(j\omega_o) + \pi = \angle L_f(j\omega_o) + \pi \quad (6.43)$$

As with the SOAS, it is seen that the ignorance of the dynamics of P_h introduces a high frequency gain factor K_f in the equivalent plant P_f , and K_f contains some parameter uncertainty. In the EEAS ω_0 is set by the excitation source, and therefore does not change with the parameters of P . Thus we shall assume ω_0 constant in this section, and it follows that there is no uncertainty associated with $|G(j\omega_0)|$. The quantities $|P_h(j\omega_0)|$ and $|A_0 + M_0 e^{j\phi}|$ both vary with plant parameters and contain the ignorance of K_f , albeit small for many practical designs.

Now, using the method in Appendix C, we wish to calculate sensitivity bounds on the Nichols chart for $L_f(j\omega_i)$; $i = 1, 2, \dots, n$. Such bounds apply to a particular plant parameter set. Specifically, we shall find bounds for $L_{fm}(j\omega_i) = G(j\omega_i)P_{fm}(j\omega_i)$, where the parameter set P_{fm} is the set maximizing the plant phase lag at ω_0 and ω_π , i.e., at high frequencies above the varying plant dynamics. In the synthesis procedure of this section we will take ω_0 larger than the maximum ω_π . Then the above selection of P_{fm} gives $L_{fm}(j\omega)$ maximum magnitude over the plant parameters, as illustrated in Fig. 6.5. The limit cycle quenching constraint is

$$M_f |L_{om}(j\omega_\pi)| / M_0 = |L_{fm}(j\omega_\pi)| \leq \rho M_f / M_0 . \quad (6.44)$$

Given a plant parameter vector w , we still require

A_o , ω_o , and G in order to evaluate P_f at some given frequency. Since ω_o and G are not available in the first stage of the design, we shall neglect the uncertainty in K_f and approximate $P_f \approx P_h$ for use in finding the first set of Nichols chart bounds. Such a set of bounds is shown in Fig. 6.10 labeled

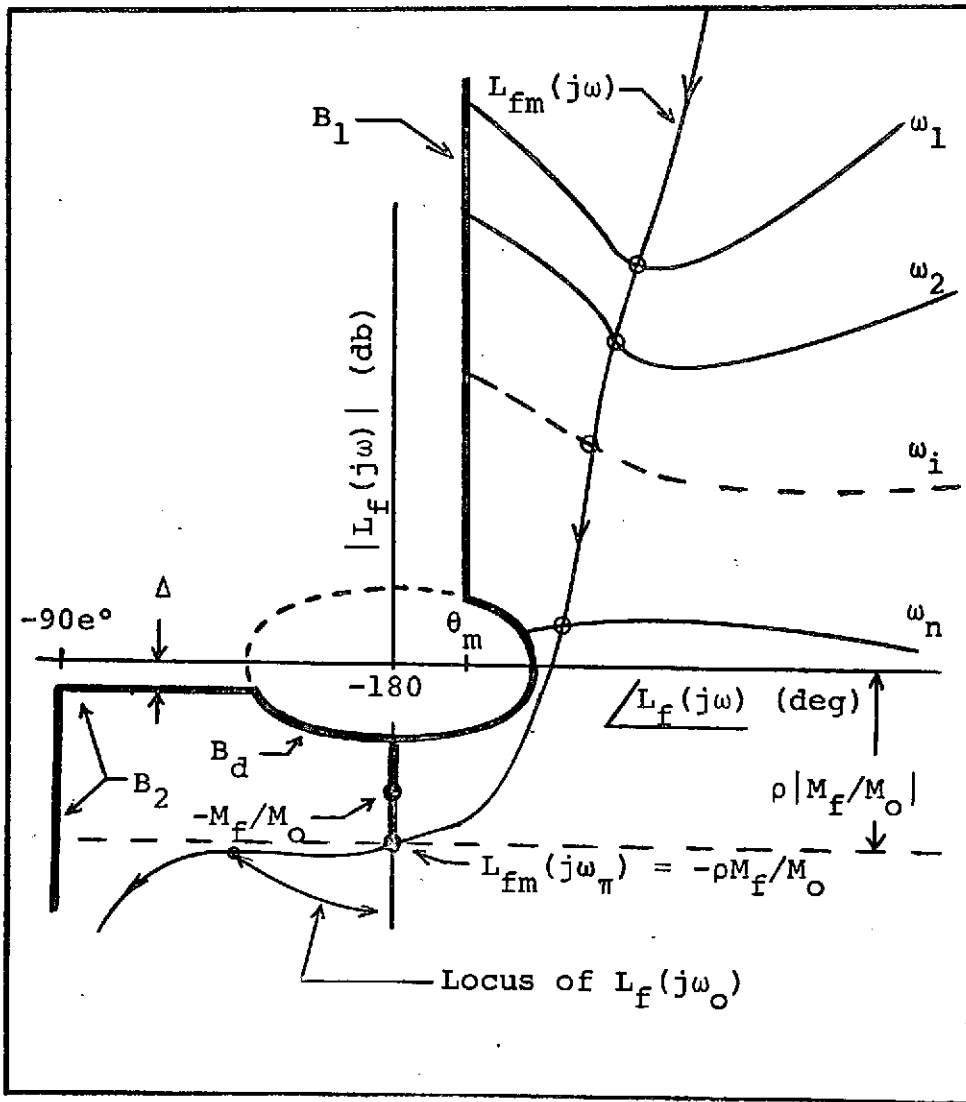


Fig. 6.10 Illustration of forced signal loop transmission shaping for the EEAS.

$\omega_1, \omega_2, \dots, \omega_n$. The remaining bounds, $B_1, B_2,$ and $B_d,$ on this figure are generated in exactly the manner explained for the SOAS in Sect. 3.3.

In Sect. 3.3 (page 82) five properties of the minimum bandwidth loop transmission were given. Properties 2. through 5. transfer directly to the EEAS by replacing L_{f1} in the Chapter III statement with L_{fm} . Property 1. is replaced by constraint (6.44). Using these properties as a guide, the designer shapes $L_{fm} = GP_{hm} = GP_{fm}$, and thus obtains the first value for L_{fm} and the compensation function G .

Now a value of ω_0 must be chosen, and it must be chosen such that $L_{fm} = M_f L_{om} / M_o$ is realizable as a solution of Eq. 6.39. At this point we have a plot of L_{fm} , say as shown in Fig. 6.10. The following method for selecting ω_0 is suggested. From consideration of Fig. 6.4 and the specified ρ , choose a reasonable $A_o > M_o$, say $A_o = 1.2M_o$. Then using the available $|L_{fm}(j\omega)|$ plot the curve of achievable $|L_{fm}^*(j\omega)|$ over the frequency range above ω_π . On the same figure plot $|L_{fm}(j\omega)|$. Both plots are depicted in Fig. 6.11, and ω_0 is chosen at the intersection. The technique is the same

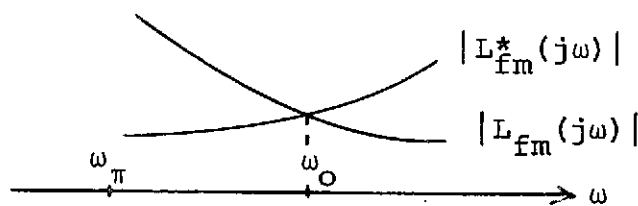


Fig. 6.11 Location of ω_0

as we have used previously in Sect. 6.4. With ω_o selected, $L_f(j\omega_o)$ will vary along a contour of constant $|L_f(j\omega)/(M_f/M_o + L_f(j\omega))|$ as depicted on Fig. 6.10.

All necessary information is now available to calculate $P_f(j\omega) = K_f P_h(j\omega)$ without neglecting K_f . Therefore P_f may be used to calculate a new set of Nichols chart bounds for $L_{fm}(j\omega_i)$. The algorithm given in Sect. 3.3 (page 85) can be applied directly to the EEAS by replacing sub-1 with sub-m throughout. Using this algorithm the designer iterates G to obtain an optimal L_f satisfying the P_h parameter sensitivity specifications.

As with the SOAS, the design steps for satisfying transfer function sensitivity specifications with minimum bandwidth are rather tedious. Hence, the designer should have some feel for whether the reduction in bandwidth is precluded by other design constraints before undertaking the procedure of this section.

6.7 EEAS Design for Disturbance Inputs

When the extreme forced input to N in Fig. 6.8 is due to a disturbance input to the system some change to the synthesis steps in Sect. 6.5 are necessary to insure quasi-linear operation. We shall denote the extreme disturbance input by $-D_e$. With this input present, there is a plant parameter set P_{he} which most nearly causes the corresponding X_e to violate

quasi-linearity constraints (6.30). Paired with this plant is loop transmission L_{fe} , and the plant output signal is written from Fig. 6.8 as $D_e L_{fe}/(1+L_{fe})$. This quantity is evaluated at ω_o and substituted in place of $R_e(j\omega_o)T_e(j\omega_o)$ (the plant output for a command input) in Eq. 6.37 to give

$$\left| \frac{X_{el}(j\omega_o)}{A_e H(j\omega_o)} \right| = \left| \frac{X_e(j\omega_o)}{A_e} \right|$$

$$\geq \frac{K_m M_o}{K_e m M_f} \left| \frac{D_e(j\omega_o) L_{fe}(j\omega_o)}{L_{om}(j\omega_o) (1+L_{fe}(j\omega_o))} \right| \left| \frac{P_{hm}(j\omega_o)}{P_{he}(j\omega_o)} \right| . \quad (6.45)$$

All quantities in this equation are defined as in Sect. 6.5. We are again faced with the problem that the quantity $|L_{fe}/(L_{om}(1+L_{fe}))|$ is not known precisely until the design is complete. Hence this factor, at $j\omega_o$, is approximated by $(M_f/M_o) |1/(1-\rho M_f/M_o)| = M_f/|M_o - \rho M_f|$, and (6.45) becomes

$$\left| \frac{X_{el}(j\omega_o)}{A_e H(j\omega_o)} \right| \geq \frac{K_m M_b}{K_e m^*} \left| \frac{D_e(j\omega_o)}{M_o - M_f} \right| \left| \frac{P_{hm}(j\omega_o)}{P_{he}(j\omega_o)} \right| . \quad (6.46)$$

m has been replaced by m^* to absorb the ignorance of the unknown factor discussed above.

For disturbance inputs the design procedure to satisfy quasi-linearity and the output oscillation magnitude constraint is precisely as detailed for command inputs in Sect. 6.5, except that we use Eq. 6.46 in place of Eq. 6.37. The ignorance in m^* must be

eliminated by iteration. For example, the first design is performed with $m^* = m$, then if the oscillation is too large m^* is reduced appropriately and the design carried out again.

As was the case for the SOAS, the EEAS design cannot be made to satisfy the frequency quasi-linearity constraint (Eq. 6.30b) for step inputs. The SOAS design for step disturbances is discussed at length in Chapter IV and the comments there apply to the EEAS as well.

The above relates to satisfying quasi-linearity and the limit on output oscillation for disturbance inputs. There may also be specifications on the disturbance attenuation as a function of frequency. If so, these are incorporated into the Nichols chart bounds on forced signal loop transmission used in Sect. 6.6. The detailed technique for doing this is covered in Sect. 4.2 and in Appendix C.

CHAPTER VII

EEAS SIMULATION

In this chapter some results are presented from digital simulation of an EEAS. Due to the strong similarity of the EEAS and SOAS design schemes an EEAS design is not detailed starting from initial specifications. Instead, an excitation signal is applied to the SOAS design of Chapter V and some theoretical predictions of Chapter VI are verified by simulation.

For reference the EEAS structure is shown again by Fig. 7.1. The nonlinear element N is taken as a sat-

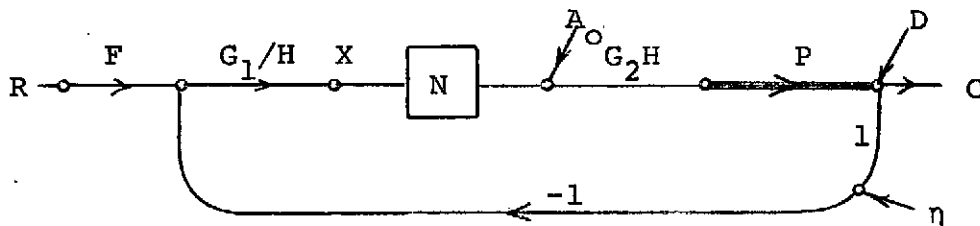


Fig. 7.1 EEAS feedback structure.

uration with the parameters given on Fig. 5.2. Study of the saturation two-sinusoid input describing function indicates the limit cycle will be suppressed for $\rho \leq 1.49$, i.e., the quenching constraint is

$$|L_o(j\omega_\pi)| \leq \rho = 1.49 . \quad (7.1)$$

The plant P in Fig. 7.1 is specified by

$$P(s) = KP_h(s) = \frac{K}{s(s+a)} ; \begin{cases} a \in [a_1, a_2] = [1, 10] \\ K \in [K_1, K_2] = [1, 10] \end{cases} \quad (7.2)$$

with K and a independent. This is the plant used for the SOAS example in Eq. 5.3. The compensations F , G_1 , G_2 , and H are given respectively by Tables 5.6, 5.3, 5.1, and 5.4. These compensations determine the phase characteristic of the loop transmission. This is shown on Fig. 7.2 for two extremes of the plant pole over a frequency band containing the oscillation frequencies of interest.

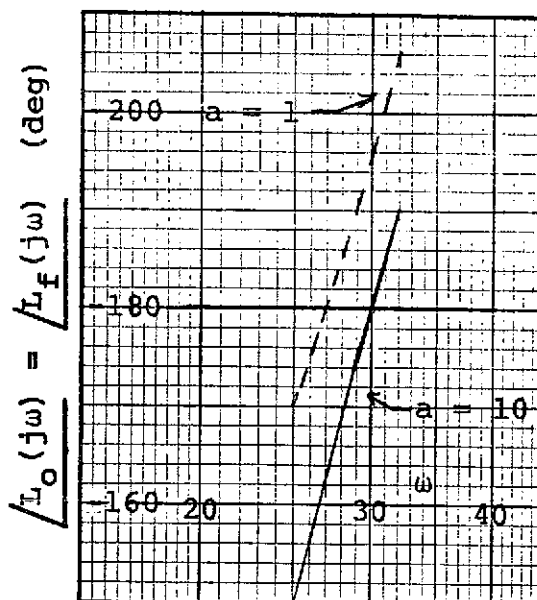


Fig. 7.2 Phase characteristic of loop transmission.

The excitation frequency is chosen at $\omega_o = 30$ rps. Using the SOAS design this choice is rather limited if ω_o is to be kept within the notch filter H (shown in Fig. 2.11). From Fig. 7.2 we see that when the plant pole is at $-a = -10$, $\omega_\pi = \omega_o = 30$ rps. With the oscillating component at the input of N written $X_o(j\omega_o) = Ae^{j\phi}$,

$\omega_o = \omega_\pi$ implies that $\phi = 0^\circ$ (see Fig. 6.3). $A_o = 1.2M_o = 3.05$ is chosen, and from

$$L_o(j\omega_o) = \frac{-e^{j\phi}}{[A_o/M_o + e^{j\phi}]} \quad (7.3)$$

this results in $|L_o(j\omega_o)| = |L_o(j30)| = .454$. For either EEAS or SOAS $L_o = \frac{M_o}{A} G_1 G_2 K P_h$. For SOAS operation $|L_o(j30)| = 1$, while for the EEAS this decreases to .454 due to an increase in A and a corresponding increase in the system output oscillating component. The input to N and the system output for a simulation started at $t = 0$ as an SOAS, and with excitation A_o applied at $t = 4$ sec. is shown in Fig. 7.3. After $t = 4$ sec. the oscillating signal magnitude should increase by $1/.454 = 2.2$ as the system assumes the EEAS mode. Fig. 7.3 verifies that this does occur. The large transients in Fig. 7.3b are present because initial conditions were not set to give an immediate steady state condition. It is evident, by tracing the effect of $|L_o(j\omega_o)|$ variation due to the plant pole change in Fig. 7.2 through Figs. 6.3 and 6.4, that the variation of $|L_o(j\omega_o)|$ will be small.

Before simulating the step response, consider briefly the sensitivity of the present EEAS to parameter changes of P_h . Recall for both systems we write the forced signal loop transmission as $L_f = K_f P_h$. Neglecting the small variation in K_f , the EEAS loop transmission is just the SOAS loop transmission of Chapter V reduced in magnitude

C-2

by $20\log(.454) = -6.8\text{db}$. This magnitude reduction causes the EEAS loop transmission to violate its respective sensitivity boundaries on the Nichols chart. Using $L_f = GP_f$ the the boundaries are computed in accord with Sect. 6.6 and Appendix C and shown on Fig. 7.4. Parameters of the EEAS L_f are tabulated on Table 7.1. The boundries apply to L_{fm} and it is seen that they are

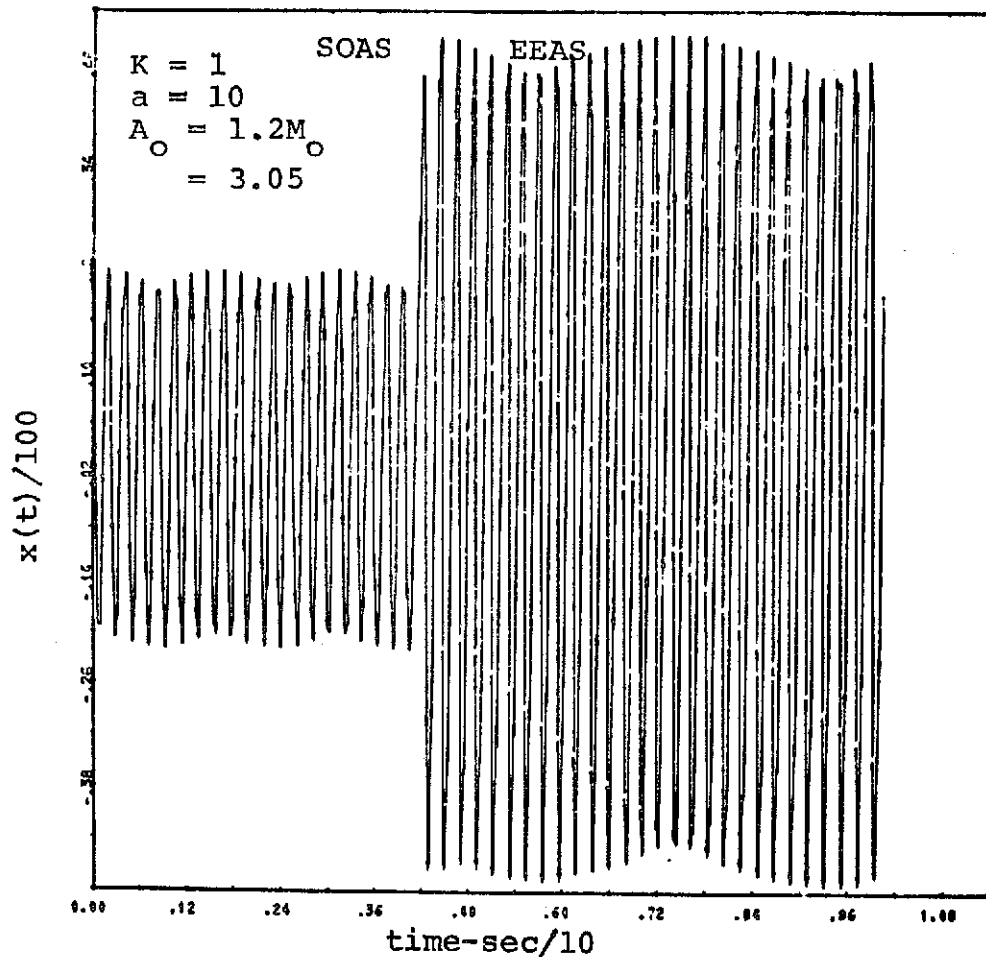


Fig. 7.3a Input signal to nonlinear element in SOAS and EEAS modes.

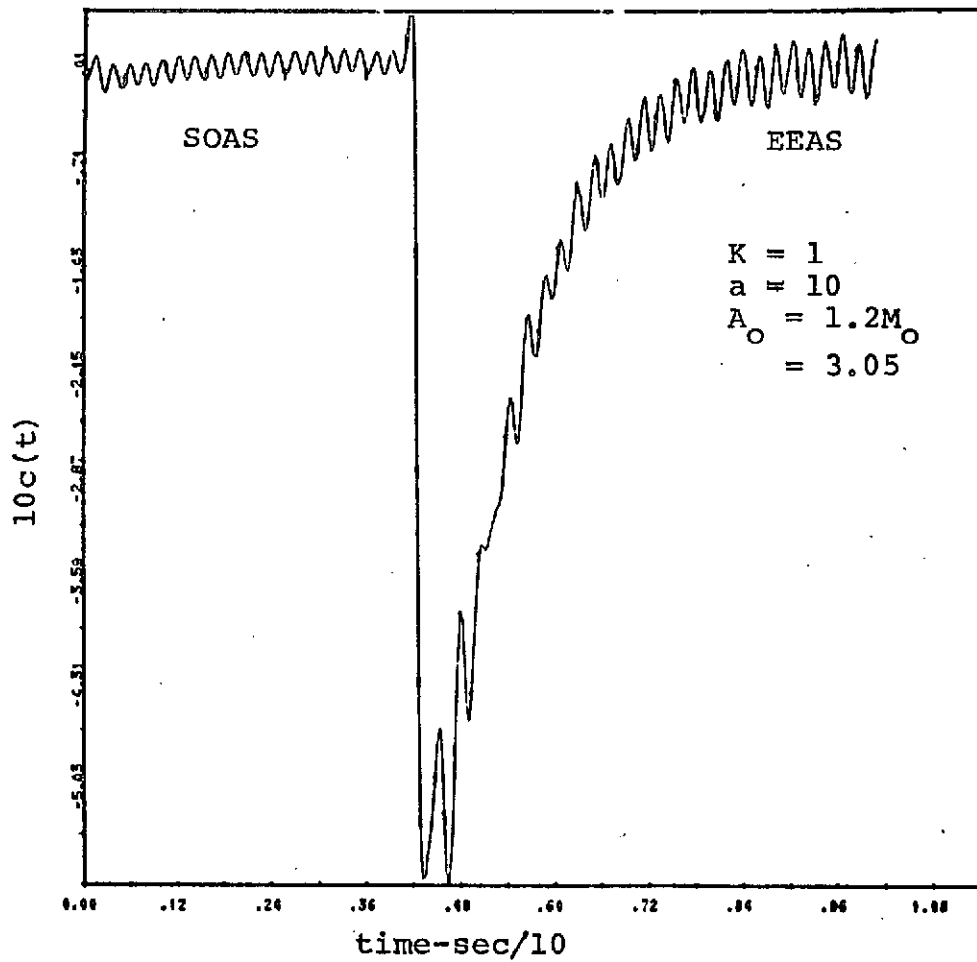


Fig. 7.3b System output in SOAS and EEAS modes.

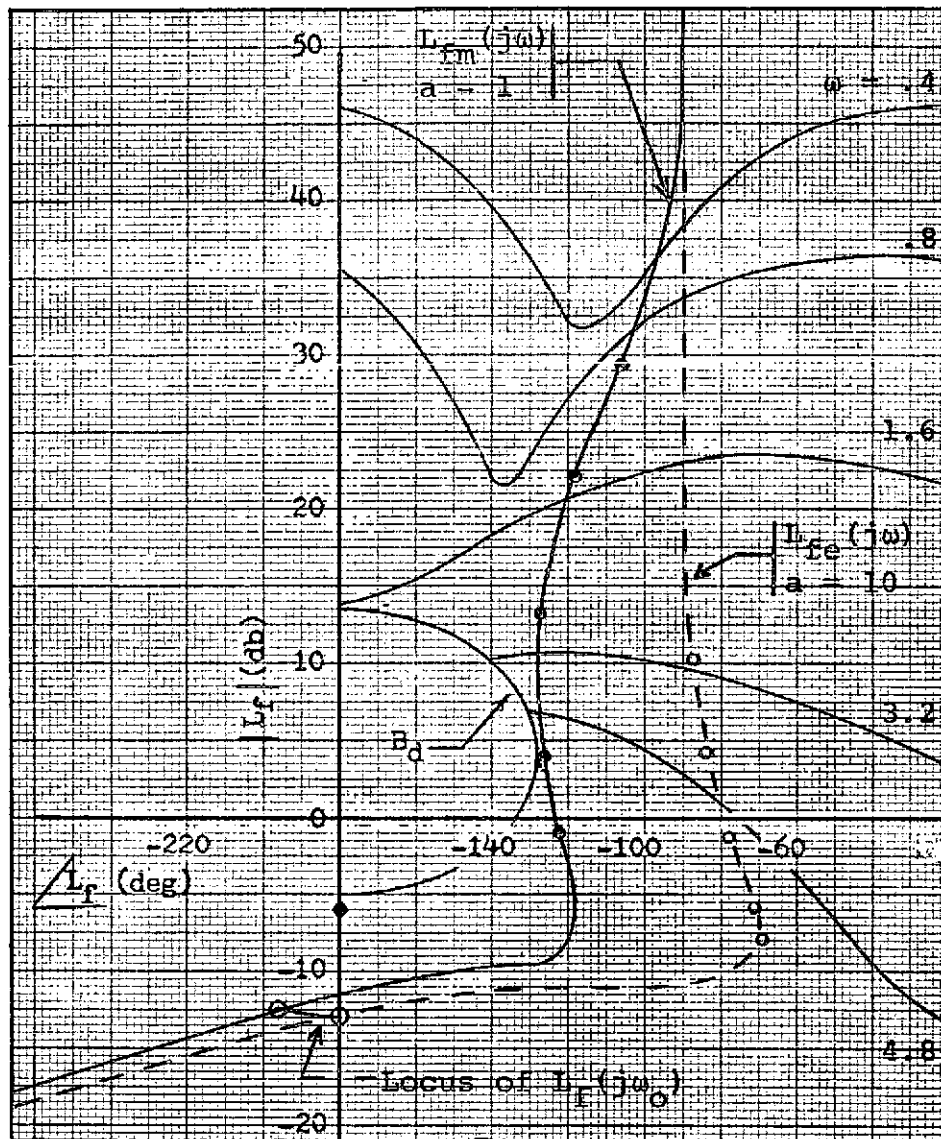


Fig. 7.4 Bounds for $L_{fm}(j\omega)$ and $L_{fm}(j\omega)$ using G of Table 5.2b and $A_0 = 1.2M_0 = 3.05$.

ω_0	K_f	ϕ (deg)	K_0	K_∞	a
30.	1.	-30.	12.7	6.66×10^{13}	1
30.	.99	-23.	4.2	6.60	3
30.	.99	-16.	2.5	6.59	5
30.	1.	-9.	1.8	6.63	7
30.	1.02	0.	1.3	6.78	10

Table 7.1 Parameters of EEAS L_f .

violated by up to 6.5db. Since $|L_f(j\omega)|$ is smaller for all ω in the EEAS it should be expected that the step response will be slower (it could of course be speeded up by changing the prefilter F). Further, since the sensitivity bounds are not satisfied, the EEAS step response can be expected to change more with P_h .

EEAS step responses for two plant pole extremes are shown in Fig. 7.5. These may be compared with similar SOAS responses (on a different time scale) in Fig. 5.11a and 5.11b. Some time parameters from the two systems are collected on Table 7.2, and these figures support the qualitative predictions made above regarding the differences expected in the two system responses.

System	a	t_r	t_s
SOAS	10	1.1	—
SOAS	1	.45	1.6
EEAS	10	2.2	—
EEAS	1	.55	1.9

Table 7.2 Comparison of SOAS and EEAS step response characteristics.

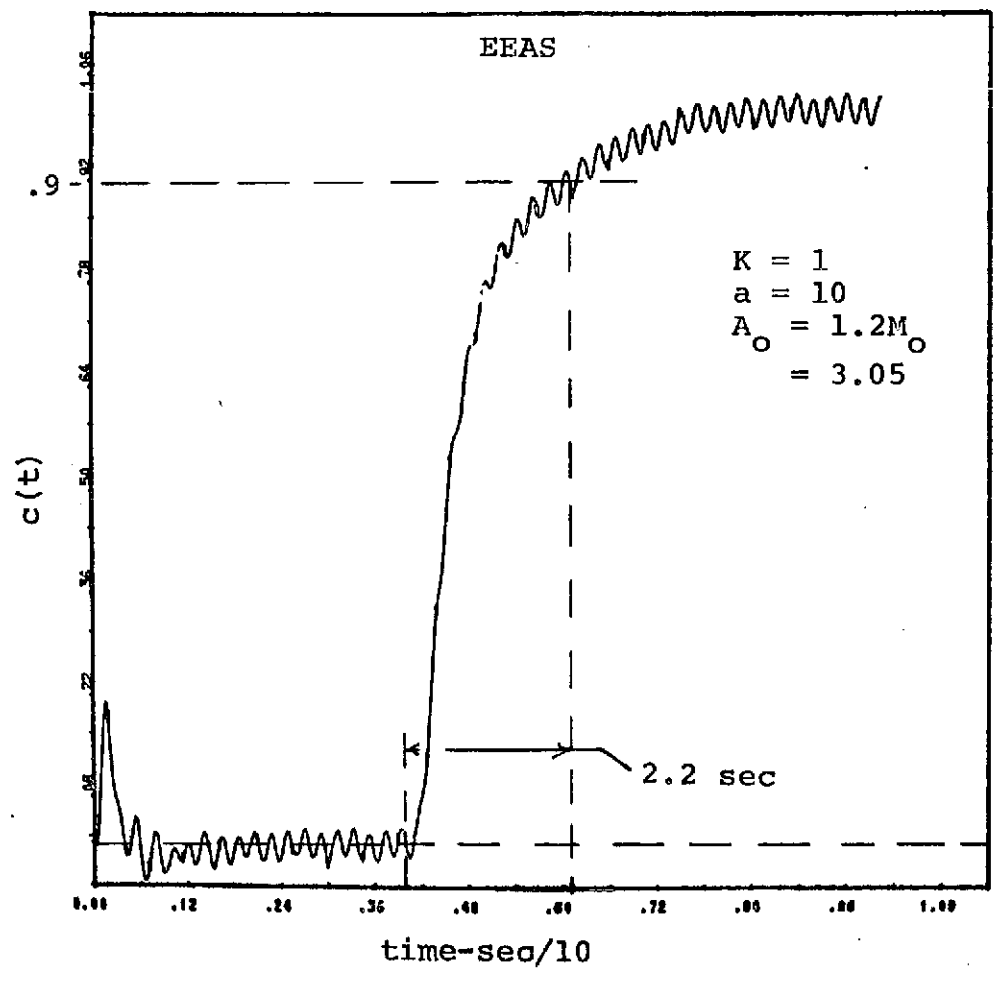


Fig. 7.5a EEAS response to unit step command applied at $t = 4$ sec.

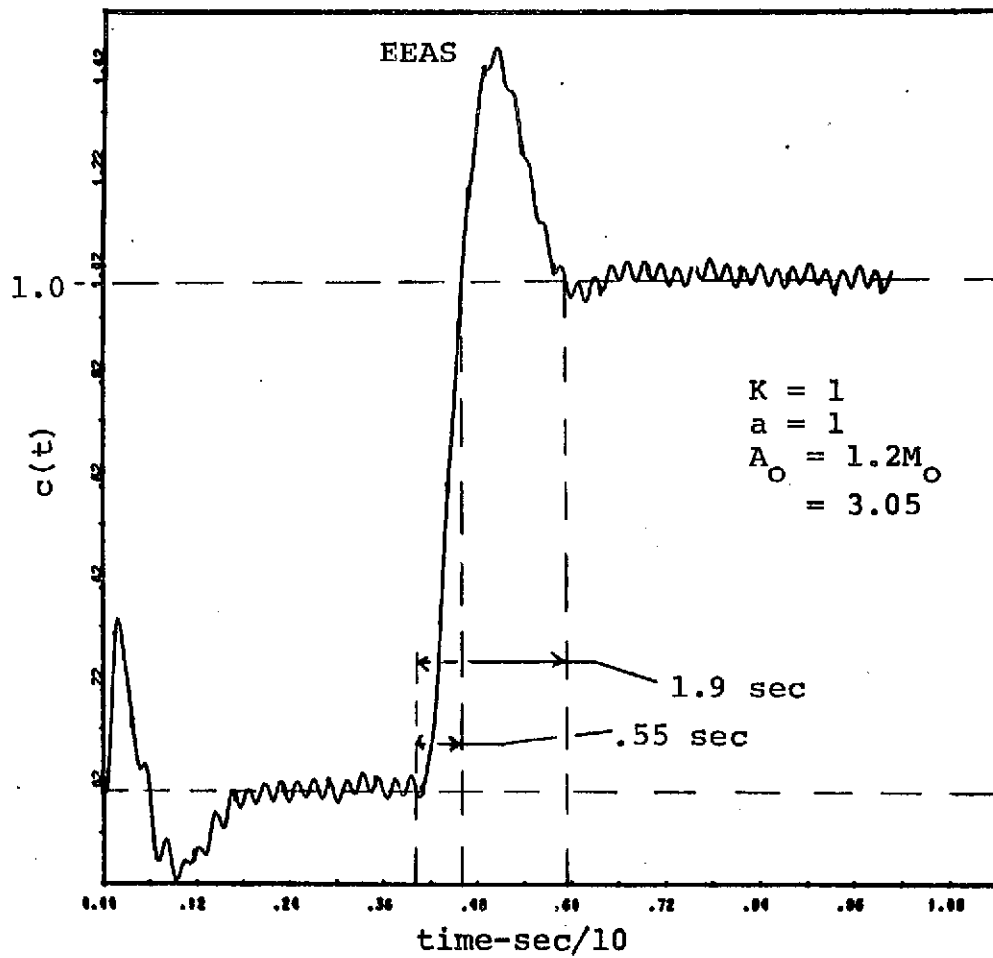


Fig. 7.5b EEAS response to unit step command applied at $t = 4$ sec.

CHAPTER IIX

SUMMARY AND CONCLUSIONS

8.1 Summary of the Oscillating System

Synthesis Philosophy

It has been found that the design of either of the oscillating systems considered herein is optimized with respect to the effect of sensor noise on the plant by designing for the minimum oscillating frequency ω_0 . Lower bounds are imposed on ω_0 by several design requirements. In particular, these are:

- a) the frequency quasi-linearity constraint which requires that the forced signal describing function component for the nonlinearity be valid over the bandwidth of the fastest forced signal input to the nonlinearity, as well as over the bandwidth of the fastest system output.
- b) the combination of magnitude quasi-linearity constraint and the upper bound on oscillating signal component at the system output.
- c) achievement of the required sensitivity reduction for ignorance or variation of plant parameters, excluding the gain factor.
- d) achievement of a specified disturbance attenuation.

Techniques have been developed in detail for determining

the lower bound on oscillating frequency for each of the factors above. The designer must first ascertain which requirement dominates in his particular design, i.e., which yields the greatest lower bound on oscillating frequency. Whenever possible, this should be done with a rough approximate design to avoid tedious optimization with respect to all of the above requirements. Once the dominant requirement is determined, the lower bound on oscillating frequency is minimized using the techniques and considering the tradeoffs detailed in the preceding chapters. Portions of the design emerge as a result of the oscillation frequency minimization procedure, and the remainder is relatively straightforward and explained herein.

8.2 Concluding Comments

The oscillating system stands out as one of the few nonlinear adaptive schemes that have been put to practical use. Heretofore, there has been no synthesis theory for designing such systems to meet practical quantitative specifications. In this paper a synthesis theory is developed which proceeds from quantitative specifications in a transparent fashion to a design that is optimal in the sense of sensor noise power at the plant input. All significant constraints on the design are considered, and the synthesis theory is demonstrated with numerical examples.

There is a distinct class of design problems for

which the oscillating adaptive scheme is superior to a linear adaptive design. The specifications and optimization criterion used in this work are sufficiently close to those used for linear adaptive design^[22] to permit a valid comparison of the best possible design by both methods. Thus, it is now possible to quantitatively evaluate which of the two design methods yields the superior solution to a given adaptive problem.

BIBLIOGRAPHY

1. L. A. MacColl, Fundamental Theory of Servomechanisms, D. Van Nostrand, N. Y., 1945, pp. 78-87.
2. J. C. Lozier, "Carrier-Controlled Relay Servos," Electrical Engineering, Vol. 69, No. 12, December 1950, pp. 1052-1056.
3. B. E. Amsler and R. E. Gorozdos, "On the Analysis of Bi-Stable Control Systems," IRE Trans. on Automatic Control, Vol. AC-4, December 1959, pp. 46-58.
4. A. Gelb, "The Foundation for Limit Cycling Adaptive Design," Proc. Northeast Electronics Res. Eng. Meeting, November 1961, pp. 76-77.
5. A. Gelb and W. E. Vander Velde, "On Limit Cycling Control Systems," IEEE Trans. on Automatic Control, AC-8, April 1963, pp. 142-157.
6. I. M. Horowitz, "Comparison of Linear Feedback Systems with Self-Oscillating Systems," IEEE Trans. on Automatic Control, AC-9, October 1964, pp. 386-392.
7. J. A. Blakelock, Automatic Control of Aircraft and Missiles, John Wiley & Sons, Inc., N.Y., 1965, p. 206.
8. L. W. Taylor, Jr. and E. J. Adkins, "Adaptive Control and the X-15," NASA Flight Research Center, Edwards, Calif., June 1, 1965 (paper presented at the Princeton University Conference on Aircraft Flying Qualities, June 17-18, 1965)
9. A. Gelb and W. E. Vander Velde, Multiple-Input Describing Functions and Nonlinear System Design, McGraw-Hill, N.Y., 1968, pp. 18-37.
10. Ibid., p. 308.
11. Ibid., p. 264, 278, 303.
12. Ibid., p. 641.

13. Ibid., pp. 401-407.
14. Ibid., pp. 560-562.
15. Ibid., p. 273.
16. R. Smisek, A Self-Oscillating Adaptive System with a Constant Time Delay Nonlinearity, M.S. Thesis, University of Colorado, Boulder, Colorado, 1969, p. 33.
17. A. Papoulis, Probability, Random Variables, and Stochastic Processes, McGraw-Hill, N.Y., 1965, pp. 475-476.
18. I. M. Horowitz, Synthesis of Feedback Systems, Academic Press, N.Y., 1963, pp. 246-249.
19. Ibid., PP 441-452.
20. Ibid., p. 332.
21. Ibid., P. 307.
22. I. M. Horowitz and M. Sidi, "Synthesis of Feedback Systems with Large Plant Ignorance for Prescribed Time Domain Tolerances," International Journal of Control, Vol. 16, No. 2, Aug. 1972, pp. 287-309.
23. I. M. Horowitz, "Optimum Loop Transfer Function in Single-Loop Minimum-Phase Feedback Systems," (to be published in the International Journal of Control).
24. G. Newton, L. Gould, and J. Kaiser, Analytical Design of Linear Feedback Controls, Wiley, N.Y., 1957, p. 43.
25. Annual Report, National Aeronautics and Space Administration Research Grant No. NGR-06-003-083, June 1970, p. 13.
26. N. Levinson and R. Redheffer, Complex Variables, Holden-Day, Inc., San Francisco, Calif., 1970, p. 227.
27. H. W. Bode, Network Analysis and Feedback Amplifier Design, D. Van Nostrand, N.Y., 1945, pp. 337-343.

28. E. O. Brigham and R. E. Morrow, "The Fast Fourier Transform," IEEE Spectrum, Vol. 4, No. 12, December 1967, pp. 63-70.
29. J. W. Cooley, Peter A. W. Lewis, and P. D. Welch, "The Fast Fourier Transform and its Applications," IEEE Trans. on Education, Vol. 12, No. 1, March 1969, pp. 27-34.

APPENDIX A

Nonlinearity Forced Input Function

In this appendix the nonlinearity forced input signal is considered in some detail. The goal is to choose this signal, subject to the appropriate constraints, such that the oscillating system loop transmission bandwidth is minimized. The structure of Fig. A.1 is assumed and the forced input to N denoted by X_f .

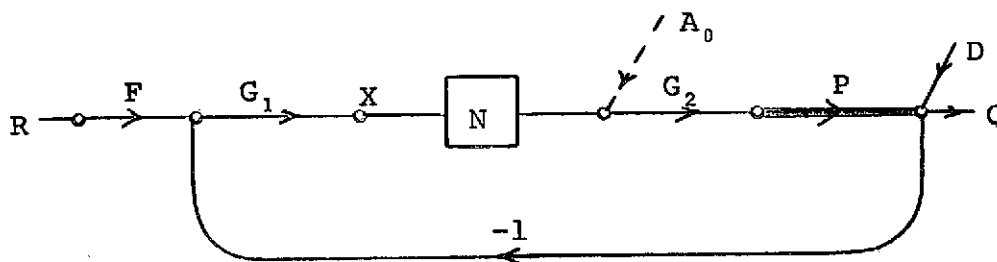


Fig. A.1 Oscillating system structure.

X_f must satisfy the quasilinearity constraints

$$\max_t |x_f(t)| \leq A_1/\alpha \quad (\text{A.1a})$$

$$\omega_b \leq \omega_0/\beta, \quad (\text{A.1b})$$

which were introduced in Sect. 1.2. In Eq. A.1, ω_0 is the oscillating frequency, ω_b is the bandwidth of $X_f(j\omega)$, A_1 is the minimum magnitude of oscillating

signal component at N , and α, β are the quasi-linearity parameters of N discussed in Sect. 1.2. In Sect. 2.1, Eq. 2.9, it was shown that X_f must satisfy

$$\mu(\omega_0) = |X_f(j\omega_0)| / \left[\max_t |x_f(t)| \right] \geq |U(j\omega_0)|, \quad (\text{A.2})$$

where U is completely determined in terms of given system parameters and specifications. In the frequency range suitable for ω_0 , $|U(j\omega)|$ is decreasing with ω so that the optimum X_f , which will permit minimum ω_0 , is the function that maximizes μ in (A.2). In Sect. 2.2 it is shown that the left side of (A.2) can, in an idealized sense, be made arbitrarily large by choosing $X_f = X_{f1} + X_{f2}$, where X_{f2} is given a constrained maximum effect on the time response and a complex pole pair at ω_0 , allowing any value for $|X_{f2}(j\omega_0)|$, and hence for $|X_f(j\omega_0)|$. However, this X_{f2} is impractical because of the acute system sensitivity to small parameter variations. The design of a practical X_{f2} is described in Sect. 2.3. In this appendix we want to determine the function X_{f1} , which is to be the relatively 'smooth' low frequency dominant portion of X_f , that will minimize the remaining burden on X_{f2} , or allow the minimum ω_0 if $X_{f2} = 0$.

For notational convenience we will consider $X_{f2} = 0$ and $X_{f1} = X_f$. In order to deal with specific

functional forms for X_f some assumptions must be made with regard to the system input and the plant. We assume the plant has one pole at the origin (Type 1) and R is a step input. Using the Final Value Theorem and Fig. A.1, $c(\infty) = \lim_{t \rightarrow \infty} c(t) = \lim_{s \rightarrow 0} sC(s) = \lim_{s \rightarrow 0} sN_f X_f(s)G_2(s)P(s)$. For $c(\infty)$ finite in the presence of step inputs, $X_f(0)$ must be finite and non-zero, excluding poles and zeros at the origin in G_2 . Summarizing, $X_f(j\omega)$ is to be a relatively smooth function having bandwidth $\omega_b \leq \omega_0/\beta$ and with $X_f(0)$ finite. The simplest such function is

$$X_f(s) = \frac{\omega_b}{s + \omega_b} \quad (\text{A.3})$$

which yields

$$\mu = \frac{1}{\omega_0 \sqrt{1 + 1/\beta^2}} \quad (\text{A.4})$$

Since $X_f = RFG_1/(1+L_f)$ with $L_f = N_f G_1 G_2 P$ in Fig. A.1, it must have the same excess of poles as RFG_1 (≥ 3), thus X_f in (A.3) can not be realized in the assumed structure. However, sufficient far poles ($\gg \omega_0$) can be added to make X_f realizable with no significance to the present discussion. On Table A.1 below several additional possibilities for X_f which allow closed form calculation of μ are tabulated. These do not of course cover all the possible choices for X_f , but by varying the several parameters in the

Trial	$X_f(s)$	μ
1	$\frac{1}{s+1}$	$\frac{1}{\sqrt{\omega_0^2+1}}$
2	$\frac{1}{(s+1)^n}; n > 1$	$\frac{(n-1)! e^{(n-1)}}{(n-1)^{(n-1)} (\omega_0^2+1)^{n/2}}$
3	$\frac{\rho}{(s+1)(s+\rho)}; 1 < \rho < \omega_0$	$\frac{\rho^{(\rho/(\rho-1))}}{\sqrt{\omega_0^2+1} \sqrt{\omega_0^2+\rho^2}}$
4	$\frac{1}{s^2+2\zeta s+1}; \zeta < 1$	$\frac{\exp[\zeta/\sqrt{1-\zeta^2} \tan^{-1}\{\sqrt{1-\zeta^2}/\zeta\}]}{\sqrt{(\omega_0^2-1)^2+4\zeta^2\omega_0^2}}$
5	$\frac{\rho_2(s+\rho_1)}{\rho_1(s+1)(s+\rho_2)};$ $\begin{cases} 1 < \rho_2 < \omega_0 \\ 0 < \rho_1 < \omega_0 \end{cases}$	$\frac{\sqrt{\omega_0^2+\rho_1^2}}{\sqrt{\omega_0^2+1} \sqrt{\omega_0^2+\rho_2^2}} \max \left[1, \frac{\rho_2}{\rho_1-1} \left\{ \frac{\rho_2(\rho_1-\rho_2)}{\rho_1-1} \right\}^{(1/(\rho_2-1))} \right]; \rho_1-\rho_2 > 1$ $\frac{\sqrt{\omega_0^2+\rho_1^2}}{\sqrt{\omega_0^2+1} \sqrt{\omega_0^2+\rho_2^2}}; \text{ otherwise}$

Table A.1 Tabulation of some trial functions $X_f(s)$.

table a wide variety of functions are considered.

For the purpose of comparing the functions in Table A.1 define ω_b as the solution of $|X_f(j\omega_b)/X_f(0)| = 1/\sqrt{2}$. For $\beta = 3$, Trial #1 gives $\mu_1 = .316$ with $\omega_0 = \beta\omega_b = 3$. For Trial #2 with $n = 2$, $\mu_2 = .575$ with $\omega_0 = \beta\omega_b = 3(.644) = 1.93$. Thus Trial #2 seems to be better than Trial #1 by the ratio $\mu_2/\mu_1 = 1.82$ (= 5.2db). This is true under the stated conditions, but it is found that $\mu_1 > \mu_2$ for $\omega_0 > \sqrt{e^2-1} = 2.53$. Thus for practical oscillating frequencies Trial #1 is superior to Trial #2 with $n = 2$, i.e., other design considerations nearly always force $\omega_0 > \beta\omega_b$. For $n = 3$, $\mu_1 > \mu_2$ for $\omega_0 > \sqrt{(e^2-2)/2} = 1.64$. It is clear that in practical design Trial #1 will provide larger μ than Trial #2.

Investigation of the remaining functions of Table A.1 is quite detailed. We shall simply summarize by stating that no acceptable combination of parameters in Trials #3, 4, and 5 produce a μ that is larger than that of Trial #1 with reasonable ω_0 .

From the above it is concluded that $X_f(s)$ from Eq. A.3 (Trial #1) gives the largest μ that is readily available and this function is used as a standard for Type 1 plants and step commands in the body of the paper. It may also serve as a standard against which any new function not considered herein may be compared.

For plants with other than a single integrator and/or other than step inputs, an investigation similar to that above should provide the designer with sufficient insight to choose a reasonable X_f .

APPENDIX B

Determination of the Extreme Plant
and Transfer Function

Using the oscillating system feedback structure on Appendix A Fig. A.1, the forced component of signal input to N is

$$X_f = \frac{Z_f}{N_f G_2 P} = \frac{AZ_f}{M_f K G_2 P_h} \quad (\text{B.1})$$

where Z_f is the forced component of plant output, A is oscillation magnitude at the input of N, and $N_f = M_f/A$ is taken as the forced signal describing function for N. The plant is characterised as

$$P(s, w) = K(w) P_h(s, w); \quad w \in W, \quad (\text{B.2})$$

where w is a parameter vector and only its bounding set W and possibly constraints among its elements are known. $P_h(s)$ is taken such that $P_h(s) \rightarrow 1/s^n$ as $|s| \rightarrow \infty$. In order that the assumed describing function hold, the quasi-linearity constraints,

$$\max_t |x_f(t)| \leq A/\alpha \quad (\text{B.3a})$$

$$\omega_b \leq \omega_0/\beta \quad (\text{B.3b})$$

are imposed. ω_b is the approximate bandwidth of $X_f(j\omega)$,

ω_0 the oscillating frequency, and α, β are the quasi-linearity parameters discussed in Chapter I. (B.3) must hold for all system inputs and all $w \in W$. Therefore, we require that these inequalities hold for the worst case X_f , which is written

$$X_e = \frac{A_e Z_e}{M_f K G_2 P_{he}} \quad (B.4)$$

The sub-e denotes that X_f and the accompanying function and parameter values which most nearly violates (B.3), i.e., the fastest and/or largest X_f . In the oscillating system synthesis theory it is assumed that the permissible Z_f are given by specifications. From this range of Z_f , and the possible P_h , the designer must select Z_e and the accompanying P_{he} that do indeed produce the extreme X_e . This selection must be made before the design is carried out, so G_2 and the precise pairings of P_h and Z_f are not known.

It is admitted at the outset that we do not know how to make the above selections in the case of an arbitrary plant and specifications on Z_f . What is done below is to make some observations that give the designer a reasonable chance to make a good selection. If this selection is incorrect, it will be revealed by the first completed design, and the designer should by then have the insight required to make the correct selection.

For a command input $Z_e = R_e T_e$, and for disturbances

it is $Z_e = -D_e L_{fe} / (1 + L_{fe})$, with $L_{fe} = \frac{M_f}{A_e} K_e G_1 G_2 P_{he}$. Presumably the expected range of inputs can be surveyed to determine R_e or D_e . Calculating the ratio X_f/X_e while the command input is held at its extreme value,

$$\frac{X_f}{X_e} = \frac{\frac{A}{M_f K_e G_2 P_h} \left[\frac{R_e F L_f}{1 + L_f} \right]}{\frac{A_e}{M_f K_e G_2 P_{he}} \left[\frac{R_e F L_{fe}}{1 + L_{fe}} \right]}$$

and canceling all the common factors

$$X_f = \left[\frac{1 + L_{fe}}{1 + L_f} \right] X_e \quad (B.5)$$

The same manipulation for a disturbance input yields exactly the same result. Therefore, P_{he} is the same parameter set regardless of whether X_e is the result of a command or a disturbance. For command input R_e we can also write

$$X_f = \frac{A K_e}{A_e K} \left[\frac{T}{T_e} \right] \left[\frac{P_{he}}{P_h} \right] X_e \quad (B.6)$$

The variation in $A K_e / A_e K$ with plant parameters is of the same order as the variation in $|P_h(j\omega_0) / P_{he}(j\omega_0)|$, which tends to be small because ω_0 is well above the varying plant dynamics and this plant ratio approaches unity for large ω_0 . Now suppose temporarily that the transfer function sensitivity is to be quite small so that $T/T_e \approx 1$ for all plants. Then

$$X_f \approx \begin{bmatrix} P_{he} \\ P_h \end{bmatrix} X_e \quad (B.7)$$

Consider a plant P_h whose poles and zeros vary independently, e.g., with $|P_h(j\omega)|$ lying in the envelope of Fig. B.1a. We have postulated in Fig. B.1a that the extreme plant is P_{he} with zeros set to minimum and poles

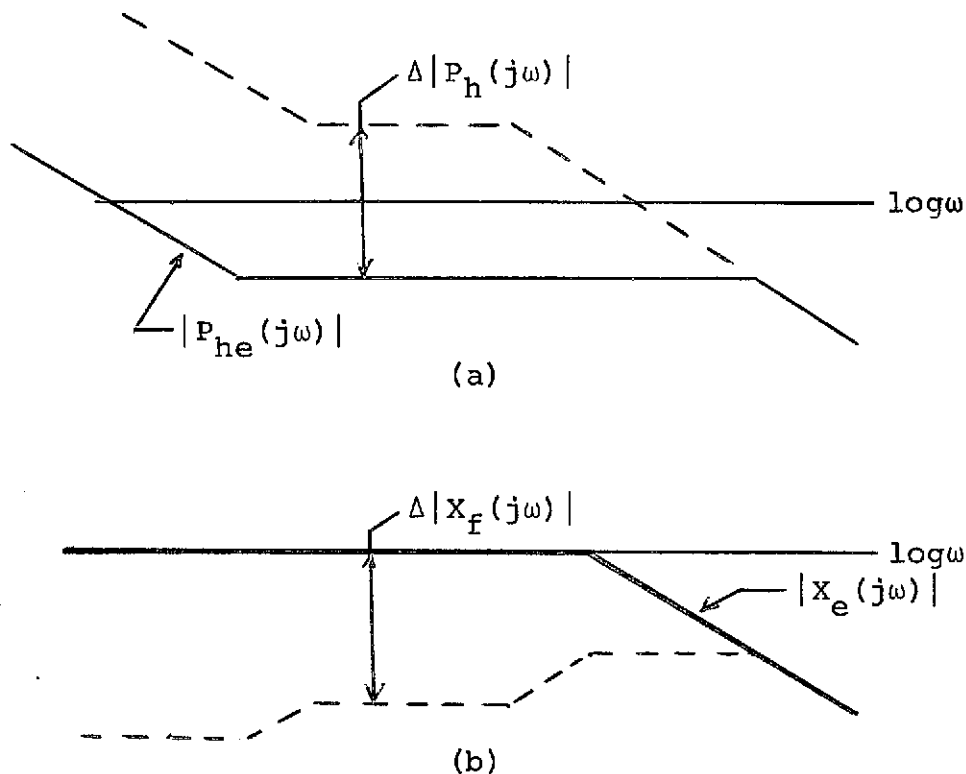


Fig. B.1 Illustration of extreme plant selection.

set to maximum. The concurrent variation in X_f in accord with (B.7) is shown in Fig. B.1b. As P_h deviates from P_{he} , $|X_f(j\omega)|$ becomes smaller than $|X_e(j\omega)|$ for all ω , but the bandwidth of $X_f(j\omega)$ increases. It is inferred from this observation that $|x_e(t)|$ will likely have the largest maximum value, but $x_e(t)$ will

be the slowest $x_f(t)$. Thus the plant that gives the extreme $X_f(t)$ with respect to (B.3a) is different from the plant giving the extreme with respect to (B.3b). This observation is supported by the following example. Let $P_h = 1/[s(s+a)]$, $a \in [1,10]$, and $P_{he} = 1/[s(s+a_e)]$. Let $X_e = 150/[(s+6)(s+25)]$. In Fig. B.2 the various $x_f(t)$ from Eq. B.7 are shown for three choices of a_e . In Fig. B.2a, with $a_e = 1$, $x_e(t)$ is simultaneously the fastest and smallest $x_f(t)$. Conversely, with $a_e = 10$ in Fig. B.2c, $x_e(t)$ is simultaneously the slowest and largest $x_f(t)$.

Recall in the synthesis steps where X_e is used (Sect. 2.3 and 6.5), that the designer is most concerned with constraint (B.3a). This constraint is used directly in the equations of that synthesis procedure to obtain a lower bound for the oscillating frequency. Once the lower bound is obtained, (B.3b) merely dictates whether it may be used in the design. Since it is not generally possible to select P_{he} to give the extreme $x_f(t)$ for both (B.3a) and (B.3b) simultaneously, it is clearly appropriate to choose the extreme with respect to (B.3a), i.e., the magnitude quasi-linearity constraint. The postulated P_{he} in Fig. B.1a is the correct selection when poles and zeros vary independently. For the more general plant, a good choice of P_{he} seems to be the parameter set that minimizes $|P_h(j\omega)|$ over the maximum portion of the system bandwidth, obtained by inspection of $|P_h(j\omega)|$

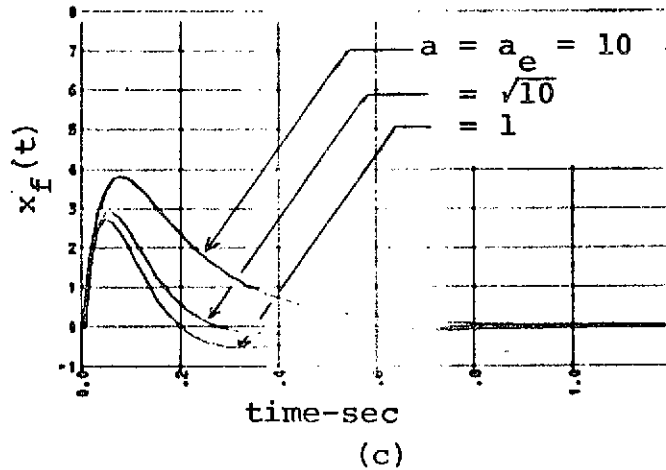
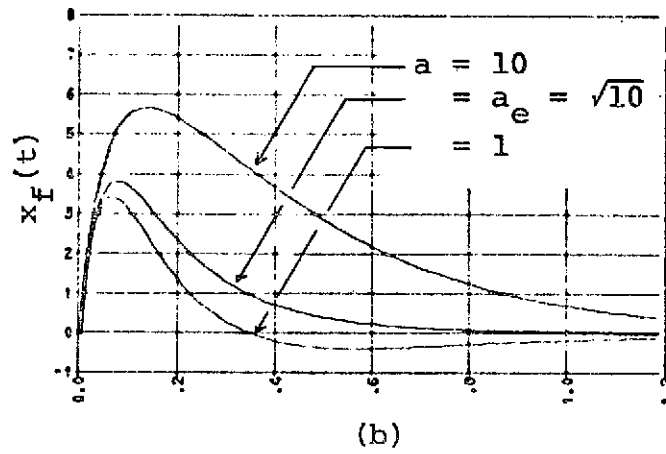
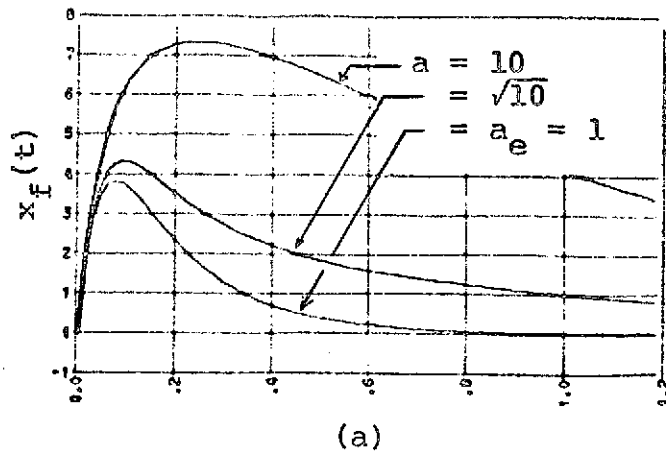


Fig. B.2 Variation of $x_f(t)$ for several selections of P_{he} .

over the permissible plant parameter sets.

Moving now to the case where the transfer function variation is not vanishingly small, it is quite reasonable that the above selection of P_{he} remains valid. Then it is necessary to determine which of the admissible transfer functions T is the T_e that is paired with P_{he} . With P_{he} selected as above (zeros minimized and poles maximized) it tends to have smallest magnitude and least phase lag over the system bandwidth. A glance at the Nichols chart, which displays the relationship between $T/F = L_f/(1+L_f)$ and $L_f = N_f G_1 G_2 K P_h$, immediately leads to the conclusion that T_e is the T for which $|T(j\omega)|$ is minimum over the system bandwidth.

In summary, the guidelines for choosing P_{he} and T_e are as follows. P_{he} is the plant with minimum $|P_h(j\omega)|$ and maximum $\frac{1}{|P_h(j\omega)|}$, while T_e is the lower bound of specifications on $|T(j\omega)|$.

Appendix C

Derivation of Bounds for $L(j\omega)$ from Transfer
Function Sensitivity or Disturbance Response
Specifications

The technique for determining bounds on acceptable loop transmission from specifications on transfer function sensitivity and/or disturbance response is detailed below. The technique applies to any linear time-invariant two degree-of-freedom feedback structure^[18] and is taken from [22]. The structure in Fig. C.1 is used, however, all two degree-of-freedom structures are equivalent with respect to the specifications considered

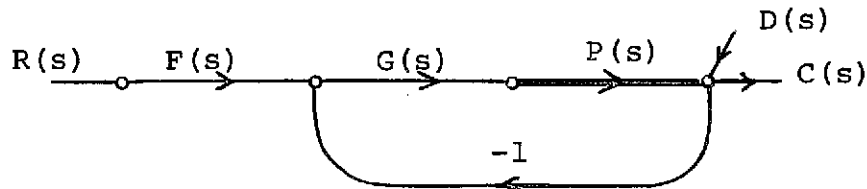


Fig. C.1 A two degree-of-freedom feedback structure.

herein; thus any other structure could be used, or could be transformed into the structure shown. For the purpose of providing insight into the meaning of the bounds for $L(j\omega)$ and how they are constructed a graphical method is first presented, then a digital computer implementation of the method is given.

In Fig. C.1 the plant $P(s)$ is the constrained part of the system given as a rational transfer function, but

with bounded uncertainty of some parameters, i.e., $P(s) = P(s, w)$; $w \in W$, where w is a parameter vector, and the bounding set W is known along with any constraining relations or correlation that may exist among the elements of w . The loop transmission is

$$L(s, w) = G(s)P(s, w). \quad (C.1)$$

Since there is no uncertainty associated with G , the plant variation may be written at some specific frequency ω_i as

$$\begin{aligned} \Delta \ln[P(j\omega_i)] &= \Delta \ln[G(j\omega_i)P(j\omega_i)] = \Delta \ln[L(j\omega_i)] \\ &= \Delta \ln|L(j\omega_i)| + j\Delta \underline{L(j\omega_i)}. \end{aligned} \quad (C.2)$$

The transfer function is

$$\frac{C}{R} = T = \frac{FL}{1+L}. \quad (C.3)$$

There is no uncertainty associated with F so that variations in $T(j\omega_i)$ are written as

$$\begin{aligned} \Delta \ln[T(j\omega_i)] &= \Delta \ln \left[\frac{F(j\omega_i)L(j\omega_i)}{1+L(j\omega_i)} \right] \\ &= \Delta \ln \left| \frac{L(j\omega_i)}{1+L(j\omega_i)} \right| + j\Delta \underline{\frac{L(j\omega_i)}{1+L(j\omega_i)}}. \end{aligned} \quad (C.4)$$

Thus both the given plant uncertainty and the specified permissible transfer function uncertainty are expressed in terms of L . Suppose that the maximum permissible transfer function uncertainty is specified by

$$\Delta \ln|T(j\omega)| \leq \ln[\beta(\omega)]; \quad \beta(\omega) \geq 1. \quad (C.5)$$

We shall show how this specification is translated to a boundary of acceptable $L(j\omega_i)$ at the frequency ω_i .

First a number of discrete parameter vectors w_r ; $r = 1, 2, \dots, m$ are selected and the plant is evaluated at ω_i for each, giving the complex numbers $P_r(j\omega_i, w_r)$; $r = 1, 2, \dots, m$. These points are plotted as shown by Fig. C.2 on Nichols chart coordinates ($\ln|P(j\omega)|$ vs.

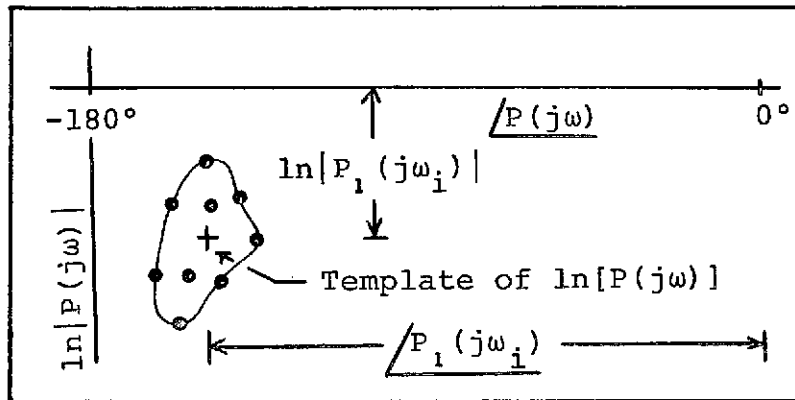


Fig. C.2 Construction of the plant template.

$\angle P(j\omega)$). The points are then enclosed to define a region of plant variation as shown, which we shall refer to as the plant template. The designer must select m large enough and the w_r with sufficient care to insure that the entire region of plant variation is included in the template with negligible error. Since $L(j\omega_i)$ will vary with the plant parameters, we will deal with a particular w_1 which gives $L_1(j\omega_i) = G(j\omega_i)P_1(j\omega_i)$. To find a point on the boundary for $L_1(j\omega_i)$ the template may be cut out of Fig. C.2 and laid on the Nichols chart for $L(j\omega)$ shown in Fig. C.3, (which has been drawn using the same scales as the plant template) keeping the coordinate axes through $P_1(j\omega_i)$ parallel to those of the $L(j\omega)$ chart at all times. The $L(j\omega)$ chart has contours of constant

$\ln|L(j\omega)/(1+L(j\omega))|$. Choose any angle $\angle G(j\omega_i)$, or equivalently $\angle L_1(j\omega_i)$, and position the plant template on

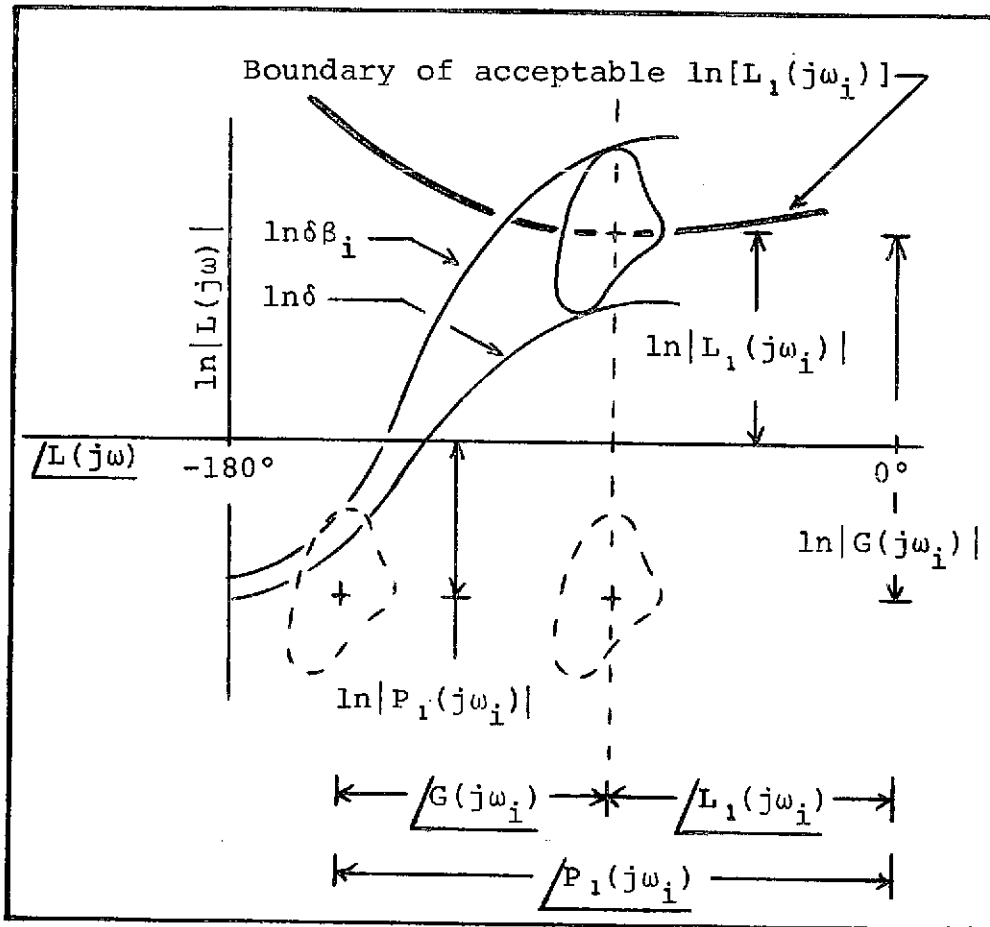


Fig. C.3 Method for locating one point on the boundary of acceptable $L_1(j\omega_i)$.

this angle grid. Next the template is moved vertically along the chosen angle grid until one finds a point where Eq. C.5 is satisfied with equality, i.e., until the template just fits between two $\ln|L(j\omega)/(1+L(j\omega))|$ contours, say $\ln\delta$ and $\ln\delta\beta_i$ ($\beta_i = \beta(\omega_i)$) as shown by Fig. C.3. In this position the origin of template coordinates determines a point on the boundary for $L_1(j\omega_i)$. Additional

points are found by repeating the process at different angles.

A plant template is prepared and the boundary for $L_1(j\omega)$ found at a sufficient number of discrete frequencies to provide a high degree of confidence that (C.5) will be satisfied closely at any ω by an L_1 satisfying the bounds at the discrete frequencies. Of course the same plant parameter set is used for P_1 at each frequency.

The Nichols chart also has contours of constant $\underline{L(j\omega)/(1+L(j\omega))}$, so that given a specification of the form

$$\underline{\Delta/T(j\omega)} \leq \Psi(\omega), \quad (C.6)$$

the boundaries for $L_1(j\omega)$ to satisfy this specification can be found in the same manner as above. For any $\underline{L_1(j\omega_i)}$, the greater of the $\ln|L_1(j\omega_i)|$ determined by (C.5) and (C.6) determines the bound that must be used to satisfy both specifications.

Next we consider the bounds on $L(j\omega)$ determined by disturbance response specifications. From Fig. C.1 the disturbance transmission is

$$\frac{C_D}{D} = T_D = \frac{1}{1+L} = \frac{1/L}{1+1/L} \equiv \frac{V}{1+V}. \quad (C.7)$$

We assume the specification on T_D is given as

$$\ln|T_D(j\omega)| \leq \ln[\rho(\omega)]. \quad (C.8)$$

Here we have a specification on the absolute value of the transmission rather than the change. However, (C.8) must be satisfied for all values of the plant. To find the

boundary for $L_1(j\omega_i)$ we first construct a template of $1/P(j\omega_i)$ since $\Delta \ln[V(j\omega_i)] = \Delta \ln[1/P(j\omega_i)]$. Positioning this template on a $\ln[V(j\omega)]$ vs. $\sqrt{V(j\omega)}$ chart, a boundary for $V_1(j\omega_i)$ is found as demonstrated in Fig. C.4a. This

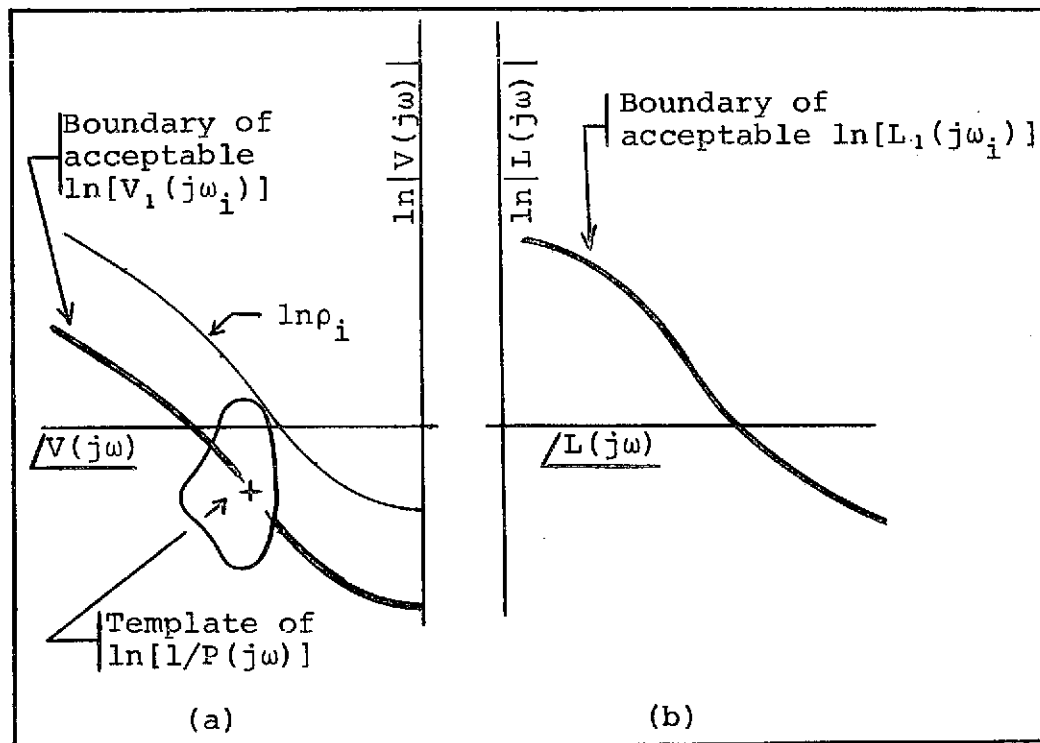


Fig. C.4 Location of boundary points for $L_1(j\omega_i)$ to satisfy disturbance transmission specification.

boundary is then translated to its equivalent for $L_1(j\omega_i) = 1/V_1(j\omega_i)$ as depicted by Fig. C.4b.

Next a digital computer implementation for finding the boundary for $L_1(j\omega_i)$ due to transfer function specification (C.5) is investigated. Let

$$G(j\omega_i) = g e^{j\theta} \quad (C.9)$$

$$P_r(j\omega_i) = p_r e^{j\phi_r}; \quad r = 1, 2, \dots, m. \quad (C.10)$$

Using T_1, T_2 , due to P_1, P_2 respectively in (C.5) with equality and squaring both sides yields

$$\left| \frac{T_1(j\omega_i)}{T_2(j\omega_i)} \right|^2 = \left[\frac{P_1}{P_2} \right]^2 \left[\frac{(gP_2)^2 + 2gP_2 \cos(\theta + \phi_2) + 1}{(gP_1)^2 + 2gP_1 \cos(\theta + \phi_1) + 1} \right] = f(g) = \beta_i^2. \quad (\text{C.11})$$

It can easily be shown that $f(\pm\infty) \rightarrow 1$, $f(g) \neq 0$, and $f(g)$ is finite for all real g and $\theta + \phi_r \neq k\pi$. Also, $f'(g) = 0$ has two real roots giving the qualitative sketch in Fig. C.5. Given P_1, P_2 , and θ , it is a simple matter to

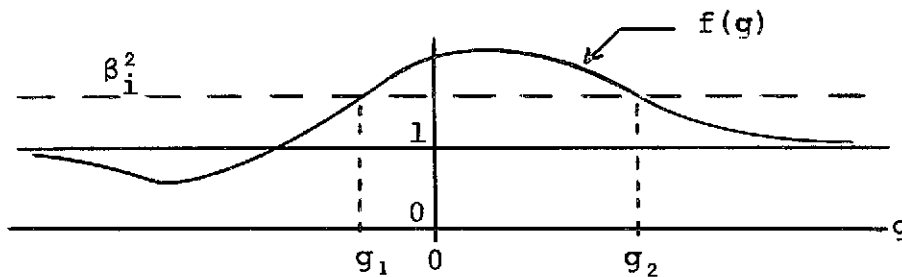


Fig. C.5 Graphical representation of Eq. C.11.

solve for the roots g_1, g_2 of (C.11). Consider the possible results in determining the boundary for $L_1(j\omega_i) = gp_1 e^{j(\theta + \phi_1)}$.

g_1, g_2 complex: For this case there is no real g satisfying (C.11) and therefore at the given $\angle L_1(j\omega_i) = \theta + \phi_1$ there is no boundary point on the Nichols chart of Fig. C.3. This case can occur if the permitted variation in transfer function is larger than the plant uncertainty.

$g_1, g_2 < 0$: This gives two boundary points on Fig.

C.3 on the angle grid at $\angle L_1(j\omega_i) = \theta + \phi_1 \pm 180^\circ$. Thus at $\angle L_1(j\omega_i) = \theta + \phi_1$ there is again no boundary for $L_1(j\omega_i)$.

$g_1 < 0, g_2 > 0$: The negative root gives a boundary point displaced 180° from the angle grid of interest at $\theta + \phi_1$. g_2 gives a valid boundary point for $L_1(j\omega_i)$.

$g_1, g_2 > 0$: This case produces upper and lower boundary points for $L_1(j\omega_i)$ on the angle grid

$\angle L_1(j\omega_i) = \theta + \phi_1$. $L_1(j\omega_i)$ must lie below the upper boundary or above the lower boundary.

The above observations allow us to construct an algorithm for obtaining a boundary for $L_1(j\omega_i)$ as follows.

Algorithm for bounds on $L_1(j\omega_i)$ due to Eq. C.5

1. Select plant parameter sets w_r ; $r = 1, 2, \dots, m \in W$ such that the plant template boundary is satisfactorily covered.
2. Choose $\theta = \angle G(j\omega_i)$ and solve Eq. C.11 $m^2 - m$ times, i.e., for all combinations of $|T_r(j\omega_i)/T_s(j\omega_i)|$; $r \neq s$, getting roots $g_{1\alpha}, g_{2\alpha}$; $\alpha = 1, 2, \dots, m^* \leq m^2 - m$.

Let

$$g_1^* = \min_{1 \leq \alpha \leq m^*} \{g_{1\alpha}\}$$

$$g_2^* = \max_{1 \leq \alpha \leq m^*} \{g_{2\alpha}\}.$$

$g_{1\alpha} < g_{2\alpha}$ for all α , so if $g_2^* < 0$ there are no bounds. Otherwise, the lower bound for $L_1(j\omega_i)$ is at $p_1 g_2^* e^{j(\theta + \phi_1)}$. If $g_1^* > 0$ there is also an upper bound at $p_1 g_1^* e^{j(\theta + \phi_1)}$. When there are two bounds the lower

bound is higher on the Nichols chart ($g_2^* > g_1^*$) and $L_1(j\omega_i)$ must avoid the region between the two bounds.

3. Repeat 2. for as many θ as desired to obtain the complete boundary for $L_1(j\omega_i)$.

Treating specification (C.6) in the same fashion

$$\frac{T_1(j\omega_i)}{T_2(j\omega_i)} = \psi_i, \quad (C.12)$$

and after some manipulation

$$g^2 p_1 p_2 [\sin(\phi_2 - \phi_1) - t \cos(\phi_2 - \phi_1)] + \quad (C.13)$$

$$g [p_2 (\sin(\theta + \phi_2) - t \cos(\theta + \phi_2)) - p_1 (\sin(\theta + \phi_1) + t \cos(\theta + \phi_1))] - t = 0,$$

where

$$t = \tan(\psi_i + \phi_2 - \phi_1). \quad (C.14)$$

The equation for g locating bounds for $L_1(j\omega_i)$ is again a quadratic. The bounds can be calculated by using the magnitude algorithm given above with Eq. C.13 substituted in step 2.

Lastly, the disturbance response specification of Eq. C.8 yields

$$(gp)^2 + 2gpc \cos(\theta + \phi) + 1 - 1/\rho_i^2 = 0. \quad (C.15)$$

The bounds for this specification are calculated using the same algorithm with (C.15) in step 2., which only needs to be solved m times because (C.15) contains only one value of the plant.

Listed below is a FORTRAN subroutine which calculates the composite boundaries for $L_1(j\omega_i)$ due to the three specifications (C.5, C.6, and C.8). A representative

output is shown using the plant $P(s) = K/[s(s+a)]$ with $K \in [1,100]$, $a \in [1,10]$, and specifications as listed on the printed output. Also listed are PLANT subroutines suitable for evaluating the forced signal equivalent plant P_f used in the SOAS and EEAS iterative designs for parameter sensitivity and disturbance attenuation.

```

SUBROUTINE NICRND(W,BETA,A1,DA,A2,PS)
C      J. W. SMAY, REVISED NOV. 72.
C      REF. HOROWITZ AND SIDI, INTERNATIONAL JOURNAL OF CONTROL,
C      VOL. 16, NO. 2, 1972, PP. 287-309.
C      ROUTINE LOCATES BOUNDS FOR G AND L1=G*P1 AT FREQUENCY W(RPS) TO
C      SATISFY THE MOST RESTRICTIVE OF
C      1.  MAX(ABS(T(JW)))/MIN(ABS(T(JW)))=BETA(1)
C      2.  MAX(ARG(T(JW)))-MIN(ARG(T(JW)))=BETA(2)(DFG)
C      3.  MAX(ABS(TD(JW)))=BETA(3)
C      IF BETA(1) IS NEGATIVE THE SPECIFICATION IS IGNORED.
C      USER MUST SUPPLY SUBROUTINE PLANT WHICH EVALUATES
C      P(1,I)=PLANT MAGNITUDE AND P(2,I)=PLANT ANGLE IN RADIANS
C      FOR N PARAMETER SETS.
C      PS IS SWITCH WHICH ALLOWS USER ROUTINE TO READ PLANT PARAMETER
C      DATA ON FIRST CALL OF PLANT.
C      BOUNDS ARE COMPUTED FOR ANGLE OF L1 ON (A1,A2) AT INCREMENTS
C      DA IN DEGREES.
      DIMENSION P(2,50),BETA(3)
      1 FORMAT(1H,10X,*NI-HOLS CHART BOUNDS AT FREQUENCY=*,F10.4,/1H ,10X*
      2,*BETA(1)=*,F8.4,* BETA(2)=*,F8.4,* BETA(3)=*,F8.4,/1H0,
      310X,*RCUND G-ANGLE*,4X,*G-MAG*,3X,*G-MAG(DB)*.2X,
      4*L1-ANGLE*,3X,*L1-MAG*,2X,*L1-MAG(DB)*//)
      2 FORMAT(1H ,15X,F10.4,22X,F10.4,* NO SOLUTION*)
      3 FORMAT(1H ,10X,*LOWFR*,7F10.4)
      4 FORMAT(1H ,10X,*UPPER*,7F10.4)
      5 FORMAT(1H ,10X,*STABILITY LIMIT ENCOUNTERED*)
      IF(PS.EQ.0.) CALL PLANT(P,W,N,PS)
      IF(PS.EQ.0.) RETURN
      WRITE(6,1) W,BETA
      BETA2=BETA(1)**2
      BETA1=1.-BETA2
      BETA3=1.-1./BETA(3)**2
      BETA4=3.1415927*BETA(2)/180.
      CALL PLANT(P,W,N,PS)
      A1=A1-180.*P(2,1)/3.1415927
10  A1=A1+3.1415927/180.
      GLM=-1.
      GUM=1.E20
      IF(BETA(1).LT.0.) GO TO 20
C      CALCULATE BOUNDS FOR TRANSFER FUNCTION MAGNITUDE SPECIFICATION.
      DO 15 I=1,N
      DO 15 J=1,N
      IF(I.EQ.J) GO TO 15
      C1=(P(1,I)*COS(A1+P(2,I))-BETA2*P(1,I)*COS(A1+P(2,J)))/(P(1,I)
      2*P(1,J)*BETA1)
      C2=(P(1,I)**2-(BETA(1)*P(1,I)**2)/((P(1,J)*P(1,I))**2*BETA1)
      C3=C1**2-C2
      IF(C3.LT.0.) GO TO 15
      G1=-C1-SQRT(C3)
      G2=-2.*C1-G1
      IF(G1.LT.GLM) GUM=G1
      IF(G2.GT.GLM) GLM=G2
15  CONTINUE
20  GLA=-1.
      GUA=1.E20
      IF(BETA(2).LT.0.) GO TO 30
C      CALCULATE BOUNDS FOR TRANSFER FUNCTION ANGLE SPECIFICATION.
      DO 25 I=1,N
      DO 25 J=1,N
      IF(I.EQ.J) GO TO 25

```

```

NICR0000
NICR0005
NICR0010
NICR0015
NICR0020
NICR0025
NICR0030
NICR0035
NICR0040
NICR0045
NICR0050
NICR0055
NICR0060
NICR0065
NICR0070
NICR0075
NICR0080
NICR0085
NICR0090
NICR0095
NICR0100
NICR0105
NICR0110
NICR0115
NICR0120
NICR0125
NICR0130
NICR0135
NICR0140
NICR0145
NICR0150
NICR0155
NICR0160
NICR0165
NICR0170
NICR0175
NICR0180
NICR0185
NICR0190
NICR0195
NICR0200
NICR0205
NICR0210
NICR0215
NICR0220
NICR0225
NICR0230
NICR0235
NICR0240
NICR0245
NICR0250
NICR0255
NICR0260
NICR0265
NICR0270
NICR0275
NICR0280
NICR0285
NICR0290
NICR0295

```

```

T=TAN(BETA4*P(2,I)-P(2,J))
C0=P(1,I)*P(1,J)*(SIN(P(2,I)-P(2,J))-T*COS(P(2,I)-P(2,J)))
C1=(P(1,I)*(SIN(A1*P(2,I))-T*COS(A1*P(2,I)))-P(1,J)*
2*(SIN(A1*P(2,J))+T*COS(A1*P(2,J))))/(2.*C0)
C2=-T/C0
C3=C1**2-C2
IF(C3.LE.0.) GO TO 25
G1=-C1-SCRT(C3)
G2=-2.*C1-G1
IF(G1.LT.GLA) GUA=G1
IF(G2.GT.GLA) GLA=G2
25 CONTINUE
30 GLD=-1.
GUD=1.E20
IF(BETA(3).LT.0.) GO TO 40
C CALCULATE BOUNDS FOR DISTURBANCE RESPONSE SPECIFICATION.
DO 35 I=1,N
C1=COS(A1*P(2,I))/P(1,I)
C2=C1**2-BETA3/P(1,I)**2
IF(C2.LT.0.) GO TO 35
G1=-C1-SCRT(C2)
G2=-2.*C1-G1
IF(G1.LT.GLD) GUD=G1
IF(G2.GT.GLD) GLD=G2
35 CONTINUE
40 GL=AMAX1(GLM,GLA,GLD)
GU=AMIN1(GUM,GUA,GUD)
A1=A1*180./3.1415927
AGP=A1+180.*P(2,1)/3.1415927
IS=0
IL=0
IF(GL.LE.0.) GO TO 50
GLDB=22.*ALOG10(GL)
GLP=GL*P(1,1)
GLPDB=20.*ALOG10(GLP)
WRITE(6,3) A1,GL,GLDB,AGP,GLP,GLPDB
C CHECK IF PRESENT LOWER BOUND IS UNSTABLE FOR ANY PLANT.
DO 45 I=1,N
AL=A1+180.*P(2,1)/3.1415927
GP=GL*P(1,I)
IF(AL.LT.(-180.).AND.GP.GT.1.) IL=1
45 CONTINUE
GO TO 55
50 IS=IS+1
55 IF(GU.LE.0.) GO TO 60
GUDB=20.*ALOG10(GU)
GUP=GU*P(1,1)
GUPDB=20.*ALOG10(GUP)
WRITE(6,4) A1,GU,GUDB,AGP,GUP,GUPDB
GO TO 65
60 IS=IS+1
IF(IS.EQ.2) WRITE(6,2) A1,AGP
65 IF(IL.EQ.1) WRITE(4,5)
IF(IL.EQ.1) RETURN
IF(AGP.LT.A2) RETURN
A1=A1-DA
GO TO 10
END
NICR0300
NICR0305
NICR0310
NICR0315
NICR0320
NICR0325
NICR0330
NICR0335
NICR0340
NICR0345
NICR0350
NICR0355
NICR0360
NICR0365
NICR0370
NICR0375
NICR0380
NICR0385
NICR0390
NICR0395
NICR0400
NICR0405
NICR0410
NICR0415
NICR0420
NICR0425
NICR0430
NICR0435
NICR0440
NICR0445
NICR0450
NICR0455
NICR0460
NICR0465
NICR0470
NICR0475
NICR0480
NICR0485
NICR0490
NICR0495
NICR0500
NICR0505
NICR0510
NICR0515
NICR0520
NICR0525
NICR0530
NICR0535
NICR0540
NICR0545
NICR0550
NICR0555
NICR0560
NICR0565
NICR0570
NICR0575
NICR0580
NICR0585

```



```

SUBROUTINE PLANT(P,W,N,PS)
C   ROUTINE GENERATES VALUES OF PLANT WITH VARYING GAIN, POLES,
C   AND ZERCS FOR CALCULATION OF NICHOLS CHART BOUNDS.
DIMENSION P(2,50),G(10),P0(10),P1(10),Z(2),ZC(2,10),PC(2,10)
1  FORMAT(13,7X,7E10.4/(8E10.4/))
2  FORMAT(1H1,10X,*PLANT PARAMETER VALUES USED TO DETERMINE NICHOLS C
  2HART BOUNDS*/1H0.1X,*ERROR CONSTANTS*/(1H ,10X,6E12.4))
3  FORMAT(1H ,10X,*POLE*,6F10.4/(1H ,17X,6F10.4/))
  IF(PS.EQ.1.) GO TO 35
C   READ AND WRITE PLANT PARAMETER VALUES.
C   ADD ONE READ AND ONE WRITE CARD FOR EACH VARYING PARAMETER.
  READ(5,1) NG,(G(I),I=1,NG)
  WRITE(6,2)(G(I),I=1,NG)
  READ(5,1) NP1,(P0(J),J=1,NP1)
  WRITE(6,3)(P0(J),J=1,NP1)
C   SET UP CONSTANT PARAMETERS OF PLANT.
  P1(1)=2.
  NP=2
  NZ=0
  NPC=0
  NZC=0
  RETURN
35 N=0
C   ADD ONE DO 60 FOR EACH VARYING PARAMETER.
  DO 60 I=1,NG
  DO 60 J=1,NP1
  P1(2)=P0(J)
  N=N+1
  CALL BCDF(W,G(I)/P1(2),NP,P1,NPC,PC,NZ,Z,NZC,ZC,PR,PI,OB,P(2,N))
60 P(1,N)=SQRT(PR**2+PI**2)
  RETURN
  END

```


PLANT PARAMETER VALUES USED TO DETERMINE NICHOLS CHART BOUNDS

ERROR CONSTANTS

1.0000E+00 1.0000E+02
 POLE 1.0000 3.0000 5.0000 7.0000 10.0000

NICHOLS CHART BOUNDS AT FREQUENCY= .1000

BETA(1)= 1.0292 BETA(2)= -1.0000 BETA(3)= -1.0000

BOUND	G-ANGLE	G-MAG	G-MAG(DB)	L1-ANGLE	L1-MAG	L1-MAG(DB)
LOWER	-4.2894	3.1479	9.9603	-100.0000	31.3223	29.9171
LOWER	-24.2894	13.7122	22.7422	-120.0000	136.4420	42.6990
LOWER	-44.2894	24.4654	27.7711	-140.0000	243.4401	47.7278
LOWER	-64.2894	31.7746	30.0416	-160.0000	316.1690	49.9984
LOWER	-84.2894	35.0682	30.8983	-180.0000	348.9412	50.8550
LOWER	-104.2894	34.0017	30.6300	-200.0000	338.3291	50.5868

STABILITY LIMIT ENCOUNTERED

NICHOLS CHART BOUNDS AT FREQUENCY= .1000

BETA(1)= -1.0000 BETA(2)= 1.0000 BETA(3)= -1.0000

BOUND	G-ANGLE	G-MAG	G-MAG(DB)	L1-ANGLE	L1-MAG	L1-MAG(DB)
LOWER	-4.2894	57.1148	35.1350	-100.0000	568.3132	55.0918
LOWER	-24.2894	52.3539	34.3790	-120.0000	520.9412	54.3358
LOWER	-44.2894	41.2784	32.3145	-140.0000	410.7355	52.2712
LOWER	-64.2894	25.2240	28.0363	-160.0000	250.9883	47.9931
LOWER	-84.2894	9.1265	15.7443	-180.0000	60.9613	35.7011
LOWER	-104.2894	15.6436	23.8867	-200.0000	155.6595	43.8435

STABILITY LIMIT ENCOUNTERED

NICHOLS CHART BOUNDS AT FREQUENCY= .1000

BETA(1)= -1.0000 BETA(2)= -1.0000 BETA(3)= .5000

BOUND	G-ANGLE	G-MAG	G-MAG(DB)	L1-ANGLE	L1-MAG	L1-MAG(DB)
LOWER	-4.2894	1.8190	5.1965	-100.0000	18.0995	25.1533
LOWER	-24.2894	2.2029	6.8599	-120.0000	21.9197	26.8167
LOWER	-44.2894	2.5757	8.2180	-140.0000	25.6294	28.1748
LOWER	-64.2894	3.8598	9.1267	-160.0000	28.4561	29.0835
LOWER	-84.2894	2.9941	9.5254	-180.0000	29.7927	29.4822
LOWER	-104.2894	2.9502	9.3970	-200.0000	29.3554	29.3537

STABILITY LIMIT ENCOUNTERED

```

SUBROUTINE PLANT(PF,W,N,PS)
  C   ROUTINE GENERATES NORMALIZED PLANT VALUES PF FOR SOAS NICHOLS
  C   CHART BOUND ITERATION.
  REAL KF,K0,KINF
  DIMENSION PF(2,50),G(12),P0(10),P1(10),Z(10),ZC(2,10),PC(2,10)
  DIMENSION KF(50)
  1  FORMAT(13,7X,7E10.4/(8E10.4/))
  2  FORMAT(1H1,10X,*PLANT PARAMETER VALUES USED TO DETERMINE NICHOLS C
  CHART BOUNDS*/)
  3  FORMAT(1H ,10X,*POLE*.6F10.4/(1H ,17X,6F10.4/))
  4  FORMAT(4I2)
  5  FORMAT(1H0,10X,*SSSS NO ITERATION FAILED TO CONVERGE SSSS*)
  6  FORMAT(1H0,10X,*COMPENSATION PARAMETERS*/)
  7  FORMAT(8E10.4)
  8  FORMAT(1H0,10X,*REAL POLES*/(1H ,10X,F10.4,))
  9  FORMAT(1H0,10X,*REAL ZEROS*/(1H ,10X,F10.4,))
 10  FORMAT(1H0,10X,*COMPLEX POLES(ZETA,OMEGA)*/(1H ,10X,2F10.4,))
 11  FORMAT(1H0,10X,*COMPLEX ZEROS(ZETA,OMEGA)*/(1H ,10X,2F10.4,))
 12  FORMAT(1H0,14X,*W0*.8X,*KF*.8X,*K0*.8X,*KINF*/)
 13  FORMAT(1H ,10X,3F10.4,E12.4)
  IF(PS.EQ.1.) GO TO 50
  GN=1.
  GI=1.
  NO=05
  NS=1
  C   READ AND WRITE PLANT PARAMETER VALUES.
  WRITE(6,2)
  READ(5,1) NP1,(P0(J),J=1,NP1)
  WRITE(6,3) (P0(J),J=1,NP1)
  P1(1)=0.
  NP=2
  NZ=0
  NPC=0
  NZC=0
  C   READ FIRST GUESS OF OSCILLATING FREQUENCY W0.
  READ(5,7) W0
  C   READ AND WRITE COMPENSATION DATA.
  READ(5,4) NPL,NZL,NPCL,NZCL
  WRITE(6,6)
  IF(NPL.EQ.NP) GO TO 20
  I0=NP+1
  READ(5,7) (P1(I),I=I0,NPL)
  DO 15 I=I0,NPL
 15  GI=GI*P1(I)
  WRITE(6,8) (P1(I),I=I0,NPL)
 20  IF(NZL.EQ.NZ) GO TO 30
  I0=NZ+1
  READ(5,7) (Z(I),I=I0,NZL)
  DO 25 I=I0,NZL
 25  GI=GI/Z(I)
  WRITE(6,9) (Z(I),I=I0,NZL)
 30  IF(NPCL.EQ.NPC) GO TO 40
  I0=NPCL+1
  READ(5,7) (PC(1,I),PC(2,I),I=I0,NPCL)
  DO 35 I=I0,NPCL
 35  GI=GI*PC(2,I)**2
  WRITE(6,10) (PC(1,I),PC(2,I),I=I0,NPCL)
 40  IF(NZCL.EQ.NZC) GO TO 50
  I0=NZC+1
  READ(5,7) (ZC(1,I),ZC(2,I),I=I0,NZCL)

```

```

DO 45 I=10,NZCL
45 GI=GI/(ZC(2,I)**2)
WRITE(6,11) (ZC(1,I),ZC(2,I),I=10,NZCL)
50 N=0
DO 70 J=1,NP1
P1(2)=P0(J)
M=N-1
CALL BODE(W,1./P1(2),NP,P1,NPC,PC,NZ,Z,NZC,ZC,PR,P1,DR,PF(2,N))
IF(NS.EQ.0) GO TO 70
C ON FIRST CALL SOLVE FOR W0 AND ADJUST GAIN SO LF(JW0)=-1/2.
A0=1000.
DO 55 K=1,25
CALL BODE(W0,GM/P1(2),NPL,P1,NPCL,PC,NZL,Z,NZCL,ZC,HR,H1,DR,A1)
CALL BODE(.95*W0,GM/P1(2),NPL,P1,NPCL,PC,NZL,Z,NZCL,ZC,FR,FI,DR,A2
2)
A1=A1+3.1415927
A2=A2+3.1415927
W1=W0-.05*W0*A1/(A1-A2)
IF(ABS(A1-A0).LE..1.AND.ABS(W0-W1).LT..05*W0) GO TO 60
A0=A1
55 W0=W1
WRITE(6,5)
60 KF(N)=.5/SQRT(HR**2+H1**2)
K0=GM*KF(N)/P1(2)
KINF=GI*K0*P1(2)
IF(N.NE.1) GO TO 65
GM=GM*KF(1)
K0=GM
KINF=GI*K0*P1(2)
KF(1)=1.
WRITE(6,12)
65 WRITE(6,13) W0,KF(N),K0,KINF
70 PF(1,N)=SQRT(PR**2+P1**2)*KF(N)
NS=0
RETURN
END

```

```

SUBROUTINE PLANT(PF,H,N,PS)
  ROUTINE GENERATES NORMALIZED PLANT VALUES PF FOR EEAS NICHOLS
  CHART BOUND ITERATION.
  REAL KF,K0,KINF
  DIMENSION PF(2,50),G(10),P0(10),P1(10),Z(10),ZC(2,10),PC(2,10)
  DIMENSION KF(50)
  1 FORMAT(13,7X,7E10.4/(8E10.4/))
  2 FORMAT(1H1,10X,*PLANT PARAMETER VALUES USED TO DETERMINE NICHOLS C
  2HART BOUNDS*/)
  3 FORMAT(1H ,10X,*P01F*.6F10.4/(1H ,17X,6F10.4/))
  4 FORMAT(4I2)
  5 FORMAT(1H0,10X,*W0=*F10.4,* A0/M0=*F10.4)
  6 FORMAT(1H0,10X,*COMPENSATION PARAMETERS*/)
  7 FORMAT(8E10.4)
  8 FORMAT(1H0,10X,*REAL POLES*/(1H ,10X,F10.4,))
  9 FORMAT(1H0,10X,*REAL ZEROS*/(1H ,10X,F10.4,))
  10 FORMAT(1H0,10X,*COMPLEX POLES(ZETA,OMEGA)*,/(1H ,10X,2F10.4,))
  11 FORMAT(1H0,10X,*COMPLEX ZEROS(ZETA,OMEGA)*,/(1H ,10X,2F10.4,))
  12 FORMAT(1H0,12X,*ARG(LF)*,3X,*MAG(LF)*,5X,*PHI*.7X,*KF*.8X,*K0*.
  28X,*KINF*/)
  13 FORMAT(1H ,10X,5F17.4,E12.4)
  IF(PS.EQ.1.) GO TO 50
  GM=1.
  GI=1.
  NS=1
C   READ AND WRITE PLANT PARAMETER VALUES.
  WRITE(6,2)
  READ(5,1) NP1,(P0(J),J=1,NP1)
  WRITE(6,3) (P0(J),J=1,NP1)
  P1(1)=0.
  NP=2
  NZ=0
  NPC=0
  NZC=0
C   READ OSCILLATING FREQUENCY W0 AND A0/M0.
  READ(5,7) W,A0
  WRITE(6,5) W,A0
C   READ AND WRITE COMPENSATION DATA.
  READ(5,4) NPL,NZL,NPCL,NZCL
  WRITE(6,6)
  IF(NPL.EQ.NP) GO TO 20
  I0=NP+1
  READ(5,7) (P1(I),I=I0,NPL)
  DO 15 I=I0,NPL
  15 GI=GI*P1(I)
  WRITE(6,8) (P1(I),I=I0,NPL)
  20 IF(NZL.EQ.NZ) GO TO 30
  I0=NZ+1
  READ(5,7) (Z(I),I=I0,NZL)
  DO 25 I=I0,NZL
  25 GI=GI/Z(I)
  WRITE(6,9) (Z(I),I=I0,NZL)
  30 IF(NPCL.EQ.NPC) GO TO 40
  I0=NPCL+1
  READ(5,7) (PC(1,I),PC(2,I),I=I0,NPCL)
  DO 35 I=I0,NPCL
  35 GI=GI*PC(2,I)**2
  WRITE(6,10) (PC(1,I),PC(2,I),I=I0,NPCL)
  40 IF(NZCL.EQ.NZC) GO TO 50
  I0=NZCL+1

```

```

READ(5,7) (ZC(1,I),ZC(2,I),I=10,NZCL)
DO 45 I=10,NZCL
45 GI=GI/(ZC(2,I)**2)
WRITE(6,11) (ZC(1,I),ZC(2,I),I=10,NZCL)
S0 NS=0
DO 70 J=1,NP1
P1(2)=P0(J)
N=N+1
CALL BODE(W,1./P1(2),NP,P1,NPC,PC,NZ,Z,N7C,ZC,PR,P1,DB,PF(2,N))
IF(NS.EQ.0) GO TO 70
C ON FIRST CALL SOLVE FOR PHI AND ADJUST GAIN SO
C LF(JW0)=-.5*EXP(PHI)/(A0/M0+EXP(PHI)).
CALL BODE(W,GM/P1(2),NPL,P1,NPCL,PC,NZL,7,NZCL,ZC,HR,HI,DB,AL)
PHI0=PHI(AL,A0)
GL0=.5/SQRT(A0**2+2.*A0*COS(PHI0)+1.)
KF(N)=GL0/SQRT(HR**2+HI**2)
K0=GM*KF(N)/P1(2)
KINF=GI*K0*P1(2)
IF(N.NE.1) GO TO 65
GM=GM*KF(1)
K0=GM
KINF=GI*K0*P1(2)
KF(1)=1.
WRITE(6,12)
65 PHJ0=PHI0*180./3.1415927
AL=AL*180./3.1415927
WRITE(6,13) AL,GL0,PHI0,KF(N),K0,KINF
70 PF(1,N)=SQRT(PR**2+P1**2)*KF(N)
NS=0
RETURN
END
FUNCTION PHI(AL,A0)
C FUNCTION SOLVES EQ. 6.11 FOR PHI(RAD). GIVEN
C AL=ARG(L0(JW0))(RAD) AND A0=A0/M0 BY SECANT METHOD.
1 FORMAT(1H0,10X,*FUNCTION PHI FAILED TO CONVERGE P0=*,E12.4.
2* P1=*,E12.4,* F1=*,E12.4./)
PI=4.*ATAN(1.)
P0=1.5*(AL+PI)
P1=1.55*(AL+PI)
F0=P0-ATAN(SIN(P0)/(A0+COS(P0)))-AL-PI
DO 2 I=1,25
F1=P1-ATAN(SIN(P1)/(A0+COS(P1)))-AL-PI
PHI=P1-F1*((P1-P0)/(F1-F0))
IF(ABS(F1).LE..01.AND.ABS(P1-P0).LE..01) RETURN
F0=F1
P0=P1
2 P1=PHI
WRITE(6,1) P0,P1,F1
STOP
END

```